# ELASTIC STABILITY OF CYLINDRICAL SHELLS WITH SOFT ELASTIC CORES: BIOMIMICKING NATURAL TUBULAR STRUCTURES

by

Gebran Nizar Karam

B. Eng. in Civil Engineering (with distinction), 1988
American Universtiy of Beirut, Beirut , Lebanon

S.M. in Civil Engineering, 1990
Massachusetts Institute of Technology, Cambridge, Massachusetts

Submitted to the Department of Civil and Environmental Engineering
in partial fulfillment of the requirements for the degree of

Doctor of Philosophy in Materials and Structures

at the

Massachusetts Institute of Technology
January, 1994

Signature of Author .................................................................................................
Department of Civil and Environmental Engineering
January 19, 1994

Certified by...........................................................................................................
Lorna J. Gibson
Associate Professor of Civil and Environmental Engineering
Thesis Supervisor

Accepted by..........................................................................................................
Professor Joseph M. Sussman
Chairman, Committee on Graduate Studies

# ELASTIC STABILITY OF CYLINDRICAL SHELLS WITH SOFT ELASTIC CORES: BIOMIMICKING NATURAL TUBULAR STRUCTURES

by

Gebran Nizar Karam

Submitted to the Department of Civil and Environmental Engineering
on January 19, 1994 in partial fulfillment of the requirements
for the degree of Doctor of Philosophy in Materials and Structures

## Abstract

Thin walled cylindrical shell structures are widespread in nature: examples include plant stems, porcupine quills and hedgehog spines. All have an outer shell of almost fully dense material supported by a low density, ᴄ 'lular core. In nature, all are loaded in some combination of axial compression and bending: failure is typically by buckling. Natural structures are often optimized. Here we have analyzed the elastic buckling of a thin cylindrical shell supported by an elastic core to show that this structural configuration achieves significant weight saving over a hollow cylinder. The results of the analysis are compared with data from an extensive experimental program on uniaxial compression and four point bending tests on silicone rubber shells with and without compliant foam cores. The analysis describes the results of the mechanical tests well. Characterization of the microstructures of several natural tubular structures with foam-like cores (plant stems, quills and spines) revealed them to be close to the optimal configurations predicted by the analytical model. Biomimicking of natural cylindrical shell structures and evolutionary design processes may offer the potential to increase the mechanical efficiency of engineering cylindrical shells.

Doctoral committee chair: Dr. Lorna J. Gibson,
   Associate Professor of Civil and Environmental Engineering, M.I.T.
Committee members: Dr. Eduardo Kausel,
   Professor of Civil and Environmental Engineering, M.I.T.
   Dr. John W. Hutchinson ,
   Professor, Division of Applied Sciences, Harvard University

*L'edication*

*In memory of my grandfather, Gebran B. Karam,*
*He would have been so proud,*
*May all his visions come true.*

*To my parents, Nada and Nizar,*
*Who made it all possible,*
*With love and respect, God bless you.*

"...Consider the Lilies of the field, how they grow;

They toil not, neither do they spin:

And yet I say unto you ,

That even Solomon in all his glory

was not arrayed like one of these."

*Matthew 6:27, 28*

"..this is the Lord's doing,

and it is marvelous in our eyes?"

*Matthew 21:42*

# Acknowledgements

An apprentice takes after his masters, and fine ones I have had.

I wish to thank Professor Eduardo Kausel for his friendship that I treasure, for his sincere involvement in this dissertation, his strong support in the course of my stay at MIT, and for his priceless advice technically and otherwise.

I wish to thank Professor John W. Hutchinson for his brilliant technical insights, the exciting discussions that helped shape this dissertation, and his enthusiasm and support throughout the course of this work.

I wish to express my appreciation and thanks to Messrs. Arthur and Steven Rudolph of the Civil Engineering machine shop without whose efforts and expertise many an experimental program would have faltered. Their excellent craftsmanship went a long way in insuring the success of my experiments, and the wisdom of Arthur helped me out of one too many depressing days.

To the one and only who has been with me through all this adventure, my wife to be Diane Zreik, I express my eternal love and gratitude for sharing, caring, and ever sustaining me by her daily offerings of love, patience, understanding and selfless dedication.

Finally I wish to acknowledge the unconditional moral support I received from my family and the unflinching financial support of my father. Nizar, Nada and Jean provided the love, trust and strength from which I drew the energy that kept me going on.

# Table of Contents

# List of Tables

# List of Figures

11

# List of Notations and Symbols

a = radius to mid-plane of thickness

b = radius of bore hole

c = core thickness

C = curvature of cylinder in bending

$D$ = flexural rigidity of shell = $\dfrac{Et^3}{12\left(1 - v^2\right)}$

E = Young's modulus of shell

$E_c$ = Young's modulus of core

$h = \dfrac{t}{\sqrt{1 - v^2}}$

I = moment of inertia

$k_e$ = spring constant for compliant core

l = length of shell

l' = half the buckling wavelength = l/m

m = longitudinal wave number

$M_{Brazier}$ = Brazier moment

$M_{lb}$ = local buckling moment

$N_x$ = uniaxial compression per unit circumferential length

$P_0$ = axial compressive buckling load of hollow shell

$P_{cr}$ = axial compressive buckling load of shell with compliant       core

q = uniform internal pressure inside shell

t = thickness of shell

$t_{eq}$ = equivalent thickness of a hollow shell of equal mass and radius as shell with a compliant core

u, v, w = deformations along x, y, z directions

U = strain energy per unit length

$w_m$ = maximum sinusoidal displacement in z-direction

$$\alpha = \left[ \frac{E_c}{E} \right]$$

$$\beta = \frac{3 - 5v_c}{(1 + v_c)(1 - 2v_c)}$$

$$\beta' = \frac{v_c^2(5 - 2v_c)}{(1 + v_c)(1 - 2v_c)}$$

$\delta$ = maximum radial displacement under ovalization

$\zeta$ = degree of ovalization = $\dfrac{\delta}{a}$

$\zeta_{cr}$ = degree of ovalization at $M_{Brazier}$

$\zeta_{lb}$ = degree of ovalization at local buckling

$\lambda$ = buckling wavelength parameter = $\dfrac{l'}{\pi}$

$\lambda_{cr}$ = value of $\lambda$ minimizing $N_x$

$v$ = Poisson's ratio of shell

$v_c$ = Poisson's ratio of core

$\rho$ = density of the shell

$\rho_c$ = density of the core

$\sigma_o$ = Theoretical buckling stress in uniaxial compression of hollow shell

$\sigma_{cr}$ = axisymmetric buckling stress of shell with compliant core under uniaxial compression

$\sigma_{max}$ = maximum normal stress in bent cylinder

$\sigma_z$ = stress in the z-direction

$\overline{\sigma_z}$ = normalized normal stress in z direction = $\dfrac{\sigma_z}{\sigma_{z/z=0}}$

$\tau_{xz}$ = shear stress in the x-z plane

$\overline{\tau_{xz}}$ = normalized shear stress in xz plane = $\dfrac{\tau_{xz}}{\tau_{xz/z=0}}$

# CHAPTER 1

## INTRODUCTION

*"... I wish to discuss the strength of hollow solids, which are employed in art - and still oftener in nature - in a thousand operations for the purpose of greatly increasing strength without adding to weight; examples of these are seen in the bones of birds and in many kinds of reeds which are light and highly resistant both to bending and brea. ing. For if a stem of straw which carries a head of wheat heavier than the entire stalk were made up of the same amount of material in solid form it would offer less resistance to bending and breaking. This is an experience which has been verified and confirmed in practice where it is found that a hollow lance or a tube of wood or metal is much stronger than would be a solid one of the same length and weight, one which would necessarily be thinner; men have discovered, therefore, that in order to make lances strong as well as light they must make them hollow. ..."*

Galileo Galilei (1638)

Thus, Galileo concluded the chapter of "Two New Sciences" dealing with the strength of materials, signaling the birth of the science of the strength and mechanics of elastic bodies and materials (Timoshenko, 1953). What the skillful artisans of the seventeenth century and their predecessors knew about the relative strengths of hollow and solid cylinders of equal weight and length, before Galileo's attempt at a scientific proof, was probably the result of observations of natural structures such as bones and plant stems used in crafting artifacts. Bamboo, for example, received a wide range of applications throughout history in weaponry, housing, utility structures and articles of everyday use; by mimicking its hollow cylindrical structure, artisans may have found they could produce lighter, stiffer and stronger pieces.

Nature has long been an important source of inspiration for scientists and engineers. Recently, there has been growing interest in the newly defined, interdisciplinary field of biomimetics which aims to analyze natural systems from an engineering perspective, understand their function, describe their behavior, and finally,

derive design principles that will allow the engineer to achieve a similar results by mimicking biology. This approach is based on the premise that Nature, be it the work of a wise Creator or the result of endless trials in biological processes over long evolutionary times, has achieved optimal results in solving many of the problems faced by living creatures. This includes structural and materials problems, chemical reactions, molecular synthesis, and thermal, electrical and sensory exchanges (Vincent and Srinivasan, 1992).

Natural materials and structural systems often have exceptional mechanical properties (such as density, $\rho$, modulus, E, and strength, $\sigma_f$) giving them high values of the mechanical performance indices defined by Ashby (1992). Woods and palms have high values of $E^{1/2}/\rho$ making them efficient materials for beams or columns (Ashby et al., 1994). Silk (Gosline et al., 1986; Vollrath, 1992) and skin (Mai and Atkins, 1989) have excellent elastic and fatigue properties; their high values of the performance index $\sigma_f^2/E$, and $\sigma_f/E$, respectively, make them excellent springs and elastic hinges. And nacre and antler are tougher than engineering ceramics by an order of magnitude (Jackson and Vincent, 1990; Gunnison et al., 1992). Limited in the choice of biologically synthesized polymers and ceramics, natural systems have adopted hierarchical design and microstructuring as the key to optimised systems (Gordon, 1988; Vincent, 1990a,b). For instance, wood and trabecular bone both combine a cellular microstructure with fibre composite cell walls (Gibson and Ashby, 1988); the cellular structure is oriented to resist the *in vivo* stresses each material sees most efficiently. Palm is made up of fibre-like vascular bundles parenchymatous matrix; the radial and longitudinal distribution of fibre bundles increases its mechanical efficiency (Rich, 1987; Tomlinson, 1990).

Other natural systems sport state of the art designs that contemporary engineering has only reached in the last few decades. Grass (Vincent, 1982), wood cell wall (Mark, 1967), and insect cuticle (Gunderson et al., 1992) for example, all have an elaborate polymeric fibre composite structure, with different fibre orientations and laminations and treatment of points of stress concentration. Sandwich beams, an elegant solution for stiff,

lightweight structures, are common in nature, as in, for instance, iris leaves (Gibson et al., 1988) and feather shafts (Purslow and Vincent, 1978) (Fig.1.1a). The internal bone of the cuttlefish, which acts as a rigid buoyancy tank (Birchall and Thomas, 1983), has a cellular microstructure, akin to a multilayered sandwich plate, that combines low weight with high compressive strength. Furthermore, its systematic compartmentalization maximizes buoyancy and reliability in the case of compressive failure, and is not without similarities to double-hulled supertanker designs (Fig. 1.1b and 1.1c).

For a structural member of a given material, the resistance to both bending deflection and Euler column buckling can most efficiently be resisted by increasing the cross-sectional shape factor $\Phi$ (Ashby, 1992) :

$$\Phi = \frac{4\pi I}{A^2} \qquad (1.1)$$

where I is the second moment of inertia and A is the area of the cross- section. For a cylindrical tube the shape factor is simply the ratio of the radius to the wall thickness, so that the most efficient section is that with the largest radius and the thinnest wall. In practice, the shape factor is limited by the onset of *local buckling*. Plant stems have developed at least two mechanisms to resist local buckling: internal pressurization and support of the shell by a foam-like core which acts as an elastic foundation (known as the "core-rind" structure to biologists). The outer shell, or rind, in plant stems is made up of sclerenchyma and collenchyma cells, with thick cell walls while the inner core is made up of thin walled parenchyma cells. This variation in the cell wall thickness gives the stem a dense, stiff outer shell supported by a light, compliant core. In certain plant varieties the parenchyma fills all of the internal volume (for instance, corn (*Zea mays* ) and sunflower (*Helianthus*)), while in others there is a central void (for instance, oat (*Avena*), barley (*Hordeum* ) and wheat (*Triticum*)) (Esau, 1977) (Fig.1.2a). Porcupine quills and hedgehog spines are also thin cylindrical shells supported by a microstructured foam core which varies from a simple three dimensional foam core in the North American porcupine (*Erethizon*) (Fig. 1.2b), to a combination of longitudinal stiffeners and a foam

core in the crested Old World porcupine (*Hystrix subcristatus* ) (Fig. 1.2c), to a lattice of struts in the European hedgehog (*Erinaceus Europaeus*) (Vincent and Owers, 1986)(Fig. 1.2d).

Thin walled cylindrical shells are widespread in engineering, too: examples include civil engineering structures (tubular trusses, silos, tanks), automotive structures, legs of offshore oil platforms, aircraft fuselages, rockets and submarines. Ranges of the ratio of cylinder radius to wall thickness, a/t, for a variety of natural and engineering structures is shown in Fig. 1.3. In contrast to natural cylindrical shells which have a uniform, compliant core, engineering structures with large ratios of a/t are typically stiffened against buckling by circumferential and longitudinal members, known as ring stiffeners and stringers, respectively. Biomimicking of natural cylindrical shell structures may offer the potential to increase the mechanical efficiency of engineering cylindrical shells.

The work presented in this thesis examines natural cylindrical structures with compliant cores, such as plant stems and animal quills, with a view to biomimicking. Plant stems resist axial load due to their own weight and bending loads due to wind. They act structurally as beam columns; their axisymmetric cylindrical tube form arises from the need to resist loads from any direction. Schwendener, in 1874, was the first to report on the internal microstructural stiffening of the stems of monocotyledons (Thompson, 1961). More recently, Niklas and O'Rourke (1987) have described the contribution of internal pressure to the flexural rigidity of the chive and Niklas (1989) has analyzed the role of pressure in stiffening plant tissues in general. Niklas (1991a,b, 1992) has also reported on the "core-rind" design of cylindrical plant organs attempting unsuccessfully to model its flexural rigidity.

This thesis analyzes the resistance of a cylindrical shell with a compliant core to local buckling, applies the results to estimate the mechanical efficiency of the natural structures described above and suggests how the natural structures might be mimicked in

engineering design. Chapter 2 reviews the engineering mechanics literature on the elastic stability of cylindrical shells, with and without a soft elastic core, under axial compression and bending loads. In Chapter 3 we derive a simple model for the axisymmetric buckling under uniaxial compression of a cylinder with an elastic core by treating a longitudinal strip of the shell as a beam on a half elastic space. We then analyze both the Brazier and local buckling of a cylindrical shell with a compliant core in pure bending; both calculations account for the ovalization of the cross-section. The local buckling moment is calculated by setting the maximum compression stress in the bent cylinder equal to the axisymmetric buckling stress for uniaxial compression. The decay in stress with depth into the core is also examined to determine the minimum core depth required to resist the stresses within the core. The results are used to perform a parametric analysis comparing the mechanical resistance of a cylinder with a compliant core to that of a hollow cylinder of the same diameter and mass. Chapter 4 describes the experimental program devised to verify the predictions of the analysis; uniaxial compression and pure bending tests were performed on model silicone rubber cylinders with either a silicone rubber foam or a flexible polyurethane foam core. Having verified the analytical results we then, in Chapter 5, compile microstructural data on natural cylindrical shells with compliant cores to estimate their mechanical efficiency compared with a hollow cylinder of equal mass and diameter. The implications of these findings for engineering design and potential applications of this research are then discussed. Our conclusions are summarized in Chapter 6 along with suggestions for future work.

**References**

Ashby, M.F., (1992), <u>Materials Selection in Mechanical Design</u>, Pergamon Press, New York

Ashby, M.F., Gibson, L.J. and Olive, R. (1994, to be submitted) "The mechanical properties of natural materials I: Material property charts" <u>Proc. Roy. Soc.</u>

Birchall, J.D. and Thomas, N.L., (1983), "On the architecture and function of the cuttlefish bone", <u>J. Mat. Sci.</u>, Vol. 18, pp 2081-2086

Esau, K., (1977), <u>Anatomy of Seed Plants</u>, 2nd ed., John Wiley and Sons, New York

Galileo Galilei, (1638) <u>Dialogues Concerning Two New Sciences</u>, English translation by H. Crew and A. de Salvio, Northwestern University Press, Evanston, Illinois (1950)

Gibson, L.J. and Ashby, M.F. (1988), <u>Cellular Solids, Structure and Properties</u>, Pergamon Press, New York

Gibson, L.J., Ashby, M.F. and Easterling, K. E., (1988), "Structure and mechanics of the iris leaf", <u>J. Mat. Sci.</u>, Vol. 23, pp 3041-3048

Gordon, J. E., (1988), <u>The Science of Structures and Materials</u>, Scientific American Library, New York

Gosline, J.M., Demont, M.E. and Denny, M.W., (1986), "The structure and properties of spider silk", <u>Endeavor</u>, Vol. 10, pp 37-43

Gunderson, S.L., Gunnison, K.E. and Sawvel, J.W., (1992) "Hierarchical structure of a natural composite", <u>Mat. Res. Soc. Symp. Proc.</u>, Vol. 255, pp 159-169

Gunnison, K.E., Sarikaya, M., Liu, J. and Aksay, I.A., (1992), "Structure-mechanical property relationships in a biological ceramic-polymer compostie nacre", <u>Mat. Res. Soc. Symp. Proc.</u>, Vol. 255, pp 171-183

Jackson, A.P. and Vincent J.F.V., (1992), "Comparison of nacre with other ceramic composites", <u>J. Mat. Sci.</u>, Vol. 25, pp 3173-3178

Mai, Y.W. and Atkins, A.G., (1989), "Further comments on J-shaped stress-strain curves and the crack resistance of biological materials", <u>J. Phys. D.: Appl. Phys.</u>, Vol. 22, pp 48-54

Mark, R.E., (1967), <u>Cell Wall Mechanics of Tracheids</u>, Princeton University Press

Niklas, K.J., (1989), "Mechanical behavior of plant tissues as inferred from the theory of pressurized cellular solids", <u>Amer. J. Bot.</u>, Vol. 76 (6), pp 929-937

Niklas, K.J., (1991a), "Bending stiffness of cylindrical plant organs with a 'core-rind' construction: evidence from juncus effusus leaves", <u>Amer. J. Bot.</u>, Vol. 78 (4), pp 561-568

Niklas, K.J., (1991b), "The elastic moduli and mechanics of populus tremoloides (salicaceae) petioles in bending and torsion", Amer. J. Bot., Vol. 78 (7), pp 989-996

Niklas, K.J., (1992), Plant Biomechanics: An Engineering Approach to Plant Form and Function, University of Chicago Press

Niklas, K.J. and O'Rourke, T.D., (1987), "Flexural rigidity of chive and its response to water potential", Amer. J. Bot., Vol. 74 (7), pp 1033-1044

Purslow, P.P. and Vincent, J.F.V., (1978), "Mechanical properties of primary feathers from the pigeon", J. Exp. Biol., Vol. 72, pp 251-260

Rich, P.M., (1987), "Mechanical structure of the stems of arborescent palms", Bot. Gaz., Vol. 148 (1), pp 42-50

Timoshenko, S.P., (1953), History of Strength of Materials, Dover Publications Inc., New York

Thompson, D'Arcy W., (1961), On Growth and From, edited by Bonner, J.T., Cambridge Universtity Press

Tomlinson, P.B., (1990), The structural biology of palms, Calrendon Press Oxford, Oxford University Press, New York

Vincent, J.F.V., (1982), "The mechanical design of grass", J. Mat. Sci., Vol. 17, pp 856-860

Vincent, J.F.V., (1990a), Structural Biomaterials rev. ed., Princeton University Press, Princeton, New Jersey

Vincent, J.F.V., (1990b), "The design of natural materials and structures", J. Intell. Mater. Syst. and Struct., Vol. 1, pp 141-146

Vincent, J.F.V. and Owers, P., (1986), "Mechanical design of hedgehog spines and porcupine quills", J. Zool. Lond., Vol. A210, pp 55-75

Vincent, J.F.V. and Srinivasan, A.V., (1992), "Introductory statement", Biomimetics, Vol. 1(1), pp 1-3

Vollrath, F., (1992), "Spider webs and silks", Sci. Am., March 1992, pp 70-76

Figure 1.1 Natural structures: (a) micrograph of seagull feather shaft section.
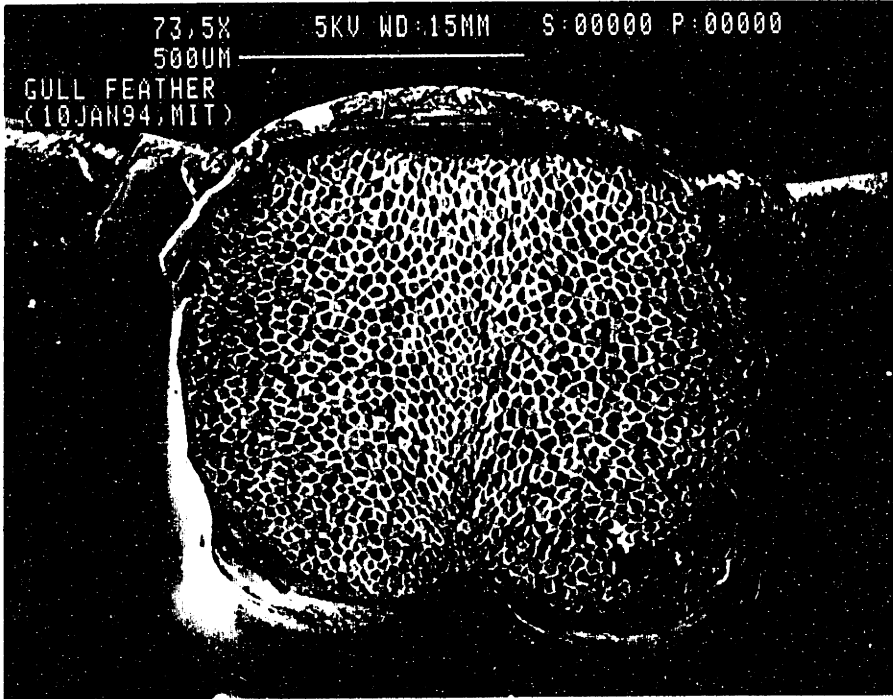
Figure 1.1 Natural structures: (b) cuttlefish bone section .

Transverse section through the cuttlebone



dorsal shield

lamellae

250 microns

pillars supporting lamellae
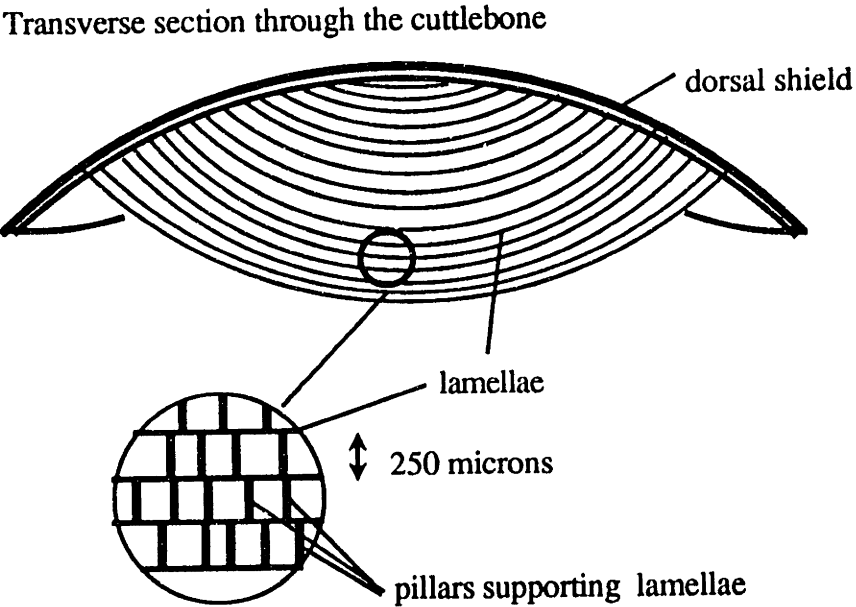
Figure 1.1 Natural structures: (c) double-hulled tanker design.
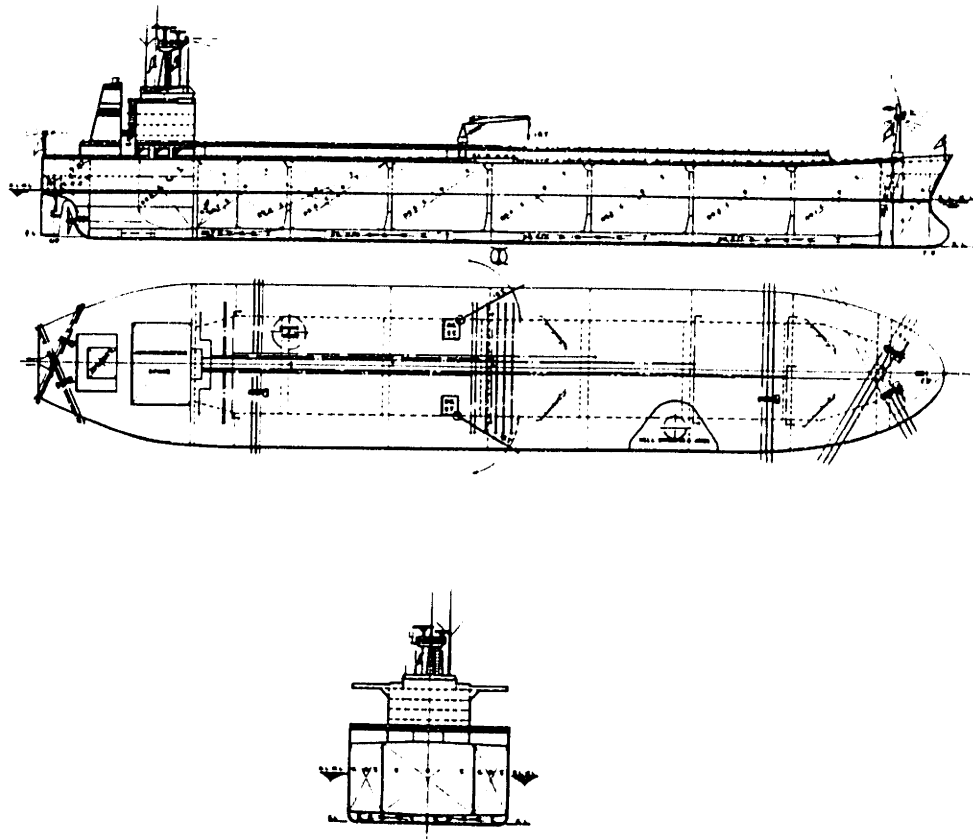
Figure 1.2 Cross sections of natural cylindrical shells with foam cores:
(a) grass (*Elytrigia repens* ) (b) North American porcupine (*Erethizon*)
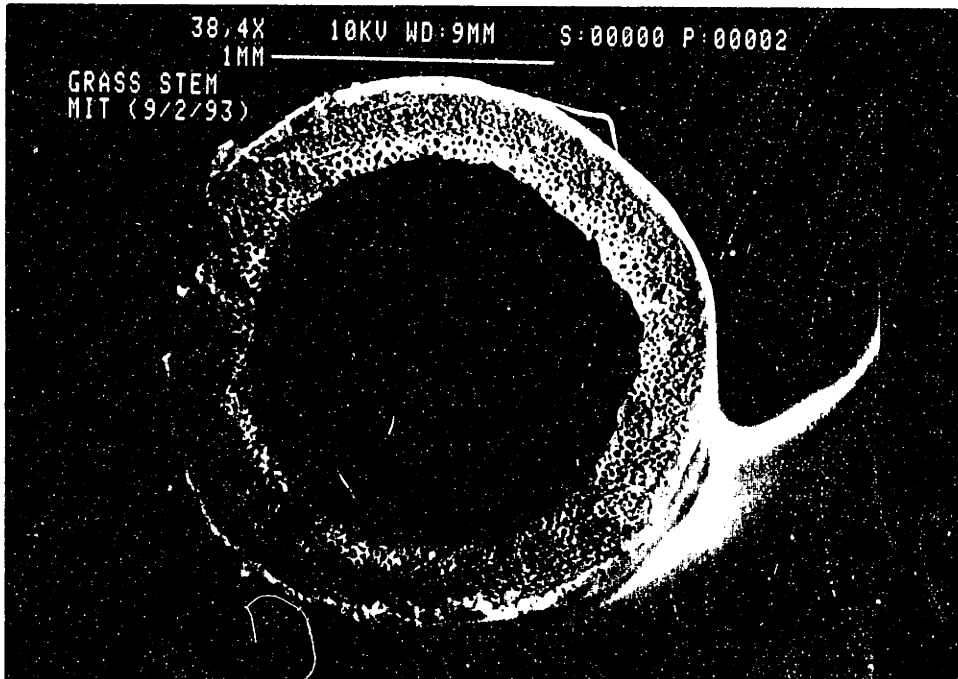


(a)
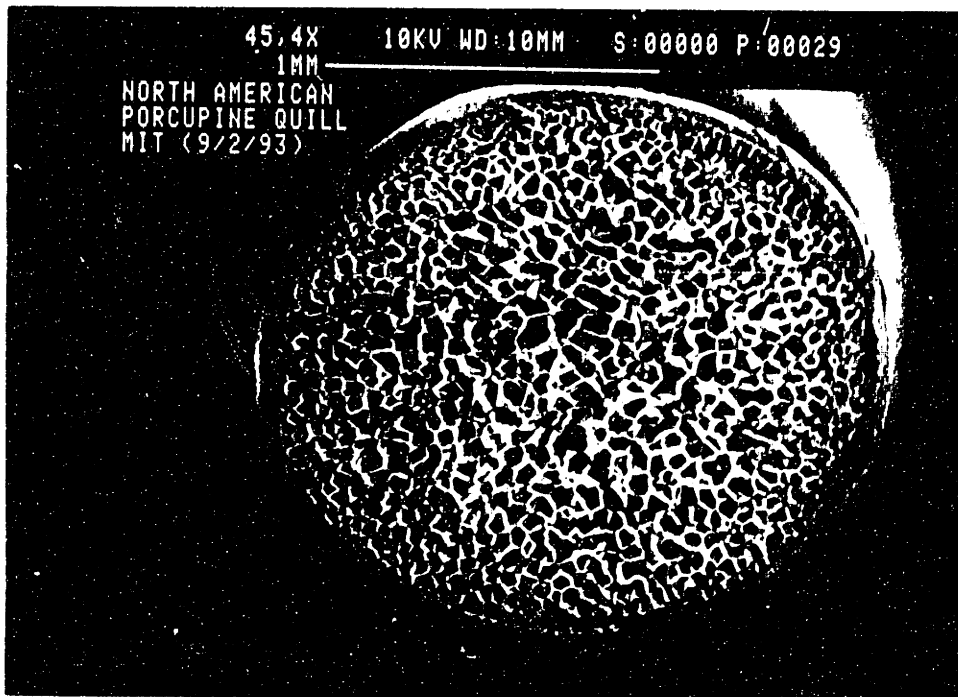


(b)

Figure 1.2 Cross sections of natural cylindrical shells with foam cores:
(c) crested porcupine (*Hystrix*) (d) hedgehog (*Erinaceus*)



(c)



(d)

27
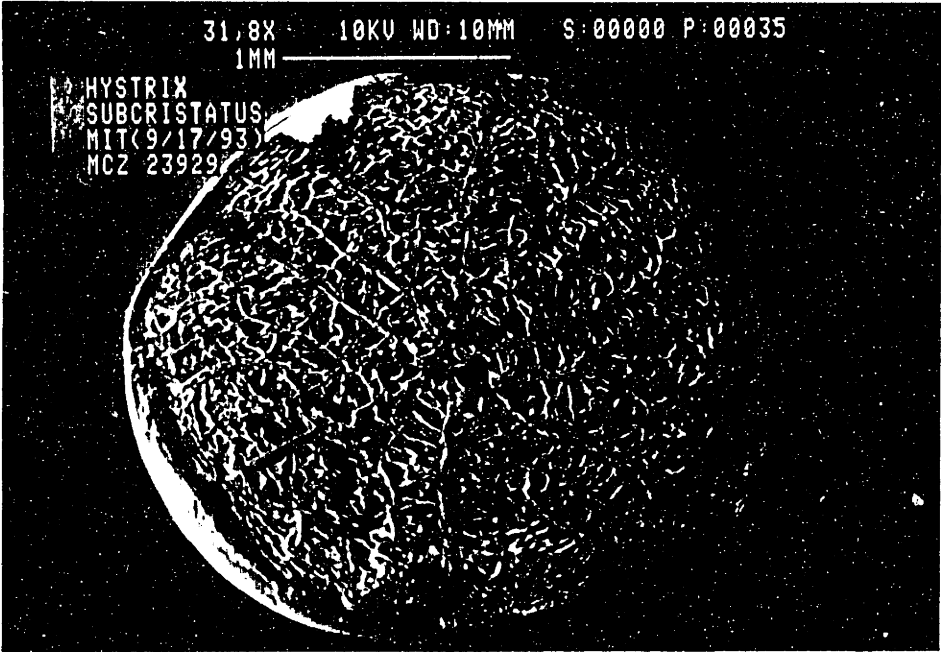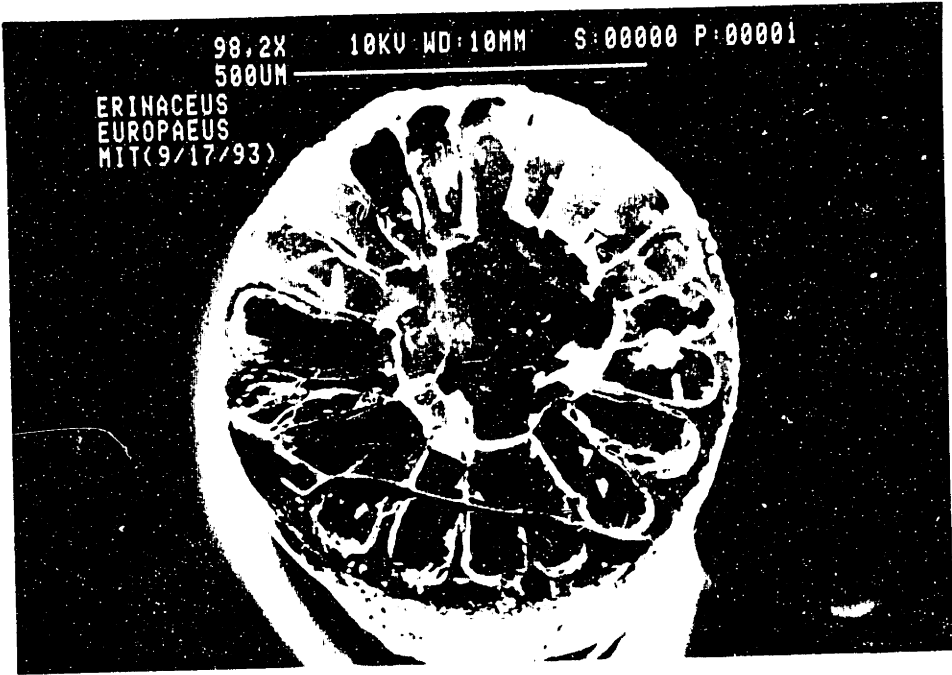
Figure 1.3 Radius to thickness ratio, a/t, for natural and engineering cylindrical shells.



Radius to thickness ratio, a/t (-)
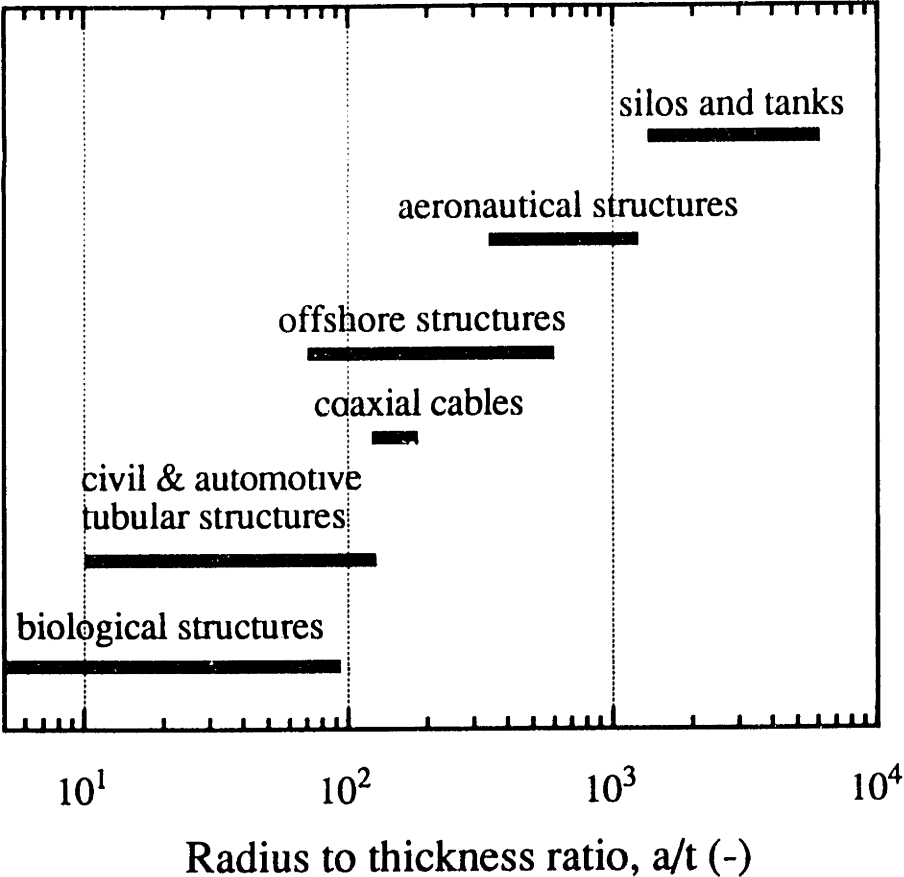
## LITERATURE REVIEW

*"Mechanics is the paradise of mathematical science because here we come to the fruits of mathematics."*

Leonardo da Vinci (ca. 1500)

Bringing his work on the calculus of variations to bear on the problem of the buckling of a uniform column under axial compression, Leonard Euler (1744) solved the first elastic stability problem by deriving the critical buckling load now known by his name. He, and many other investigators, later expanded his treatment of the strength of columns. But it wasn't until the end of the nineteenth century and the beginning of the twentieth, as more ambitious bridges were built, larger metallic ships and submarines were ordered by navies, and the first airplanes were constructed that the practical importance of the elastic stability of structures was revealed (Timoshenko, 1953). The stability of columns and beams, flat plates, curved panels, cylindrical and spherical shells has since received extensive treatment.

### 2.1 Elastic stability of cylindrical shells

So much has been written about the buckling of cylindricals shells that it is foolhardy to attempt a full review save to mention a few key contributions. In a recent review Arbocz (1981) has counted no less than sixteen hundred references treating shell buckling. The elastic stability of circular cylindrical shells has been analyzed under axial compression, bending, torsion, internal and external pressure and the combined effects of these loads. Shells reinforced with longitudinal and/or circumferential stiffeners have

also received wide attention. A good summary and state of the art can be found in the works of Timosenko and Gere (1961), Yamaki (1984), Kollár and Dulácska (1984), Calladine (1983), Kenny (1984) and Harding (1992) which are dedicated to the topic. The cases of elastic buckling under axial compression and bending are presented below.

## 2.1.1 Elastic stability under axial compression

The classical theory for the case of axial compression buckling was developed by Lorenz (1908, 1911), Southwell (1914) and Timoshenko (1910, 1914). Using the assumptions of small-deflection, linear bending shell theory, the critical elastic buckling stress $\sigma_0$ of a long cylinder was found to be:

$$\sigma_0 = \frac{Et}{a\sqrt{3\left(1 - v^2\right)}} \qquad (2.1)$$

where E is the modulus of elasticity of the shell, n is Poisson's ratio, and a and t are the radius and wall thickness respectively. This result is obtained whether a sinusoidal axisymmetric or a non-axisymmetric buckling mode is assumed (Timoshenko and Gere, 1961). The buckling wavelength in the longitudinal direction is given by :

$$\frac{L}{m} = \frac{\pi}{\sqrt[4]{12\left(1 - v^2\right)}}\sqrt{at} \qquad (2.2)$$

where L is the length of the cylinder and m the number of half buckling wavelengths. The number of circumferential buckles is dependent on the boundary conditions and the length of the cylinder; it was later derived by de Neufville and Connor (1968).

The experimental work of Robertson (1928), Lundquist (1933), Wilson and Newmark (1933), and Donnell (1934) gave data that were 1/5 to 1/3 of the theoretical

values, prompting an important research effort to resolve this situation. To add to the confusion these tests were performed on metallic specimens without clear distinction between elastic, plastic and elasto-plastic buckling (de Neufville, 1965). Large-deflection theories with non-linear bending were proposed to analyze buckling and postbuckling behavior (Flügge, 1932 and Donnell, 1934). But it wasn't until the work of von Kármán and Tsien (1941) that an approximate large deflection shell theory, the so-called Donnell-von Kármán equations, emerged with an analysis that proved the existence of stable postbuckled configurations that can be maintained at much lower loads than the critical one. It was then postulated that initial geometric imperfections, dynamic vibrations or any perturbation in the energy state of a compressed shell would cause it to jump prematurely into a buckled mode. Tsien (1942) provided a theoretical foundation to this line of argument by showing that bifurcation actually takes place at the energy level causing the sudden jump from one configuration to another. Donnell and Wan (1950) studied the effect of initial geometric imperfections in the shape of the buckling mode. Their results showed that two types of buckling failure could occur in elasto-plastic materials: a purely elastic one with a reduced buckling load or one in which buckling is precipitated by local yielding due to large deformations. The minimum postbuckling load in the case of elastic material behavior is dependent on the buckling mode and the boundary conditions. For cylinders which are longer than their radius, end effects can be neglected. Batdorf (1947) found the effect of length on the buckling mode of a shell to be a function of a dimensionless number, Batdorf's parameter Z:

$$Z = \left(\frac{L}{a}\right)^2 \left(\frac{a}{t}\right)\sqrt{1-v^2} \qquad (2.3)$$

For $Z < 2.85$, the cylindrical shell buckles in axisymmetric mode only, while for $2.85 \leq Z < 8.314\sqrt{1-v^2}\left(\frac{a}{t}\right)^2$ the cylinder buckles in a chessboard/diamond pattern, and for $Z \geq 8.314\sqrt{1-v^2}\left(\frac{a}{t}\right)^2$ Euler column buckling occurs. For metallic materials with elasto-plastic behavior, elastic buckling can only occur at large enough radius to thickness

31

ratios, $\left(\frac{a}{t}\right)$, such as to have buckling before yielding. For steel this limiting condition was found to be $\left(\frac{a}{t}\right) \geq 300$ (Timoshenko and Gere, 1961; de Neufville, 1965).

As powerful computing machines became available, the analysis of von Kármán and Tsien (1941) was refined and more complicated buckling patterns were investigated, yielding lower and lower postbuckling loads (Leggett and Jones, 1942, Michielsen, 1948, Kempner, 1950, Almroth, 1963). Hoff and co-workers investigated the effect of edge conditions on the buckling of thin cylinders. They also showed that, when the buckling displacement is represented by a Fourier series with a number of terms tending to infinity, the absolute minimum postbuckling load for long cylindrical shells, where end conditions can be neglected, is actually zero (Hoff et al., 1966). At the limit, the buckling pattern tends towards the Yoshimura displacement pattern (Yoshimura, 1955), involving infinitesimal displacements as the number of circumferential buckling waves tends to infinity.

In his doctoral thesis Koiter (1945) developed a non-linear theory of elastic stability which he applied to the buckling of a cylindrical shell in axial compression. He showed that the buckling load was extremely sensitive to initial deviations from the exact cylindrical geometry. Assuming an imperfection in the form of the axisymmetric buckling mode he derived an upper bound for the reduced buckling load based on his general theory (Koiter, 1962):

$$\frac{P^*}{P_{cr}}|\mu| = \frac{2}{3\sqrt{3(1-v^2)}}\left(1 - \frac{P^*}{P_{cr}}\right)^2 \qquad (2.4)$$

where $P^*$ and $P_{cr}$ are the reduced and the critical buckling loads respectively, and m is the ratio of the amplitude of the imperfection to the wall thickness of the shell. Hutchinson (1965a and b) refined Koiter's results and extended them to include the effects of internal and external pressure. Assuming axisymmetric and asymmetric imperfections in the shape of the buckling modes, he found the reductions in the buckling

load to be more important than those predicted by Koiter. He also showed that the most critical type of imperfection was the one in the form of the axisymmetric buckling mode. Further refinements to Koiter's theory were introduced and the exact numerical solutions verified by experiments on specially manufactured plastic cylindrical models with sinusoidal, localized or random axisymmetric imperfections (Tennyson and Muggeridge, 1969, Hutchinson et al., 1971, Amazigo and Budiansky, 1972).

As the theoretical work described in the previous paragraphs proceeded, a large number of experimental investigations were carried out to solve the practical side of the problem and recommend design procedures to the booming defense and aerospace industries. The main results are summarized in a the contributions by Donnell and Wan (1950), Weingarten et al. (1965), Budiansky (1976), Kollár and Dulácska (1984) and Yamaki (1984). When experimental cylindrical specimens were manufactured with conventional techniques, such as used in engineering structures, experimental buckling loads were always found to fall below the theoretical predictions and to decrease with increasing radius to thickness ratios. This was explained by the inherent geometric imperfections that are bound to occur in any cylindrical structure in light of the postbuckling and imperfection sensitivity analyses that were developed. This interpretation was further supported by experiments on special near-perfect laboratory-prepared specimens that yielded buckling loads within 10% of the classical theory (Tennyson, 1963, 1964, 1967 and Kollár and Dulácska, 1984). For engineering design purposes Weingarten et al. (1965) proposed an empirically fitted lower bound to the elastic axial buckling stress of metallic cylinders, $\sigma_{lower}$, with $\nu = 0.3$:

$$\sigma_{lower} = \left(0.606 - 0.546\left(1 - \exp\left(-\tfrac{1}{16}\sqrt{a/t}\right)\right)\right)\exp\left(-\tfrac{1}{16}\sqrt{a/t}\right)\frac{Et}{a} \qquad (2.5)$$

Note that Eq. 2.5 tends to Eq. 2.1 as $\left(\frac{a}{t}\right)$ tends to zero. Similar formulas for knock down factors can be found in design codes for cylindrical structures (Kenny, 1984).

In engineering practice cylindrical shells are stiffened with longitudinal stringers or circumferential rings or both. The use of massive stiffeners, as in naval construction, offshore oil platforms and airframes, subdivides the shell into curved panels that are less sensitive to defects and achieve higher buckling loads (von Kárman et al., 1940, Timoshenko and Gere, 1961, and Kenney 1984). Closely spaced stiffeners, whether placed longitudinally, circumferentially or orthogonally are the most common (Kollár and Dulácska, 1984). The close spacing of the stiffeners insures that they buckle integrally with the skin. One or two way ribbed cylindrical shells exhibit the same types of buckling behavior as isotropic shells with the difference that the stiffeners increase the stretching and bending stiffnesses in the direction along which they are placed. They can be analyzed as orthotropic shells and their buckling loads obtained accordingly. The differential equations of this problem were established by Flügge (1932), and tackled first by Dschou (1935). Van der Neut (1947) analyzed the eccentric stiffening effect due to external and internal stiffening, finding external stiffeners more efficient than internal ones. Given the large number of geometric variables and stiffness constants involved in the formulation of the stiffened shell problem, a stiffening geometry has to be assumed to allow a numerical evaluation of the axial compression buckling load (Kollár and Dulácska, 1984). This, combined with the complications that plagued the investigation of the stability of unstiffened shells, has rendered the task of investigators even more formidable. In a manner similar to that for unstiffened shells the postbuckling behavior and minimum load of orthotropic cylinders was investigated by Almroth (1964). Postbuckling and imperfection sensitivity analysis of stiffened cylindrical shells were also performed along the lines of Koiter's theory of elastic stability (Hutchinson and Amazigo, 1967, Hutchinson and Frauenthal, 1969, and Byskov and Hutchinson, 1977).

More recently Ellinas and co-workers revisited the problem in depth. Previous contributions were reviewed and a new method to determine minimum postbuckling loads of stringer and ring stiffened cylinders was proposed based on the assumption that the components of energy that are eroded from the classical buckling load in the postbuckling stage can be neglected (Ellinas and Croll, 1981, and Ellinas et al., 1981). Numerical modeling was performed for a few typical stiffening configurations to study the imperfection sensitivity of the stiffened cylinders. In light of this new analysis the results of more than 240 past experiments on axially compressed stringer stiffened cylinders were re-examined (Ellinas et al., 1983); the results suggested that the observed buckling behaviors exhibited a degree of imperfection sensitivity higher than that previously ascribed to them.

Theoretical investigations and experiments on near perfect ribbed shells have shown that ring stiffened cylinders always have a lower buckling load in axial compression than geometrically perfect isotropic equivalent weight cylinders (Calladine 1983 and Tennyson, 1976). Stringer reinforced cylinders can be marginally more efficient (Tennyson, 1976). Ellinas and Croll (1981) and Ellinas et al. (1981) reached the same conclusions after an elaborate analysis; they, however, show that when imperfection sensitivity is taken into account, the improved knock down factors for circumferentially reinforced shells may reverse these conclusions for some stiffening ratios.

With powerful computers and finite element codes (FEM), most recent research has concentrated on refined numerical investigations of the stability of stiffened and unstiffened circular cylindrical shells with realistic imperfections such as those measured in welded silos and tension legs of offshore platforms (for example, the work of Arbocz and Williams, 1977, Rotter and Teng, 1989, Rotter and Zhang, 1990, Teng and Rotter, 1991, Chryssanthopoulos et al., 1991a,b, and Hunt and Neto, 1991).

## 2.1.2 Elastic stability under pure bending

Long cylindrical elastic tubes subjected to a bending moment can theoretically collapse by one of two modes of failure. In the first mode the ovalization of the cross section of the tube causes a non-linear moment-curvature relation, resulting in a maximum moment carrying capacity. The second failure mode is a bifurcation type of instability characterized by local buckling or wrinkling of the compressive side of the bent tube when local compressive stresses reach a critical value. Local buckling occurs before the limit moment of the first mode is reached.

In a unique contribution, Brazier (1927) was the first to succeed in determining the limit moment for an infinitely long cylindrical shell under pure bending. Assuming an inextensional flattening of the section in the shape of an ellipse, he derived an expression for the strain energy per unit length in terms of the change in axial curvature. Minimizing this expression with respect to the change in curvature he obtained the limit moment $M_{Brazier}$, as :

$$M_{Brazier} = \frac{2\sqrt{2}\pi Eat^2}{9\sqrt{1-v^2}} = \frac{0.987Eat^2}{\sqrt{1-v^2}} \qquad (2.6)$$

Reissner (1962) derived a more general formulation of this problem dealing with thin walled cylindrical tubes of arbitrary cross section subjected to pure biaxial bending moments, and with it, calculated the state of stresses in the ovalized circular bent tube (Reissner and Weinitschke, 1963).

The local buckling of thin cylindrical tubes under pure bending was first investigated by Flügge (1932) whose preliminary calculations showed the critical compressive stress to be about 30% higher than that for an axially compressed cylindrical shell. For thirty years Flügge's result was adopted by the engineering mechanics

36

community (Timoshenko, 1953 and Timoshenko and Gere, 1961). Seide and Weingarten (1961) dispelled that misconception showing that the critical bending stress is, for all purposes, equal to the critical compressive stress. Weingarten (1962) investigated the effect of internal pressure on the buckling of bent circular cylindrical shells showing that, unlike the case of pressurized cylinders under compression, the critical bending stress increases with internal pressure. Similar to the case of axially compressed cylinders, experimental results on cylinder under bending fell short of the theoretical predictions and semi-empirical design procedures were proposed (Suer et al., 1958).

If a shell is considered to be short, then the prebuckling ovalization can be ignored and the analysis of Seide and Weingarten (1961) is appropriate. For a bent intermediate length shell the supports will hold the ends of the tube circular and hamper ovalization to some extent. An infinitely long tube will ovalize unhampered under pure bending until bifurcation takes place. The effects of length were first studied theoretically by Akselrad (1965). Stephens et al. (1975) investigated numerically the effect of length for four different specific geometries of thin walled circular tubes. Calladine (1983) re-analyzed the problem in terms of the geometric parameter $\Omega$:

$$\Omega = \left(\frac{L}{a}\right)\left(\frac{t}{a\sqrt{(1-v^2)}}\right)^{1/2} \qquad (2.7)$$

For $\Omega < 0.5$ there is little ovalization and local buckling occurs as described by Seide and Weingarten (1961); for $0.5 \leq \Omega \leq 2.0$ the end conditions affect the ovalization behavior; and for $\Omega > 2.0$ the behavior of the tube corresponds essentially to that of an infinite cylinder under pure bending. The interaction of ovalization with the bifurcation behavior was analyzed by Fabian (1977) who showed that elastic bifurcation occurs prior to reaching the limit state. Reddy and Calladine (1978) obtained an approximate closed form solution for the buckling stress, the buckling mode and the critical load combinations between bending moment and internal pressure. They found the maximum

compressive stress at bifurcation, $\sigma_{max}$, to be slightly larger than the axial compressive stress, $\sigma_0$:

$$\sigma_{max} \cong \sigma_0\left(1 + 0.35\left(\tfrac{t}{a}\right)^{2/3}\right) \qquad (2.8)$$

Further refinements to the analysis of the problem were contributed by Gellin (1982) who found more conservative bifurcation load estimates than those previously obtained.

Taking account of the ovalization under bending of a long tube as estimated by Brazier (1927), and using the critical axial compressive stress as a buckling criterion, Calladine (1983) calculated the local buckling moment, $M_{lb}$, as:

$$M_{lb} = \frac{0.939 E a t^2}{\sqrt{1 - v^2}} \qquad (2.9)$$

Comparing with Eq. 2.6, the moment required for local buckling is always slightly lower than the Brazier moment.

Very little experimental work was performed on the elastic ovalization of thin walled cylinders under pure bending save for the original experiments of Brazier (1927) on celluloid tubes and some unpublished tests on silicone rubber tubes reported by Calladine (1983).

## 2.2 Stability of beams on elastic foundation

The problem of the beam on elastic foundation is doubly relevant to the work presented in this thesis. First, from a mathematical point of view, all axisymmetric stability problems of cylindrical, conical, and spherical shells are amenable to treatment by the bending theory of straight beams on an elastic foundation. Second, the role of a soft elastic core inside a cylindrical shell, as found in natural structures, is that of an elastic supporting medium.

In conjunction with the analysis of railroad tracks, Winkler (1867) introduced the assumption that the reaction forces of the foundation are proportional at every point to the deflection of the beam at that point. This assumption allowed a practical and very popular approximate solution to the soil reaction problem, and a rigorous solution to problems dealing with thin shells and networks of beams. Hetényi (1946) has written an authoritative treatise on the theory of beams on a Winkler-type elastic foundation.

Very seldom, however, does it happen that a foundation acts as a continuously distributed set of independent springs; in fact a foundation is typically an elastic continuum where shear between contiguously loaded columns of material is very important, and the interaction between vertical elements dominates the response. Biot (1937) has provided the solution for an infinite beam resting on an elastic foundation represented as an isotropic continuum defined by its Young's modulus and Poisson's ratio. Reissner (1937) obtained the results of Biot in a more general way, allowing different kinds of foundations ranging from elastic to elastic-plastic.

As early as 1913, Timoshenko derived the buckling stress, $\sigma_{cr}$, of an infinite beam resting on water, or a Winkler foundation, of modulus k, as (Timoshenko and Gere, 1961):

$$\sigma_{cr} = 2\frac{\sqrt{kEI}}{A} \qquad (2.10)$$

where EI is the bending rigidity of the beam and A its cross sectional area. Reissner (1937) made some progress in treating the buckling problem of the beam supported by a two-dimensionally infinite medium. Using the results of Biot (1937), Gough et al. (1940) have analyzed the stability of a thin sheet supported by a continuous elastic medium, under the conditions that the surface of the medium has the same vertical displacements as the beam and that it carries no strain parallel to the direction of the beam axis. They obtained full solutions for the cases of a beam on an elastic half-space, a beam on an elastic foundation of limited depth with free or rigid back, and for a sandwich

configuration. For a perfectly bonded infinitely long sheet on an elastic half space they found the buckling stress, $\sigma_{cr}$, to be:

$$\sigma_{cr} = \left( \frac{3}{2(1+v_c)(3-v_c)} \right)^{2/3} \left( E_c^2 E \right)^{1/3} \qquad (2.11)$$

where $E_c$, and $v_c$ are the Young's modulus and the Poisson's ratio of the foundation, and E is the Young's modulus of the sheet or beam. The assumed buckling mode was sinusoidal and its wavelength dependent on the relative properties of the beam and foundation. The half buckling wavelength, $l'$, was found to be:

$$\frac{l'}{\pi t} = \left[ \frac{(3-v_c)(1+v_c)}{12} \right]^{1/3} \left[ \frac{E}{E_c} \right]^{1/3} \qquad (2.12)$$

where t is the thickness of the beam.

Very recently, in the context of investigating fiber microbuckling in unidirectional fiber composites, Waas et al. (1990) have revisited the two-dimensional problem of the beam on an infinite elastic foundation. Their generalized analysis allowed for a complete description of the beam-foundation interface, and included boundary conditions to permit modeling of actual conditions in fiber composites. Their results agreed very closely with those obtained previously by Gough et al. (1940) for the infinite beam problem.

## 2.3 Stability of circular cylindrical shells with an elastic core

In the late 1950's, in the context of the cold war and the space program, a major effort in basic research on solid propellant rocket launchers and missiles was undertaken. The rocket motor casing is a circular cylindrical shell that contains rubbery or plastic-like solid propellant mix. This solid propellant core may or may not contain a central bore hole to control the burning of the propellant (Sutton, 1986). This spurred numerous

investigations of the elastic buckling of a thin, isotropic cylindrical shell filled with a compliant elastic core. A variety of loading configurations have been analyzed, including: axial load (Seide, 1962, Yao, 1962, Lu and Nash, 1964, Myint-U, 1966, Vlasov, 1973); torsion (Weingarten, 1962); uniform radial pressure (Seide and Weingarten, 1962, Seide, 1962, Herrmann and Forrestal, 1965, Vlasov, 1973); circumferential band of pressure (Yao, 1965); axial load plus uniform radial pressure (Seide, 1962; Brush and Almroth, 1962, Vlasov, 1973); axial load plus axially varying radial pressure (Brush and Almroth, 1962) ; axial load with axially varying thermal stresses (Zak and Bollard, 1962); axial load plus circumferential band of pressure (Brush and Almroth, 1962); and bending (Yabuta, 1980). More recently, the analysis has been extended to orthotropic cylindrical shells (Holston, 1967; Bert, 1971; Vlasov, 1975; and Malyutin et al., 1980) and to an elastic-plastic core (Babich and Cherevko, 1983). The literature on the stability of an isotropic circular cylindrical shell under axial load and bending is reviewed in more detail below.

Seide (1962) and Yao (1962) have analyzed the buckling under axial compression of cylindrical shells with a soft elastic core. Using Batdorf's (1947) modification to Donnell's shell equations Seide (1962) treated the cases of axial compression and lateral pressure. He considered the role of the core to be that of a spring that counteracts the normal displacements of the shell. He neglected the shearing stresses between the core and the cylinder and assumed the core to be stress free in the longitudinal direction in the pre-buckling stage. He derived the spring constant of the core, with and without a central bore hole, by treating it as a three dimensional solid and applying to its surface the assumed buckling mode of the shell. Using Timoshenko's differential equations for a cylindrical solid (Timoshenko and Goodier, 1970) he found the exact solution to the state of stresses in terms of modified Bessel functions. For any given geometry and assumed buckling mode the spring constant of the core can be found and the axial load calculated. Seide's calculations showed that the axisymmetric buckling mode yields lower

compressive buckling stresses, in agreement with experimental observations. By minimizing the compressive stress in the shell with respect to the axisymmetric buckling wavelength, the critical compressive stress and the buckling wavelength are determined. As expected, the buckling wavelength decreases, and the buckling load increases, with increasing core stiffness. He also found that for a filled core, the solution for the uniaxial, axisymmetric buckling stress, $\sigma_{cr}$, can be approximated by:

$$\frac{\sigma_{cr}}{\sigma_o} = 1 + \phi \qquad (2.13)$$

for $\phi < 0.5$ and by:

$$\sigma_{cr} = \frac{1}{4}\left[9\left(\frac{E_c}{\left(1-v_c^2\right)}\right)^2 \frac{E}{\left(1-v^2\right)}\right]^{1/3} \qquad (2.14)$$

for $\phi > 3$, where:

$$\phi = \frac{\left[12\left(1-v^2\right)\right]^{1/4}}{4\left(1-v_c^2\right)}\left[\frac{E_c}{E}\right]\left[\frac{a}{t}\right]^{2/3} \qquad (2.15)$$

and $E_c$ and $v_c$ are the Young's modulus and Poisson's ratio for the elastic core. The solution for $\phi > 3$ (Eq. 2.14) is similar to that for wrinkling of a beam on an elastic foundation (Eq. 2.11).

Yao (1962) obtained a theoretical solution to the buckling load of axially compressed cylindrical shells by a different method. His working assumptions were: a solid core with or without a bore hole, a core modulus much lower than the shell modulus, all compressive forces are taken by the shell prior to buckling, and there is no relative movement between the shell and the core prior to buckling. He derived the state of stresses in the three-dimensional core by using stress functions and the three function theorem. Matching the displacements of the boundary of the core to those of the mid-section of the shell he obtained a system of non-linear equations that can be solved

numerically for the compressive stress given an assumed buckling mode. The buckling load was numerically evaluated for $v=0.3$, $v_c=0.45$, a/t ranging from 50 to 1000, and $E_c/E$ ranging from 2.9 to $12\times10^{-5}$. Yao found that for the number of circumferential buckling waves varying from 0 (axisymmetric mode) to 8 the critical compressive stress converged to essentially the same value. Yao's derivation included the shear stresses between the core and the shell, but for the numerical range investigated his numerical results were practically the same as Seide's. The final results of both methods (Seide, 1962 and Yao, 1962) were found to be consistent with finite element calculations (Weingarten and Wang, 1976)

Lu and Nash (1964), numerically analyzed the buckling of cylindrical shells stiffened by a core under axial compresion and bending, assuming a buckling mode similar to those observed in experiments and a Winkler-foundation for the core effect. Using a Galerkin procedure with a finite-deformation formulation for the shell they showed that for an even moderately rigid foundation the increases in buckling strength of the shell are significant.

Myint-U (1966) modeled the core as a Pasternak or a two parameter foundation with k being the Winkler foundation modulus and g the shear layer constant. Using Donnell's (1934) shell equations and the buckling modes assumed by von Kármán and Tsien (1941) he found the critical compressive stress of the axially loaded shell to be:

$$\sigma_{cr} = \sigma_o\left(\sqrt{\left(1+\frac{ka^2}{Et}\right)} + \sqrt{3\left(1-v^2\right)}\frac{g}{t}\right) \qquad (2.16)$$

where $\sigma_o$ is the buckling load of the empty shell (Eq. 2.1). The result for a Winkler foundation can be obtained by putting g=0. Myint-U neglected the effect of the core on the buckling wavelength of the shell and hence his results give a lower bound estimate of the real critical buckling stress.

43

Vlasov (1973), numerically solved the three-dimensional linearized equations of elastic stability for a/t ratios varying from 100 to 600 and $E_c/E$ from $10^{-9}$ to $10^{-3}$, with the Poisson ratios of the shell and core equal to 0.3. He carried out his analysis for two cases: axisymmetric buckling and nonaxisymmetric buckling with both longitudinal and circumferential buckles. His results showed that nonaxisymmetric buckling appeared only at $E_c/E < 10^{-5}$, and that the buckling load calculated for either buckling modes were equal.

Data for the uniaxial elastic buckling stress of cylinders with a compliant core lie significantly below Seide's (1962) estimates, although the discrepancy decreased with increasing $\phi$ (Eq. 2.15) (Kachman, 1959; Fitzgibbon, 1960; and Goree and Nash, 1962). These experimental investigations concentrated on metallic shells ($v=0.3$) with a rubber core ($v_c=0.5$) having a/t between 250 and 700, and $E_c/E$ between $10^{-6}$ and $10^{-4}$. Similar to the postbuckling analyses carried out for empty shells (von-Kárman and Tsien, 1941, Kempner, 1954 and Almroth, 1963), a lower bound given by the minimum postbuckling load was calculated by Almroth and Brush (1963). Observations of the buckling mode indicated that there was a transition between the classical diamond pattern for the empty cylinders to a circumferentially elongated diamond pattern in cylinders with a very low modulus core ($E_c/E = 3 \times 10^{-5}$, Kachman, 1959) to, finally, the axisymmetric mode in cylinders with a stiffer core ($E_c/E = 10^{-4}$, Kachman, 1959). More recently Malyutin et al. (1980) have reported results on fiberglass cylinders with rubber cores having a/t betweem 90 and 160 with $E_c/E$ between $10^{-4}$ and $10^{-3}$. Their results were in closer agreement with the theoretical predictions due to the larger stiffening effect.

Local buckling arising from pure bending has been analyzed by extending Seide's work and neglecting any ovalization of the cross-section (Yabuta, 1980) to model the bending behavior of submarine coaxial cables whose outer conductor is a thin cylindrical

shell with an inner dielectric elastic core and an outer rubber sheath. The relationships between the local buckling stress and $E_c/E$ and $a/t$ are plotted for a limited set of values. Bend tests were performed on four Mylar cylinders ($a/t=100$), two of which were empty and two of which were filled with silicone rubber ($E_c/E=10^{-3}$). The empty and filled cylinders buckled at roughly 60% and 80% of the calculated load in a trend similar to that reported for the uniaxial load case.

The goal of this thesis is to compare the buckling resistance of cylindrical shells of equal mass with and without a compliant core for uniaxial compression, pure bending and combined compression and bending. The axial buckling loads obtained by Seide (1962), Yao (1962) and Vlasov (1973) for a three-dimensional treatment of the core are complicated and require the simultaneous solution of a system of six non-linear equations by numerical methods. The one-dimensional analysis of Lu and Nash (1964) and Myint-U (1966) treated the core as a Winkler or a two parameter foundation, and can at best give a lower bound estimate of the buckling load. The stability in bending has received a very limited treatment (Yabuta, 1980). In the following chapter, the elastic buckling of a thin, isotropic cylindrical shell with a compliant elastic core is re-analyzed to develop a two-dimensional, more tractable analysis for axisymmetric buckling in uniaxial compression and a new analytical model is derived for the ovalization, Brazier moment and local buckling moment in pure bending.

## References

Akselrad, E.L., (1965), "Refinement of the upper critical loading of pipe bending, taking into account the geometrical non-linearity ", Izv. Akad. Nauk. USSR. Otdelenie Teknicheskikh Nauk. Mech., Vol. 4, pp 123-139

Almroth, B.O., (1963), "Postbuckling behavior of axially compressed circular cylinders", AIAA J., Vol. 1, pp 630-633

Almroth, B.O., (1964), "Postbuckling behavior of orthotropic cylinders under axial compression", AIAA J., Vol. 2, pp 1795-1799

Almroth, B.O. and Brush, D.O. (1963), "Postbuckling behaviour of pressure- or core-stabilized cylinders under axial compression", AIAA J., Vol. 1, pp 2338-2341

Amazigo, J.C. and Budiansky, B., (1972), "Asymptotic formulas for the buckling stresses of axially compressed cylinders with localized or random axisymmetric imperfections", J. Appl. Mech., Vol. 39, pp 179-184

Arbocz, J., (1981), Past, Present and Future of Shell Stability Analysis, Delft Universtity of Technology, Dept. of Aerospace Eng., Rept. LR-320

Arbocz, J. and Williams, J.G., (1977), "Imperfection surveys on a 10-ft-diameter shell structure", AIAA J., Vol. 15, pp 949-956

Babich, I.Y. and Cherevko, M.A. (1984),"Stability of cylindrical shells with an elastic-plastic filler under axial compression", Prikladnaya Mekhanika, Vol. 20, pp 60-64

Batdorf, S.B., (1947), A Simplified Method of Elastic Stability Analysis for Thin Cylindrical Shells, N.A.C.A. Technical Reports No. 874 and 1342

Bert, C.W. (1971),"Buckling of axially compressed, core-filled cylinders with transverse shear flexibility" J. Spacecraft, Vol. 8, pp 546-548

Biot, M.A., (1937), "Bending of an infinite beam on an elastic foundation", Trans. ASME, Vol. 59, pp A1-A7, also J. Appl. Mech., Vol. 4, pp 1-8

Brazier, L.G. (1927),"On he flexure of thin cylindrical shells and other thin sections" Proc. Royal Soc. London., Series A, Vol. 116, pp 104-114

Brush, D.O. and Almroth, B.O. (1962),"Buckling of core-stabilized cylinders under axisymmetric external loads", J. of the Aerospace Sciences, Vol. 29, pp 1164-1170

Budiansky, B., (1976), editor, Buckling of Structures, (IUTAM Symposium Cambridge, June 17-21, 1974) Springer-Verlag, New York

Byskov, E. and Hutchinson, J.W., (1977), "Mode interaction in axially stiffened cylindrical shells", AIAA J., Vol. 15, pp 941-948

Calladine, C.R., (1983) Theory of Shell Structures, Cambridge University Press

Chryssanthopoulos, M.K., Baker, M.J. and Dowling, P.J., (1991a), "Statistical analysis of imperfections in stiffened cylinders", J. Struct. Eng. ASCE, Vol. 117, pp 1979-1997

Chryssanthopoulos, M.K., Baker, M.J. and Dowling, P.J., (1991b), "Imperfection modeling for buckling analysis of stiffened cylinders", J. Struct. Eng. ASCE, Vol. 117, pp 1998-2017

Donnell, L.H., (1934), "A new theory for the buckling of thin cylinders under axial compression and bending", Transactions ASME, Vol. 56, pp 795-806

Donnell, L.H. and Wan, C.C., (1950). "Effect of imperfections on buckling of thin cylinders and columns under axial compression", J. Appl. Mech., Vol. 17, pp 73-83

Dschou, D.D., (1935), "Die Druckfestigkeit versteifter zylindrischer Schalen", Luftfahrt-Forschung, Vol. 11, pp 223-234

Ellinas, C.P. and Croll, J.G.A. (1981) "Overall buckling of ring stiffened shells", Proc. Inst. of Civil Engrs, Part 2, Vol. 71, pp 637-661

Ellinas, C.P., Batista, R.C. and Croll, J.G.A. (1981) "Overall buckling of stringer stiffened shells", Proc. Inst. of Civil Engrs, Part 2, Vol. 71, pp 479-512

Ellinas, C.P. and Croll, J.G.A. (1983) "Experimental and theoretical correlations for elastic buckling of axially compressed stringer stiffened cylinders", J. Strain Analysis, Vol. 18, pp 41-67

Euler, Leonard (1744), De Curvis Elasticis, Additamentum I to Methodius Inveniendi...., English translation by Oldfather W.A., Ellis, C.A. and Brown D.M. in Isis, Vol. XX, pp 72-160

Fabian, O., (1977), "Collapse of cylindrical elastic tubes under combined bending, pressure and axial loads", Int. J. Solids Structures, Vol. 13, pp 1257-1270

Fitzgibbon, D.P. (1960), Preliminary results of sub-scale tests on cylinders filled with an elastic core, Space Technology Labs, Inc. GM 60-7520.6-11, 25 April 1960

Flügge, W., (1932), "Die Stabilität der Kreiszylinderschale", Ing. Arch., Vol. 3, pp 463-506

Gellin, S. (1982), "A new class of solutions for buckling of a short cylindrical shell in pure bending", Int. J. Mech. Sci., Vol. 24, pp 691-697

Goree, W.S. and Nash, W.A. (1962), "Elastic stability of circular cylindrical shells stabilized by a soft elastic core", Experimental Mechanics, Vol. 2, pp 142-149

Gough, G.J., Elam, C.F., and de Bruyne, N.A. (1940), "The stabilization of a thin sheet by a continuous supporting medium", Journal of the Royal Aeronautical Society, Vol. 44, pp 12-43

Harding, J.E., (1992), "The behaviour and design of cylindrical shell structures" in Stability Problems of Steel Structures edited by Ivanyi M. and Skaloud, M., Springer-Verlag, New York

Herrmann, G. and Forrestal, M.J. (1965) "Buckling of a long cylindrical shell containing an elastic core", AIAA J.,Vol. 3, pp 1710-1715

Hetényi, M., (1946), <u>Beams on Elastic Foundation</u>, The University of Michigan Press, Ann Arbor, Michigan

Hoff, N.J., Wayne, A.M. and Mayers, J., (1966), "Postbuckling equilibrium of axially compressed circular cylindrical shells", <u>AIAA J.</u>, Vol. 4, pp 126-133

Holston, A. (1967),"Stability of inhomogeneous anisotropic cylindrical shells containing elastic cores" <u>AIAA J.</u>, Vol. 5, pp 1135-1138

Hunt, G.W. and Neto, E.L., (1991), "Localized buckling in long axially loaded cylindrical shells", <u>J. Mech. Phys. Solids</u>, Vol. 39, pp 881-894

Hutchinson, J.W., (1965a), "Axial buckling of pressurized imperfect cylindrical shells", <u>AIAA J.</u>, Vol. 3, pp 1461-1466

Hutchinson, J.W., (1965b), "Buckling of imperfect cylindrical shells under axial compression and external pressure", <u>AIAA J.</u>, Vol. 3 , pp 1968-1970

Hutchinson, J.W. and Amazigo, J.C., (1967),"Imperfection-sensitivity of eccentrically stiffened cylindrical shells", <u>AIAA J.</u>, Vol. 5, pp 392-401

Hutchinson, J.W. and Frauenthal, J.C., (1969), "Elastic post-buckling behaviour of stiffened and barreled cylindrical shells", <u>J. Appl. Mech.</u>, Vol. 36, Series E, pp 784-790

Hutchinson, J.W., Tennyson, R.C. and Muggeridge, D.B., (1971), "Effect of a local axisymmetric imperfection on the buckling behavior of a circular cylindrical shell under axial compression", <u>AIAA J.</u>, Vol. 9 pp 48-52

Kachman, D.R. (1959), <u>Test report on buckling of propellant cylinders under compressive loads</u>, Space Technology Labs, Inc. GM 59-7520.6-24, 30 November

Kármán, Th. von, and Tsien, H.S., (1941), "The buckling of thin cylindrical shells under axial compression", <u>J. Aeronautical Sci.</u>, Vol. 8, pp 303-312

Kármán, Th. von, Dunn, L.J. and Tsien, H.S., (1940), "The influence of curvature on the buckling characteristics of structures", <u>J. Aeronautical Sci.</u>, Vol. 7, pp 276-289

Kempner, J., (1954), "Postbuckling behavior of axially compressed circular cylindrical shells", <u>J. Aeronautical Sci.</u>, Vol. 21, pp 329-342

Kenny, J.P. and Partners (1984) <u>Buckling of Offshore Structures</u>, Granada Pub., London

Koiter, W.T., (1945), <u>On the Stability of Elastic Equilibrium</u>, Ph.D. thesis, Delft, H.J. Paris, Amsterdam, (english translation AFFDL-TR-70-25 Wright Patterson Air Force Base, 1970)

Koiter, W.T., (1963),"Elastic stability and post-buckling behavior", in <u>Proceedings Symposium Non-Linear Problems</u>, ed. Langer, R.E., University of Wisconsin Press, Madison, Wisconsin pp 257-275

Kollár, L. and Dulácska, E. (1984) <u>Buckling of Shells for Engineers</u>, John Wiley and Sons

Leggett, A. and Jones, R.P.N., (1942), The Behaviour of a Cylindrical Shell under Axial Compression when the Buckling Load Has Been Exceeded, RAE Report No. SME 3204 (ARC No. 6135)

Lorenz, R., (1908, 1911), "Achsenssymmetrische Verzerrungen in dünnwandingen Hohlzylinderen", Zeit. Ver. Deut. Ing., Vol. 52, pp 1706-1713 and "Die nicht achnsensymmetrische Knickung dünnwandingen Hohlzylinderen", Phys. Zeit., Vol. 13, pp 241-260

Lu, S.Y. and Nash, W.A., (1964), "Buckling of thin cylindrical shells stiffened by a soft elastic core", Simplified Calculation Methods of Shell Structures, Paduart, A. and Dutron, R. editors, North Holland Publishing Co., Amsterdam, pp 475-481

Lundquist, E.E., (1933), Strength Tests of Thin-Walled Duralumin Cylinders in Compression, N.A.C.A. Technical Report No.473

Malyutin, I.S., Pilipenko, P.B., Georgievskii, V.P. and Smykov, V.I. (1980) "Experimental and theoretical study of the stability in axial compression, of cylindrical shells reinforced with an elastic filler", Prikladnaya Mekhanika, Vol. 16, pp 56-60

Michielsen, H.F., (1948), "The behavior of thin cylindrical shells after buckling under axial compression", J. Aeronautical Sci., Vol. 15, pp 738-744

Myint-U, T. (1966), "Stability of axially compressed core-filled cylinders", AIAA J., Vol. 4, pp 552-553

Neufville, R.L. de, (1965) "Influence of geometry on the number of buckles in cylinders", AIAA J., Vol. 3 (2), pp 364-365

Neufville, R.L. de, and Connor, J.J., (1968), "Postbuckling behavior of thin cylinders", J. Eng. Mech. Div., Proc. ASCE, Vol. 94 EM2, pp 585-603

Neut, A. van der, (1947), General Instability of Stiffened Cylindrical Shells under Axial Compression, National Luchtvaartlaboratorium, Holland, Vol. 13, Report S 314

Reddy, B.D. and Calladine, C.R., (1978),"Classical buckling of a thin-walled tube subjected to bending moment and internal pressure", Int. J. Mech. Sci., Vol. 20, pp 641-650

Reissner, E., (1937), "On the theory of beams resting on a yielding foundation", Proc. Nat. Acad. of Sci., Vol. 23, pp 328-333

Reissner, E., (1961), "On finite pure bending of cylindrical tubes", Österr. Ing. Arch., Vol. 15, pp 165-172

Reissner, E. and Weinitschke, H.J. (1963), "Finite pure bending of circular cylindrical tubes", Quart. Appl. Math., Vol. 20, pp 304-319

Robertson, A., (1928), "The strength of tubular struts", Proc. Roy. Soc. London, Series A, Vol. 121, pp 558-585

Rotter, J.M. and Teng, J.G., (1989), "Elastic stability of cylindrical shells with weld depressions", J. Struct. Eng. ASCE, Vol. 115, pp 1244-1263

Rotter, J.M. and Zhang, Q., (1990), "Elastic buckling of imperfect cylinders containing granular solids", J. Struct. Eng. ASCE, Vol. 116, pp 2253-2271

Seide, P. (1962),"The stability under axial compression and lateral pressure of circular-cylindrical shells with a soft elastic core", J. of the Aerospace Sciences, Vol. 29, pp 851-862

Seide, P. and Weingarten, V.I., (1961), "On the buckling of circular cylindrical shells under pure bending", J. Appl. Mech., Transactions ASME, Vol. 28, pp 112-116

Seide, P. and Weingarten, V.I. (1962),"Buckling of circular rings and long cylinders enclosing an elastic material under uniform external pressure", American Rocket Society J., Vol. 32, pp 680-688

Southwell, R.V., (1914),"On the general theory of elastic stability", Phil. Trans. Roy. Soc. London, Series A, Vol. 213, p 187

Stephens, W.B., Starnes, J.H. and Almroth, B.O., (1975), "Collapse of long cylindrical shells under combined bending and pressure loads", AIAA J., Vol. 13, pp 20-25

Suer, H.S., Harris, L.A., Skene, W.T. and Benjamin, R.J., (1958), "The bending stability of thin-walled unstiffened circular cylinders including the effects of internal pressure", J. Aeronatical Sci., Vol. 25, pp 281-287

Sutton, G.P., (1986), Rocket Propulsion Elements, An Introduction to the Engineering of Rockets, Fifth edition, John Wiley and Sons

Teng, J.G. and Rotter, J.M., (1992), "Buckling of pressurized axisymmetrically imperfect cylinders under axial loads", J. Eng. Mech. ASCE, Vol. 118, pp 229-247

Tennyson, R.C. (1963) " A note on the classical buckling of load of circular cylindrical shells under axial compresion" AIAA Journal, Vol. 1, No. 2, pp 475-476

Tennyson, R.C. (1964) " Buckling of circular cylindrical shells in axial compresion" AIAA Journal, Vol. 2, No. 7, pp 1351-1353

Tennyson, R.C. (1967) " Photoelastic circular cylinders in axial compression", STP 419, American Society for Tes ing and Materials, Philadelphia, PA, USA

Tennyson, R.C. (1976) "The effect of shape imperfections and stiffening on the buckling of circular cylinders", in Buckling of Structures, ed. B. Budiansky, Springer-Verlag, NY

Tennyson, R.C. and Muggeridge, D.B., (1969), "Buckling of axisymmetric imperfect circular cylindrical shell under axial compression", AIAA J., Vol. 7, pp 2127-2131

Timoshenko, S.P., (1910, 1914), "Einige Stabilitätsprobleme der Elastizitätstheorie", Zeit. Math. Phys., Vol. 58, pp 337-385 and Bull. Electrotech. Inst. St. Petersburg, Vol. 11

Timoshenko, S.P., (1953), History of Strength of Materials, Dover Publications Inc., New York

Timoshenko, S.P. and Gere, J.M. (1961) Theory of Elastic Stability, Second edition, McGraw Hill

Timoshenko, S.P. and Goodier, J.N., (1970) Theory of Elasticity, Third edition, McGraw Hill

Tsien, H.S., (1942), "Atheory for the buckling of thin shells", J. Aeronautical Sci., Vol. 9, pp 373-384

Vlasov, V.V. (1973) "Stability of cylindrical shells containing a filler on being subjected to axial compression and external pressure" , Prikladanya Mekhanika (trans. in English), Vol. 9, No.1, pp 117-121.

Vlasov, V.V. (1975) "Stability of composite shells with an elastic core", Mekhanika Polimerov, (trans. in English), No. 3, pp 544-547

Waas, A.M., Babcock, C.D. and Knauss, W.G., (1990), "A mechanical model for elastic fiber microbuckling", J. Appl. Mech., Vol. 57, pp 138-149

Weingarten, V.I., (1962), "Effects of internal pressure on the buckling of circular cylindrical shells under pure bending", J. Aeronautical Sci., Vol. 29, pp 804-807

Weingarten, V.I., (1962), "Stability under torsion of circular cylindrical shells with an elastic core", American Rocket Society J., Vol. 32, pp 637-639

Weingarten, V. I., Morgan, E.J. and Seide, P., (1965) "Elastic stability of thin-walled cylindrical and conical shells under axial compression", AIAA J., Vol. 3, pp 500-505

Weingarten, V.I. and Wang, Y.S. (1976), "Stability of shells attached to elastic core", Journal of the Engineering Mechanics Division, ASCE, Vol. 102, pp 839-849

Wilson, W.N. and Newmark, N.M., (1933), The Strength of Thin Cylindrical Shells, University of Illinois Bulletin No. 255

Winkler, E., (1867), Die Lehre von Elastizität und Festigkeit, Prag, p. 182

Yabuta, T. (1980), "Effects of elastic supports on the buckling of circular cylindrical shells under bending", J. Appl. Mech., Vol. 47, pp 866-870

Yamaki, N. (1984) Elastic stability of circular cylindrical shells, North-Holland Series in Applied Mathematics and Mechanics, Elsevier Science Publishing Co., New York

Yao, J.C. (1962) "Buckling of axially compressed long cylindrical shell with elastic core", J. Appl. Mech., Vol. 29, pp 329-334.

Yao, J.C. (1965) "Bending due to ring loading of a cylindrical shell with an elastic core", J. Appl. Mech., Vol. 32, pp 99-103.

Yoshimura, Y., (1955), On the Mechanism of Buckling of a Circular Cylindrical Shell under Axial Compression, NACA TM 1390

Zak, A.R. and Bollard, R.J.H. (1962), "Elastic buckling of cylindrical thin shells filled with an elastic core", American Rocket Society J., Vol. 32, pp 588-593

## CHAPTER 3

## ELASTIC BUCKLING OF CYLINDRICAL SHELLS WITH ELASTIC CORES I: ANALYSIS

*"For since the fabric of the universe is most perfect, and is the work of a most wise Creator, nothing whatsoever takes place in the universe in which some relation of maximum and minimum does not appear. Wherefore there is absolutely no doubt that every effect in the universe can be explained as satisfactorily from final causes, by the aid of the method of maxima and minima, as it can from the effective causes themselves."*

Leonhard Euler (De Curvis Elasticis, 1744)

### 3.1 Introduction

Thin walled cylindrical shell structures are widespread in nature: examples include plant stems, porcupine quills and hedgehog spines (Fig.1.2). All have an outer shell of almost fully dense material supported by a low density, cellular core: biologists refer to this as a "core-rind" structure (Niklas, 1992). The cellular core can be made up of either foam-like cells (as in the parenchyma in the grass and hawthorne) or of a lattice of struts (as in the hedgehog spine). In nature, all of these structures are loaded in some combination of axial compression and bending: failure is typically by buckling. Natural structures are often optimized; the results of our analysis of the elastic buckling of a thin cylindrical shell supported by an elastic coi ∿, described below, suggests that this structural configuration achieves significant weight saving over a hollow cylinder.

Thin walled cylindrical shells are widespread in engineering, too: examples include civil engineering structures, offshore oil platforms and aircraft fuselages. Ranges of the ratio of cylinder radius to wall thickness, a/t, for a variety of natural and engineering structures is shown in Fig. 1.3. In contrast to natural cylindrical shells which have a uniform, compliant core, engineering structures with large ratios of a/t are typically stiffened against buckling by circumferential and longitudinal members, known as ring

stiffeners and stringers, respectively. Biomimicking of natural cylindrical shell structures may offer the potential to increase the mechanical efficiency of engineering cylindrical shells. As a first step in evaluating this possibility, we have analyzed the elastic buckling of a cylindrical shell with a compliant core and compared its buckling resistance with that of a hollow cylindrical shell of equal mass. The results suggest that a compliant core significantly reduces the weight of a cylindrical shell. The results of the analysis are compared with data in the following chapter.

## 3.2 Literature Review

We first review the elastic buckling behaviour of a thin walled, hollow, cylindrical shell of radius, a, and wall thickness, t, made of an isotropic material of Young's modulus, E and Poisson's ratio, $v$. In uniaxial compression, buckling takes place at a critical stress of (Timoshenko and Gere, 1961):

$$\sigma_o = \frac{Et}{a\sqrt{3(1 - v^2)}} \qquad (3.1)$$

for any assumed buckling mode. Experimentally, it has been observed that thick, low modulus shells buckle axisymmetric-ally while thin, high modulus shells tend to buckle in a non-axisymmetric, diamond mode (Timoshenko and Gere, 1961; Kollár and Dulácska, 1984). In pure bending, the circular cross section ovalizes, reducing its moment of inertia. As the curvature is increased, the bending moment reaches a theoretical maximum, the Brazier moment (Brazier, 1927):

$$M_{Brazier} = \frac{2\sqrt{2}\pi Eat^2}{9\sqrt{1 - v^2}} = \frac{0.987 Eat^2}{\sqrt{1 - v^2}} \qquad (3.2)$$

In pure bending, local buckling occurs when the stress on the compressive face of the shell reaches the critical stress to cause axisymmetric buckling under uniaxial compression (eqn 3.1). Taking account of the ovalization of the cross section, the result is (Calladine, 1983):

$$M_{1b} = \frac{0.939\,\mathrm{Eat}^2}{\sqrt{1 - v^2}} \qquad (3.3)$$

The moment required for local buckling is always lower than the Brazier moment.

The elastic buckling of a thin, isotropic cylindrical shell filled with a compliant elastic core has been analyzed for a variety of loading configurations including: axial load (Seide, 1962; Yao, 1962; and Myint, 1966); uniform radial pressure (Seide and Weingarten, 1962; Seide, 1962; Herrmann and Forrestal, 1965); circumferential band of pressure (Yao, 1965); axial load plus uniform radial pressure (Seide, 1962; Brush and Almroth, 1962; Vlasov, 1972); axial load plus axially varying radial pressure (Brush and Almroth, 1962) or temperature (Zak and Bollard, 1962); axial load plus circumferential band of pressure (Brush and Almroth, 1962); and bending (Yabuta, 1980). More recently, the analysis has been extended to orthotropic cylindrical shells (Holston, 1967; Bert, 1971; Vlasov, 1975; and Malyutin et al., 1980) and to an elastic-plastic core (Babich and Cherevko, 1983). Natural cylindrical shell strucures are typically loaded uniaxially and in bending; we consider the results for these two cases here.

The uniaxial load case has been solved by using the differential equations for equilibrium of the shell, modified to account for the spring constant of the compliant core (Seide, 1962) and by the use of stress functions (Yao, 1962). Both methods assume that the shell is thin and that the core modulus is lower than the shell modulus. Both treat the core as a three-dimensional solid and allow the core to be hollow. And both methods allow for both longitudinal and circum-ferential buckling of the shell. The final results of both methods, which must be solved numerically, are similar and are consistent with finite

element calculations (Weingarten and Wang, 1976). As expected, the buckling wavelength decreases, and the buckling load increases, with increasing core stiffness. Seide (1962) notes that for a filled core the axisymmetric buckling mode gives the lowest buckling load. He also notes that for a filled core, the solution for the uniaxial, axisymmetric buckling stress, $\sigma_{cr}$, can be approximated by:

$$\frac{\sigma_{cr}}{\sigma} = 1 + \phi \qquad (3.4)$$

for $\phi<0.5$ and by:

$$\sigma_{cr} = \frac{1}{4}\left[9\left(\frac{E_c}{1-v_c^2}\right)^2\left(\frac{E}{1-v^2}\right)\right]^{1/3} \qquad (3.5)$$

for $\phi>3$, where:

$$\phi = \frac{\left[12\left(1-v^2\right)\right]^{1/4}}{4\left(1-v_c^2\right)} \frac{E_c}{E}\left(\frac{a}{t}\right)^{3/2} \qquad (3.6)$$

and $E_c$ and $v_c$ are the Young's modulus and Poisson's ratio for the elastic core. The solution for $\phi>3$ is similar to that for wrinkling of the compressive face of a sandwich beam (Allen, 1969).

Data for the uniaxial elastic buckling stress of cylinders with a compliant core lie significantly below Seide's (1962) estimates, although the discrepancy decreases with increasing $\phi$ (Kachman, 1959; Fitzgibbon, 1960; and Goree and Nash, 1962). A lower bound on the data is given by the minimum postbuckling load calculated by Almroth and Brush (1963). Observations of the buckling mode indicate that there is a transition between the classical diamond pattern for the empty cylinders to a circumferentially elongated diamond pattern in cylinders with a very low modulus core ($E_c/E = 3 \times 10^{-5}$, Kachman,

1959) to, finally, the axisymmetric mode in cylinders with a stiffer core ($E_c/E = 10^{-4}$, Kachman, 1959).

Local buckling arising from pure bending has been analyzed by extending Seide's work and neglecting any ovalization of the cross-section (Yabuta, 1980). The relationships between the local buckling stress and $E_c/E$ and $a/t$ are plotted for a limited set of values. Bend tests were performed on four Mylar cylinders, two of which were empty and two of which were filled with silicone rubber ($E_c/E = 10^{-3}$). The empty and filled cylinders buckled ~ roughly 60% and 80% of the calculated load in a trend similar to that reported for the uniaxial load case.

Our goal is to compare the buckling resistance of cylindrical shells of equal mass with and without a compliant core for uniaxial compression, pure bending and combined compression and bending. We reanalyze the elastic buckling of a thin, isotropic cylindrical shell with a compliant elastic core to develop a simplified, more tractable analysis for axisymmetric buckling in uniaxial compression and for the ovalization, Brazier moment and local buckling moment in pure bending. We then compare the buckling resistance of hollow cylindrical shells to that of cylindrical shells with a compliant core to evaluate mechanical efficiency. Finally, we describe the potential for biomimicking of natural cylindrical shells in engineering design.

## 3.3 Analysis

*Axial compression - axisymmetric buckling*

A circular cylindrical shell of radius, a, and wall thickness, t, with a compliant elastic core is shown in Fig. 3.1. The shell has a density, $\rho$, a Young's modulus, E, and a Poisson's ratio, $\nu$; the core has a density, $\rho_c$, a Young's modulus, $E_c$, and a Poisson's ratio, $\nu_c$. We define coordinate x, y, and z axes as shown with corresponding deformations u, v, and w. We calculate the critical stress for axisymmetric elastic buckling under uniaxial compression by modifying Timoshenko and Gere's (1961) results for the symmetric deformation and axisymmetric buckling of a hollow cylindrical shell to account for the compliant core as a two-dimensional elastic foundation stabilizing a longitudinal strip of the shell. The differential equation for bending of a strip mn of the shell subject to uniaxial tension or compression, $N_x$, and a uniformly distributed internal pressure, q, is (Timoshenko and Gere, 1961):

$$D\frac{d^4w}{dx^4} = q + \frac{1}{a}\nu N_x - \frac{w}{a^2}Et + N_x\frac{d^2w}{dx^2}$$

(3.7)

where D is the flexural rigidity of the shell $(D=Et^3/12(1-\nu^2))$. For the shell with the compliant core the internal pressure arises from the deformation of the core and

$$q = -k_e w$$

(3.8)

where $k_e$ is the spring constant for the compliant core.

Following Timoshenko and Gere's (1961) analysis of the critical buckling stress we measure the displacement w from the middle surface of the shell after uniform compression requiring replacement of w by $w + (\nu N_x a)/(Et)$. Taking $N_x$ as positive in compression leads to the result:

$$D\frac{d^4w}{dx^4} + N_x\frac{d^2w}{dx^2} + \frac{w}{a^2}(Et + k_e a^2) = 0$$

(3.9)

Assuming that the radial displacements during buckling can be written:

$$w = w_m \sin\left(\frac{m\pi x}{1}\right)$$

(3.10)

we find:

$$-D\left(\frac{m\pi}{1}\right)^4 + N_x\left(\frac{m\pi}{1}\right)^2 - (Et + k_e a^2)\frac{1}{a^2} = 0$$

(3.11)

The critical buckling stress is simply $N_x/t$; for a constant value of $k_e$, independent of buckling wavelength, the minimum value is:

$$\sigma_{cr} = \frac{Et}{a\sqrt{3(1-v^2)}}\sqrt{1 + \frac{a^2 k_e}{tE}}$$

(3.12)

Note that for zero spring stiffness this reduces to the result for a hollow cylindrical shell. Assuming that the shell thickness is much smaller than its radius, the spring constant $k_e$ can be found from the result for the stress in the z direction for an elemental flat strip on an elastic foundation undergoing a sinusoidal displacement in the z direction (Gough et al. 1940, Allen, 1969):

$$q = \sigma_2 = -\frac{2\pi E_c}{(3 - v_c)(1 + v_c)}\frac{w}{1'}$$

(3.13)

where l' is one half the buckled wavelength = l/m. Setting

$$\lambda = 1/m\pi = 1'/\pi$$

(3.14)

and

$$\alpha = \frac{E_c}{E}$$

(3.15)

we find:

58

$$k_e = \frac{2 E_c}{(3 - v_c)(1 + v_c)} \frac{1}{\lambda} \qquad (3.16)$$

Substituting in eqn (3.11) gives:

$$N_x = D \frac{1}{\lambda^2} + \frac{Et}{a^2} \lambda^2 + \frac{2 E \alpha \lambda}{(3 - v_c)(1 + v_c)} \qquad (3.17)$$

The minimum buckling load is found by taking the derivative of $N_x$ with respect to $\lambda$:

$$\frac{\partial N_x}{\partial \lambda} = -2D \frac{1}{\lambda^3} + \frac{2 Et}{a^2} \lambda + \frac{2 E \alpha}{(3 - v_c)(1 + v_c)} = 0 \qquad (3.18)$$

The root $\lambda_{cr}$ can be solved for using a numerical procedure such as Newton-Raphson for given values of a, t, $\alpha$ and E: it is plotted in Fig. 3.2. Note that for $(a/t)^2(E_c/E)<0.1$, $\lambda_{cr}$ is given by the result for an empty cylinder:

$$1 / m = \frac{\pi}{\left[12\left(1 - v^2\right)\right]^{1/4}} (at)^{1/2}$$

or

$$\frac{\lambda_{cr}}{t} = \frac{1}{\left[12\left(1 - v^2\right)\right]^{1/4}} \left(\frac{a}{t}\right)^{1/2}$$

For $(a/t)(E_c/E)>10$, $\lambda_{cr}$ is given by the result for wrinkling of a flat sheet on an elastic foundation (Allen, 1969):

$$\frac{\lambda_{cr}}{t} = \left[\frac{(3 - v_c)(1 + v_c)}{12\left(1 - v^2\right)}\right]^{1/3} \left[\frac{E}{E_c}\right]^{1/3}$$

The critical buckling stress can then be found from eqn (3.17). Alternatively, noting that $\sigma_{cr} = N_x/t$ and $D = Et^3/12(1-v^2)$ we can write the critical buckling stress in the shell as:

$$\sigma_{cr} = \sqrt{3(1 - v^2)}\sigma_0 f_1 \qquad (3.19)$$

where

$$f_1 = \frac{1}{12(1 - v^2)} \frac{a/t}{(\lambda_{cr}/t)^2} + \frac{(\lambda_{cr}/t)^2}{a/t} + \frac{2\alpha}{(3 - v_c)(1 + v_c)}\left(\frac{\lambda_{cr}}{t}\right)\left(\frac{a}{t}\right)$$

where $\sigma_0$ is the buckling stress for the hollow cylinder (eqn 3.1). The total axial buckling load, $P_{cr}$, found by assuming that the core has to deform along with the shell in compression prior to buckling, and neglecting any other interaction prior to buckling is then:

$$P_{cr} = 2\pi a t \sigma_{cr}\left(1 + \frac{a}{2t}\frac{E_c}{E}\right) \qquad (3.20)$$

*Pure bending- the Brazier effect*

In pure bending, the cross section of a hollow cylindrical shell *ovalizes*, decreasing the moment of inertia and flexural rigidity of the section (Fig. 3.3). The moment carrying capacity of the cross-section reaches a maximum at the *Brazier* moment, $M_{Brazier}$ (Brazier, 1927). The Brazier moment can be calculated by writing the strain energy, U, of the cylinder in terms of the curvature, C, and the degree of ovalization, $\zeta$, noting that for a given curvature the degree of ovalization is that which minimizes strain energy (i.e. $dU/d\zeta$ = 0) and finding the maximum moment by taking $dU/dC$ = 0. Using this procedure for a hollow cylindrical shell, Calladine (1983) finds:

$$M_{Brazier} = \frac{0.987 E a t^2}{\sqrt{1 - v^2}}$$

The degree of ovalization, $\zeta$, at $M_{Brazier}$ is 2/9. Here, we use the same procedure for calculating the Brazier moment for a cylindrical shell with a compliant core.

The strain energy per unit length of a hollow cylindrical shell under a pure bending moment is (Calladine, 1983):

$$U = \frac{1}{2}C^2 E\pi a^3 t\left(1 - \frac{3}{2}\zeta + \frac{5}{8}\zeta^2\right) + \frac{3}{8}\pi E\frac{t}{a}h^2\zeta^2 \qquad (3.21)$$

where

$$h = \frac{t}{\sqrt{1 - v^2}}$$

and

$$\zeta = \delta/a$$

The first term describes the contribution of longitudinal stretching to the strain energy while the second describes that of circumferential bending. For a cylindrical shell filled with a compliant core, the strain energy is increased by the energy of ovalization of a circular disk of foam core and the energy to counter Poisson's effects due to bending of the foam core. The moment of inertia of the cross-section is also increased by the presence of the compliant core. Each of these effects is calculated in the Appendix. The final result for the strain energy of the cylindrical shell with a compliant core is:

$$U = \frac{1}{2}C^2 E\pi a^3 t\left(1 + \frac{\alpha a}{4t}\right)\left(1 - \frac{3}{2}\zeta + \frac{5}{8}\zeta^2\right) + \frac{3}{8}\pi E\frac{t}{a}h^2\zeta^2 + \frac{\pi}{4}\alpha\beta E\zeta^2 a^2 + \frac{\pi}{16}\alpha\beta' E C^2 a^4$$

$$(3.22)$$

where $\alpha = E_c/E$,

$$\beta = \frac{3 - 5v_c}{(1 + v_c)(1 - 2v_c)} \quad \text{and} \quad \beta' = \frac{v_c^2(5 - 2v_c)}{(1 + v_c)(1 - 2v_c)}$$

For a given curvature C the ovalization that minimizes strain energy is (neglecting the term $\frac{5}{8}\zeta^2$ in eqn 3.22):

$$\zeta = C^2 \frac{a^4}{h^2} \left( \frac{1 + \frac{\alpha a}{4t}}{1 + \frac{2}{3}\alpha\beta \frac{a^3}{th^2}} \right)$$

(3.23)

Substituting this value in eqn (3.22) and taking $\partial^2 U/\partial C^2 = \partial M/\partial C = 0$ we obtain the Brazier moment:

$$M_{Brazier} = \frac{2\sqrt{2}}{9}\pi Eath \left(1 + \frac{2}{3}\alpha\beta\frac{a^3}{th^2}\right)^{1/2} \left(1 + \frac{\alpha a}{4t} + \frac{\alpha\beta a}{8t}\right)^{3/2} \left(1 + \frac{\alpha a}{4t}\right)^{-1}$$

(3.24)

At the Brazier moment the ovalization is:

$$\zeta_{cr} = \frac{2}{9}\left[1 + \frac{\alpha\beta \cdot \frac{a}{8t}}{\left(1 + \frac{\alpha a}{4t}\right)}\right]$$

(3.25)

The maximum compressive stress in the shell at the Brazier moment is:

$$\sigma_{\substack{max \\ brazier}} = ECa\left(1 - \zeta_{cr}\right)$$

(3.26)

at the Brazier moment it is:

$$\sigma_{\substack{max \\ Brazier}} = \frac{Et}{a\sqrt{1 - v^2}} \left(\zeta_{cr}\right)^{1/2} \left(1 - \zeta_{cr}\right) \frac{\left(1 + \frac{2\alpha\beta a^3\left(1 - v^2\right)}{3 t^3}\right)^{1/2}}{\left(1 + \frac{\alpha a}{4t}\right)^{1/2}}$$

(3.27)

*Pure bending- local buckling*

True local buckling corresponding to a bifurcation point occurs if the normal stress in the compressive side of the cylindrical shell reaches the critical stress for axisymmetric buckling calculated above. Following Calladine's analysis for an empty cylindrical shell we observe that (Calladine, 1983):

$$\sigma_{max} = \sigma_{cr}(1 - 3\zeta)$$  (3.28)

where $\sigma_{cr}$ is the uniaxial compresssive stress for axisymmetric buckling. Substituting eqns (3.19) (3.23) (3.26) we obtain:

$$\frac{\zeta^{\frac{1}{2}}(1 - \zeta)}{\sqrt{1 - v^2}(1 - 3\zeta)} = f_1 \frac{\left(1 + \dfrac{\alpha a}{4t}\right)^{\frac{1}{2}}}{\left[1 + \dfrac{2\alpha\beta a^3(1 - v^2)}{3t^3}\right]^{\frac{1}{2}}}$$  (3.29)

which can be solved numerically for the ovalization at which local buckling occurs, $\zeta_{lb}$ or using the nomograph in Fig. 3.4. The critical moment for local buckling is found by substituting the result of eqn (3.29) in (3.22) and (3.23) and writing $M = \partial U/\partial C$. Writing the moment in terms of the ovalization at which local buckling occurs we obtain:

$$M_{lb} = \frac{\pi E a t^2 \sqrt{\zeta_{lb}}}{\sqrt{1 - v^2}} \left(1 + \frac{\dfrac{\alpha\beta' a}{8t}}{1 + \dfrac{\alpha a}{4t}} - \frac{3}{2}\zeta_{lb}\right) \left(1 + \frac{2\alpha\beta a^3}{3th^2}\right)^{1/2} \left(1 + \frac{\alpha a}{4t}\right)^{1/2}$$

(3.30)

The moment to cause local buckling is always lower than the Brazier moment.


*Combined axial load and bending moment*


Local buckling can also take place under the combined action of an axial load, P, and a bending moment, M. The combined load at any section of the core filled cylinder can

63

be replaced by an axial load applied with an eccentricity, e, with respect to the axis of the cylinder, with M=Pe. Local buckling will take place when the maximum compressive stress in the shell reaches the axisymmetric axial compression buckling stress. The maximum compressive stress is the sum of the stress due to the axial load and that due to bending. Noting that the curvature is given by C=M/EI, and replacing M and I by their values we find:

$$C = \frac{Pe}{\pi Ea^3 t(1 - \frac{3}{2}\zeta)(1 + \frac{\alpha a}{4t})} \qquad (3.31)$$

Using eqn (3.23) the ovalisation can be solved numerically from:

$$\zeta(1 - \frac{3}{2}\zeta)^2 = \left(\frac{Pe}{\pi Eath}\right)^2 \frac{1}{(1 + \frac{\alpha a}{4t})(1 + \frac{2\alpha\beta a^3}{3th^2})} \qquad (3.32)$$

The stress due to bending is :

$$\sigma_{bending} = \frac{Pea(1 - \zeta)}{\pi a^3 t(1 - \frac{3}{2}\zeta)(1 + \frac{\alpha a}{4t})} \qquad (3.33a)$$

and that due to axial compression is:

$$\sigma_{axial} = \frac{P}{2\pi at(1 + \frac{\alpha a}{2t})} \qquad (3.33b)$$

Summing the two stresses, equating them to the axisymmetric buckling stress (eqn 3.19) and solving for P we get:

$$P_{cr} = \frac{\frac{Et}{a}(1 - 3\zeta)f_1}{\frac{ea(1 - \zeta)}{\pi a^3 t(1 - \frac{3}{2}\zeta)(1 + \frac{\alpha a}{4t})} + \frac{1}{2\pi at(1 + \frac{\alpha a}{2t})}} \qquad (3.34)$$

64

For a given eccentricity, e, this equation can be solved for the critical axial load, $P_{cr}$. Conversely, given the load $P_{cr}$, the maximum eccentricity can be obtained by simultaneously solving eqn (3.32).

*Stress decay within the core*

The buckling analyses described above treat the core as an elastic foundation resisting buckling of the shell. The normal and shear stresses developed in the core are maximum at the interface between the shell and the core (z=0) and decay within the core with increasing z. The decay of normal and shear stresses within the core can be closely approximated using the solution for a buckled flat strip supported by an elastic half-space (Fig. 3.5). The normal stress in the z direction and the shear stress in the xz plane are given by Allen (1969) as:

$$\sigma_z = \frac{2\pi}{l'} \frac{E_c}{(3-v_c)(1+v_c)} w_m \sin\left(\frac{\pi x}{l'}\right)\left[1 + \left(\frac{1+v_c}{2}\right)\frac{\pi z}{l'}\right]\exp\left(-\frac{\pi z}{l'}\right)$$

(3.35a)

and

$$\tau_{xz} = \frac{\pi}{l'} \frac{E_c(1-v_c)}{(3-v_c)(1+v_c)} w_m \sin\left(\frac{\pi x}{l'}\right)\left[1 + \left(\frac{1+v_c}{1-v_c}\right)\frac{\pi z}{l'}\right]\exp\left(-\frac{\pi z}{l'}\right)$$

(3.35b)

Normalizing $\sigma_z$ and $\tau_{xz}$ by $\sigma_z$ (z=0) and $\tau_{xz}$ (z=0), respectively, we obtain:

$$\bar{\sigma}_z = \frac{\sigma_z}{\sigma_{z/z=0}} = \left[1 + \left(\frac{1+v_c}{2}\right)\frac{\pi z}{l'}\right]\exp\left(-\frac{\pi z}{l'}\right)$$

(3.36a)

and

$$\bar{\tau}_{xz} = \frac{\tau_{xz}}{\tau_{xz/z=0}} = \left[ 1 + \left( \frac{1 + v_c}{1 - v_c} \right) \frac{\pi z}{l'} \right] \exp\left( -\frac{\pi z}{l'} \right) \qquad (3.36b)$$

Both stresses are plotted as a function of $(\pi z/l')$ in Fig. 3.6, for $v_c = 0$ and $v_c = 0.5$. We observe that the stresses decay to about 5% of their maximum value at $\pi z/l' = 5$, or at a depth of 1.6 half wavelengths. Similar results are found for a strip supported by an elastic foundation of finite thickness. Core material at $z > 1.6 \, l'$ does not resist any load and can be removed without reducing the axisymmetric buckling stress in uniaxial compression or the local buckling stress in bending.

The buckling resistance of the cylindrical shell with a compliant core of thickness, c $\geq 1.6l'$, with a central bore hole of radius, b, is obtained by modifying the previous results. The uniaxial compressive stress at which axisymmetric buckling occurs remains unchanged. The Brazier moment is modified as follows. The moment of inertia of the cross-section becomes:

$$I = \pi a^3 t + \frac{E_c}{E} \frac{\pi a^4}{4} \left( 1 - \frac{b^4}{a^4} \right)$$

Setting b = a-c and c = 5l gives:

$$I = \pi a^3 t \left[ 1 + \frac{E_c}{E} \frac{a}{4t} \left\{ 1 - \left( 1 - \frac{5\lambda_{cr}\,/\,t}{a\,/\,t} \right)^4 \right\} \right] \qquad (3.37)$$

The strain energy of ovalization for the core becomes:

$$U = \frac{\pi}{4} \alpha\beta E\zeta^2 \left(a^2 - b^2\right) = \frac{\pi}{4} \alpha\beta E\zeta^2 a^2 \left[1 - \left(1 - \frac{5\lambda_{cr} / t}{a / t}\right)^2\right]$$

(3.38)

And the strain energy due to Poisson's effect becomes:

$$U = \frac{\pi}{16} \alpha\beta' EC^2 a^4 \left(1 - \frac{b^4}{a^4}\right) = \frac{\pi}{16} \alpha\beta' EC^2 a^4 \left[1 - \left(1 - \frac{5\lambda_{cr} / t}{a / t}\right)^4\right]$$

(3.39)

The moment at which local buckling moment occurs is found, as before, by setting the moment equal to the derivative of the strain energy with respect to curvature, using the ovalization at which local buckling occurs. The prodedure is identical to the previous analysis with the strain energy of the core modified by eqn (3.37, 3.38, and 3.39). The ovalization at which local buckling occurs is given by the solution to:

$$\sqrt{\frac{\zeta}{1 - v^2}} \frac{1 - \zeta}{1 - 3\zeta} = f_1 \frac{\left(1 + \frac{5}{4} \frac{E_c}{E} \frac{\lambda_{cr}}{t}\right)}{\left[1 + 8.74 \left(\frac{a}{t}\right)^2 \frac{E_c}{E} \frac{\lambda_{cr}}{t} \left(2 - 5 \frac{\lambda_{cr}/t}{a/t}\right)\right]^{1/2}}$$

(3.40)

The solution can be found numerically or by using the nomograph in Fig. 3.7 (for $v = v_c = 0.3$). The moment at which local buckling occurs is then given by eqn (3.30) using the value of $\zeta = \zeta_{lb}$ that satisfies the above equation and the modificiations given in eqns (3.37-3.39).

67

The above analysis for the stress decay within the core assumes that the core continues to function as an elastic foundation. In practice, if the core thickness is sufficiently reduced, the core will deform sinusoidally, as a unit, along with the shell. The buckling load is that given for a hollow cylinder by Timoshenko and Gere (1961) with D and t replaced by values for the transformed section, D' and t'. The moment of inertia for a unit circumferential length of shell and core is:

$$I = \left( \frac{\alpha^3 c^3 + t^3}{12} \right) + t\left( c + \frac{t}{2} - y_o \right)^2 + \alpha c\left( y_o - \frac{c}{2} \right)^2$$

giving the equivalent bending rigidity of the section as:

$$D' = \left( \frac{E}{1 - v^2} \right)\left[ \left( \frac{\alpha^3 c^3 + t^3}{12} \right) + t\left( c + \frac{t}{2} - y_o \right)^2 + \alpha c\left( y_o - \frac{c}{2} \right)^2 \right]$$

where $y_o$ is the location of the centroid of the section measured from the free face of the core, and $v_c = v$.

The equivalent thickness of the section is:

$$t' = t + \alpha c$$

The generalized buckling stress is then:

$$\sigma_{cr} = \frac{2}{at'} \sqrt{ED't'} \qquad (3.41)$$

## 3.4 Comparison of buckling resistance of thin walled cylindrical shells with and without a compliant elastic core

The performance of a thin walled cylindrical shell with a compliant elastic core can be evaluated by comparing its buckling resistance to that of an empty shell of equal diameter and mass (Fig. 3.8). The outer cylindrical shells both have a density, $\rho$, a Young's modulus, E, and a Poisson's ratio, $\nu$. The elastic core properties are: density, $\rho_c$, Young's modulus, $E_c$, and Poisson's ratio, $\nu_c$. The elastic core has a central bore-hole of radius, b, removing the stress-free core material, and leaving a core thickness, c, equal to 1.6 times the buckling half wavelength. The thickness of the empty shell, $t_{eq}$, at equal mass, is:

$$t_{eq} = t\left[1 + \frac{c}{2t}\cdot\frac{\rho_c}{\rho}\left(2 - \frac{c}{a}\right)\right] \qquad (3.42)$$

Noting that $c = 5l/\pi = 5\lambda_{cr}$ we obtain:

$$t_{eq} = t\left[1 + 5\frac{\lambda_{cr}\rho_c}{t\rho}\left(1 - 2.5\frac{\lambda_{cr}/t}{a/t}\right)\right] \qquad (3.43)$$

where, as before, $\lambda_{cr}$ is the buckling wavelength for axisymmetric buckling under a uniaxial load (Fig. 3.4).

The ratio of the uniaxial buckling stress for the cylinder with the core to that without the core is then given by dividing eqn (3.19) by eqn (3.1) and setting the thickness of the empty cylinder equal to $t_{eq}$ (eqn 3.43). We obtain, assuming $\nu = \nu_c = 0.3$:

$$\frac{\sigma_{cr}}{(\sigma_o)_{eq}} = \frac{\dfrac{a/t}{10.9(\lambda_{cr}/t)^2} + \dfrac{(\lambda_{cr}/t)^2}{a/t} + 0.57\dfrac{E_c}{E}\dfrac{a}{t}\dfrac{\lambda_{cr}}{t}}{0.605\left[1 + 5\dfrac{\lambda_{cr}}{t}\dfrac{\rho_c}{\rho}\left(1 - 2.5\dfrac{\lambda_{cr}/t}{a/t}\right)\right]}$$

$$= \frac{f_1}{0.605 \left[ 1 + 5 \frac{\lambda_{cr}}{t} \frac{\rho_c}{\rho} \left( 1 - 2.5 \frac{\lambda_{cr}/t}{a/t} \right) \right]} \qquad (3.44)$$

The uniaxial buckling load for the empty cylinder is found by multiplying the critical buckling stress (eqn 3.1) by the shell area $2\pi a t_{eq}$. That for the cylinder with the core is found by multiplying the critical buckling stress by the shell area plus $E_c/E$ times the core area. The resulting ratio of critical buckling loads with and without the core is (for $\nu = \nu_c = 0.3$):

$$\frac{P_{cr}}{(P_0)_{eq}} = \frac{\left[ 1 + 5 \frac{\lambda_{cr}}{t} \frac{E_c}{E} \left( 1 - 2.5 \frac{\lambda_{cr}/t}{a/t} \right) \right] f_1}{0.605 \left[ 1 + 5 \frac{\lambda_{cr}}{t} \frac{\rho_c}{\rho} \left( 1 - 2.5 \frac{\lambda_{cr}/t}{a/t} \right) \right]^2} \qquad (3.45)$$

The ratio of critical buckling loads for uniaxial loading is plotted in Fig. 3.9. The plots have been made assuming that the ratio of the core to shell Young's moduli vary as the ratio of the core to shell density raised to a power one or two, corresponding to a honeycomb or foam core supporting a shell made from the same solid material. Support of the shell by a core following $E_c/E = \frac{\rho_c}{\rho}$ leads to substantial increases in the axial buckling load, especially at large $a/t$. Support of the shell by a core following $E_c/E = \left( \frac{\rho_c}{\rho} \right)^2$ shows increases in the axial buckling load only for dense cores at high $a/t$.

The Brazier moment for a cylindrical shell with a compliant core is given by the second derivative of eqn (3.22) modified by eqns (3.37-3.39). Setting $\nu = \nu_c = 0.3$ we obtain the ratio of the Brazier moment for a cylindrical shell with a compliant core with a central bore hole to that of a hollow cylindrical shell of equal radius and mass:

$$\frac{M_{Brazier}}{\left(M_{Brazier}\right)_{eq}} = \frac{\left[1 + 1.747\left(\frac{a}{t}\right)^3 \frac{E_c}{E} \frac{5\lambda_{cr}/t}{a/t}\left(2 - \frac{5\lambda_{cr}/t}{a/t}\right)\right]^{1/2}}{\left[1 + \frac{5\lambda_{cr}}{t} \frac{\rho_c}{\rho}\left(1 - \frac{5\lambda_{cr}/t}{2a/t}\right)\right]^2}$$

$$\times \frac{\left[1 + \frac{5}{4}\frac{\lambda_{cr}}{t}\frac{E_c}{E} + 0.095\frac{a}{t}\frac{E_c}{E}\left(1 - \left(1 - \frac{5\lambda_{cr}/t}{a/t}\right)^4\right)\right]^{3/2}}{\left[1 + \frac{5}{4}\frac{E_c}{E}\frac{\lambda_{cr}}{t}\right]}$$

(3.46)

The ratio of Brazier moments is plotted in Fig. 3.10, again for cores obeying $E_c/E = \rho_c/\rho$ and $E_c/E = (\rho_c/\rho)^2$. The cores are much more effective in resisting Brazier buckling than uniaxial compression: both plots suggest an increase in Brazier moment of several fold for even the medium density core at a/t > 20. But in practice, local buckling precedes Brazier buckling, and it is the improvement in local buckling resistance that is most significant.

The ratio of the moments at which local buckling occurs for a cylindrical shell with and without a core is found from:

$$\frac{M_{lb}}{(M_{lb})_{eq}} = \frac{\left(1 + 1.25\frac{E_c}{E}\frac{\lambda_{cr}}{t}\right)\left[1 + \frac{0.119\frac{E_c}{E}\frac{\lambda_{cr}}{t}}{1 + 1.25\frac{E_c}{E}\frac{\lambda_{cr}}{t}} - \frac{3}{2}\zeta\right](1 - 3\zeta)f_1}{0.312\left[1 + 5\frac{\lambda_{cr}}{t}\frac{\rho_c}{\rho}\left(1 - 2.5\frac{\lambda_{cr}/t}{a/t}\right)\right]^2 (1 - \zeta)}$$

(3.47)

where $f_1$ is given by eqn (3.19) and $\zeta$ by eqn (3.40) or Fig. 3.7, for $v = v_c = 0.3$. The ratio of the local buckling moments is plotted in Fig. 3.11, again for cores obeying $E_c/E = \rho_c/\rho$ and $E_c/E = (\rho_c/\rho)^2$. Cores following the linear relationship produce large increases in local buckling resistance, even for low relative densities and low ratios of a/t. Cores

71

following the square relationship give rise to increases in local buckling resistance only at high relative densities.

Uniaxial compression and four point bending tests have been performed on silicone rubber cylindrical shells with and without a compliant core. The above analysis describes the results, detailed in the following, chapter, well.

## 3.5 Implications for engineering design: biomimicking

In nature, cylindrical shells are commonly stabilized by a compliant core. The theoretical analysis described here shows that the presence of a compliant core increases the buckling resistance in both axial compression and bending over that of a hollow cylinder of equal mass and radius. Honeycomb cores are more effective than foam cores. For the natural structures shown in Fig. 1.2, we estimate the increase to be a factor of between 1.5 and 4.

Cylindrical shells are used in a variety of engineering applications (Fig. 1.3). In practice, the measured elastic buckling loads are always less than the theoretical due to unavoidable geometric and material defects that cause premature loss of stability (Timoshenko and Gere, 1961, Kollár and Dulácska, 1984). In design elastic buckling loads are reduced by safety factors, termed "knock down" factors, to 30 to 40% of theoretical predictions (Kollár and Dulácska, 1984, Kenney 1984). A compilation of published experimental results (Fig. 3.12) and more recent ones (see Chapter 4) show a consistent trend of cylinders with a compliant core achieving close to 100% of their theoretical strength as the core stiffness and the radius to thickness ratio increase. This difference in knock down factors further increases the elastic buckling resistance of cylinders with a compliant core relative to equivalent hollow cylinders.

In practice engineers stiffen cylindrical shells with longitudinal stringers or circumferential rings or both. The use of massive stiffeners, as in naval construction, offshore oil platforms and airframes, subdivides the shell into curved panels that are less sensitive to defects and achieve higher buckling loads (Timoshenko and Gere, 1961, Kenney 1984). In some cases where high reliability is required such as in aircraft design, the ribs supporting the shell may be designed to carry most of the external loads with the shell reduced to the role of an enclosure (Kollár & Duláscka, 1984) While this is a safe design it requires more material and is heavier than an unreinforced shell. A better way of reinforcing shells is with closely spaced longitudinal, circumferential or orthogonal stiffeners (Kollár and Dulácska, 1984): the close spacing of the stiffeners insures that they buckle integrally with the skin. One or two way ribbed cylindrical shells exhibit the same types of buckling behavior as isotropic shells with the difference that the stiffeners increase the stretching and bending stiffnesses in the direction along which they are placed. Their buckling loads can be obtained by analyzing them as orthotropic shells.

For the case of buckling in axial compression and the associated local buckling problem in bending, theoretical investigations and experiments on near perfect ribbed shells have shown that ring stiffened cylinders have always a lower buckling load in axial compression than isotropic equivalent weight cylinders (Calladine 1983, Tennyson, 1976). Stringer reinforced cylinders can be marginally more efficient (Tennyson, 1976). Ellinas and Croll (1981) and Ellinas et al. (1981) reached the same conclusions after an elaborate analysis, they however show that when imperfection sensitivity is taken into account, the improved knock down factors for circumferentially reinforced shells may reverse these conclusions for some stiffening ratios.

The thinner and deeper the stiffeners are, the higher the bending stiffness of the shell and hence the efficiency of the reinforcement. The depth of the stiffeners can be increased until local buckling of the stiffeners becomes the controlling failure mechanism. In the most general case an optimal reinforcing geometry would be one with both longitudinal and circumferential stiffeners equally distributed. The efficiency of this orthogonal reinforcement can be improved by making the stiffeners deeper and thinner, local buckling being prevented by the bracing provided by the closely spaced orthogonal elements. This optimisation scheme can be pursued until such a point where the orthogonal stiffening cannot buckle integrally with the shell, but instead becomes akin to a square honeycomb foundation stabilizing it. Honeycomb cores have Young's modulus proportional to density; their efficiency is given by the plots in Figs. 3.9a, 3.10a and 3.12a.

Metal honeycombs, made by the expansion of adhesively bonded sheets of foil, have been widely used in lightweight structural sandwich panels in the aerospace industry. Recently, higher density metal honeycombs have been made by spot welding thicker sheets of material together. Metal foams are becoming more common; a low cost, $270kg/m^3$, closed cell, aluminum foam is currently being tested by Alcan (Alcan International Ltd., Kingston, Ontario, Canada) and the Dnepropetrovsk Metallurgical Institute (DMI) in Ukraine is producing a range of metal honeycombs and foams (copper, iron, nickel, aluminum) with cell sizes from 10m to 5mm in relative densities from 0.3-0.9 (Walukas, 1992). The DMI materials can be made as laminates of alternating fully dense and cellular layers. Of particular interest, solid cylindrical shells with either a honeycomb or foam core can be produced as a single monolithic unit. The development of such engineering materials opens up the possibility of biomimicking of the natural structures shown in Fig. 1.2.

## 3.6  Conclusions

The simplified analysis of the buckling in axial compression of core filled cylindrical shells captures the most important elements of the full 3-D analysis and provides excellent analytical predictions in a tractable mathematical form. The axial buckling stress was used as a criterion for local buckling to develop a general solution for the elastic stability in pure bending of cylindrical shells with an elastic core including Brazier's ovalisation and Poisson's ratio effects in the core. The analysis of stress decay in the core showed that the stresses in the core are negligible at a depth of roughly 1.6 half buckling wavelengths; the removal of core material beyond this depth does not affect the buckling stress of the shell. A parametric analysis showed that cylinders with this core depth have higher buckling loads than equivalent hollow cylinders.

The results of the analysis suggest that there is great potential for biomimicking of natural structures in engineering. A uniform honeycomb or foam foundation can become a more efficient substitute for stiffened shells; in addition to offering improved theoretical buckling resistance shells with a compliant core offer reduced sensitivity to imperfections. The recent development of denser honeycomb materials, foamed metals and monolithic metal cylindrical shells with metal honeycomb or foam cores opens up the possibility of biomimicking of the natural structures shown in Fig. 1.2.

# References

Allen, H.G. (1969) Analysis and Design of Structural Sandwich Panels, Pergamon.

Almroth, B.O. (1963) Postbuckling behaviour of axially compressed circular cylinders. AIAA Journal 1, 630-633.

Almroth, B.O. and Brush, D.O. (1963) Postbuckling behaviour of pressure- or core-stabilized cylinders under axial compression. AIAA Journal 1, 2338-2341.

Babich, I.Y. and Cherevko, M.A. (1984) Stability of cylindrical shells with an elastic-plastic filler under axial compression. Prikladnaya Mekhanika 20, 60-64.

Bert, C.W. (1971) Buckling of axially compressed, core-filled cylinders with transverse shear flexibility. J. Spacecraft, 8, 546-548.

Brazier, L.G. (1927) On the flexure of thin cylindrical shells and other thin sections. Proc. Royal Soc. London. A116, 104-114.

Brush, D.O. and Almroth, B.O. (1962) Buckling of core-stabilized cylinders under axisymmetric external loads. J. of the Aerospace Sciences, 29, 1164-1170.

Calladine, C.R. (1983) Theory of Shell Structures Cambridge University Press.

Ellinas, C.P. & Croll, J.G.A. (1981) "Overall buckling of ring stiffened shells", Proc. Inst. of Civil Engrs, Part 2, 71, 637-661.

Ellinas, C.P., Batista, R.C. & Croll, J.G.A. (1981) "Overall buckling of stringer stiffened cylinders", Proc. Inst. of Civil Engrs, Part 2, 71, 479-512.

Fitzgibbon, D.P. (1960) "Preliminary results of sub-scale tests on cylinders filled with an elastic core", Space Technology Labs, Inc. GM 60-7520.6-11, 25 April.

Goree, W.S. and Nash, W.A. (1962) Elastic stability of circular cylindrical shells stabilized by a soft elastic core. Experimental Mechanics, 2, 142-149.

Gough, G.J., Elam, C.F., and de Bruyne, N.A. (1940) "The stabilization of a thin sheet by a continuous supporting medium", The Journal of Royal Aeronautical Society, 44, 12-43.

Herrmann, G. and Forrestal, M.J. (1965) Buckling of a long cylindrical shell containing an elastic core. AIAA Journal 3, 1710-1715.

Holston, A. (1967) Stability of inhomogeneous anisotropic cylindrical shells containing elastic cores. AIAA Journal 5, 1135-1138.

Kachman, D.R. (1959) "Test report on buckling of propellant cylinders under compressive loads", Space Technology Labs, Inc. GM 59-7520.6-24, 30 November.

Kenny, J.P. and Partners (1984) Buckling of Offshore Structures, Granada Pub., London.

Kollár, L. and Dulácska, E. (1984) Buckling of Shells for Engineers, John Wiley and Sons.

Malyutin, I.S., Pilipenko, P.B., Georgievskii, V.P. and Smykov, V.I. (1980) Experimental and theoretical study of the stability in axial compression, of cylindrical shells reinforced with an elastic filler. Prikladnaya Mekhanika 16, 56-60.

Myint-U, T. (1966) Stability of axially compressed core-filled cylinders, AIAA Journal, 4, 552-553.

Niklas, K.J. (1992) Plant Biomechanics: An Engineering Approach to Plant Form and Function University of Chicago Press.

Seide, P. (1962) The stability under axial compression and lateral pressure of circular-cylindrical shells with a soft elastic core. J. of the Aerospace Sciences 29, 851-62.

Seide, P. and Weingarten, V.I. (1962) Buckling of circular rings and long cylinders enclosing an elastic material under uniform external pressure. American Rocket Society J., 32, 680-688.

Tennyson, R.C. (1976) "The effect of shape imperfections and stiffening on the buckling of circular cylinders" ,in Buckling of Structures, ed. B. Budiansky, Springer Verlag, NY.

Timoshenko, S.P. and Gere, J.M. (1961) Theory of Elastic Stability, Second edition. McGraw Hill.

Vlasov, V.V. (1972) "Stability of cylindrical shells containing a filler on being subjected to axial compression and external pressure" Pukladanya Mekhanika (trans. in English), 9, No. 1, 117-121.

Vlasov, V.V. (1975) "Stability of composite shells with an elastic core", Mekhanika Polimerov, (trans. in English), No. 3, 544-547.

Walukas, D.M. (1992) GASAR materials: a novel approach in the fabrication of porous materials. Internal report USP Holdings, Ann Arbor, MI.

Weingarten, V.I. and Wang, Y.S. (1976) Stability of shells attached to elastic core. Journal of the Engineering Mechanics Division, ASCE. 102, 839-849.

Yabuta, T. (1980) Effects of elastic supports on the buckling of circular cylindrical shells under bending. J. Appl. Mech. 47, 866-870.

Yao, J.C. (1962) Buckling of axially compressed long cylindrical shell with elastic core. J. Appl. Mech., 29, 329-334.

Yao, J.C. (1965) Bending due to ring loading of a cylindrical shell with an elastic core, J. Appl. Mech., 32, 99-103.

Zak, A.R. and Bollard, R.J.H. (1962) Elastic buckling of cylindrical thin shels filled with an elastic core. American Rocket Society Journal, 32, 588-593.

# Appendix

The total strain energy of the cylindrical shell with the compliant core is the sum of the strain energies of the hollow cylindrical shell and of the compliant core. The strain energy of the hollow cylindrical shell is the sum of the energy to ovalize the circular cross-section and that to bend the ovalized tube: it is given by eqn (3.21). The strain energy of the compliant core is the sum of the energy to ovalize the circular cross-section of the core, bend the ovalized core and to maintain the ovalized cross-section against Poisson ratio effects. Each of these terms is derived below. In calculating the strain energy terms we assume that the cylinder is long in comparison with its radius, producing plane strain conditions. We also assume that the cylindrical shell is much stiffer than the core so that it will fully restrain against Poisson ratio effects that tend to distort the core: i.e., the core will maintain the ovalized shape of the shell.

*Strain energy associated with ovalization of compliant core.*

The radial and tangential displacements, u and v respectively, of a hollow cylindrical shell ovalized by $\zeta$ are (Calladine, 1983):

$$u = r\zeta\cos 2\theta \quad \text{and} \quad v = \frac{-r}{2}\zeta\sin 2\theta$$

Assuming that the compliant core ovalizes to the same shape the radial and circumferential strains are, then:

$$\varepsilon_r = \frac{\partial u}{\partial r} = \zeta\cos 2\theta$$

$$\varepsilon_\theta = \frac{u}{r} + \frac{\partial v}{r\partial\theta} = 0$$

$$\gamma_{r\theta} = \frac{\partial u}{r\partial \theta} + \frac{\partial v}{\partial r} - \frac{v}{r} = -2\zeta \sin 2\theta$$

The corresponding components of stress are:

$$\sigma_r = \frac{E_c}{(1 + v_c)(1 - 2v_c)}\left[(1 - v_c)\varepsilon_r + v_c\varepsilon_\theta\right] = \frac{(1 - v_c)E_c}{(1 + v_c)(1 - 2v_c)}\zeta \cos 2\theta$$

$$\sigma_\theta = \frac{E_C}{(1 + v_C)(1 - 2v_C)}\left[(1 - v_c)\varepsilon_\theta + v\varepsilon_r\right] = \frac{vE_C}{(1 + v_C)(1 - 2v_C)}\zeta \cos 2\theta$$

$$\tau_{r\theta} = \frac{E_C}{2(1 + v_C)}\gamma_{r\theta} = \frac{-E_c\zeta \sin 2\theta}{(1 + v_C)}$$

The strain energy per unit length in the ovalized core is:

$$U = \frac{1}{2}\int_0^{2\pi}\int_0^a (\sigma_r\varepsilon_r + \sigma_\theta\varepsilon_\theta + \tau_{r\theta}\gamma_{r\theta})r dr d\theta$$

Substituting for the stresses and strains we obtain:

$$U = \frac{\pi E\zeta^2 a^2}{4}\frac{(3 - 5v)}{(1 + v_C)(1 - 2v_C)}$$

*Strain energy associated with bending of the core filled cylinder*

The strain energy per unit length to bend a member of flexural rigidity EI to a curvature C is:

$$U = \frac{1}{2}EIC^2$$

79

For a hollow tube with ovalization $\zeta$ the moment of inertia is  (Calladine, 1983)

$$I = \pi a^3 t \left( 1 - \frac{3}{2} \zeta + \frac{5}{8} \zeta^2 \right)$$

And for a circular shell filled with a compliant core of modulus $E_c$ this becomes

$$I = \left( \pi a^3 t + \frac{\pi a^4}{4} \frac{E_c}{E} \right) \left( 1 - \frac{3}{2} \zeta + \frac{5}{8} \zeta^2 \right) = \pi a^3 t \left( 1 + \frac{E_c}{E} \frac{a}{4t} \right) \left( 1 - \frac{3}{2} \zeta + \frac{5}{8} \zeta^2 \right)$$

*Strain energy associated with Poisson's effects due to bending*

Here we calculate the radial and circumferential strains that would be induced in a beam of circular cross-section  deforming freely in pure bending (Fig. 3.A1).  We then calculate the strain energy required to maintain the circular cross-section.

The strain in the longitudinal (z) direction is simply:

$$\varepsilon_z = -Cy = -Cr \sin \theta$$

while the strains in the radial and circumferential directions are:

$$\varepsilon_r = \varepsilon_\theta = -v_c \varepsilon_z = v_c Cr \sin \theta$$

Noting that

$$\varepsilon_r = \frac{\partial u}{\partial r}$$

and

$$\varepsilon_\theta = \frac{u}{r} + \frac{1}{r}\frac{\partial v}{\partial \theta}$$

we find

$$u = \frac{v_c}{2}\, Cr^2 \sin\theta \quad \text{and} \quad v = \frac{-v_c}{2}\, Cr^2 \cos\theta$$

Substituting in

$$\gamma_{r\theta} = \frac{1}{r}\frac{\partial u}{\partial \theta} + \frac{\partial v}{\partial r} - \frac{v}{r}$$

gives

$$\gamma_{r\theta} = -v_c Cr \cos\theta$$

The strain energy per unit length of cross-section to maintain the circular cross-section is then (noting that $\varepsilon_r = \varepsilon_\theta$ and $\sigma_r = \sigma_\theta$):

$$U = \frac{1}{2}\int_o^a \int_o^{2\pi} \left(2\sigma_r \varepsilon_r + \tau_{r\theta}\gamma_{r\theta}\right) r\,d\theta dr$$

$$= \frac{1}{2}\int_o^a\int_o^{2\pi}\left(\frac{2v_c^2 E_c C^2 r^2 \sin^2\theta}{(1+v_c)(1-2v_c)} + \frac{v_c^2 E_c C^2 r^2 \cos^2\theta}{2(1+v_c)}\right) r\,d\theta dr$$

$$= \frac{\pi}{16}\frac{v_c^2(5-2v_c)}{(1+v_c)(1-2v_c)}E_c C^2 a^4$$

## Notation

a = radius to mid-plane of thickness

b = radius of bore hole

c = core thickness

C = curvature of cylinder in bending

$D$ = flexural rigidity of shell = $\dfrac{Et^3}{12\left(1 - v^2\right)}$

E = Young's modulus of shell

$E_c$ = Young's modulus of core

$h = \dfrac{t}{\sqrt{1 - v^2}}$

I = moment of inertia

$k_e$ = spring constant for compliant core

l = length of shell

$l'$ = half the buckling wavelength = l/m

m = longitudinal wave number

$M_{Brazier}$ = Brazier moment

$M_{lb}$ = local buckling moment

$N_x$ = uniaxial compression per unit circumferential length

$P_o$ = axial compressive buckling load of hollow shell

$P_{cr}$ = axial compressive buckling load of shell with compliant    core

q = uniform internal pressure inside shell

t = thickness of shell

$t_{eq}$ = equivalent thickness of a hollow shell of equal mass and    radius as shell with a compliant core

u, v, w = deformations along x, y, z directions

U = strain energy per unit length

$w_m$ = maximum sinusoidal displacement in z-direction

$$\alpha = \left[ \frac{E_C}{E} \right]$$

$$\beta = \frac{3 - 5v_c}{\left(1 + v_c\right)\left(1 - 2v_c\right)}$$

$$\beta' = \frac{v_c^2\left(5 - 2v_c\right)}{\left(1 + v_c\right)\left(1 - 2v_c\right)}$$

$\delta$ = maximum radial displacement under ovalization

$$\zeta = \text{degree of ovalization} = \frac{\delta}{a}$$

$\zeta_{cr}$ = degree of ovalization at $M_{Brazier}$

$\zeta_{lb}$ = degree of ovalization at local buckling

$$\lambda = \text{buckling wavelength parameter} = \frac{l'}{\pi}$$

$\lambda_{cr}$ = value of l minimizing $N_x$

$v$ = Poisson's ratio of shell

$v_c$ = Poisson's ratio of core

$\rho$ = density of the shell

$\rho_c$ = density of the core

$\sigma_0$ = Theoretical buckling stress in uniaxial compression of a hollow shell

$\sigma_{cr}$ = axisymmetric buckling stress of shell with compliant core under uniaxial compression

$\sigma_{max}$ = maximum normal stress in bent cylinder

$\sigma_z$ = stress in the z-direction

$$\overline{\sigma_z} = \text{normalized normal stress in z direction} = \frac{\sigma_z}{\sigma_{z/z=0}}$$

$\tau_{xz}$ = Shear stress in the x-z plane

$\bar{\tau}_{xz}$ = normalized shear stress in xz plane = $\dfrac{\tau_{xz}}{\tau_{xz/z=0}}$

Figure 3.1 A thin-walled cylindrical shell with a compliant, elastic core.
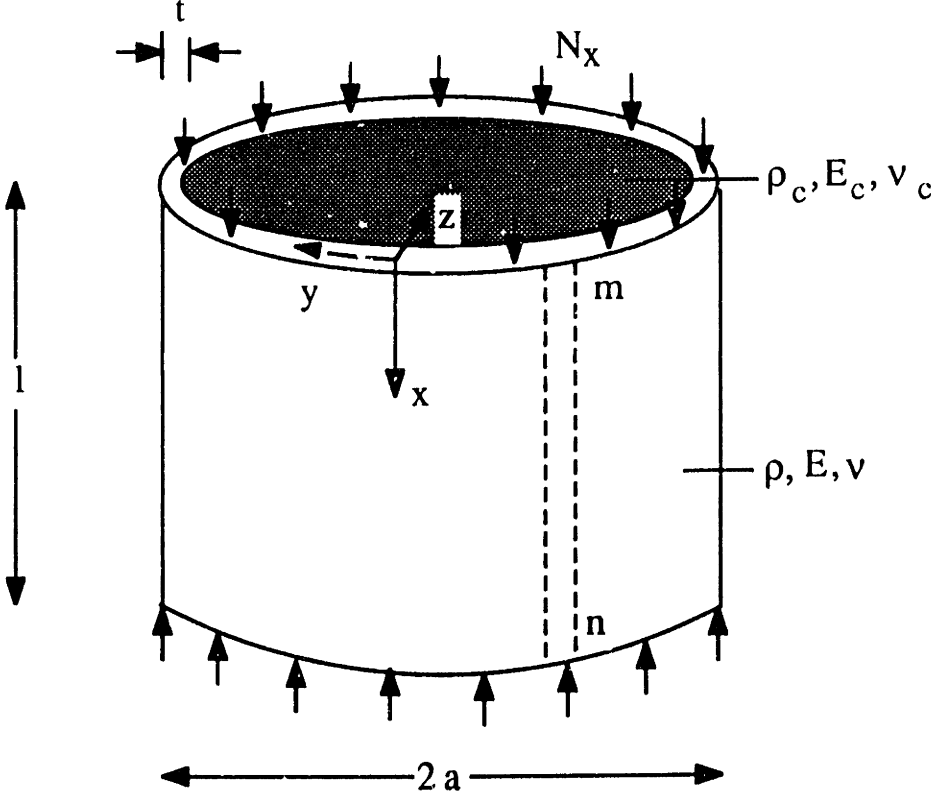
Figure 3.2 The normalized axisymmetric buckling wavelength parameter, $\lambda/t$, for a cylindrical shell plotted against radius to thickness ratio, $a/t$, for various values of $E_c/E$. Each curve can be approximated by a bilinear relationship. $\lambda$ is the buckling half wavelength divided by $\pi$.
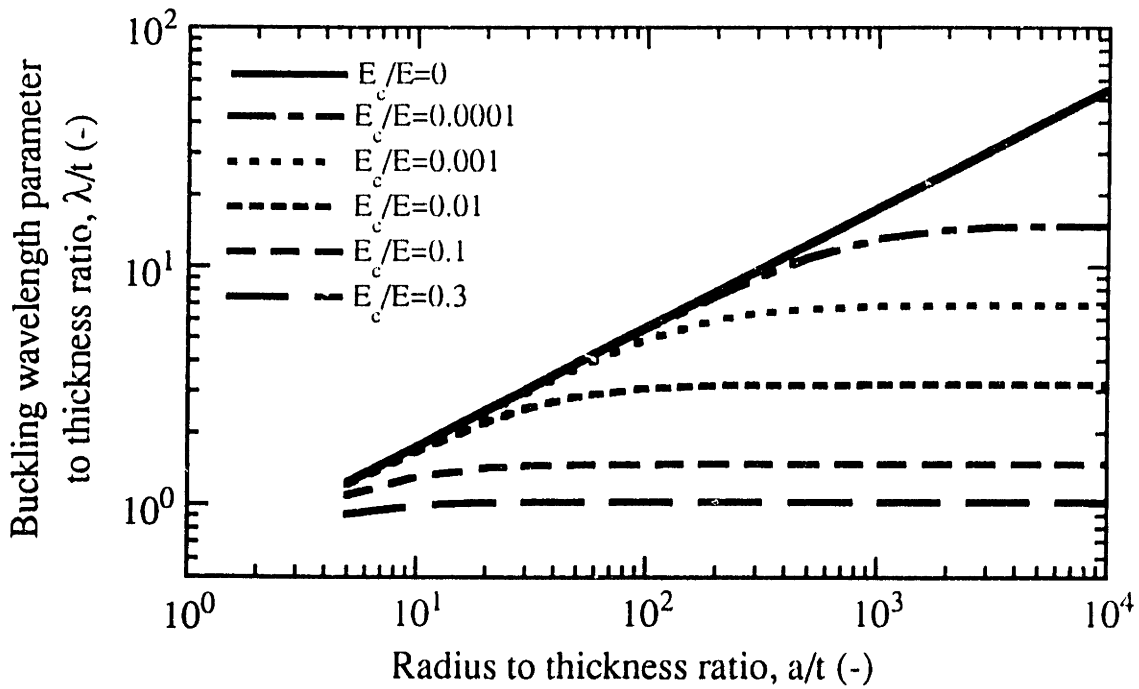
Figure 3.3(a) A hollow cylindrical shell in pure bending.



(a)
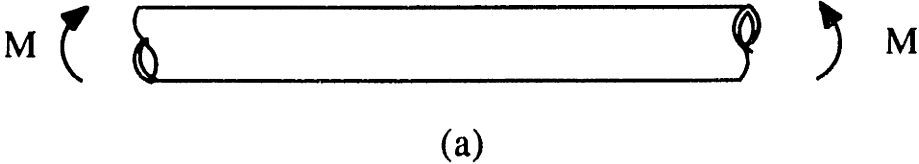
Figure 3.3(b) Ovalization of the initially circular cross-section. The degree of ovalization is $\zeta = \delta/a$.



(b)

$\xi = \delta/a$
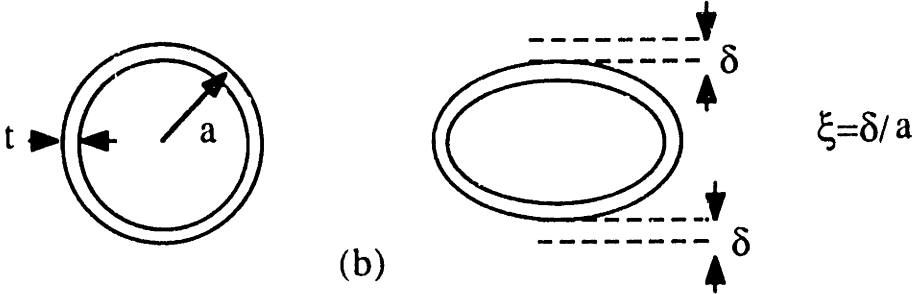
Figure 3.3(c) A cylindrical shell of modulus E filled with a compliant core of modulus $E_c$.



(c)
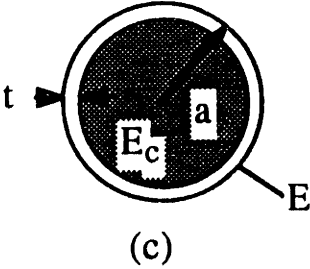
Figure 3.4 Nomograph for solution of $\zeta_{lb}$ for cylindrical shell with compliant core.
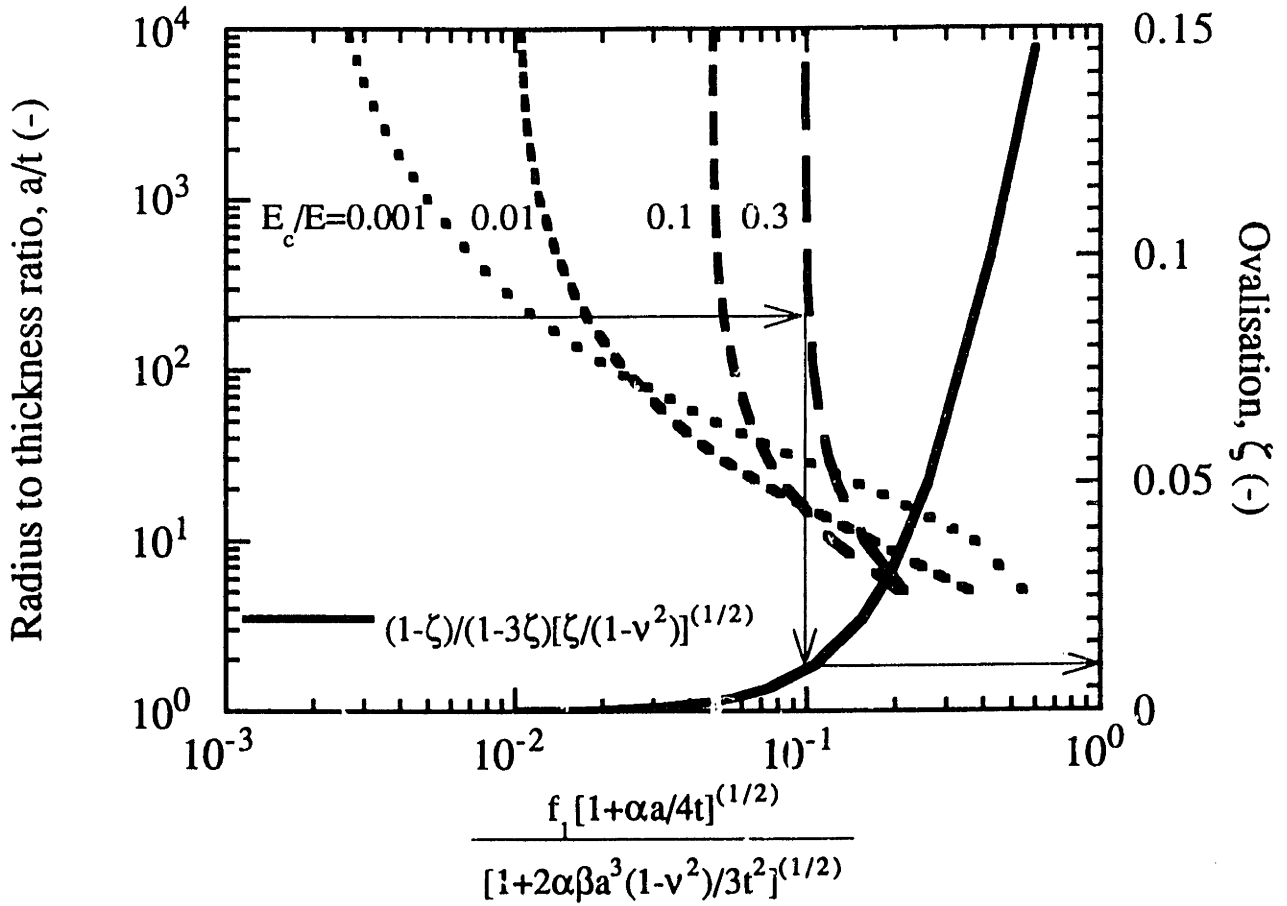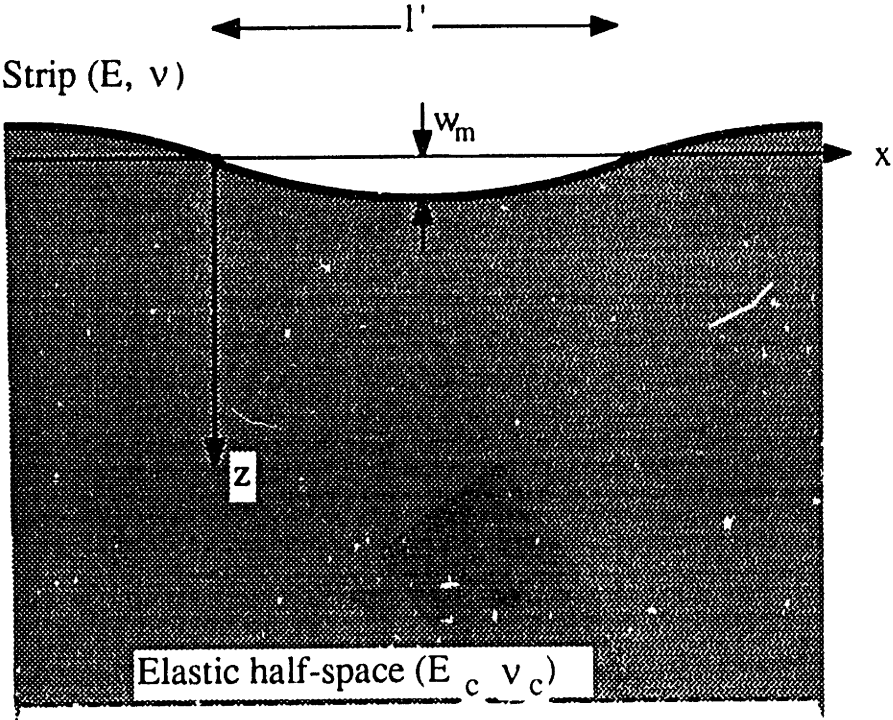
Figure 3.5 A buckled flat strip on an elastic half-space.

Figure 3.6(a) Decay of normal stress in the z direction with normalized depth into the core, $\pi z/l'$.
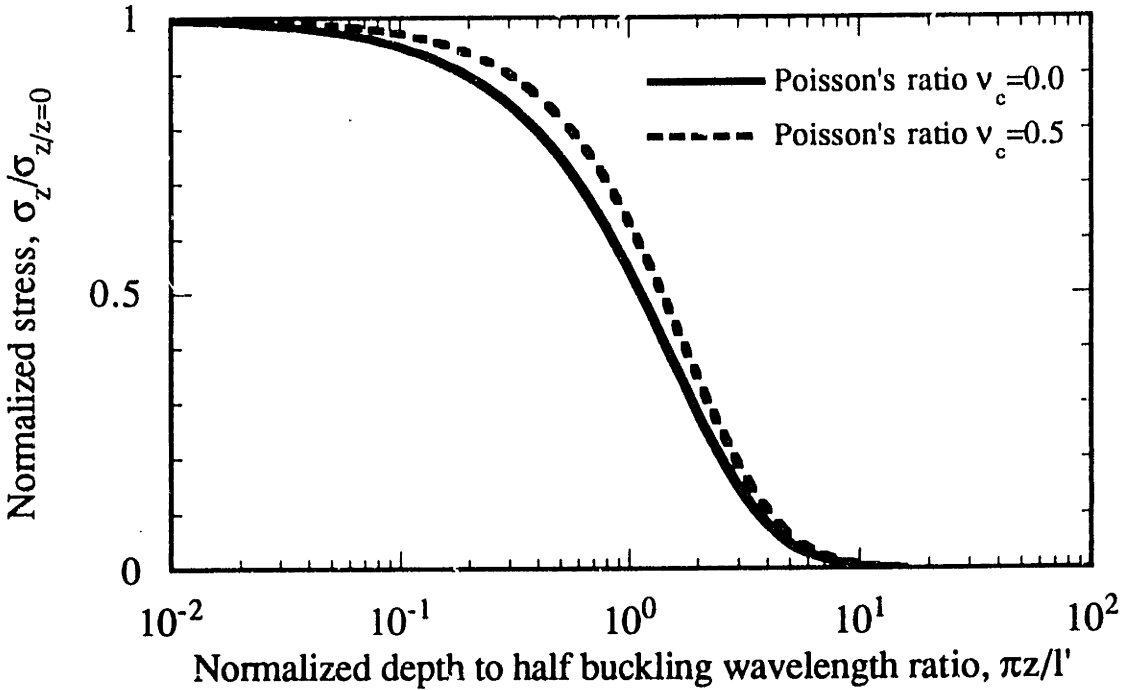
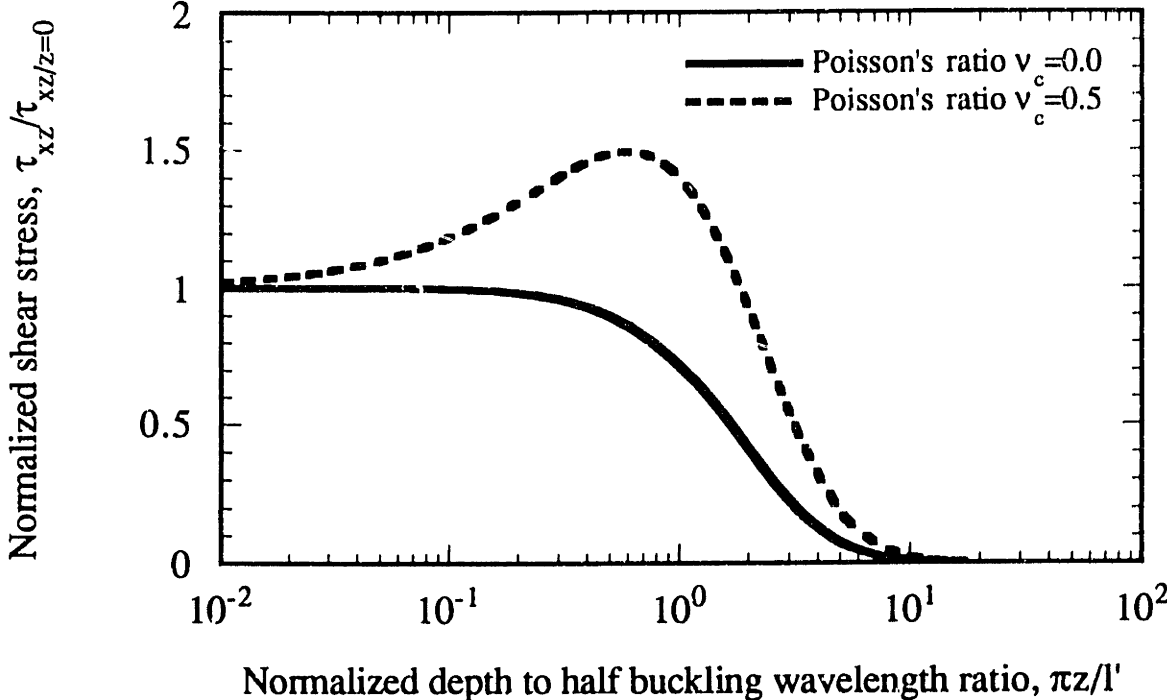Figure 3.6(b) Decay of shear stress in the xz plane with normalized depth into the core, $\pi z/l'$.

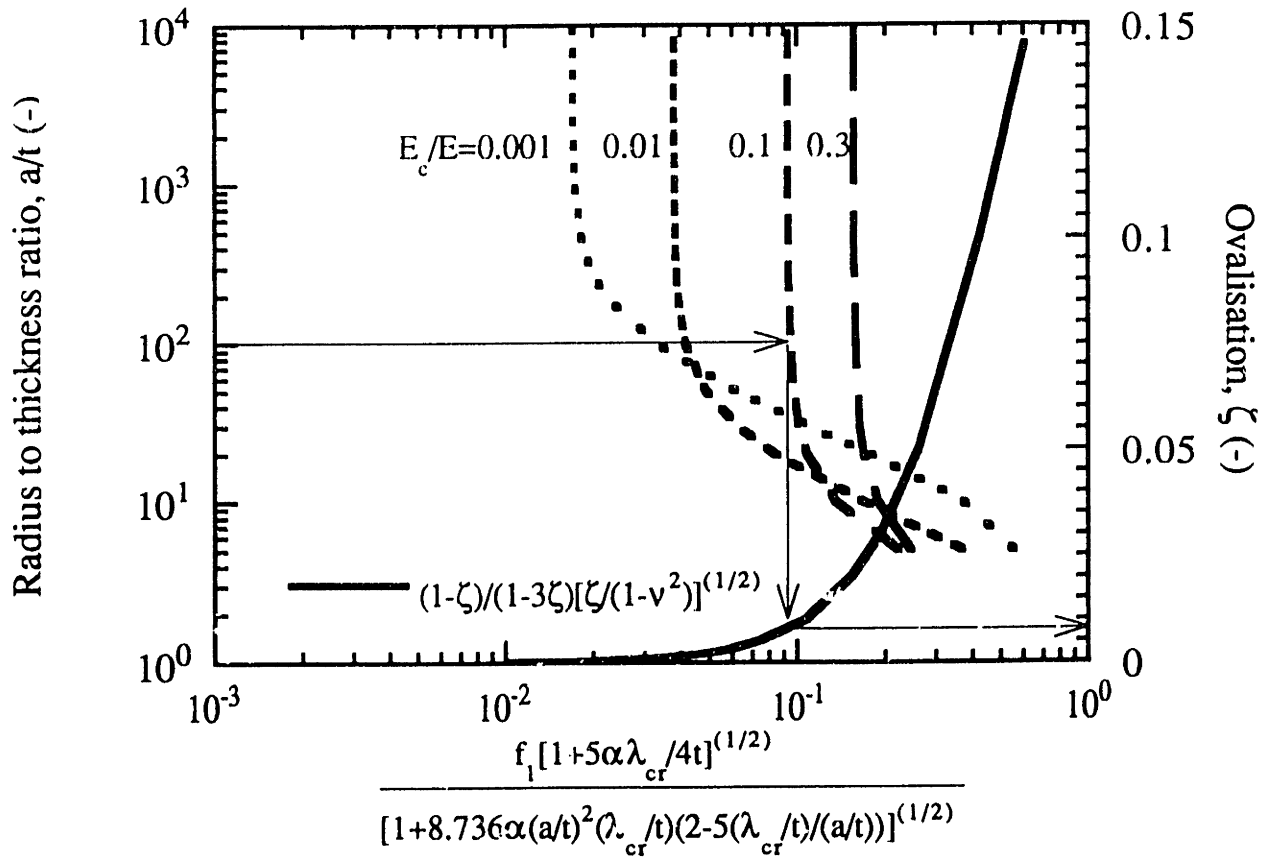Figure 3.7 Nomograph for solution of $\zeta_{lb}$ for cylindrical shell with compliant core with central bore hole.

Figure 3.8(a) Thin walled cylindrical shell (no core).

(b) Thin walled cylindrical shell with a compliant core of depth c of equal radius and mass as shell in (a).
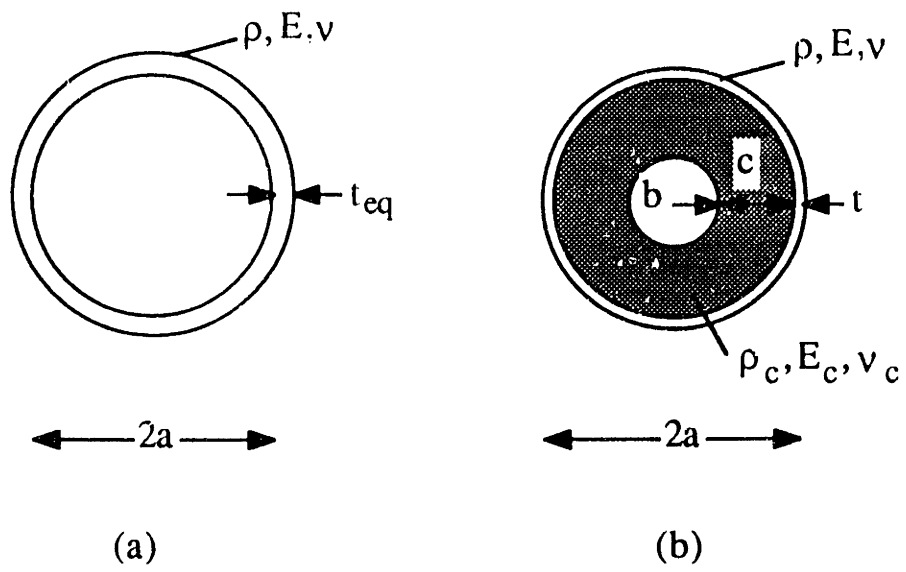


(a)

(b)

Figure 3.9 The ratio of the elastic buckling load for uniaxial loading of a cylindrical shell with an elastic core to that without a core plotted against the ratio of shell radius to thickness for the shell with the core. (a) $E_C/E = \rho_C/\rho$.

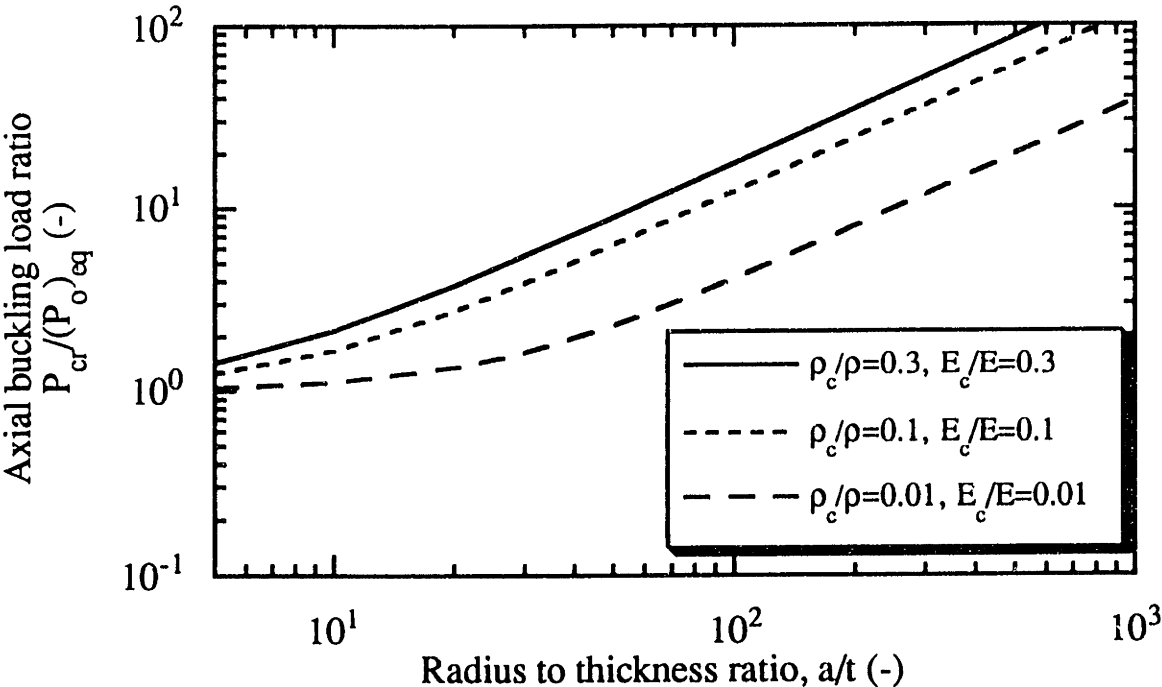Figure 3.9 (b) $E_C/E = (\rho_c/\rho)^2$.



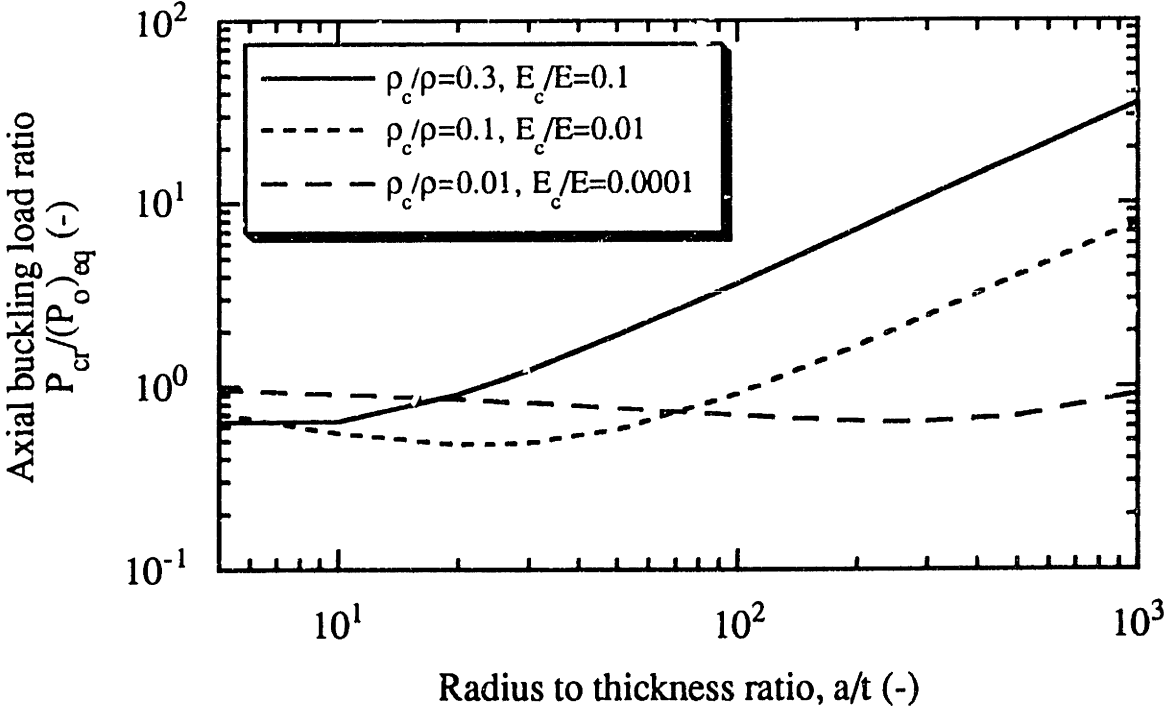Figure 3.9 (b) $E_C/E = (\rho_c/\rho)^2$.

Figure 3.10 The ratio of the Brazier moment for a cylindrical shell with an elastic core to that without a core plotted against the ratio of shell radius to thickness for the shell with the core. (a) $E_c/E = \rho_c/\rho$.
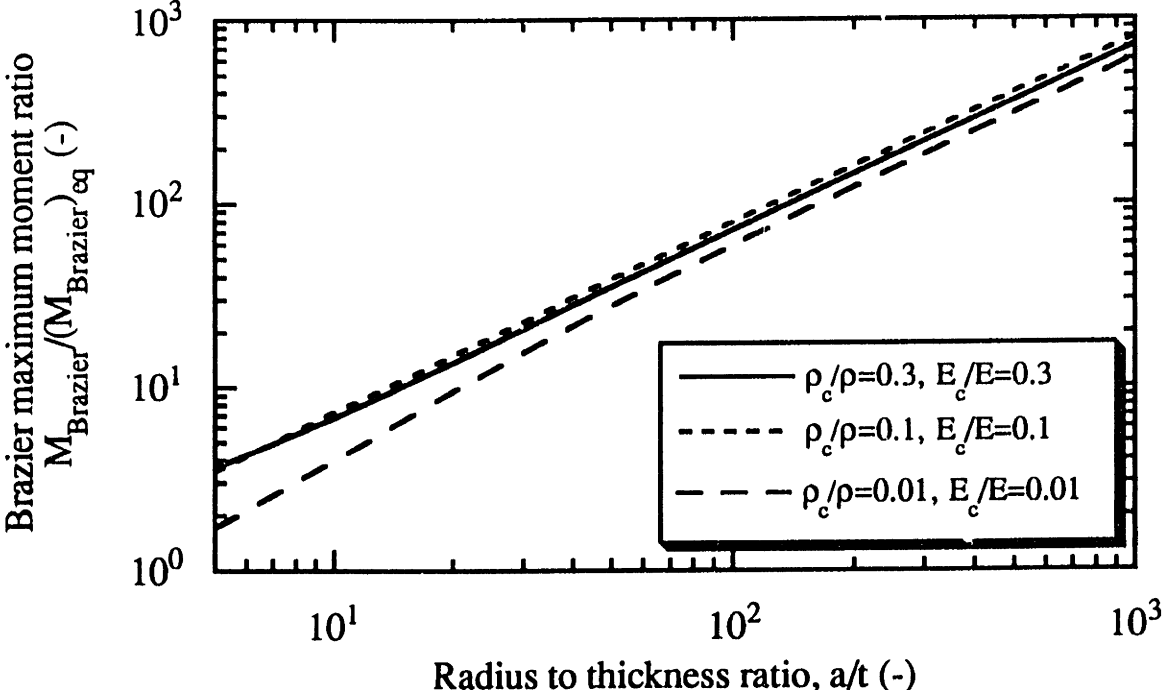
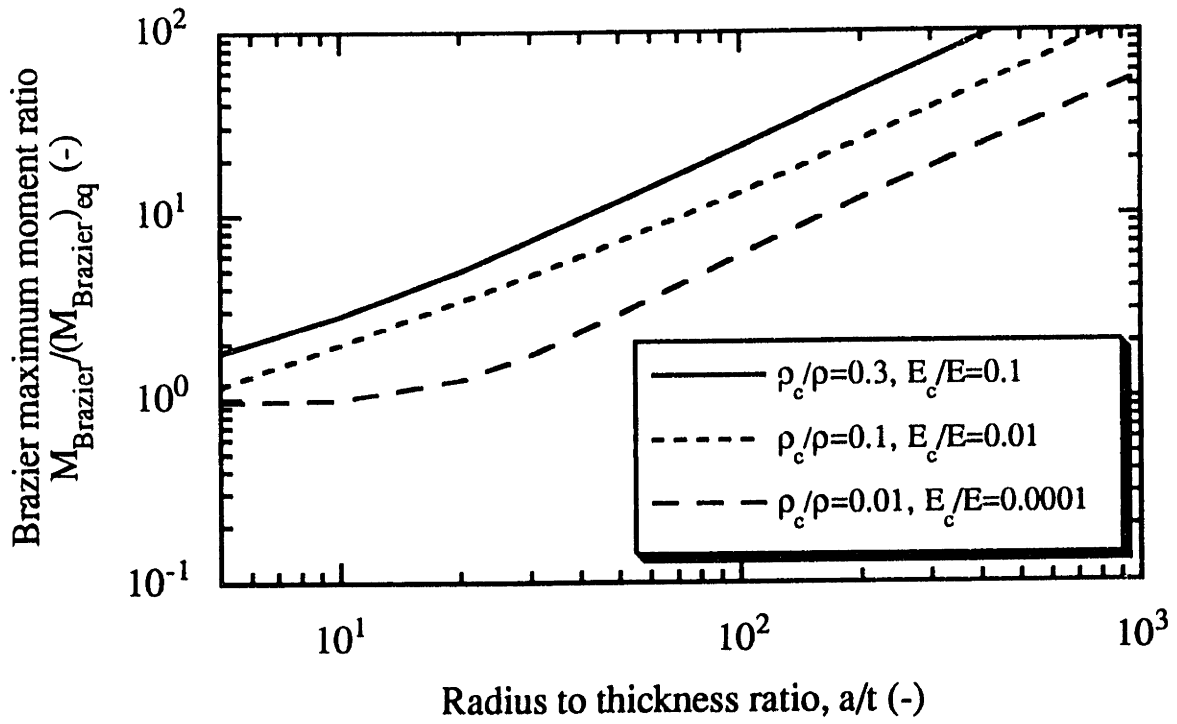Figure 3.10 (b) $E_c/E = (\rho_c/\rho)^2$.

Figure 3.11 The ratio of the local buckling moment of a cylindrical shell with an elastic core to that without a core plotted against the ratio of shell radius to thickness for the shell with the core. (a) $E_c/E = \rho_c/\rho$.
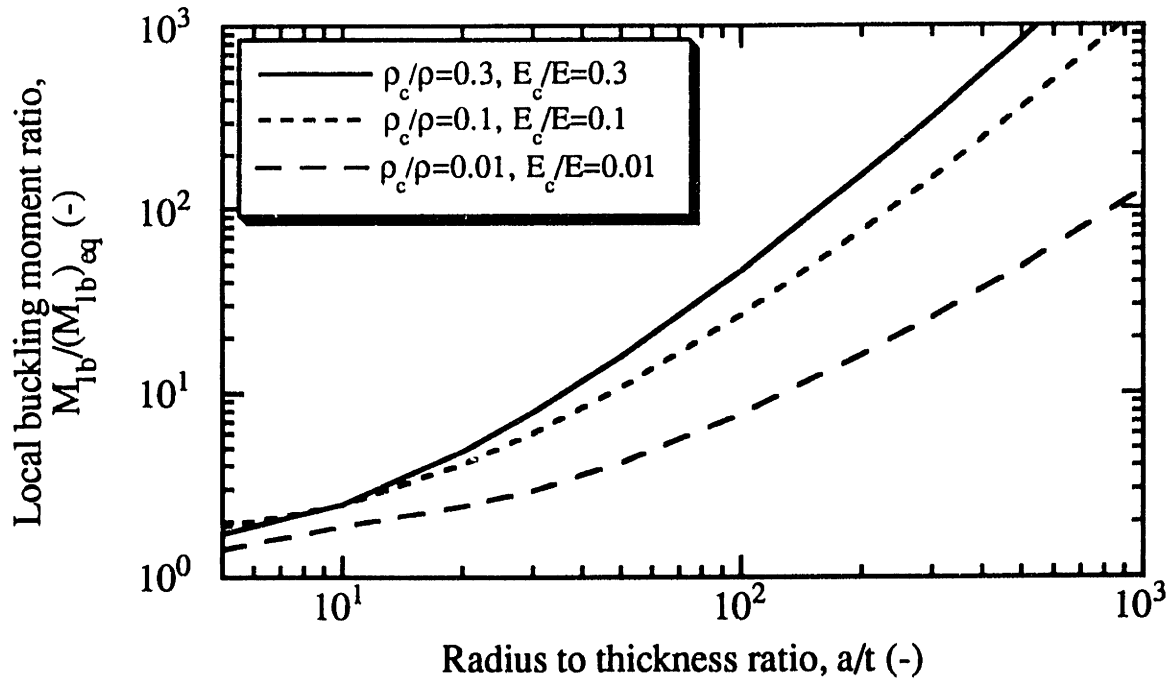
Figure 3.11 (b) $E_c/E = (\rho_c/\rho)^2$.
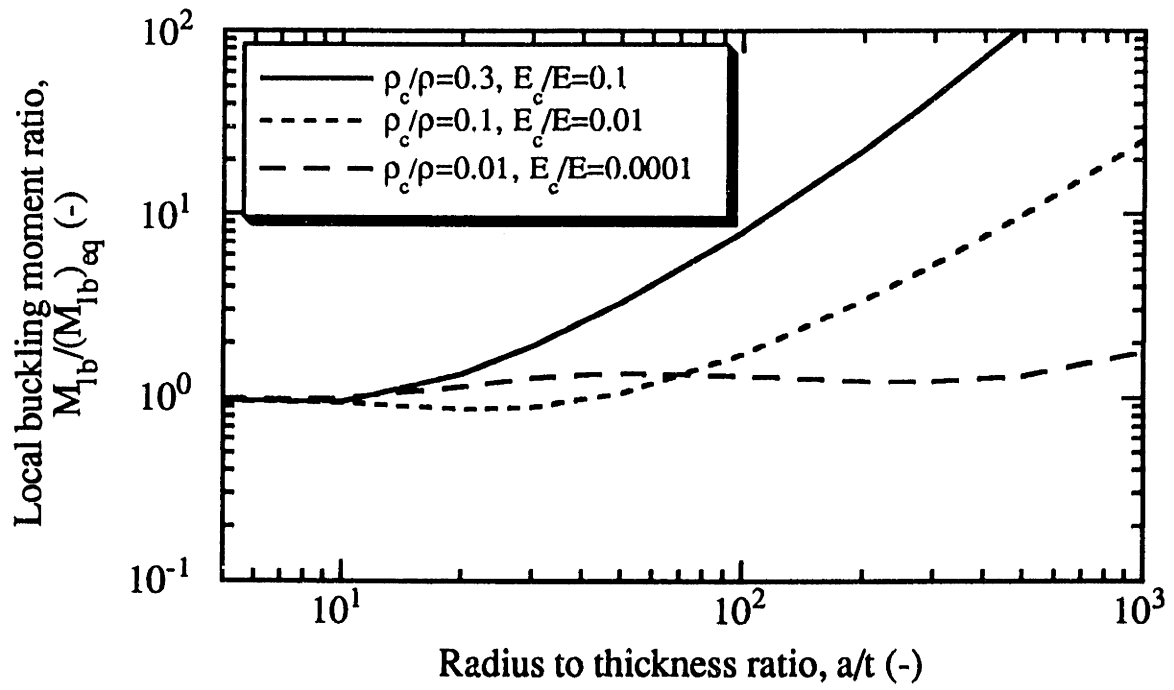
Figure 3.12 Uniaxial compression buckling stress ratio, $\sigma_{cr}/\sigma_0$ plotted against the dimensionless stiffening parameter, $(a/t)^{3/2}(E_c/E)$ comparing our simplified analysis with the theoretical results of Seide (1962) and Yao (1962), the finite element analysis of Weingarten and Wang (1976) and data.

Figure 3.A1(a)  A beam of circular cross-section in pure bending with coordinate axes defined. (b) The distortion of the circular cross-section of the beam due to Poisson's ratio effects.



(a)



(b)

## ELASTIC BUCKLING OF CYLINDRICAL SHELLS WITH ELASTIC CORES II: EXPERIMENTS

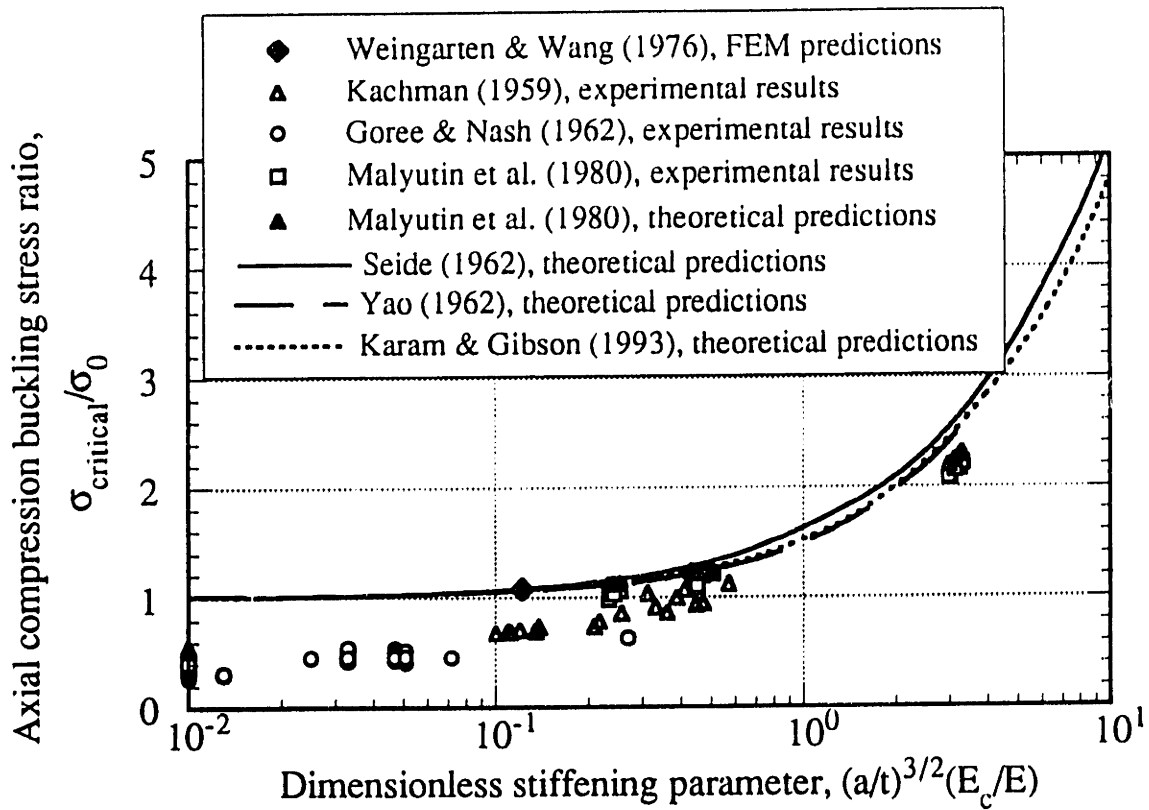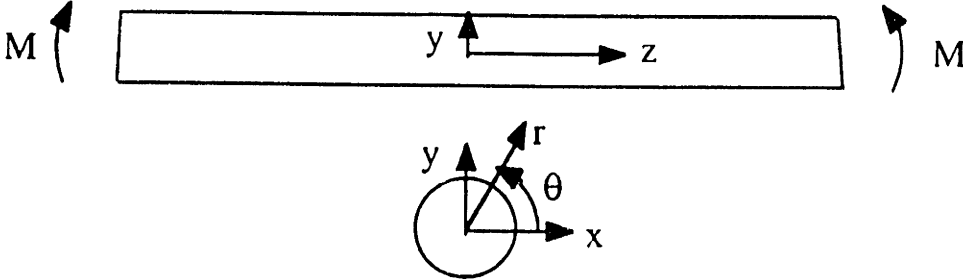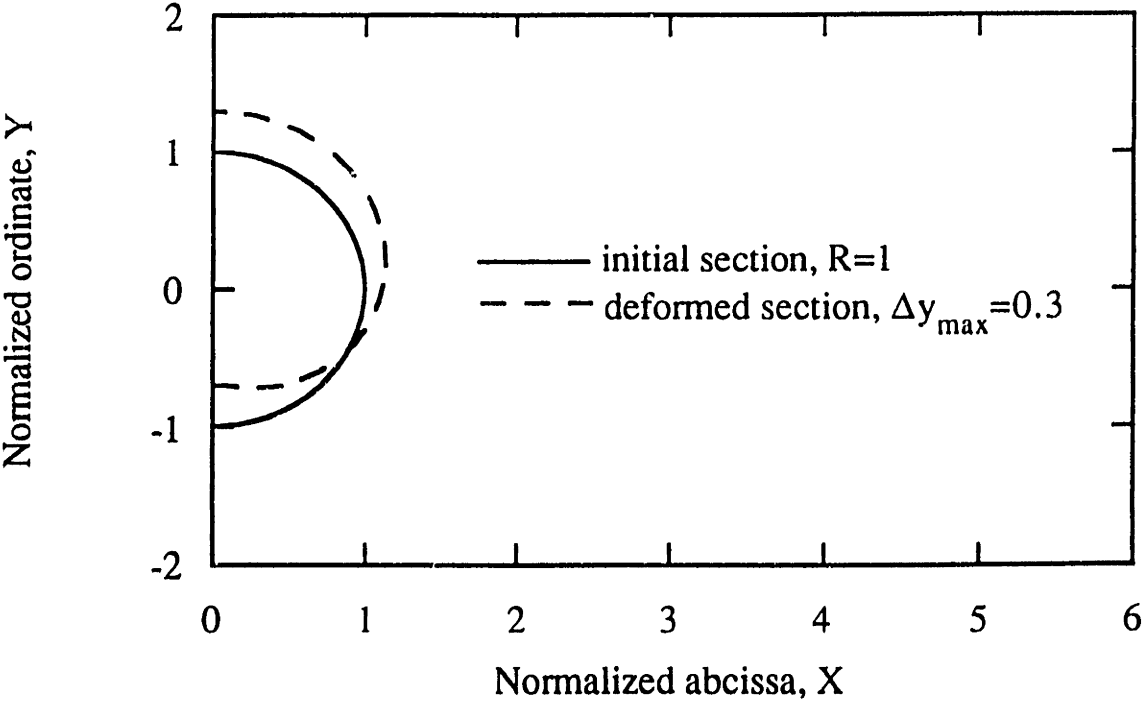*"The principle which makes this development possible is hidden to the eyes but not to the mind; but whether such a development must necessarily come about is completely unknown to us. We know that the principle which makes it possible is in the very nature of body; but there is no clear evidence in that body that there is a principle by which it must necessarily take place."*

St.Augustine (ca. 400)

### 4.1 Introduction

In nature, thin cylindrical shells are often supported by a compliant elastic core. In the previous chapter, we analyzed the local buckling under axial compression and bending of a thin walled cylindrical shell with a compliant core. The results indicated that such shells can be designed to have a higher buckling resistance than hollow shells of equal mass. The results were used to suggest that the elastic core in natural cylindrical shells gives rise to increased buckling resistance. In this chapter we describe experiments to measure the elastic buckling response of silicone rubber shells with and without a compliant core under uniaxial compression and four point bending. The experimental results are well described by the analysis of the previous chapter.

### 4.2 Experimental Methods

Silicone rubber cylindrical shells with and without compliant foam cores were tested in uniaxial compression and four point bending. The uniaxial compressive buckling strength was first measured on hollow cylindrical shells with no compliant core. The shells were then filled with a compliant core and retested. Each specimen was then cored to produce a central bore hole and retested; this procedure was then repeated for

incrementally larger diameter bore holes. The local buckling strength in bending was measured on hollow cylinders and on cylinders partially filled with a compliant core. Typical uniaxial compression and four point bend specimens are shown in Fig. 4.1.

*Uniaxial compression specimens*

Silicone rubber cylindrical shells with nominal shell radius to wall thickness ratios, a/t, of 4.3, 10, 22, 31, 48 were made. The two thickest shells (a/t = 4.3 and 10) were made by mixing liquid rubber (RTV 3110, Dow Corning Corp. Midland, Michigan) with a slow acting catalyst, de-airing with a vaccuum pump for three to five minutes, and pouring the mixture into concentric plexiglass molds for curing. The thinner shells (a/t = 22, 31 and 48) were made by mixing the liquid rubber with a fast acting catalyst, pouring it into a cylindrical mold and rotating the mold around its longitudial axis at 500 rpm until curing was complete. This spin casting technique does not require de-airing as centrifugal force collapses all entrapped air bubbles and ensures nearly perfect thin walled cylinders. Each shell was 150 mm long. Three cylinders of each a/t ratio were made. A detailed tabular description of the specimens is given in Table 4.A1 of the appendix. Three tensile dogbone specimens were cast from each batch of silicone rubber for subsequent measurement of Young's modulus and Poisson's ratio.

The wall thickness of each cylinder was measured at three circumferential locations at two positions along the length using a spring loaded, weighted micrometer accurate to within 0.025 mm (Ames S-4325, B.C.Ames Co., Waltham, MA). Only cylinders with a coefficient of variation of wall thickness of less than 5% were used in subsequent mechanical tests. The mass of each cylinder was measured using an electronic balance (Sauter-E49, Ebingen, Germany), allowing the density of the silicone to be calculated.

After initial testing of the hollow shells in uniaxial compression each shell was filled with a compliant core of foamed silicone rubber (RTV 3-6548, Dow Corning Corp.,

Midland, Michigan) with a nominal relative density of 0.3. The rubber was foamed in place to ensure a good bond between the foam and the shell. The shells were supported in a split cylinder plexiglas mold during the foaming process to minimize distortions to the shell due to foam expansion. Four twenty millimeter cubes of foam cut from blocks cast in the same batch were used to determine its Young's modulus. Four rectangular strips 127mm x 32mm x 10mm were used to determine Poisson's ratio of the foam. Foam densities were calculated from volume and weight measurements on four small rectangular block specimens (140mm x 32mm x 20mm). The dimensions were measured with an electronic digital caliper (Max-Cal, Japan) and the weights measured on the Sauter-E49 balance. After testing the filled cylinders in uniaxial compression a central cylinder of foam was removed using a hole saw in a drill press. The cylinder was then retested in uniaxial compression, the central bore hole diameter increased by some increment and the cylinder retested. This procedure was repeated for bore hole diameters between 25mm and 102mm for each cylinder.

In addition, four pairs of hollow and partially filled cylinders of equal mass were made to compare their buckling resistance. The shells were made from silicone rubber while the cores were made of polyurethane foam. The core:shell modulus ratio was 0.013; the core depth was equal to ~1.6 half buckling wavelengths.

*Four point bending specimens.*

Four point bending tests were performed on hollow silicone rubber cylinders and on silicone rubber cylinders partially filled with a compliant core. The cylindrical shells were spun in the same manner as uniaxial compression specimens using a larger mold operating at a higher speed (1200 rpm). The cylindrical shells had a length of 889 mm, an outside diameter of 146 mm and had radius to wall thickness ratios of a/t= 17.6, 22, 23, 32, 34, 40, 42, and 55. Two cylinders were made with a/t=23 and a/t = 32; a single cylinder was made for each of the remaining a/t ratios. A detailed tabular description of

these specimens is given in Table 4.A2 of the appendix. Each cylinder was then cut longitudinally and bonded to a 25.4 mm thick flat sheet (889 mm long by 458 mm wide) of flexible polyurethane foam ($\rho$ = 15 kg/m$^3$) using a thin layer of freshly mixed silicone rubber. The composite silicone rubber shell lined with the polyurethane foam sheet was then wrapped around a cylindrical mandrel, inserted into a split cylinder mold and bonded together along the seam line with more liquid silicone rubber to form a cylindrical shell with a compliant core. The thickness of the silicone rubber shells was measured in the same manner as the uniaxial compression shells while the shell was cut into a flat sheet. Measurements were made at 152 mm intervals across the sheet; only sheets with coefficients of variation of less than 10% were used in subsequent mechanical tests. The weight of the rubber used to bond the foam to the shell and to bond the longitudinal seam was measured by weighing the different components of the foam-core cylinder as it was made. This weight was then added to the initial weight of the empty rubber tube and a corrected cylinder thickness calculated. Three 25.4 mm cubes of the flexible polyurethane were cut to determine its density and Young's modulus. Nine strips 152mm x 25.4mm x 13mm were cut along each of three mutually perpendicular planes in the sheet to determine Poisson's ratio.

*Mechanical tests*

The Young's modulus and Poisson's ratio of the solid rubber was calculated from data from tensile tests on dog-bone specimens using a universal testing machine (Instron Model 4201, Instron, Corp. Canton, MA). Three specimens from each batch were used to measure Young's modulus and one specimen from each batch was used to measure Poisson's ratio. One batch, from which a single cylindrical shell was made, was represented by only one dogbone specimen. The load was monitored through a 50N load cell. The longitudinal and transverse displacements were monitored using a travelling optical microscope (Titan Tool Supply Co., Buffalo, NY) over a 51 mm and 12.7 mm

gage lengths, respectively; the gauge lengths were marked by either steel pins or by a thin strip of rubber glued to the specimen. Both load and displacements were measured at increasing increments of crosshead displacement.

The Young's moduli of the silicone rubber and polyurethane foams were calculated from compression tests on cubic specimens using the same Instron testing machine. The load was measured with the 50N cell and the displacement was taken as that of the crosshead. The Poisson's ratio of the silicone rubber foam was calculated from longitudinal and transverse elongations monitored with the travelling microscope over gauge lengths of 38 mm and 28 mm, respectively, in tensile tests on thin strips. The Poisson's ratio of the polyurethane foam was measured in a similar fashion, with longitudinal and transverse gage lengths of 25mm, respectively.

The uniaxial compression tests on the cylindrical shells were also performed using the Instron Model 4201 testing machine. The hollow shells were tested first. The top and bottom edges of the shells were fitted into a grooved platen to maintain their circular cross-section at the ends. The top platen had two holes drilled into it to allow air inside the specimen to escape, preventing any internal pressure buildup. The specimens were centered along the loading axis of the machine using the special jig shown in Fig. 4.2. The load, applied through a steel ball centered to within 3mm, was recorded from the load cell while displacements were measured using the crosshead displacement transducer in the machine. The load-deflection data was obtained on an x-y plotter and recorded digitally by a data acquisition system (Hewlett-Packard HP 3497A, Data Control Unit) connected to a personnal computer (Hyundai PC-XT). After buckling each test was stopped and the buckling pattern photographed.

On completion of the tests on empty cylinders, the specimens were filled with silicone rubber foam and retested using the same procedure. Central bore-holes of increasing diameter were then made in the specimens. After each boring, the cylinders

were again retested. Each buckling test was performed three times to verify the repeatability of the results.

While the axial compression tests followed an established and widely accepted procedure (Tennyson, 1963, 1964, 1967; Weingarten et al., 1965a and 1965b; de Neufville, 1965; and Yamaki, 1983), there is no consensus on how to test thin walled tubes in bending. In order to study the moment-curvature relationship and buckling phenomena, a uniform bending moment has to be applied to all or part of the cylinder and maintained to relatively large deflections. Conventional four point bending is the simplest way to achieve a constant bending moment (Rhodes and Harvey, 1971), but at large deflections the loads transmitted through the vertical loading knives apply a drawing action on the rotated specimen (Cimpoeru and Murray, 1993) resulting in undesirable end restraints (Sherman, 1976). In the original work of Brazier (1927) and later Sherman (1983) a pure moment was applied at the ends of specimens rigidly attached to a rotating fixture; the prevention of axial movement of the fixtures caused unwanted axial tensile forces to develop at large deflections. McIvor et al. (1977) used a modified four-point bending set up that was suitable for large deflections but prevented the horizontal translation of the specimen, also leading to axial tensile forces. Reddy (1979) developed a modified four point test restraining the ends of the specimens by spring steel strips that allowed relatively large deflections and partial axial movement. Kyriakides and Shaw (1982, 1987) used a unique experimental rig that maintained constant force, direction and moment arm at large deflections while allowing some axial specimen movement. In their rig the specimen ends are inserted into two wheels each carrying two points of a four point loading set up. The wheels are rotated in opposite directions by shortening a chain running around them, applying a uniform bending moment to the tube in between the wheels. Cimpoeru and Murray (1993) proposed additional improvements on this set up to eliminate friction and the development of tensile forces at very large deflections. Given the requirements of our experimental

program (large beam curvatures, free rotation at the supports, free axial movement, special grips to transmit loading to the beams) we have found it necessary to design and build a modified four point testing rig that can be used with conventional testing machines and yet provide the required characteristics.

The specially built loading rig, designed to be used in the Instron testing machine, is shown in Fig. 4.3. The specimens were gripped at the ends with a closely fitting external cylinder and a tapered conical insert. Each specimen had two 3mm diameter holes drilled into it near the end grips to allow air inside the specimen to escape, preventing any internal pressure buildup. The end grips were extended by solid hardened steel rods fitted into linear bearings, allowing free axial movement in and out of the block supports. Each block support rested on two rotational bearings allowing free rotation in the plane of loading. The load was applied through a universal joint at the midpoint of a loading beam with rollers at fixed locations at its ends. The self-equilibrating loading beam splits the load applied by the machine into two equal forces applied to the end grips at a constant horizontal distance, d, from the center of the support blocks. Sliding counterweights were fitted to the steel rods extending beyond the supports allowing an initial constant moment to be applied to the specimen if needed.

The load was measured using a 500N load cell while the curvature of the beams was monitored with an angular displacement transducer (Model 0605, Transtek Inc., Ellington, CT) measuring the rotation at the supports (Fig. 4.3). The load cell and rotation transducer were both connected to the computerized data acquisition system described above. The bending stiffness of the grips and extension rods was designed to be much larger ( about $2.5 \times 10^3$) than that of the specimens tested so as to concentrate all deformation in the free spanning part of the cylinder. By adjusting the free span of the cylinder, l, and the moment arm, d (Fig. 4.3) in the loading set up the magnitude of the moments and curvatures applied can be widely varied while keeping the support rotations

small and the loading geometry constant. For small end rotations, $\theta \leq 15°$, the curvature of the cylinder, C, and the moment, M, due to the applied load are given by :

$$C = \frac{2\theta}{l}$$

$$M = \frac{Pd}{2}$$

(4.1)

where q is in radians.

Under their self weight, the cylinders deflect, rotating the ends. This initial end rotation was then reduced to zero by setting the counterweights appropriately. At the beginning of the test, then, the cylinder was in a fixed-fixed end condition with zero rotation and curvature at the supports. At this point, the cylinder was subject to its own dead weight between the grips and the end moment from the counterweights causing an initial moment, $M_{dl}$, and curvature, $C_{dl}$, at the midspan of the beam. The cylinders were then loaded to failure using the Instron Model 4201 with a crosshead speed of 5mm/min. Under these conditions the cylinders buckled locally in the middle away from t! . end grips. Failure was defined as the loss of moment carrying capacity.

In a separate series of tests, the ovalization of the midspan of the beams was measured with the travelling microscope for fixed bending moments applied by the counterweights. The rotation at the support was measured with the angular rotation transducer.


## 4.3 Experimental Results

The measured density, Young's modulus and Poisson's ratio of the solid silicone rubber, foamed silicone rubber and foamed polyurethane used in the experimental program are listed in Table 4.1. The ratio of the core to shell moduli for the rubber foam is $E_c/E \approx 0.1$, while for the polyurethane foam it is $E_c/E \approx 0.01$.

Under uniaxial compression, the hollow cylinders buckled in a diamond pattern showing buckling wavelengths in both the circumferential and longitudinal directions, while the cylinders with the compliant core buckled in the axisymmetric mode with only longitudinal wavelength (Fig. 4.4). The longitudinal buckling wavelength of the hollow cylinders was, as expected, several times that of the foam core cylinders. For a given cylinder with a compliant core, increasing the bore-hole diameter had little effect on the buckling wavelength until the core became very thin (core to shell ratios, c/t, of about 5). At this point the shell and underlying foam acted as an equivalent isotropic shell and buckled together as a unit. Typical load deflection curves for two hollow cylinders are shown in Fig. 4.5. The normalized uniaxial buckling stress, $\sigma_{cr}/E$, for the hollow cylinders is plotted against the ratio of shell radius to wall thickness, a/t, in Fig. 4.6. Each point represents the average buckling load of tests on three cylinders; the vertical lines represent the maximum and minimum buckling loads. The buckling load for each cylinder was obtained by averaging three repeated buckling measurements; the variation in single cylinder measurements did not exceed 5%. The calculated buckling load, given by eqn (3.1) in Chapter 3, is represented by the solid line in the figure: the theory describes the data well. The load deflection curves for the fully and partially filled cylinders show several distinct behaviors (Fig. 4.7). In the thicker walled cylinders (a/t = 4.3, 10) buckling causes a decrease in load; if the core is sufficiently deep it can carry additional load at reduced stiffness after buckling of the shell (Fig. 4.7a). This behavior is consistent with the numerical predictions of Almroth and Brush (1963) for the postbuckling behavior of core-stabilised cylinders. At a/t = 22 there is a transition in behaviour: cylinders with thick cores show bilinear behaviour with reduced slope at higher loads while the cylinders with thin cores show a maximum load at which buckling occurs (Fig. 4.7b). And the thinnest walled cylinders (a/t = 31, 48) all show a bilinear load deflection curve (Fig. 4.7c). Axisymmetric buckling was observed to occur at the peak load in curves with a maximum or at the point at which the slope of the load-

deflection curve reduced in the bilinear curves. Data for the uniaxial buckling loads are plotted against the core to thickness ratio, c/t, in Fig. 4.8. The measured buckling loads are normalized by the theoretical buckling load for the hollow cylinder of the same a/t. Each point represents the average buckling load of tests on three cylinders; the vertical lines represent the maximum and minimum buckling loads. The leftmost point on each plot represents the hollow cylinder (c/t=0), while the rightmost point represents the fully filled cylinder (c/t = a/t-1/2). Intermediate points at increasing c/t correspond to increasing core thickness. The value of c/t for which the stresses within the core decay to a negligible level is indicated by $(c/t)_o$.

In Fig. 4.9, the number of axisymmetric buckling wavelengths for the fully filled tubes is plotted against the radius to shell thickness ratio, a/t. The solid line represents the number of wavelengths calculated from eqn (3.14) of the previous chapter based on the initial length of the cylinder while the dashed line respresents that based on the actual shortened length of the cylinder at the instant of buckling. Figure 4.10 shows the uniaxial buckling stress for the fully filled cylinder of given a/t divided by the buckling stress of a hollow cylinder of same a/t, $\sigma_{cr}/\sigma_o$, plotted against the dimensionless core stiffening parameter suggested by Seide (1962), $(a/t)^{3/2}(E_c/E)$, comparing our results with theoretical predictions and a compilation of data from the literature.

Four pairs of hollow and partially filled cylinders of equal mass were tested in uniaxial compression to compare their buckling resistance. The cores of the partially filled cylinders were made of polyurethane foam with a core:shell modulus ratio of 0.013; the core depth was equal to 1.6 buckling half wavelengths. The buckling loads are compared in Table 4.2. The partially filled cylinders had measured buckling loads ranging from 1.35 to 3.70 times those of the hollow cylinders of equal weight, in comparison to theoretical buckling load ratios of 1.8 to 5.22.

The results of the four point bend tests are shown in Figs. 4.11-4.15. Figure 4.11 shows photographs of local buckling of the compressive face and final collapse of a

partially filled cylinder. Figure 4.12 shows moment-curvature relationships for typical hollow and partially filled cylinders. The two measurements shown on each graph are made with the seam of the tube at the neutral axis rotated either plus or minus $180\infty$; the local buckling moment was taken to be the maximum moment capacity of the beam and was calculated from the average of the two measurements. The initial offset arises from the initial dead load, as described in the methods section. The average local buckling moment for the hollow cylinders is plotted against the shell radius to wall thickness ratio, a/t, in Fig. 4.13a. The degree of ovalization of one of the hollow cylinders is plotted against curvature in Fig. 4.13b. The degree of ovalization of the partially filled cylinders was measured to be less than 1.5% for curvatures up to 0.6 $m^{-1}$, which we took to be negligible. The average local buckling moment of the partially filled cylinders is plotted against the shell radius to wall thickness ratio, a/t, in Fig. 4.14. Figure 4.15 plots the ratio of the measured local buckling moments of the partially filled cylinders to the theoretical local buckling moment of hollow cylinders of equal weight. Superimposed on the figure are the ratios predicted from the analysis of the previous chapter (eqn 3.47). Table 4.3 compares the theoretical and experimental local buckling moments of four pairs of partially filled and hollow cylinders of equal weight. The partially filled cylinders had measured buckling moments ranging from 2.43 to 4.84 times those of the hollow cylinders of equal weight, in comparison to theoretical buckling load ratios of 2.15 to 2.99.

### 4.4 Discussion

*Uniaxial compression*

The load deflection curves for the hollow cylinders in uniaxial compression show a well-defined maximum load at which buckling occurs (Fig. 4.5). The measured buckling loads are described well by the analysis of the previous chapter (eqn 3.1) (Fig. 4.6). The excellent agreement between the analysis and data is due to the near perfect

specimens produced by the spin-casting manufacturing technique (Tennyson, 1963, 1967) and to the relatively small radius to thickness ratios used.

Data for the effect of increasing the central bore hole diameter on the uniaxial buckling load are compared with the analysis in Fig. 4.8. The solid line represents the calculated normalized buckling load, using eqn (3.1, 3.20 and 3.42) of the previous chapter. For values of c/t < (c/t)$_0$ (that is, core thicknesses less than that required for the stresses in the core to decay to a negligible value) the modulus of the elastic foundation k$_e$, was modified as follows (Gough et al., 1940):

$$k_e = \frac{2E_c}{\lambda} \frac{\sinh(\frac{c}{\lambda})\cosh(\frac{c}{\lambda}) - \frac{c}{\lambda}}{(3 - v_c)(1 + v_c)\sinh^2(\frac{c}{\lambda}) + (1 + v_c)^2(\frac{c}{\lambda})^2 + 4} \qquad (4.2)$$

where the variables are defined in the previous paper. The dashed lines describe combined buckling of the shell and core (eqn (3.41) of the previous chapter). The mean buckling load is indicated by the filled diamond points with a vertical line representing the range. The theory describes the data well for a/t = 4.3 and 10, confirming the use of the analysis for stress decay within the core. For a/t = 22 and 48, the mean measured buckling loads are about 75% of the expected. And for a/t = 31, they are about 50% of the expected. The discrepancies arise from imperfections in the thinner walled shells and, at very low c/t, due to accumulated damage, namely shell-core debonding, from repeated coring and testing. Imperfections arose from internal pressure in the core during the foaming process causing barrelling of the thinner shells such that an originally straight longitudinal strip of the shell bowed out slightly. Profile measurements of the thicker walled shells (a/t=4.3 and 10) (Fig. 4.A1a) showed negligible barreling with maximum magnitudes of between 1 and 2 mm, corresponding to one tenth to one third of the shell thicknesses. Some of the thinner walled shells (a/t=22, 31 and 48) (Fig. 4A1b), on the other hand, gave an approximately sinusoidal profile with a maximum amplitude varying between 3 and 5 mm, or one to three times the shell thickness. The profiles fit the

equation $z = z_{max}\sin(\pi x/152)$ with a correlation factor $R > 0.92$, where z is the outward displacement, $z_{max}$ is the maximum barreling amplitude in mm given in the appendix (Table 4.A3), x is the distance in mm along the length and z and x are measured in mm. Given the long wavelength of the imperfection it seems that the decrease in the buckling load is dependent on the maximum amplitude of the barreling. For the profiles measured, specimens D4 (a/t=31), D5 (a/t=31) and E2 (a/t=48) showed the most barreling along with the highest reduction in the buckling stress.

Previous investigations indicated that for an axisymmetric imperfection in the shape of the buckling mode of amplitude equal to the thickness of the shell, the buckling load of a hollow shell is reduced by 75% (Koiter, 1963). The presence of relatively small internal pressures can reduce the drop in the buckling loads to less than 30% (Hutchinson, 1965): the effect of the compliant core in our specimens is similar to that of internal pressure, reducing the effect of initial imperfections.

To verify that barreling was the correct cause of the decrease in buckling loads three "quasi-perfect" cylinders of a/t=22,31,48 whe·e made and tested (Table 4.A1). The cores were separately foamed in rigid molds, precisely machined to the inside dimensions of the empty shells, then slipped in and bonded with a minimal amount of liquid rubber. The effect of the bonding rubber was included in the analysis similarly to the bending specimens. These specimen showed almost no barreling (Table 4.A3, Fig. 4A1c). The buckling loads of these special specimens are represented in Figs.4.8c,4.8d and 4.8e, by the open diamond symbols showing very good agreement with the theoretical predictions.

The contribution of the foam core in resisting axial compression results in a stable postbuckling regime. If serviceability is taken as the failure criterion, then the load carried by the imperfect buckled cylinder at the deflection predicted by the linear classical solution should be substituted for the bifurcation load. This will result in higher failure loads for the imperfect cylinders and improved agreement with theoretical predictions.

The number of axisymmetric buckling wavelengths for the filled cylinders is plotted against a/t in Fig. 4.9. The solid line represents theoretical values based on the initial length of the cylinder while the dashed line takes account of the axial shortening of the cylinder in the linear elastic range before buckling occurs. Agreement is good.

The data from this study are compared with those of previous studies and with various theoretical models in Fig. 4.10. The new results, with the exception of the points corresponding to the most barreled specimens with a/t=22,31,and 48, agree well with the theoretical predictions and extend the range of experimental verification by about one log cycle.

*Local buckling*

Typical moment curvature relationships for the four point bend specimens are presented in Fig. 4.12. The theoretical moment curvature relationship can be derived from the results of the companion paper as:

$$M = \pi E t a^3 C \left[ \left( 1 + \frac{\alpha a}{4t}\left( 1 - \frac{b^4}{a^4} \right) + \frac{\alpha \beta' a}{8t} \right) - \frac{3}{2}\frac{a^4}{t^2}(1 - v^2)\frac{\left( 1 + \frac{\alpha a}{4t}\left( 1 - \frac{b^4}{a^4} \right) \right)^2}{\left( 1 + \frac{2\alpha \beta a^3}{3t^3}(1 - v^2) \right)}C^2 \right] \quad (4.3)$$

with the variables defined as the companion paper, and b and b' modified to account for the central bore hole of radius b. Note that in Fig. 4.12 the experimental moment curvature curves start with an offset equal to the initial conditions caused by the dead load. The experimental plots of the partially filled cylinders are linear up to about half of the theoretical critical curvature, $C_{cr}$, and then become nonlinear, reaching a maximum. The initial linear behavior is slightly stiffer than expected due to an increase in the gripping area of the conical inserts of the bending jig as the curvature increases; this

117

increased stiffness is most pronounced in the most compliant tubes with high a/t ratios. The last part of the plots shows a small plateau corresponding to stable local buckling which is usually followed by the localization of one buckle, the formation of an elastic hinge and the collapse of the bent cylinder (Fig. 4.11b). In the unique case of the cylinder with a/t=40, collapse did not take place and the tests were stopped when the maximum range of the x-y plotter was reached. The measured buckling wavelength was found to be between 25 and 32mm, close to the theoretical buckling wavelength of 31mm.

The measured local buckling moments of the hollow tubes are plotted against the radius to thickness ratio, a/t, in Fig. 4.13a. The data lie between 70-95% of the theoretical values represented by the solid line. The discrepancies are caused by the variability in the thickness of the long bending specimens. The buckling moment is proportional to the square of the thickness of the tube; some individual thickness measurements deviated from their average by up to 15%. The ovalization-curvature relationship for hollow tubes was well described by theory (eqn (3.23) of the previous chapter) with stable ovalizations of up to 8% measured (Fig. 4.13b).

The local buckling moments of the silicone rubber tubes with flexible polyurethane foam cores are well described by the analysis of the previous chapter (eqns 3.30 and 3.37 to 3.40) (Fig. 4.14). With one exception all of the data points lie slightly below the expected values; the discrepancies are due to local imperfections and eccentricities. The buckling load for a/t = 40 exceeded predictions by about 15%. This is within the statistical variability of the different experimentally measured properties, especially the modulus of the rubber which showed a standard deviation of around 10%. The measured ovalizations of the partially filled four point bend tubes were found to be less that 1.5% at 80% of the critical curvatures for buckling.

Yabuta (1980) used the results of Seide (1962) for axial compression as the local buckling criterion for cylindrical shells under buckling, neglecting any ovalisation or

Brazier buckling. His limited data for Mylar cylinders filled with an elastic silicone rubber core are within 20% of the numerical predictions, consistent with our observation that ovalization can be neglected in a cylindrical shell with a compliant core. But his data for hollow cylinders are less than 60% of the predicted loads as a result of neglecting the ovalization at local buckling. Accounting for ovalization ($\zeta_{lb}=0.145$) the theoretical buckling stress is reduced to $(1-3\zeta_{lb}) = 56\%$ of its axial compression value bringing the theory into good agreement with the data.

In Fig. 4.15 the ratios of the measured local buckling moment of the partially filled cylinders to the theoretical local buckling moment of hollow cylinders of equal weight, show gains of 50 to 400% in strength for a/t = 20 to 50. The data points show the same increasing trend with increasing a/t that the theory predicts, falling at most 25% below predictions. The range of a/t are characteristic of plant stems and grasses, which have a/t ratios from 10 to 70.

## 4.5 Conclusions

The uniaxial compression data for the buckling load, the effect of core depth and the buckling wavelength are well described by the analysis of the companion paper. The measured buckling stresses of foam filled cylinders fell along the trend compiled from the literature and have substantially extended the experimental verification range of the theoretical predictions (Fig. 4.10). Cylinders with foam cores showed a reduced sensitivity to imperfections caused by the manufacturing process and displayed a stable postbuckling behavior, both missing characteristics in conventional hollow shells.

The elastic buckling of both hollow and partially filled cylindrical shells in pure bending was shown to be well described by combining an axial buckling stress criterion with Brazier's ovalisation analysis. The presence of a foam core reduced the ovalisation at incipient local buckling from 15% for an empty tube to less than 1.5%. The measured moment curvature relationships showed a nonlinear behavior while the analysis predicted

an almost linear relationship. The discrepancy was found to be due to gripping friction and premature local buckling. The critical buckling loads and bending moments of partially filled cylinders increased by up to 400% above those of equivalent hollow cylinders, as suggested by the analysis in Chapter 3.

The results suggest that biomimicking of natural cylindrical shells such as plant stems may lead to improved design of engineering cylindrical shell structures.

## References

Almroth, B.O. and Brush, D.O (1963) " Postbuckling behavior of pressure or core-stabilized cylinders under axial compression" *AIAA Journal*, Vol. 1, No. 10, pp 2338-2341

Brazier, L.G. (1927) " On the flexure of thin cylindrical shells and other thin sections" *Proc. Roy. Soc. Lond.*, Vol. 116 A, pp 104-114

Calladine, C.R. (1983) Theory of shell structures Cambridge University Press, Cambridge, Great Britain

Cimpoeru, S.J. and Murray, N.W. (1993) " The large deflection pure bending properties of a square thin-walled tube" *Int. J. Mech. Sci.*, Vol. 35, No. 3/4, pp 247-256

de Neufville, R.L. (1965) " Buckling mechanism of thin cylinders under axial load" Ph.D. Thesis, Massachusetts Institute of Technology, Cambridge, Massachusetts, USA

Gibson, L.J. and Ashby, M.F. (1988) " Cellular solids: structure and properties" Pergammon Press, New York, NY, USA

Gough, G.S., Elam, C.F. and deBruyne, N.A. (1940) " The stabilisation of a thin sheet by a continuous supporting medium" *J. Roy. Aero. Soc.*, Vol. 44, pp 12-43

Hutchinson, J.W. (1965a) " Axial buckling of pressurized imperfect cylindrical shells" *AIAA Journal*, Vol. 3, No. 8, pp 1461-1466

Hutchinson, J.W. (1965b) " Buckling of imperfect cylindrical shells under axial compression and external pressure" *AIAA Journal*, Vol. 3, No. 10, pp 1968-1970

Hutchinson , J.W. (1968) " Buckling and initial postbuckling behavior of oval cylindrical shells under axial compresion" *J. Appl. Mech. ASME*, Vol. 35, pp 66-72

Hutchinson, J.W., Tennyson, R.C. and Muggeridge, D.B. (1971) " Effect of local axisymmetric imperfection on the buckling behavior of a circular cylindrical shell under axial compression" *AIAA Journal*, Vol. 9, No. 1, pp 48-52

Koiter, W.T. (1945) " On the stability of elastic equilibrium" Ph.D. thesis, Delft, H.J. Paris Pub., Amterdam, Holland

Koiter, W.T. (1963) " Elastic stability and post-buckling behavior" Proceedings Symposium Non-Linear Problems, R.E. Langer ed., University of Wisconsin Press, Madison, WI pp 257-275

Kyriakides, S. and Shaw, P.K. (1982) " Response and stability of elastoplastic circular pipes under combined bending and external pressure" *Int. J. Solids Structures*, Vol. 18, No. 11, pp 957-973

Kyriakides, S. and Shaw, P.K. (1987) " Inelastic buckling of tubes under cyclic bending" *J. Pressure Vessel Tech.*, Vol. 109, 169-178

McIvor, I.K., Anderson, W.J. and Bijak-Zochowski, M. (1977) " An experimental study of the large deformation of plastic hinges" *Int. J. Solids Structures*, Vol. 13, pp 53-61

Reddy, B.D. (1979) "An experimental study of the plastic buckling of circular cylinders in pure bending" *Int. J. Solids Structures*, Vol. 15, pp 669-683

Rhodes, J. and Harvey, M. (1971) " Alternative approach to light gage beam design" *J. Struct. Div. Proc. ASCE*, Vol. 97, pp 2119-2135

Seide, P. and Weingarten, V.I. (1961) " On the buckling of circular cylinders under pure bending" *J. Appl. Mech. ASME*, Vol. 28, pp 112-116

Seide, P. (1962) " The stability under axial compression and lateral pressure of circular cylindrical shells with a soft elastic core" *J. Aerosp. Sci.*, Vol. 29, No. 7, pp 851-862

Sherman, D.R. (1976) " Tests of circular steel tubes in bending" *J. Struct. Div. ASCE*, Vol. 102, ST11, pp 2181-2195

Sherman, D.R. (1983) " Bending capacity of fabricated pipes" Report, Department of Civil Engineering, University of Wisconsin-Milwaukee, Wisconsin, USA

Tennyson, R.C. (1963) " A note on the classical buckling of load of circular cylindrical shells under axial compresion" *AIAA Journal*, Vol. 1, No. 2, pp 475-476

Tennyson, R.C. (1964) " Buckling of circular cylindrical shells in axial compresion" *AIAA Journal*, Vol. 2, No. 7, pp 1351-1353

Tennyson, R.C. (1967) Photoelastic circular cylinders in axial compression, STP 419, American Society for Testing and Materials, Philadelphia, PA, USA

Tennyson, R.C. and Muggeridge, D.B. (1969) " Buckling of axisymmetric imperfect circular cylindrical shells under axial compresion" *AIAA Journal*, Vol. 7, No. 11, pp 2127-2131

Weingarten, V.I., Morgan, E.J. and Seide, Paul (1965a) " Elastic stability of thin-walled cylindrical and conical shells under axial compression" *AIAA Journal*, Vol. 3, No. 3, pp 500-505

Weingarten, V.I., Morgan, E.J. and Seide, Paul (1965b) " Elastic stability of thin-walled cylindrical and conical shells under combined internal pressure and axial compression" *AIAA Journal*, Vol. 3 No. 3, pp 500-505

Yabuta, T. (1980) " Effects of elastic supports on the buckling of circular cylindrical shells under bending" *J. Appl. Mech. ASME*, Vol. 47, pp 866-870

Yamaki, N. (1984) Elastic stability of circular cylindrical shells, North-Holland Series in Applied Mathematics and Mechanics, Elsevier Science Publishing Co., New York, NY, USA

## Table 4.1 Material Properties

| Property | Solid Rubber | Foam Rubber | Foam Polyurethane |
|---|---|---|---|
| Density (Mg/m³) | 1.17(0.022)† | 0.40(0.01) | 0.015(0.002) |
| Young's modulus (MPa) | 2.2* | 0.20(0.024) | 0.028(0.0032) |
| Poisson's ratio (-) | 0.48(0.009) | 0.32(0.073) | 0.45(0.10)†† |

† number between parenthesis is the standard deviation

* Values for the Young's modulus varied between 1.41 and 2.39 GPa, depending on the type of catalyst and the amount of thinner used. The theoretical buckling loads and local bending moments were calculated using the value of E corresponding to the batch from which each cylinder was made (see Appendix Table 4.A1 and 4.A2).

†† The polyurethane foam showed anisotropic with Poisson's ratios averaging 0.3, 0.46 and 0.55 along three orthogonal axes. In the numerical model, $n_c$ was set to 0.3. Both 0.3 and 0.45 give negligible ovalisations, and the use of 0.45 instead of 0.3 for the local buckling stress results in an overestimate of the buckling stress of less than 5%.

Table 4.2 Uniaxial Compression Buckling Loads for Hollow and Partially Filled
Cylinders of Equal Weight

| Mass (g) | a/t | c/t | $P_{expt}(N)$ | $P_{theory}(N)$ | $P_{core}/P_{empty}(-)$ (expt) | $P_{core}/P_{empty}(-)$ (theory) |
|---|---|---|---|---|---|---|
| 228 | 32.5 | 12.5 | 160 | 166 | 1.54 | 1.80 |
| 218 | 22 | - | 104 | 92 | | |
| 157 | 40 | 15 | 73 | 108 | 1.35 | 2.00 |
| 150 | 26 | - | 54 | 54 | | |
| 671 | 65 | 11 | 290 | 400 | 2.44 | 3.01 |
| 710 | 37 | - | 119 | 133 | | |
| 352 | 125 | 21 | 85 | 235 | 3.70 | 5.22 |
| 350 | 65 | - | 23 | 45 | | |

Notes:
Cylinders had solid silicone rubber shells with a flexible polyurethane core with c/t≈1.6
buckling half wavelengths

**Table 4.3 Local Buckling Moments for Empty and Partially Filled Cylinders of Equal Weight**

| Mass (g) | a/t | c/t | $M_{lb}$ expt(Nm) | $M_{lb}$ theo(Nm) | $M_{lb\ core}/M_{lb\ empty}$ expt (-) | $M_{lb\ core}/M_{lb\ empty}$ theo (-) |
|---|---|---|---|---|---|---|
| 1971 | 20 | 7 | 5.10 | 6.34 | 2.43 | 2.15 |
| 1976 | 17.6 | - | 2.10 | 2.95 | | |
| 1566 | 25 | 8.7 | 4.20 | 4.66 | 3.00 | 2.77 |
| 1550 | 23 | .. | 1.40 | 1.68 | | |
| 1505 | 27 | 9.5 | 3.50 | 4.16 | 2.50 | 2.48 |
| 1540 | 23 | - | 1.40 | 1.68 | | |
| 1172 | 40 | 14 | 3.05 | 2.60 | 4.84 | 2.99 |
| 1101 | 32 | - | 0.63 | 0.87 | | |

## Appendix : Dimensions and Properties of the Specimens Used in the Experimental Program

Table 4.A1.Elastic Moduli of the Solid Rubber Hollow Uniaxial Compression Specimens

| Specimen Designation | D(mm) | t (mm) | a/t (-)† | E (Mpa) |
|---|---|---|---|---|
| A2(S 10%,nd) | 113 | 11.80 | 4.3 | 1.97 (0.126)†† |
| A3(S 10%,d) | 113 | 11.90 | 4.3 | 2.204 (0.023) |
| A4(S 10%,d) | 113 | 11.82 | 4.3 | 2.197 (0.022) |
| B3(S 10%,nd) | 133 | 6.23 | 10 | 1.97 (0.126) |
| B4(S 10%,d) | 133 | 6.30 | 10 | 2.204 (0.023) |
| B5(S 10%,d) | 133 | 6.28 | 10 | 2.197 (0.022) |
| C1(S 10%,sp) | 132 | 2.77 | 22 | 2.197 (0.022) |
| C2(FT 10%,sp) | 132 | 2.92 | 22 | 1.412 (0.078) |
| C3(F 10%,sp) | 132 | 2.83 | 22 | 2.388 (0.144) |
| C4*(F 10%,sp) | 132 | 3.02 | 22 | 2.388 (0.144) |
| D3(F 10%,sp) | 132 | 2.02 | 31 | 2.33  - |
| D4(F 10%,sp) | 132 | 2.12 | 31 | 2.388 (0.144) |
| D5(F 10%,sp) | 132 | 2.05 | 31 | 2.388 (0.144) |
| E1(FT 10%,sp) | 132 | 1.37 | 48 | 1.412 (0.078) |
| E2(F 10%,sp) | 132 | 1.26 | 48 | 2.388 (0.144) |
| E3(F 10%,sp) | 132 | 1.46 | 48 | 2.388 (0.144) |

"Quasi-perfect" specimens

| Specimen Designation | D(mm) | t (mm) | a/t (-)† | E (Mpa) |
|---|---|---|---|---|
| C5(F 10%, sp) | 132 | 2.565 | 22 | 2.110 (0.090) |
| D7(F 10%, sp) | 132 | 2.014 | 31 | " |
| E5(F 10%, sp) | 132 | 1.338 | 48 | " |

Note: in the specimen designation, S stands for slow catalyst, F for fast catalyst, FT for fast catalyst and thinner, nd, d and sp for not de-aired, de-aired and spun respectively

† a/t ratios are the mean values of the actual a/t ratios calculated from the outer diameter, D, and the measured thicknesses, t, of the shell as a/t=(D-t)/2t, for the five size groups

†† numbers between parenthesis are standard deviations

* cylinder C4 was kept empty

Table 4.A2.Elastic Moduli of the Solid Rubber Hollow Four Point Bending Specimens

| Specimen Designation | t (mm) | a/t (-)† | a/t_cor. (-)†† | E (Mpa) |
|---|---|---|---|---|
| C7(F 10%,sp) | 1.73 | 42 | 29 | 2.2 (0.204)** |
| C8(F 10%,sp) | 1.32 | 55 | 40 | " |
| C9(F 10%,sp) | 2.25 | 32 | 25 | " |
| C11*(F 10%,sp) | 2.25 | 32 | - | " |
| C12(F 10%,sp) | 1.83 | 40 | 28 | " |
| C13(F 10%,sp) | 2.16 | 34 | 27 | " |
| C15(F 10%,sp) | 3.28 | 22 | 19 | " |
| C16(F 10%,sp) | 3.12 | 23 | 20 | " |
| C17*(F 10%,sp) | 3.12 | 23 | - | " |
| C18*(F 10%,sp) | 4.15 | 17.6 | - | " |

Note: in the specimen designation, F stands for fast catalyst,and sp for spun

† a/t ratios are calculated from the outer diameter, D=146mm, and the measured thicknesses, t, of the shell as a/t=(D-t)/2t

†† (a/t)_cor.are the a/t ratios of the foam filled cylinders corrected to account for the additional solid rubber used to bond the foam and seal the shell

* cylinders C11, C17 and C18 were kept empty

** numbers between parenthesis are standard deviations

Table 4.A3. Maximum amplitude of profile barreling in axially compressed cylinders with a foamed in place core

| Specimen designation | Maximum barreling amplitude (mm) | $z_{max}/t$ (-) |
|---|---|---|
| A4 | 1.25 | 0.1 |
| B5 | 2.0 | 0.3 |
| C3 | 4.03 | 1.4 |
| D4 | 4.95 | 2.3 |
| D5 | 4.11 | 2.0 |
| E1 | 3.68 | 2.7 |
| E2 | 5.0 | 3.9 |

*"Quasi-perfect" specimen, core not foamed in place*

| | | |
|---|---|---|
| C5 | 1.15 | 0.4 |
| D7 | 1.65 | 0.8 |
| E5 | 1.15 | 0.9 |

Figure 4.1: a) hollow b) fully filled and c) partially filled uniaxial compression specimens; and d) bending specimen.
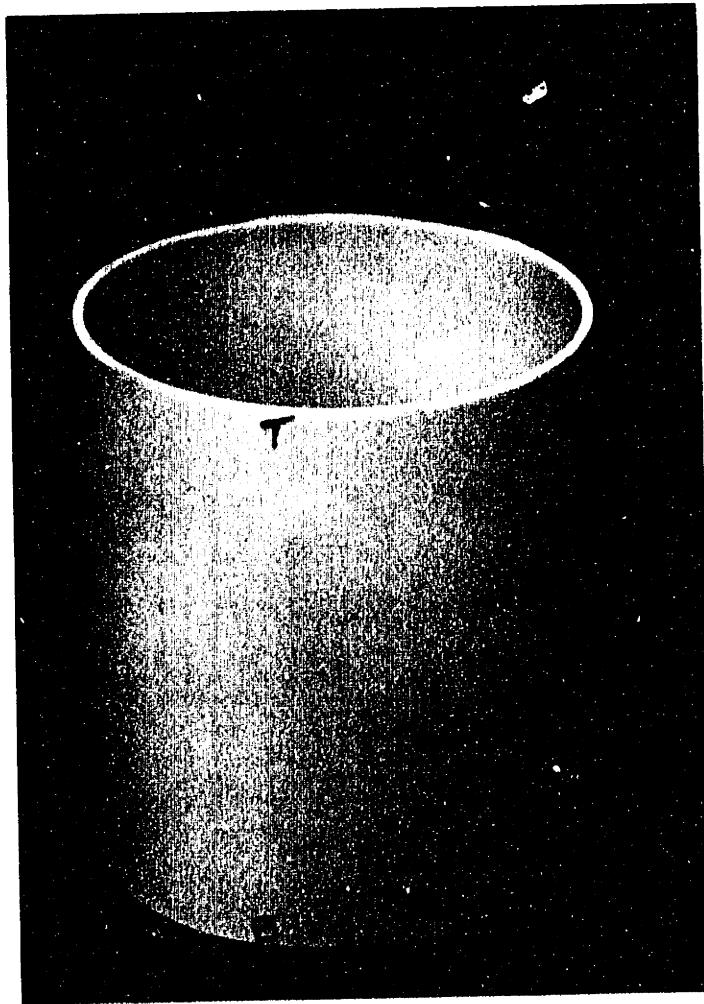


(a)

Figure 4.1: (b)
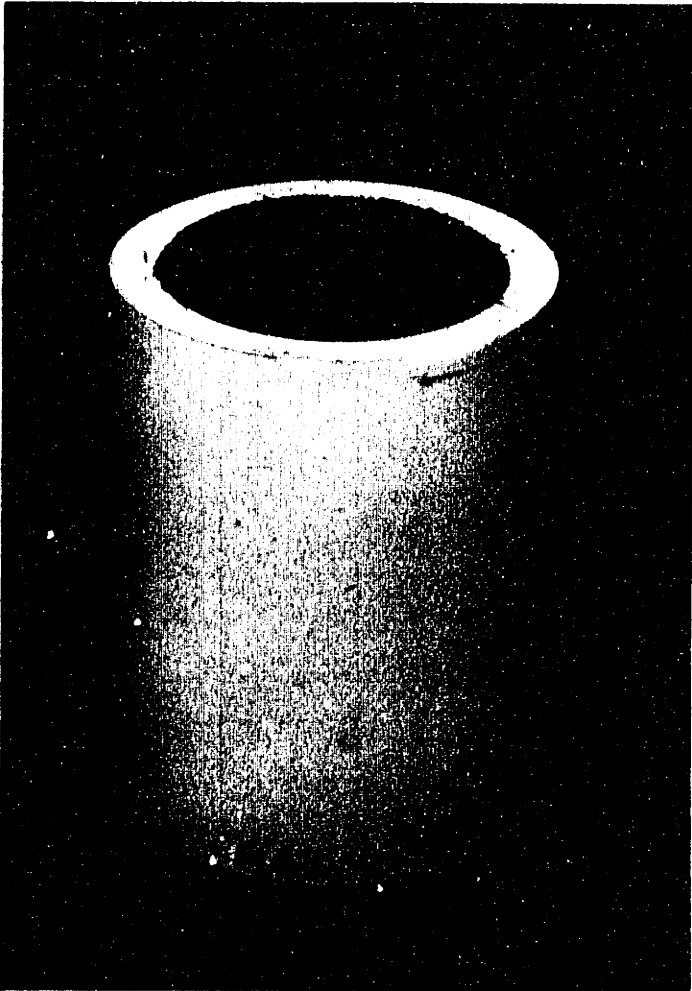
Figure 4.1: (c)

Figure 4.1: (d)
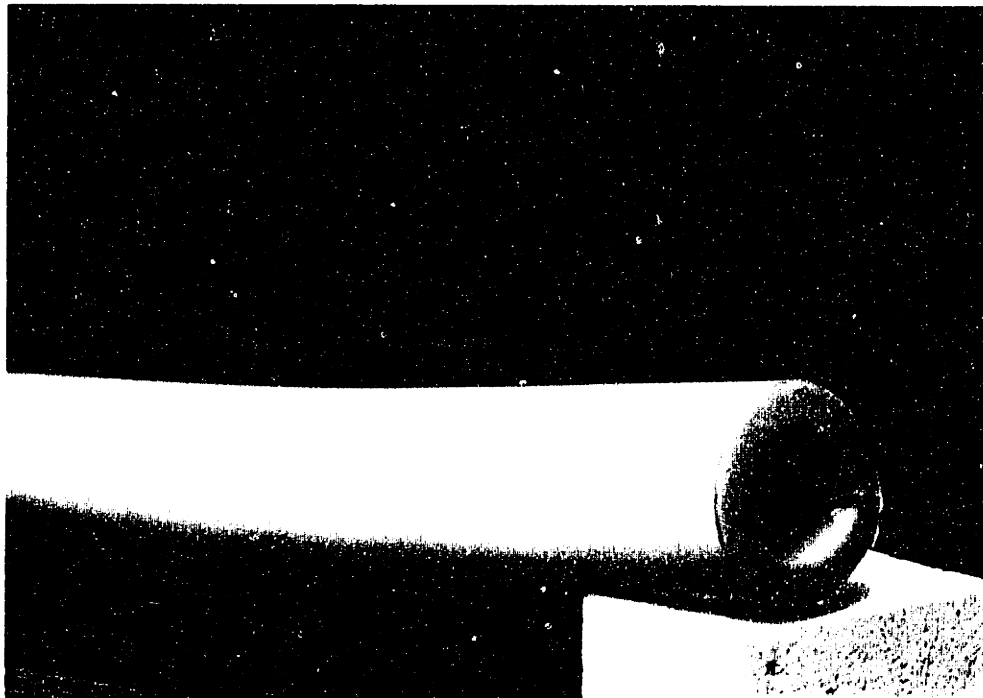
Figure 4.2: Centering jig for uniaxial compression tests.
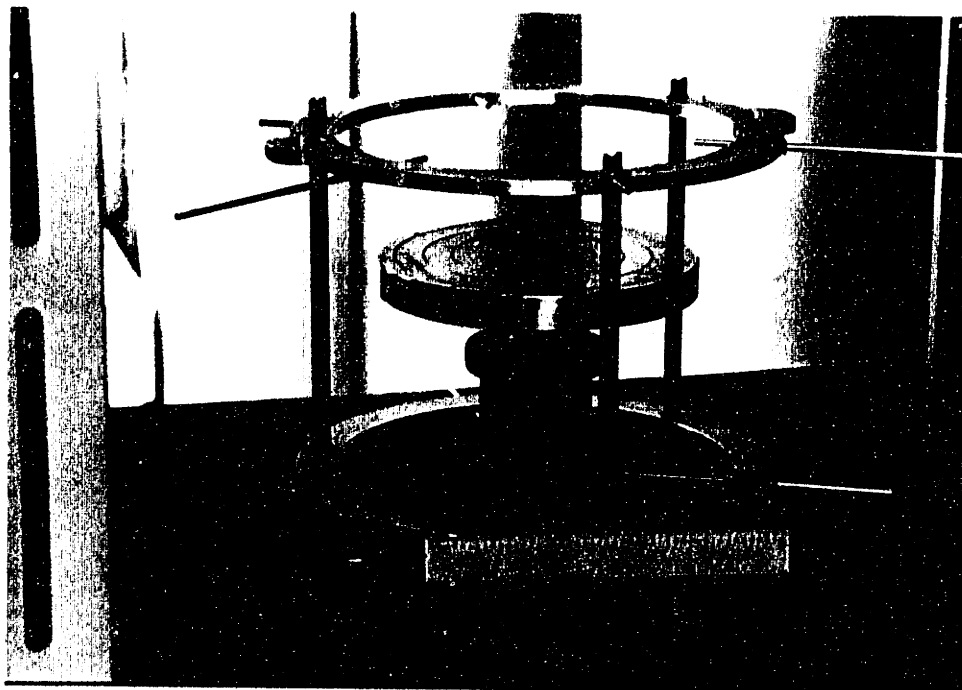
Figure 4.3: Four-point bending rig a) schematic of end fixture b) schematic of test set-up



extension rod

alum. cyl.

solid plate
connected
to extension rod, alum. cyl. and cone insert

machined conical insert
rigid PU-foam



P

d

Load cell

Universal joint

Channel section loading beam

Roller

Counterweight

θ

Rubber cylinder

l

End grips

Linear bearing

Extension rod

Angular transducer

Rotating block

(not to scale)
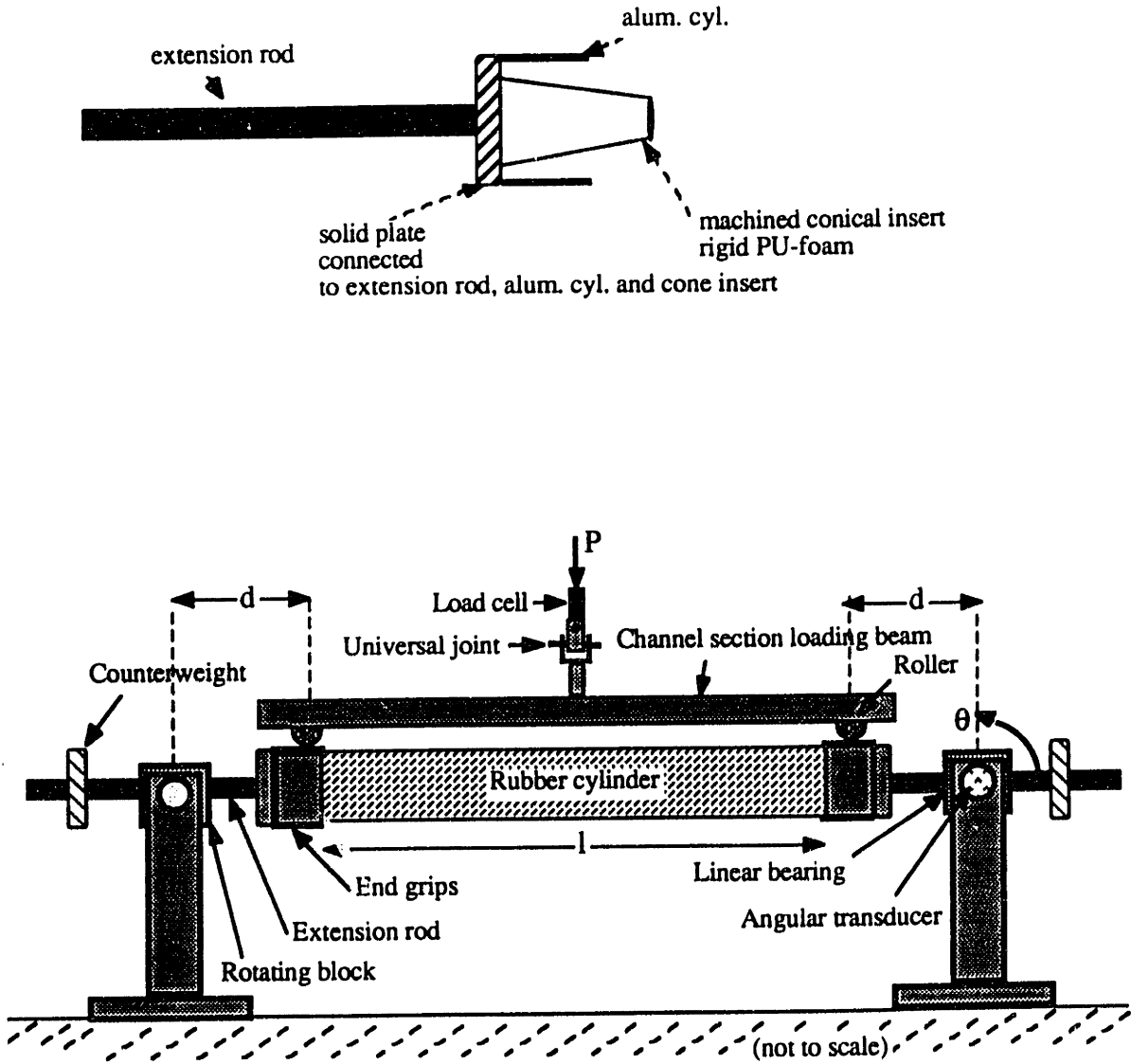
Figure 4.3: c) photograph of test set up.
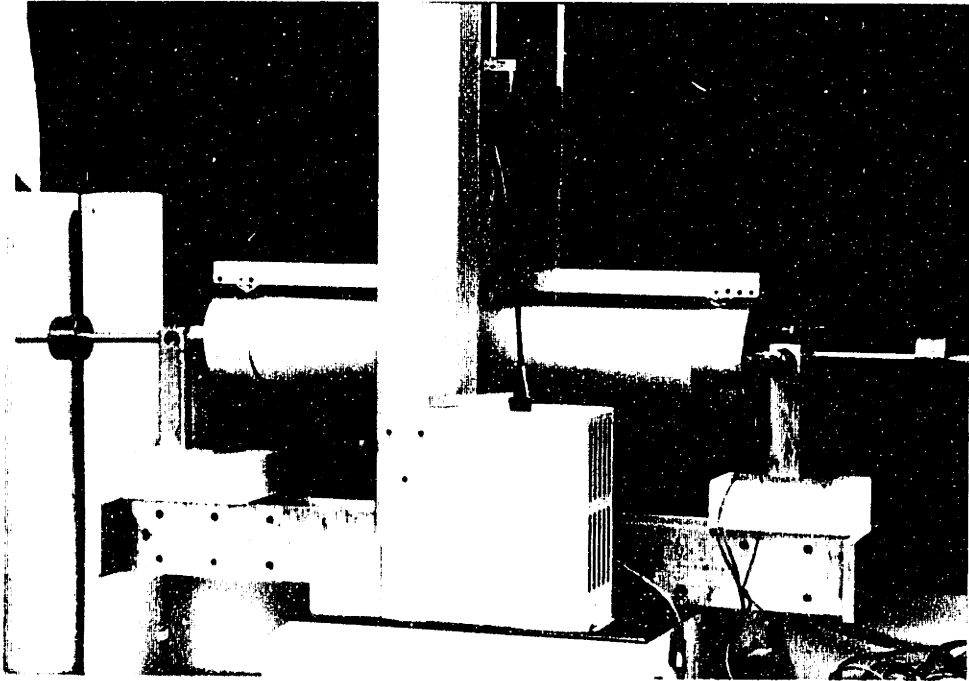
Figure 4.4: Buckling patterns of cylinders in uniaxial compression a) a/t=22, c/t=0
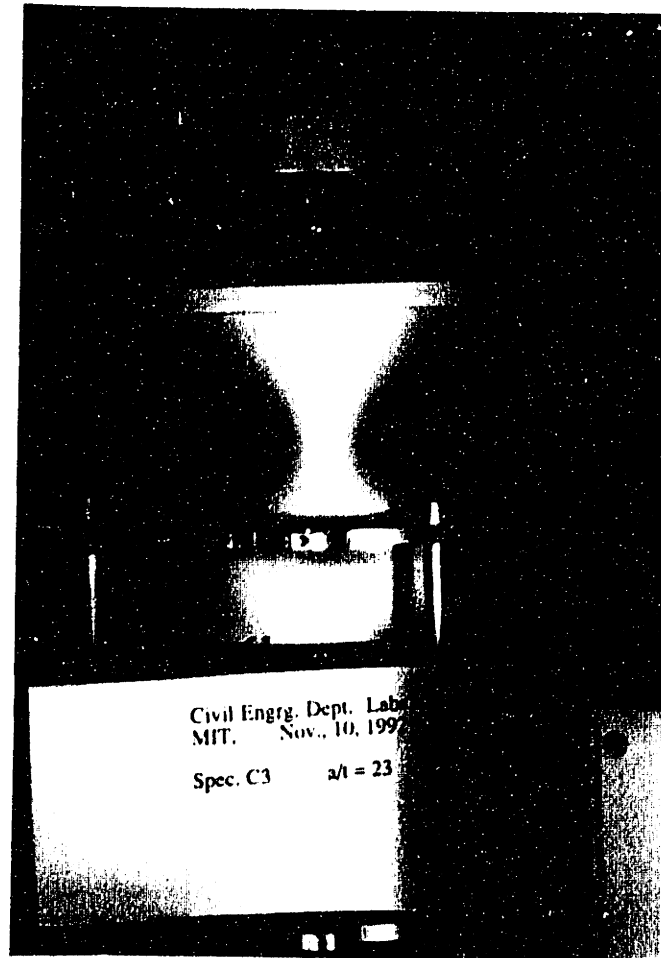
Figure 4.4: b) a/t=22, c/t=21.5
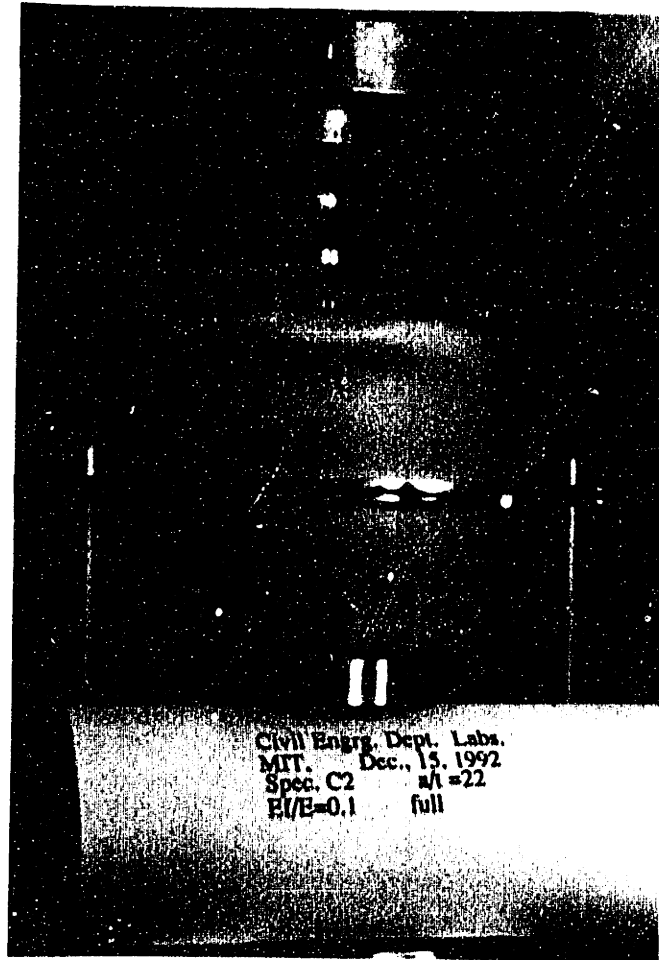
Figure 4.4: c) a/t=22, c/t=13.5



Civil Engrg. Dept. Labs.
MIT.        Dec., 15, 1992
Spec. C2        a/t =22
EI/E=0.1        2.0" hole
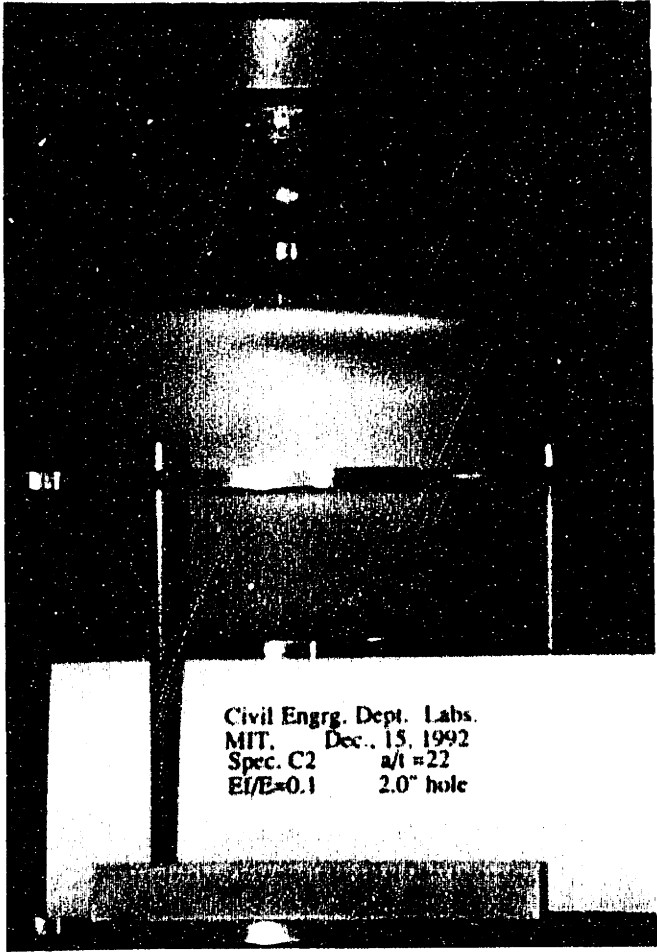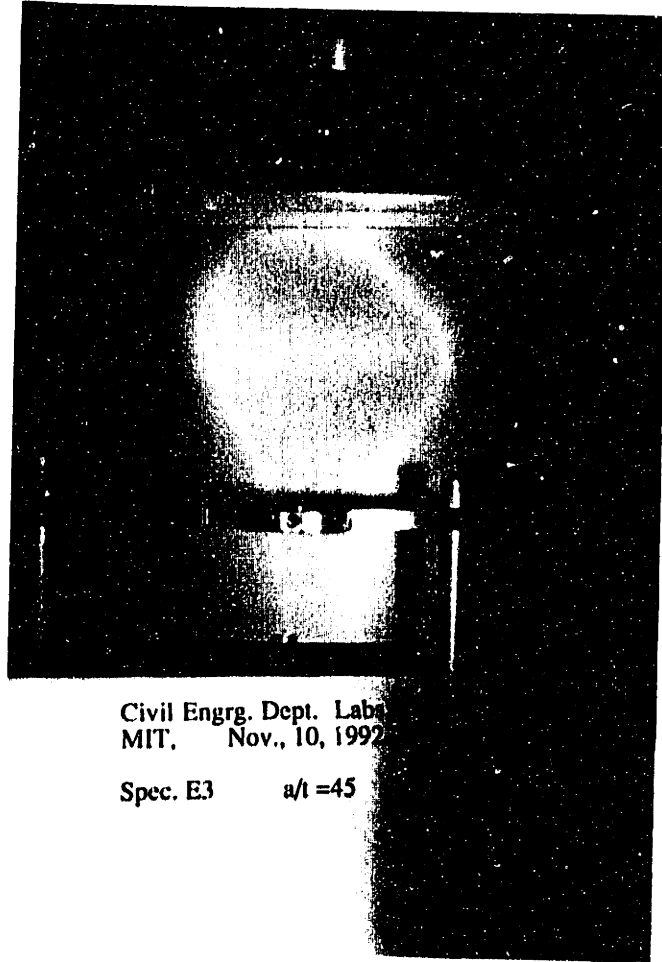
Figure 4.4: d) a/t=48, c/t=0



Civil Engrg. Dept. Lab
MIT. Nov., 10, 1992

Spec. E3    a/t =45

Figure 4.4: e) a/t=48, c/t=47.5

Figure 4.4: f) a/t=48, c/t=28.5

Figure 4.5: Load-axial shortening curves for hollow cylinders in uniaxial compression.
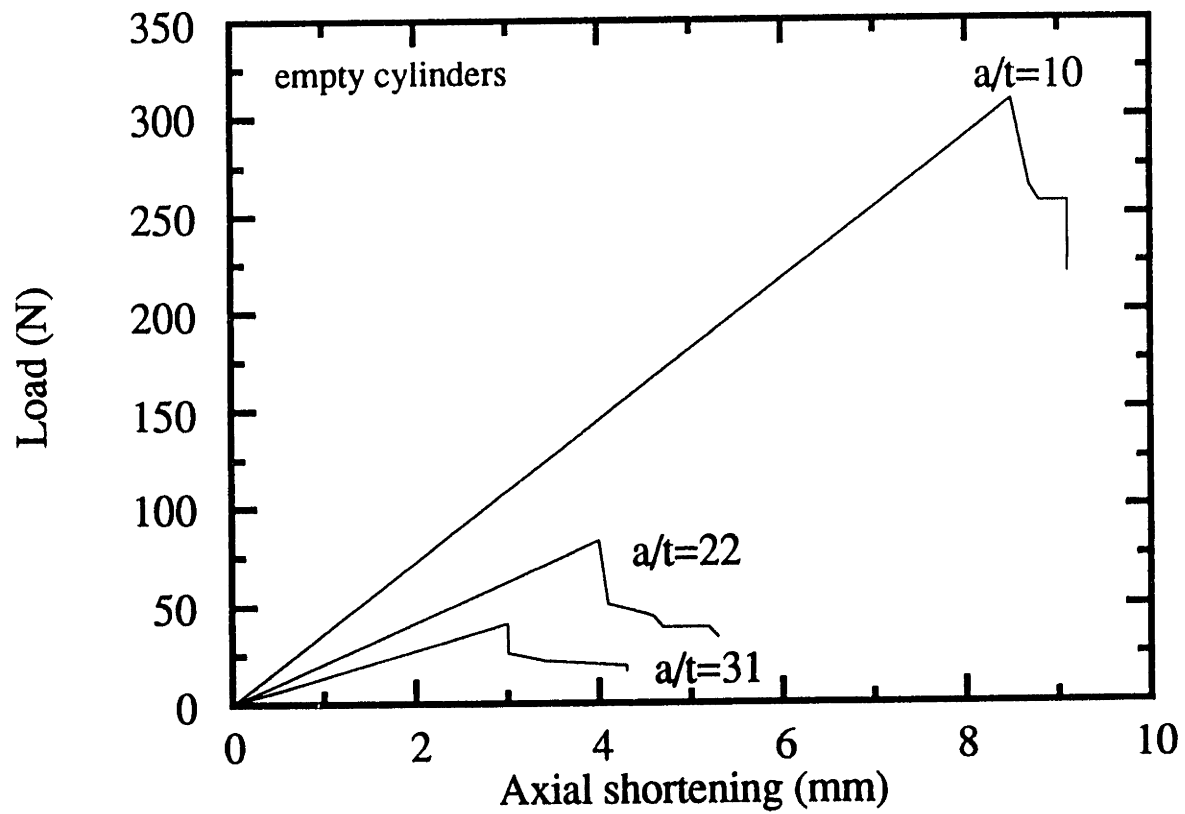
Figure 4.6: Normalized buckling stress $\sigma_{cr}/E$ plotted against radius to wall thickness ratio, a/t, for hollow cylinders loaded in axial compression.
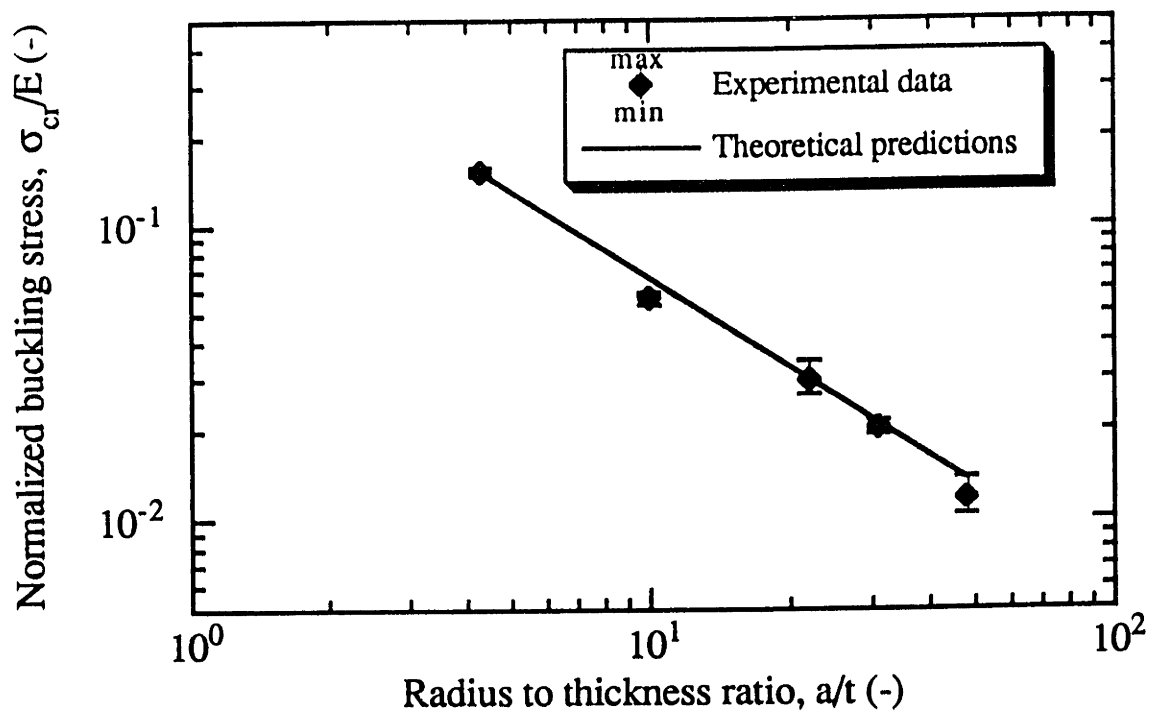
Figure 4.7: Load-axial shortening curves for foam filled cylinders, a) a/t=10



144
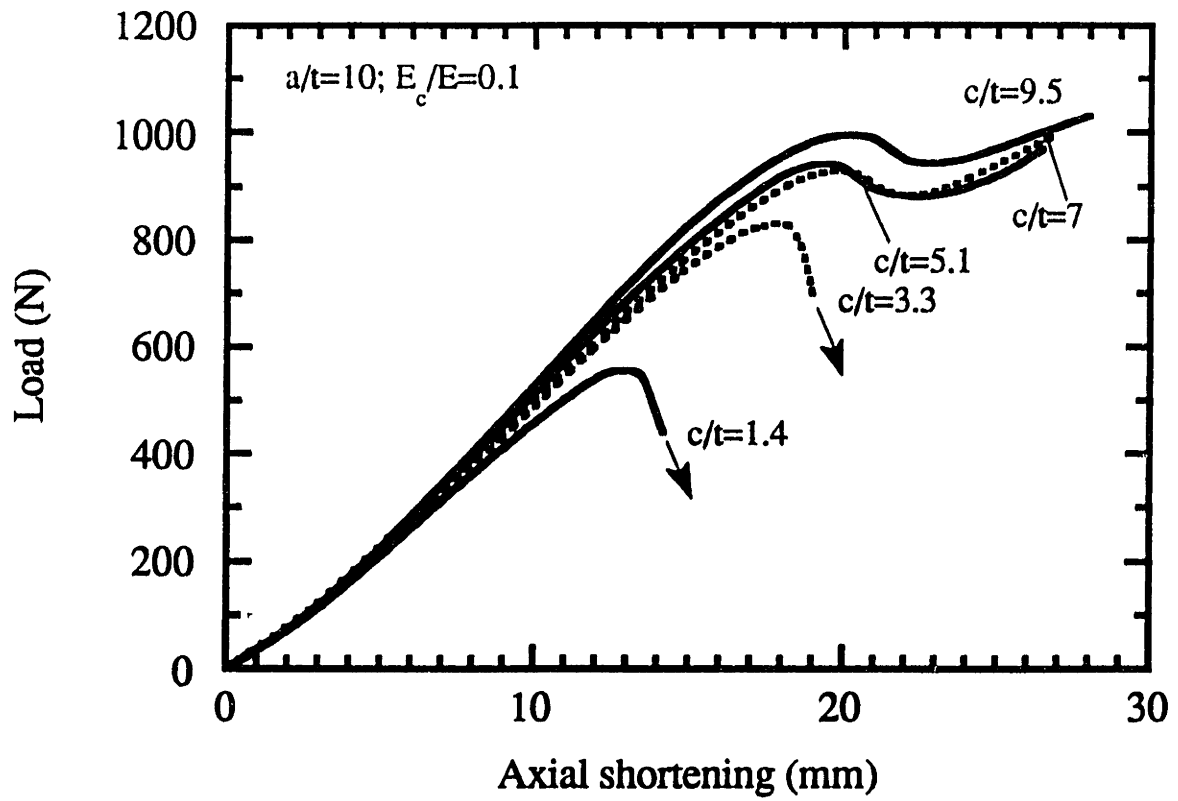
Figure 4.7: b) a/t=22

Figure 4.7: c) a/t=31



146
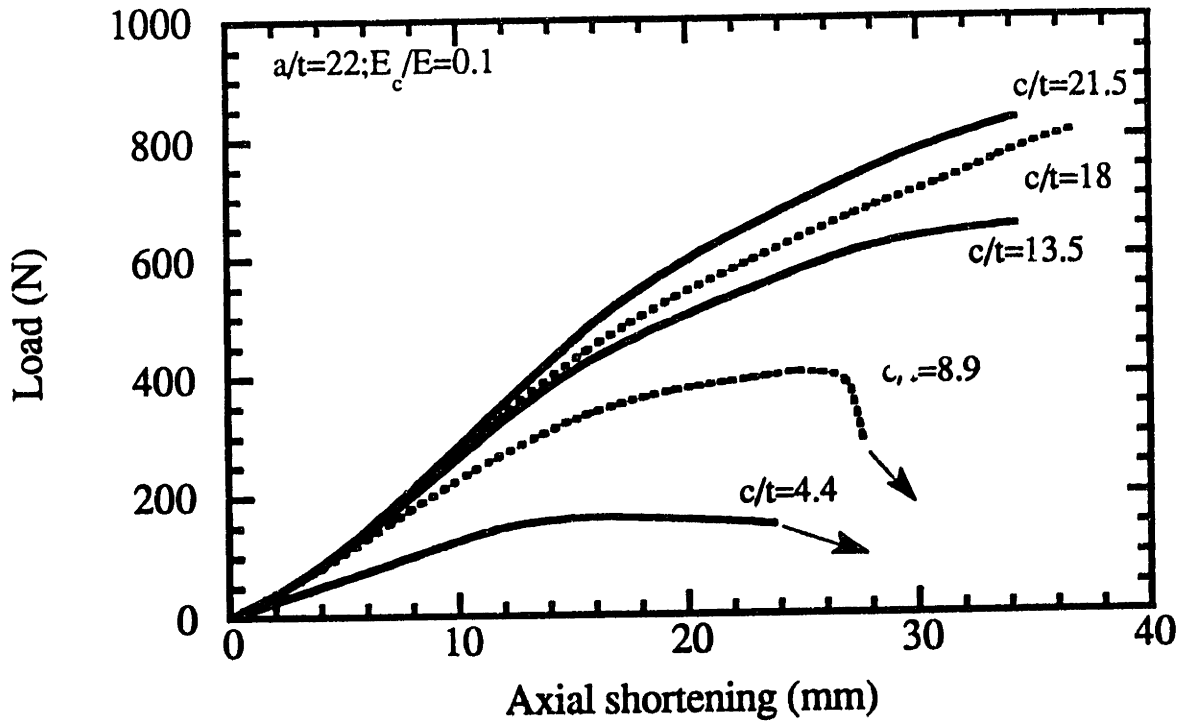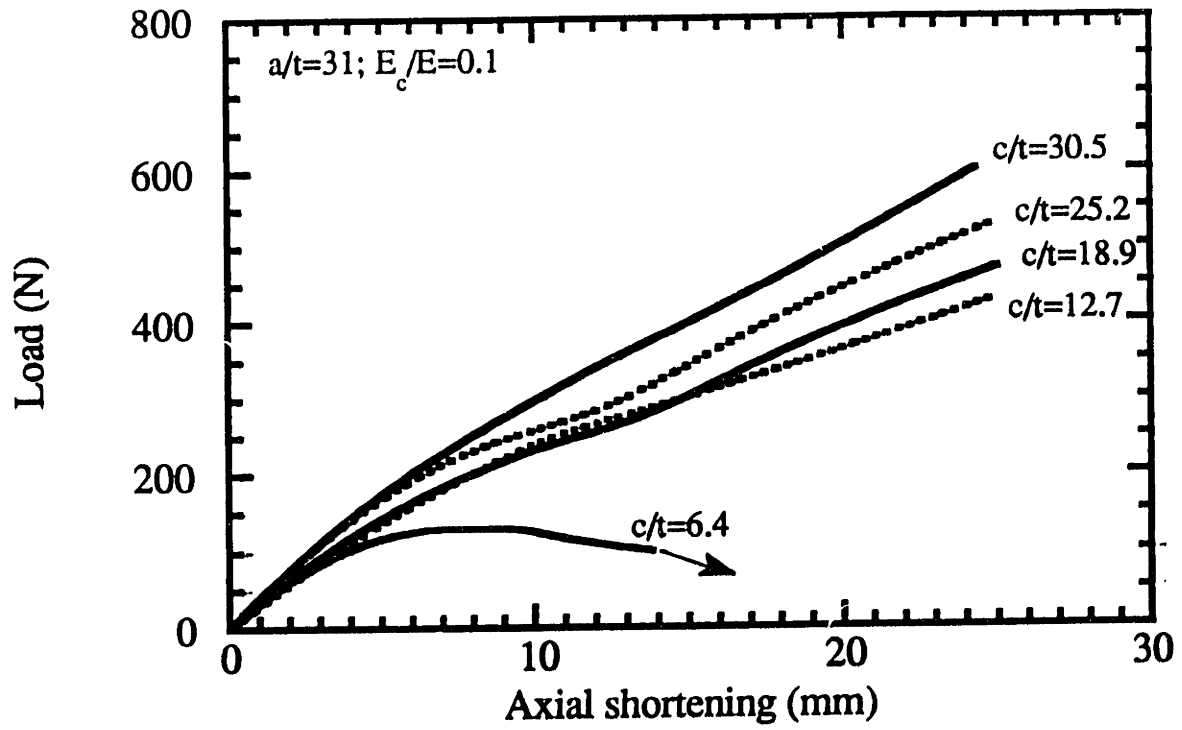
Figure 4.8: Measured buckling load in uniaxial compression normalized by the theorectical buckling load of a hollow cylinder of the same a/t plotted against the core to shell thickness, c/t. a) a/t=4.3
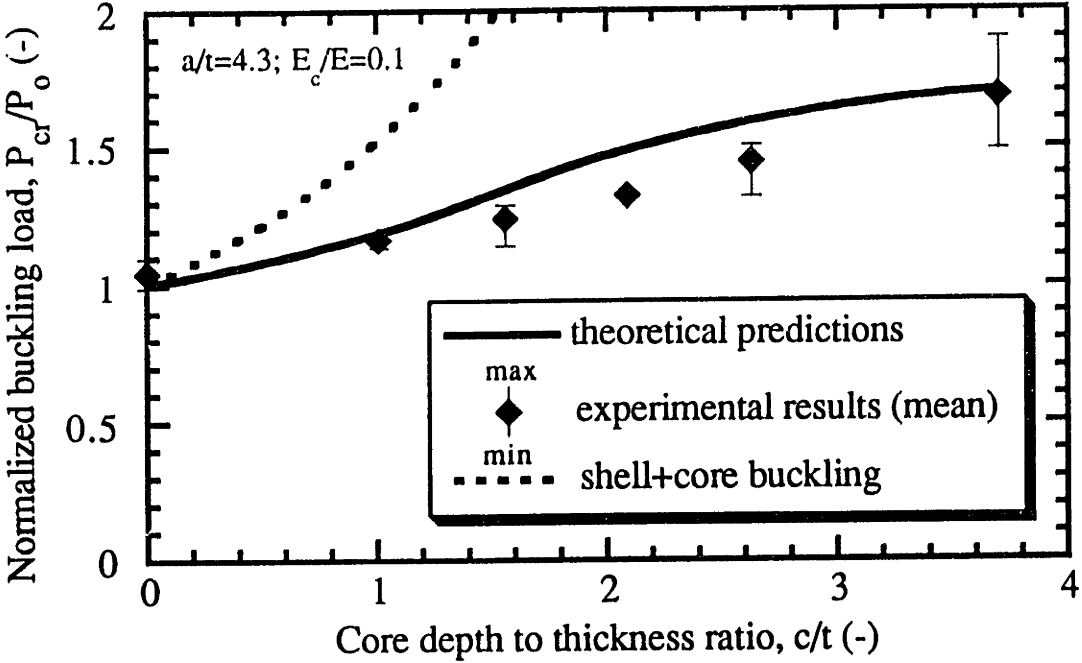
Figure 4.8: b) a/t=10
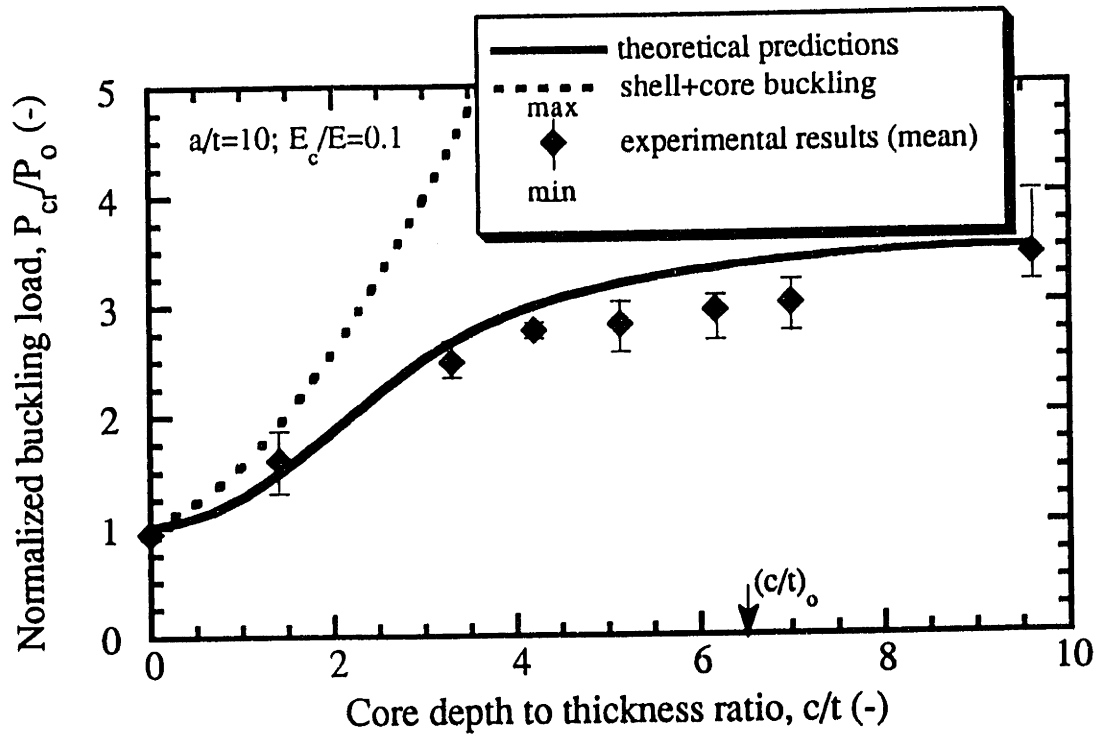
Figure 4.8: c) a/t=22
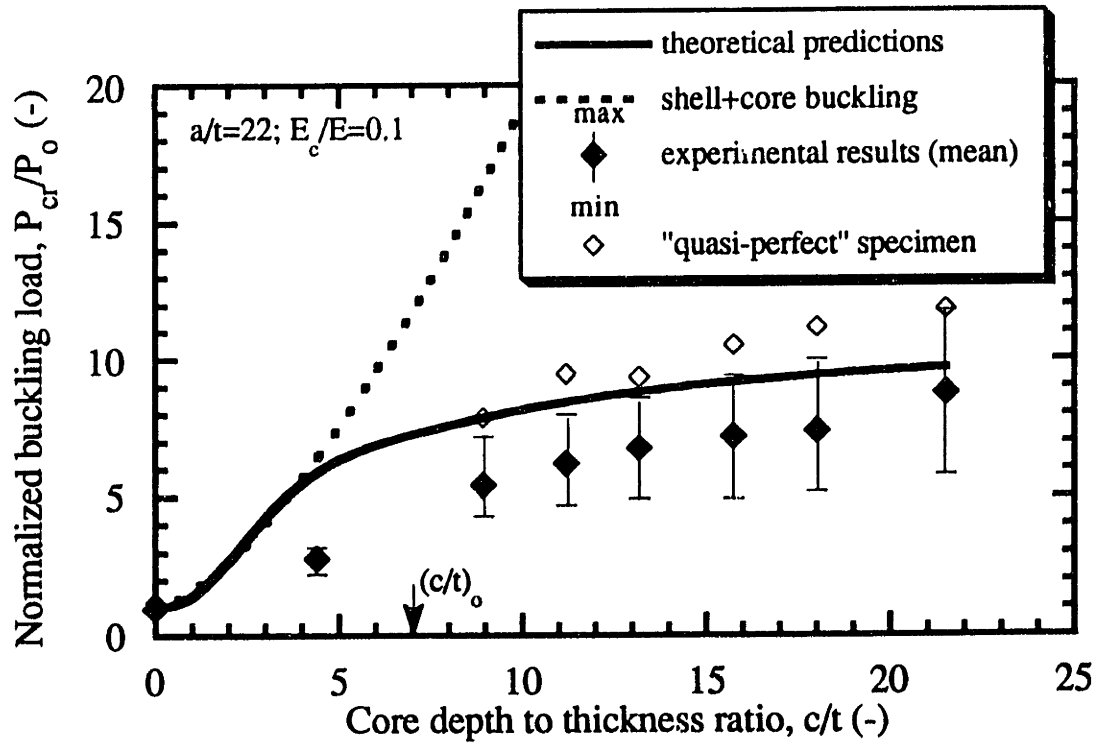
Figure 4.8: d) a/t=31
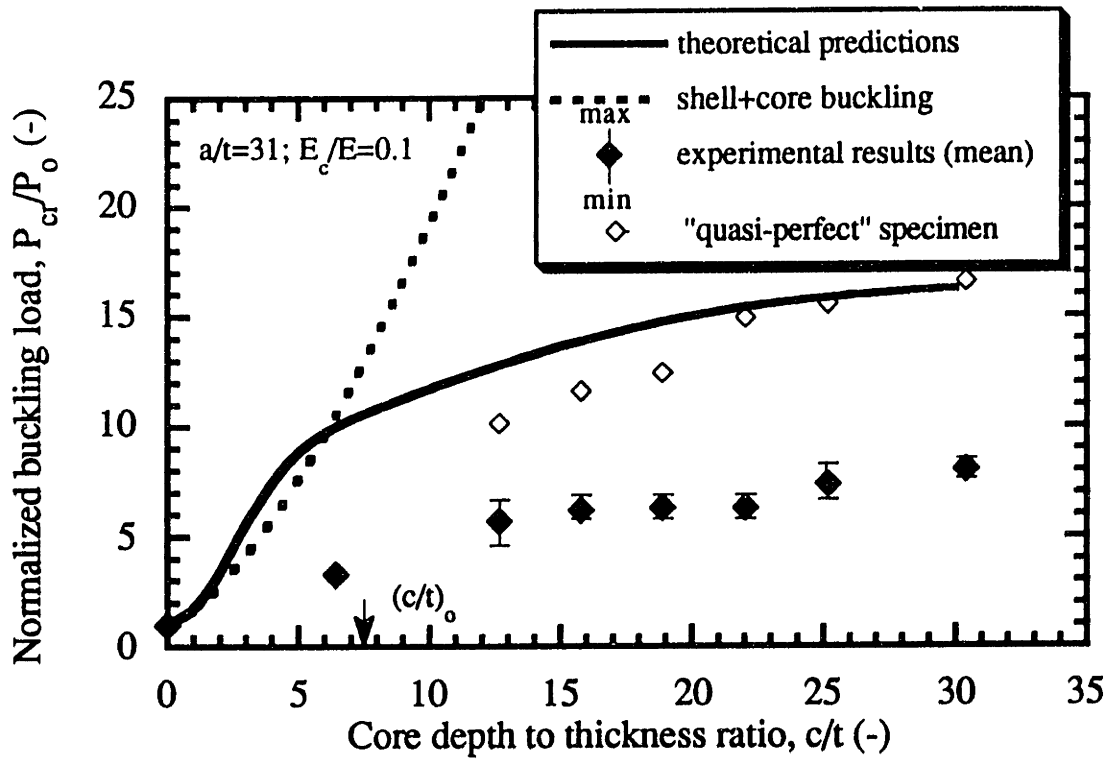
Figure 4.8: e) a/t=48
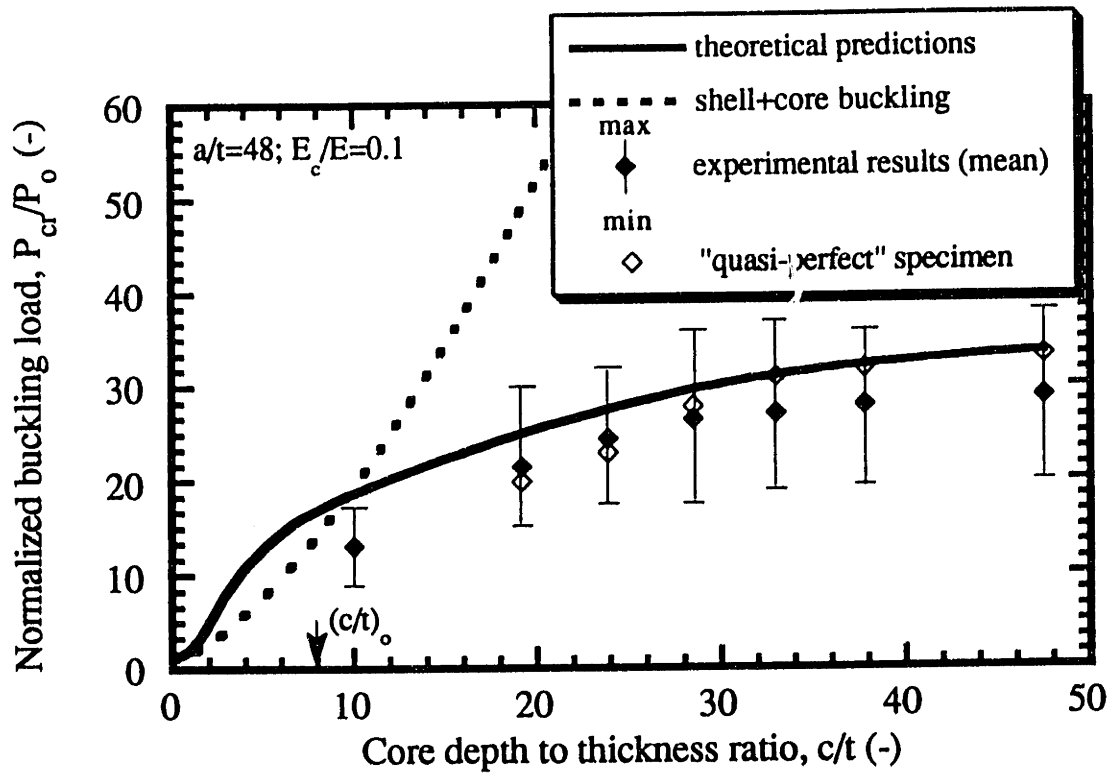
Figure 4.9: Number of axisymmetric buckling wavelengths for foam filled cylinders in axial compression plotted against radius to shell thickness ratio, a/t.
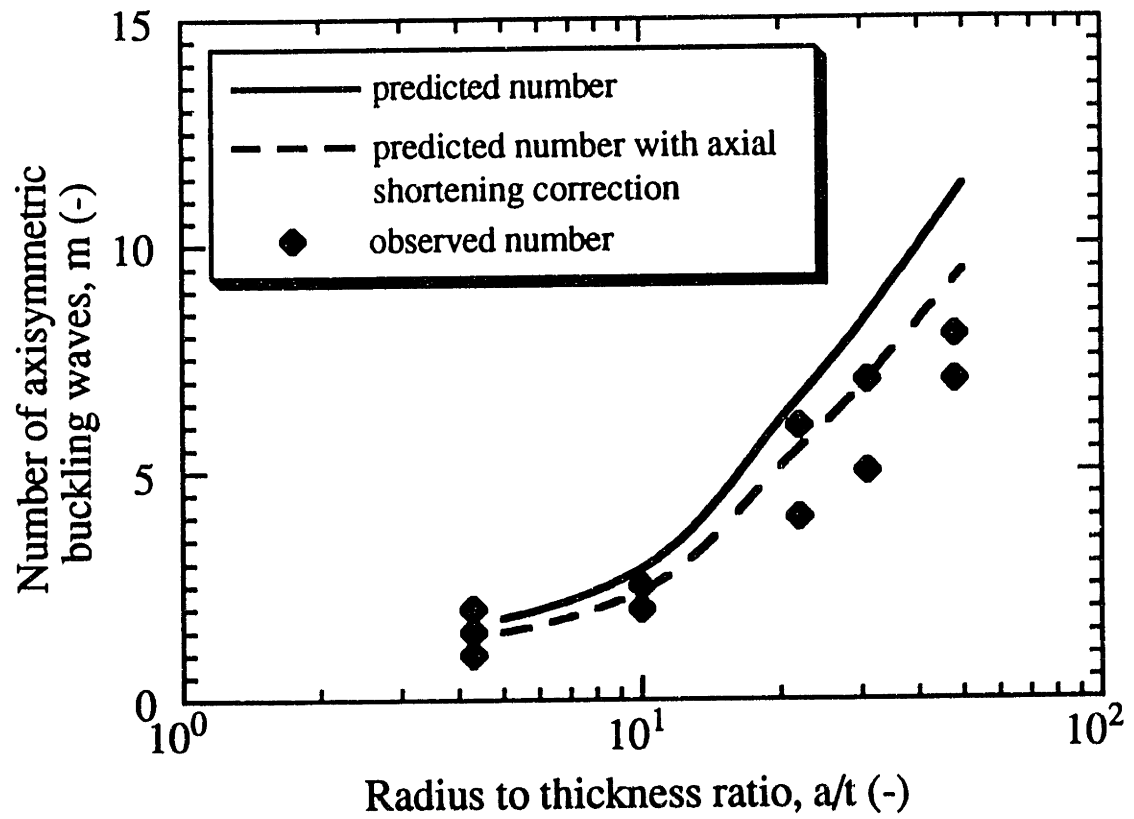
Figure 4.10: Uniaxial buckling stress ratio plotted against Seide's dimensionless stiffening parameter.
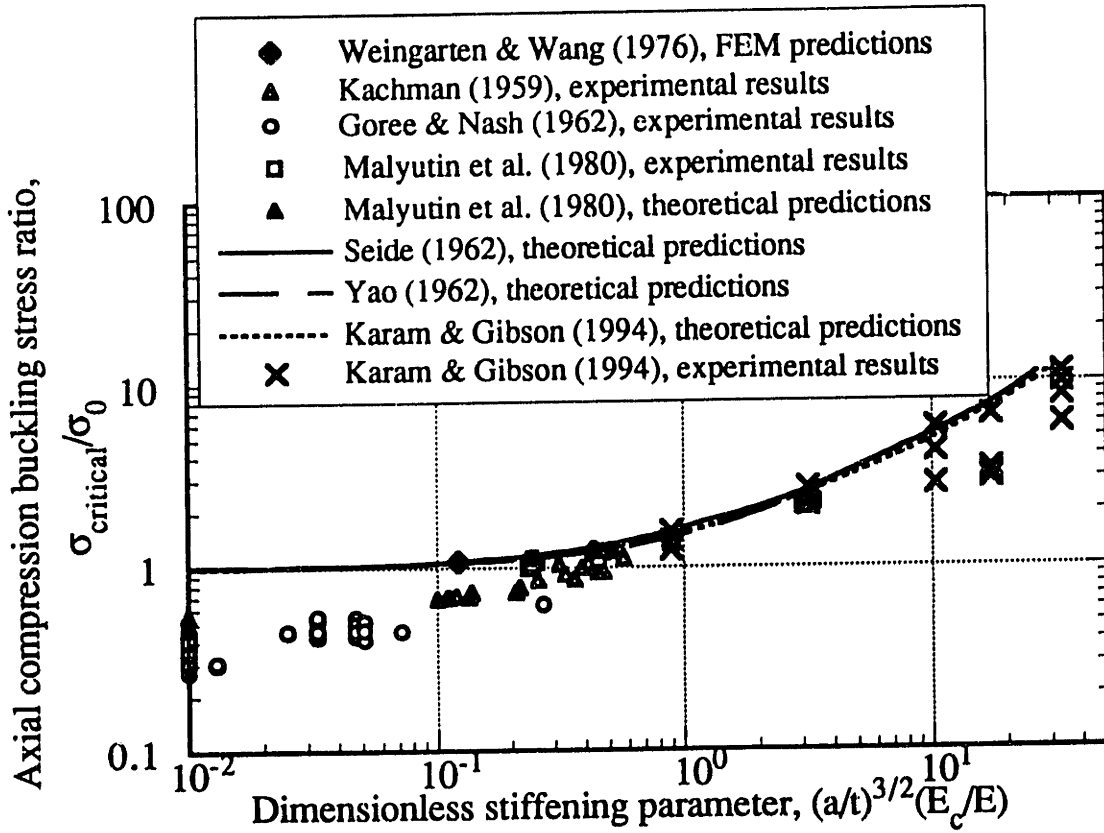
Figure 4.11: a) Photograph showing short wavelength buckling on the compressive side of the beam (a/t=28, c/t=10)
b) Photograph showing final collapse of the same beam.



(a)



(b)

154

Figure 4.12: Moment-curvature curves for cylinders in four-point bending. The theoretical critical curvature at which local buckling initiates is indicated by the arrow. a) hollow cylinder, a/t=23
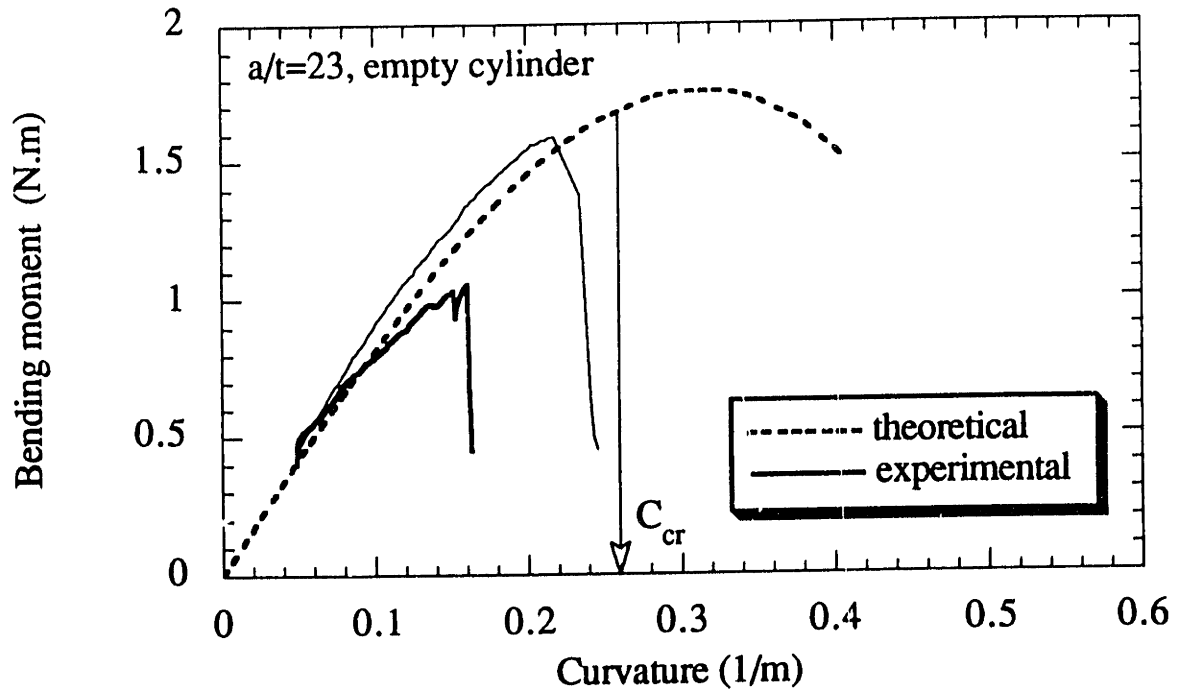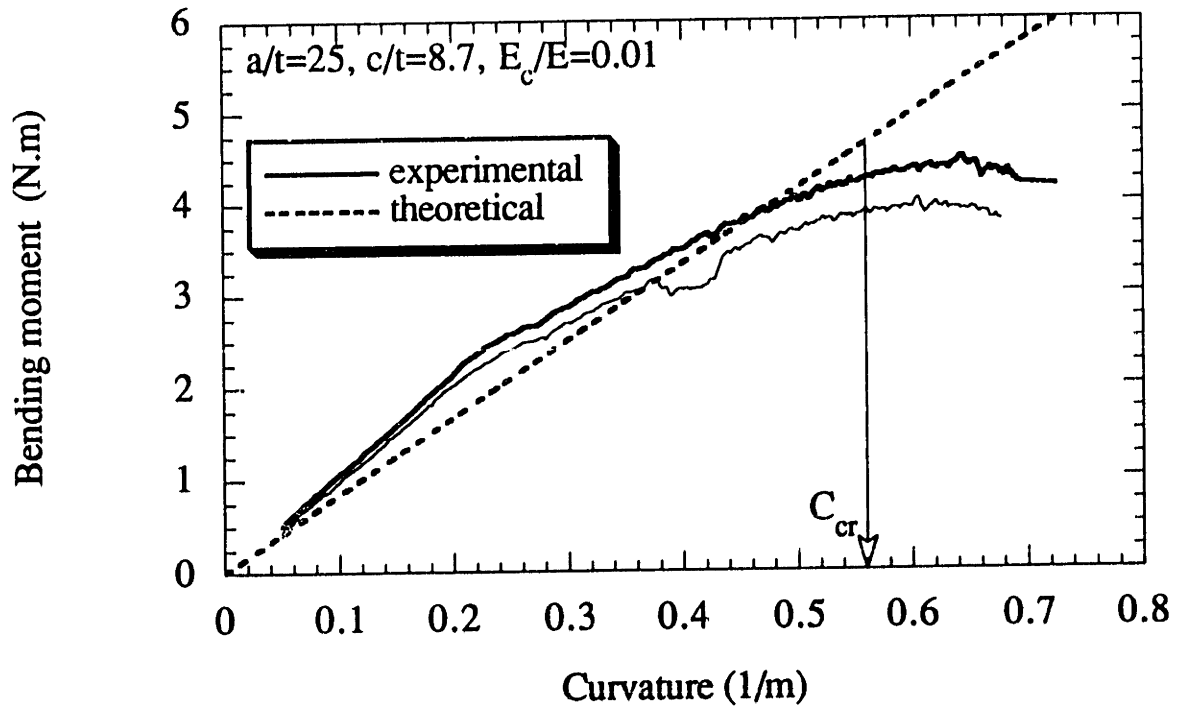
Figure 4.12: b) partially filled cylinder, a/t=25, c/t=8.7

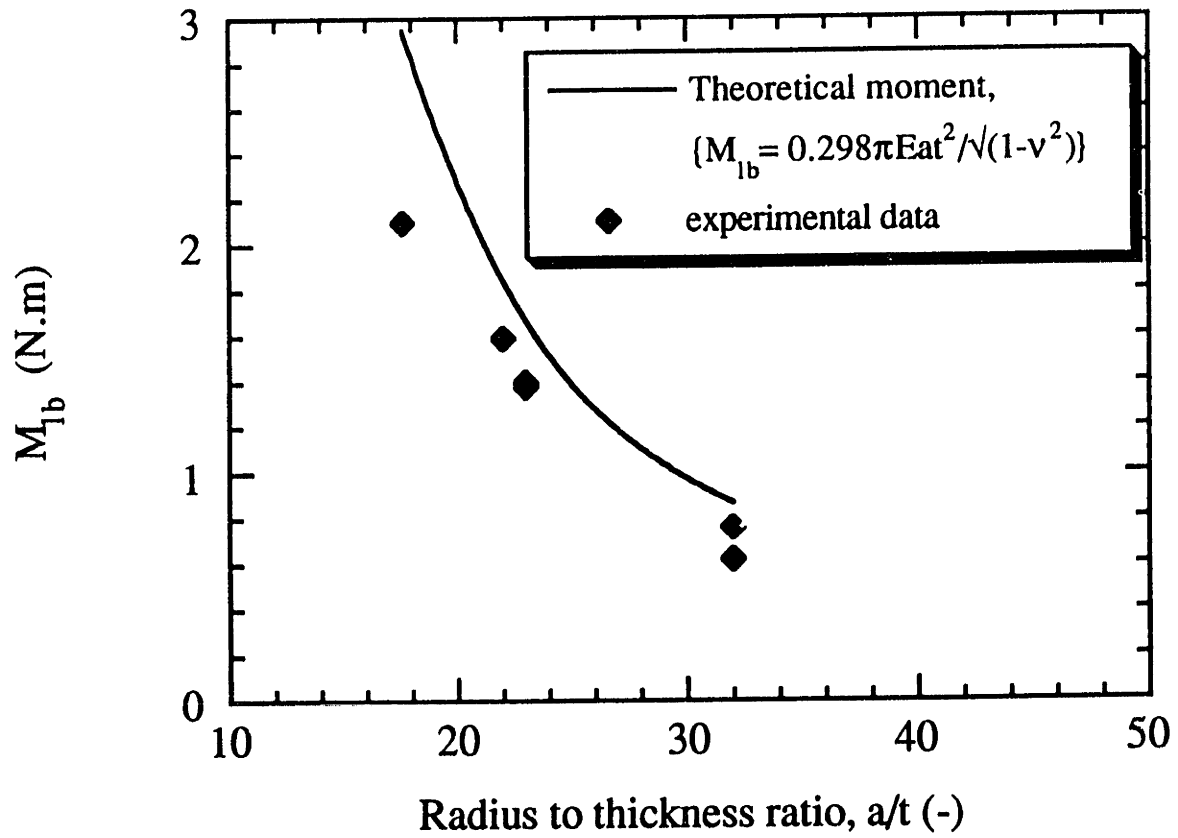Figure 4.13: a) Local buckling moment for hollow cylinders plotted against radius to thickness ratio, a/t.



Figure 4.13: a) Local buckling moment for hollow cylinders plotted against radius to thickness ratio, a/t.

The figure plots $M_{lb}$ (N.m) on the vertical axis against Radius to thickness ratio, a/t (-) on the horizontal axis. Legend: Theoretical moment, $\{M_{lb} = 0.298\pi Eat^2/\sqrt{(1-v^2)}\}$; experimental data.

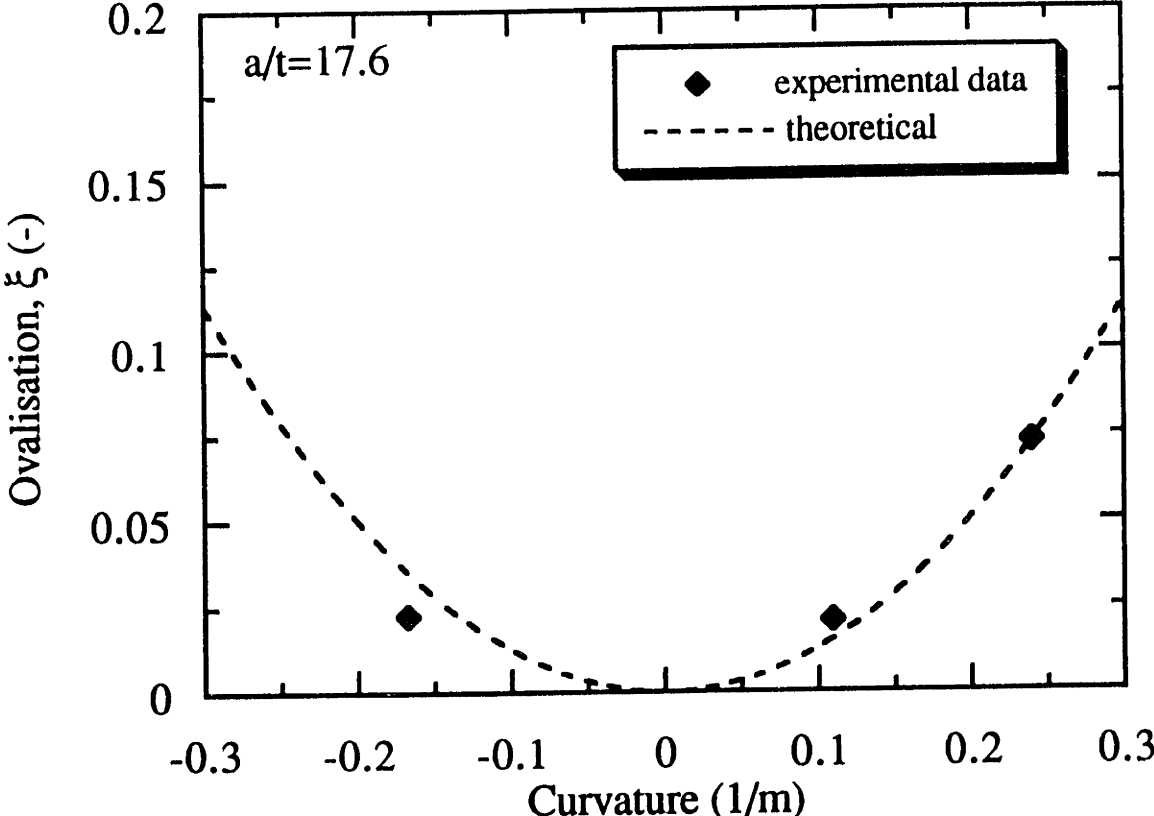Figure 4.13: b) Ovalisation-curvature relationship for a hollow cylinder, (a/t=17.6).

Figure 4.14: Local buckling moment for partially filled cylinders plotted against radius to wall thickness ratio, a/t.
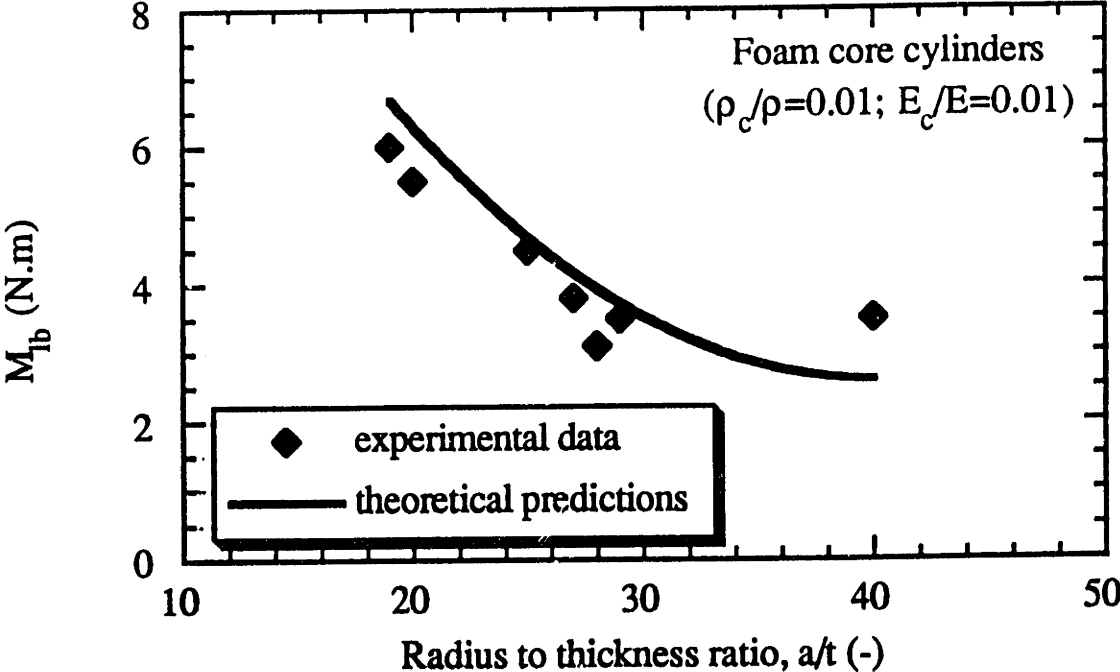
Figure 4.15: Ratio of measured local buckling moment of partially filled cylinders to theoretical predictions for empty cylinders of equal weight plotted against a/t for the partially filled cylinders.
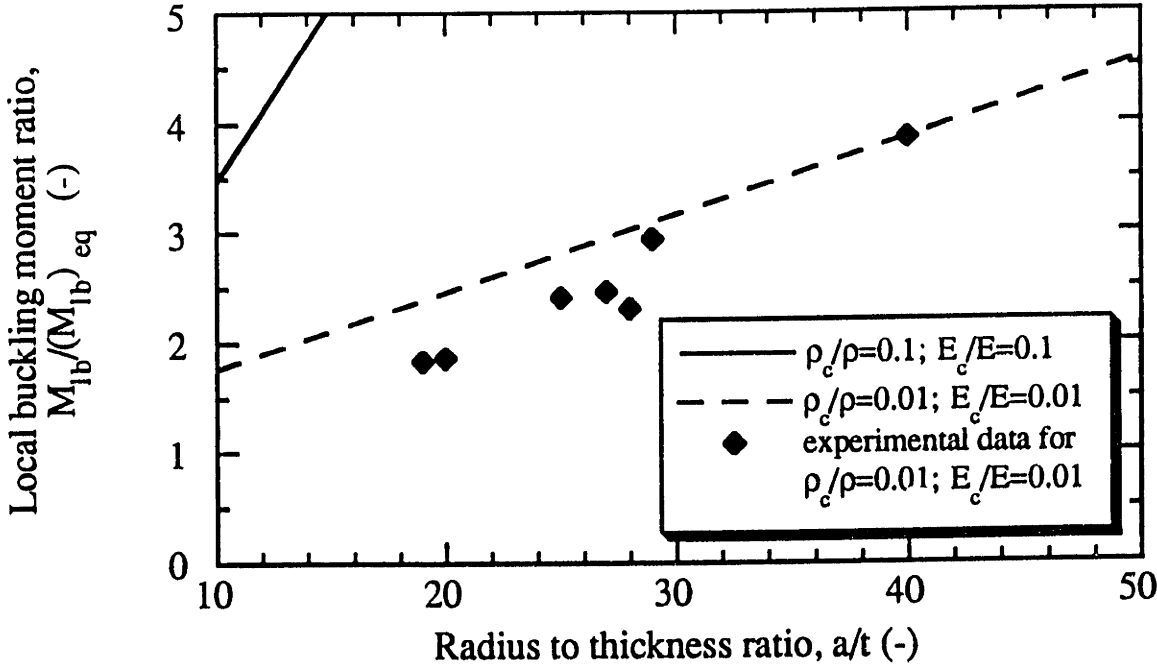
Figure 4.A1: Profile deviation from original straight shape for uniaxial compression specimens, (a) a/t=4.3, foamed in place core
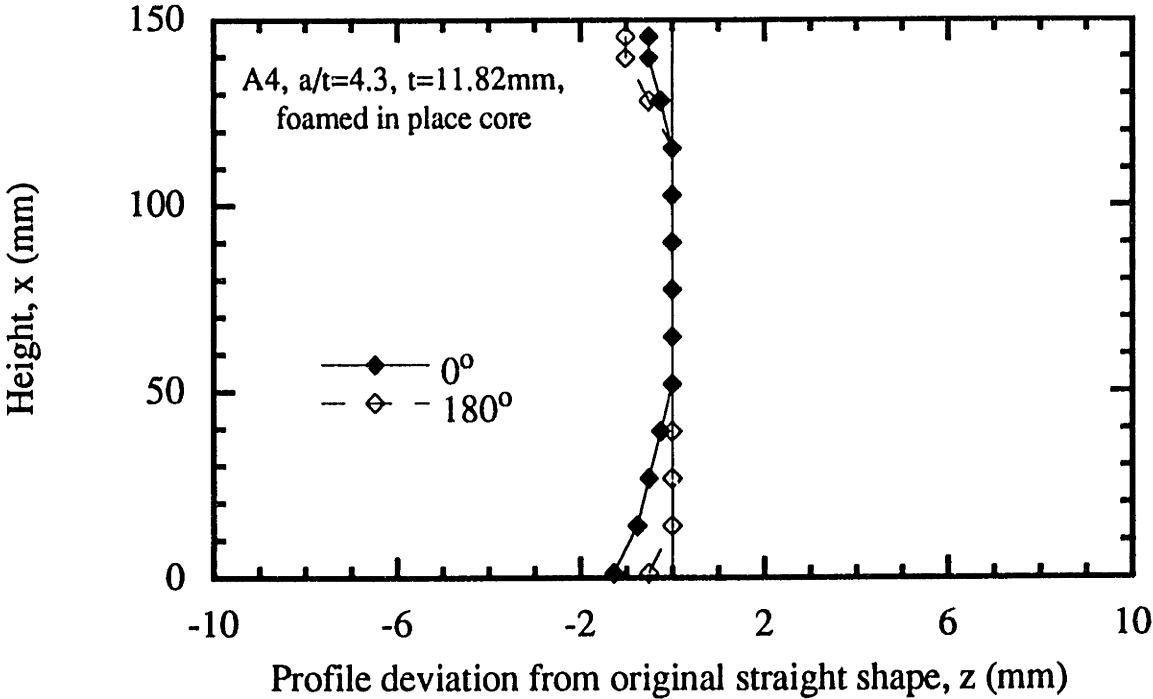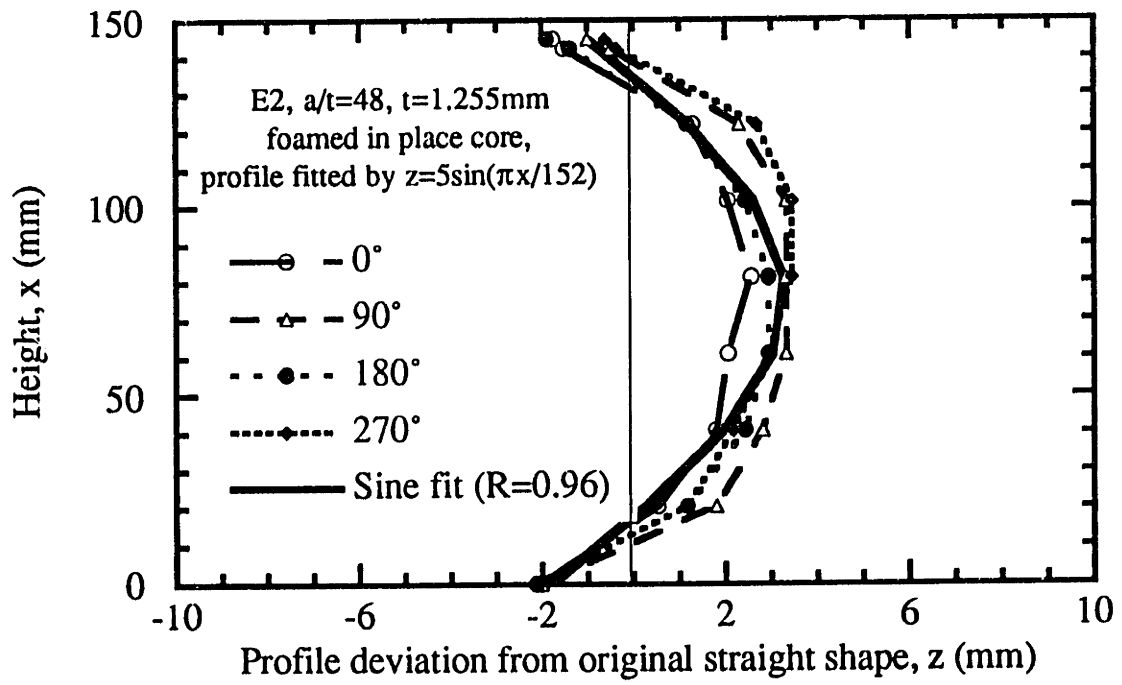


A4, a/t=4.3, t=11.82mm,
foamed in place core

0°
180°

Height, x (mm)

Profile deviation from original straight shape, z (mm)

Figure 4.A1: (b) a/t=48, foamed in place core

E2, a/t=48, t=1.255mm
foamed in place core,
profile fitted by z=5sin(πx/152)

— ⊖ — 0°
— △ — 90°
- • - - 180°
....♦.... 270°
——— Sine fit (R=0.96)

Height, x (mm)

Profile deviation from original straight shape, z (mm)

Figure 4.A1: (c) a/t=48, "quasi-perfect" specimen, machined core.



E5, a/t=48, t=1.338mm,
"quasi-perfect" specimen

●   0°

△   180 °
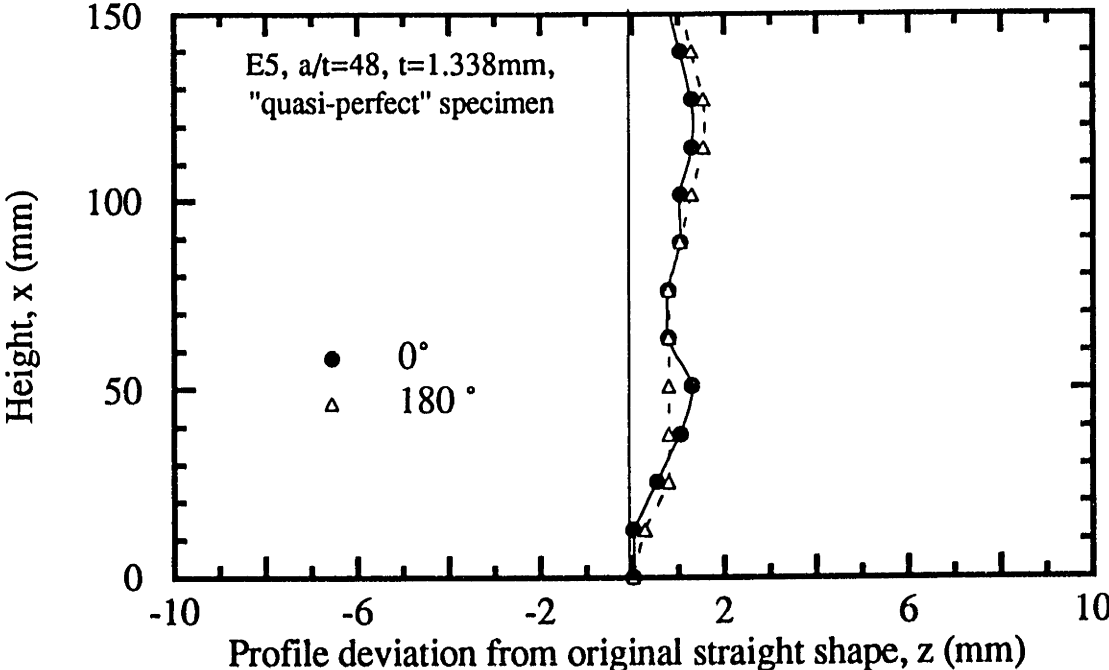
# CHAPTER 5

## NATURAL TUBULAR STRUCTURES,

## DESIGN AND BIOMIMETICS

*"Very different from human art, whose productions are only dead works, Nature is herself a work perpetually alive, an active and never ceasing operator who knows how to employ every material, and, though always labouring on the same invariable plan, her power, instead of being lessened, is perfectly inexhaustible."*

George-Louis de Buffon (Histoire Naturelle, 1764)

In light of the theoretical and experimental work presented in the previous chapters, the microstructure of different plant stems and animal quills and spines was characterized and their resistance to buckling estimated. The geometry of these tubular structures was measured from optical and scanning electron micrographs. The elastic moduli of the core was estimated from measurements of its relative density using models for cellular solids (Gibson and Ashby, 1988). Data from our own specimens were supplemented by measurements on micrographs taken from the published literature on the microstructure of stems and quills. The measured core depth was compared to that predicted by the stress decay analysis of Chapter 3. The mechanical efficiency of the natural structures was evaluated by calculating the ratios of the axial buckling load, the Brazier moment and the local buckling moment, to those of a hollow cylinder of equal radius and mass. Potential biomimetic applications of these structures are described.

## 5.1 Materials and methods

Fully grown live plant specimens were collected from the natural wild growth in the New England area and identified at the Herbarium of Harvard University (Stevens, 1993). Stem cross sections were obtained from the lower quarter of the stems by sectionning with a sharp razor blade. Measurements of the microstructure of the larger specimens were performed with an electronic caliper (Max-Cal, Japan) and a direct measurement optical microscope with a precision glass reticle (Edmund Scientific Co, Barrington, New Jersey). Smaller specimens were gold coated, examined and photographed in the scanning electron microscope (SEM) (Cambridge Instruments, Model S240).

North American porcupine quills, 50 to 60 mm long, were obtained from live animals at the Franklin Park Zoo in Boston while English hedgehog spines, 15 to 20 mm long, were obtained from recently sacrificed animals at the Zoology Department of Harvard University. We also obtained, from the Museum of Comparative Zoology at Harvard University, conserved quill specimens for three other species: *Hystrix Galeata, Hystrix Subcristata* and *Tachyglossus Aculeatus* , of lengths 235, 360 and 35 mm respectively. Sections were prepared by freezing in liquid nitrogen and sectionning with a sharp razor blade. Specimens were then gold coated and prepared for examination in the SEM. Geometric property measurements were made on cross sections obtained from the central part of the quills where the diameter is more or less constant along the length.

The recent botanical and zoological literature was also surveyed for micrographs of plant stems and animal quills from which microstructural measurements could be made ( Esau, 1977, Cenci et al., 1984, Vincent and Owers, 1986, Dunn and Briggs, 1988, Ueno et al., 1989, Wilson et al. 1989).

The radius, shell thickness and core depth of each natural tubular structure were measured either by direct optical microscopy, or on SEM micrographs. The solid fractions, or relative densities of the outer shell and of the inner core were obtained by the

classical stereological method of point counting: the relative density was found from the ratio of the number of grid points that fell on solid material to the total number of grid points falling in the observed region (Underwood, 1970). In the case of the optical measurements, the glass reticle grid was used as a reference while in the case of the micrographs a grid was overlain on top of the micrograph.

## 5.2 Microstructure and material properties of natural cylindrical shells with compliant cores

### Microstructures

The porcupine quills and hedgehog spines all had a dense outer shell with a more compliant inner core; their geometrical measurements are listed in Table 5.1A. Four types of core microstructure were observed. The simplest microstructure, a foam-like core filling the outer shell, was observed in the North American porcupine (*Erethizon*), (Fig. 5.1), in the Brazilian tree porcupine (*Coendou prehensilis*) (Vincent and Owers, 1986), and in one of the two specimens of the echidna (*Tachyglossus Aculeatus*) that were investigated (Fig. 5.2a-c). The other echidna specimen was hollow (Fig. 5.2d). The cell wall thickness is uniform over the cross section while the cell size decreases from the center of the cross section to the outer shell, resulting in a radially increasing relative density, (Figs. 5.1a-c). The foam relative density reported in Table 5.1A is an average across the section.

The second core microstructure resembled the first, but with additional thin, solid, longitudinal stiffeners running radially from the outer shell of the quill towards the center; this microstructure was observed in the Old World porcupine quills *Hystrix Subcristata* (Fig. 5.3), *H. Galeata*, (Fig. 5.4), and *H. Indica x Cristata*, (Vincent and Owers, 1986). The stiffeners decrease in thickness as they converge at the central axis. The foam filling the remaining core stabilizes both the outer shell and the thin stiffeners (Figs. 5.3c,d). The volume fraction of the cross section occupied by the stiffeners was

reported as the core relative density due to the ribs and it was obtained by dividing the area occupied by the solid ribs by the total area of the section. The three dimensional foam relative density was reported separately (Table 5.1A).

In the third microstructure the outer shell is stabilized by closely spaced longitudinal and radial stiffeners; this structure was observed in the spines of the hedgehog (*Erinaceus Europaeus*) (Vincent and Owers, 1986) (Fig. 5.5) and the spiny rat (*Hemiechinus spinosus*) (Vincent and Owers, 1986). The longitudinal stiffeners do not fully extend into the center of the cross section (Figs. 5.5a,b). The radial ring stiffeners span the spaces between the longitudinal stiffeners; at the radius at which the longitudinal stiffeners end, every three to four ring stiffeners converge to form a thin diaphragm or septum that spans across the open central core (Figs. 5.5c,d). This configuration acts as a square honeycomb supporting the inside surface of the shell (Figs. 5.5d,e). The relative density of the honeycomb reported in Table 5.1A does not include the central septa.

The fourth microstructure type was observed only in the tenrec (*Setifer*) spine which has a filled foam core exclusively made out of thin closely spaced septa (Vincent and Owers, 1986).

The plant stems surveyed (Table 5.1B) had a microstructure with a foam like core similar to the first type observed in the porcupine quills. They could however be divided into two main groups depending on the location of the vascular bundles in the stem. In the first group,( *Avena, Eleocharis, Elytrigia, Hordeum, and Secale*), the outer shell was made of close to cylindrical sclerenchyma and collenchyma cells, aligned along the main axis (Fig. 5.6). The cells in the core were elongated parenchyma cells that are much shorter, more equiaxed and of less regular geometry than the sclerenchyma and collenchyma cells making up the outer shell (Esau, 1977). The cells in the outer shell layer have small diameters, very thick walls and virtually no lumen, while those in the core have thinner walls and much larger diameters resulting in a clear density change

(Fig. 5.6a,b). The vascular bundles (xylem and phloem) through which water and nutrients circulate, and the stiff bundle sheath enclosing them, are part of the core and were included in its estimated density. All of the specimens surveyed in this first group had a central hole.

In the second group the outer shell, again made up of elongated cells, contained the vascular bundles while the core was made up of foam-like, roughly equiaxed parenchyma cells (Fig. 5.7). Most specimens in this groups had fully filled cores. Examples include *Artemisia, Cenchrus Ciliaris,  Latuca Biennis* and *Phytolacca Americana.*

The dimensionless geometrical parameters needed for the analysis of mechanical efficiency were calculated from the information in Tables 5.1A and 5.1B and are presented in Tables 5.2A and 5.2B. along with the required material properties. The radius to thickness ratio, a/t, was obtained from the outer radius and shell thickness measurements by subtracting half the thickness from the outer radius and dividing the result by the thickness. The core to shell density ratio, $r_c/r$, was obtained as the ratio of the core relative density to that of the shell. The core depth to thickness ratio, c/t, was calculated as the ratio of the measured values. In the case of a foam-like core filling the shell c/t = a/t-1/2.

*Material properties*

If the shell and the core are assumed to be made of the same material, the ratio of the Young's modulus of the core to that of the shell, $E_c/E$, can be estimated from the core to shell density ratio, $\rho_c/\rho$, as $(\rho_c/\rho)^n$, where the exponent n depends on the geometry of the cellular core as described by Gibson and Ashby (1988). Spines and porcupine quills have no physiological function and are essentially modified hairs made of alpha keratin (Vincent and Owers, 1986). Here we assume, like Vincent and Owers (1986), that the

168

solid material in the shell and the core has the same mechanical properties. We also make the same assumption for the plant stems.

In the analysis of Chapter 3, it was assumed that the shell and core were both made of an isotropic material. The shells of the quills and spines are made of lay ups of a fibre reinforced composite which most likely has its keratin microfibrils oriented to resist stresses in the most efficient way, as was observed, for example, in the bessbeetle cuticle (Gunderson et al., 1992). The shells of the plant stems, consisting of longitudinally oriented, thick walled fibres, are obviously anisotropic to some degree (Niklas, 1992).

Due to the lack of published information on this topic and for the sake of analytical simplicity, we assume the shell material in the observed natural structures to be isotropic. On the other hand, the properties of the cores are dependent on their microstructure which in some cases is clearly anisotropic.

Figure 5.9 shows schematically the different microstructures surveyed and the models used to estimate the core to shell stiffness ratio, $E_c/E$. For the echidna and the porcupine quills with a simple, isotropic, closed-cell foam-like core microstructure, classified as type 1 microstructure (*Coendou, Erethizon, and Tachyglossus Aculeatus*) (Fig. 5.9a):

$$\left(\frac{E_c}{E}\right)_x = \left(\frac{E_c}{E}\right)_y = \left(\frac{E_c}{E}\right)_z = \left(\frac{\rho_c}{\rho}\right)^2$$

as suggested by Gibson and Ashby (1982,1988) for similar synthetic foams. In this model the major contribution to the stiffness of the foam was assumed to come from the solid material accumulated at the edges of the packed cells neglecting the bending rigidity of the walls themselves. Under loading these walls also undergo stretching which can increase the stiffness significantly. This increase is a function of the fraction of solid

material in the edges, $\phi$, and the walls, 1-$\phi$, and can be represented in a refined form as (Gibson and Ashby, 1988):

$$\frac{E_c}{E} = \phi^2 \left(\frac{\rho_c}{\rho}\right)^2 + (1-\phi)\left(\frac{\rho_c}{\rho}\right)$$

A conservative estimate of the foam stiffness will be used in the following analysis, neglecting the wall stretching contribution.

The second type of microstructure, exhibited by the Old World porcupines (*Hystrix Galeata, Subcristatus and Indica x Cristata*, Fig. 5.9b), has an isotropic foam core with longitudinal rib stiffeners, producing orthotropic properties. Their relative moduli in the longitudinal and radial directions, x and z, can be estimated from an upper bound rule of mixtures, as:

$$\left(\frac{E_c}{E}\right)_x = \left(\frac{E_c}{E}\right)_z = \left(\frac{\rho_c}{\rho}\right)_{ribs} + \left(1-\left(\frac{\rho_c}{\rho}\right)_{ribs}\right)\left(\frac{\rho_c}{\rho}\right)^2_{foam}$$

and the relative modulus in the circumferential direction, y, can be conservatively estimated by:

$$\left(\frac{E_c}{E}\right)_y = \frac{1}{\left(1-\left(\frac{\rho_c}{\rho}\right)_{ribs}\right)^2}\left(\frac{\rho_c}{\rho}\right)^2_{foam}$$

where $(\rho_c/\rho)_{ribs}$ and $(\rho_c/\rho)_{foam}$ represent the relative density of the ribs and foam, obtained by dividing the solid cross sectional area occupied by the ribs and the foam respectively over that of the total cross section (Table 5.1A).

In the case the third type of microstructure, typified by the hedgehog spines (*Erinaceus and Hemiechinus*) (Fig.5.9c), the square honeycomb core has a radial relative stiffness equal to its relative density, while the longitudinal and circumferential stiffnesses are equal to half that value because only half the core material is oriented in those directions:

$$2\left(\frac{E_c}{E}\right)_x = 2\left(\frac{E_c}{E}\right)_y = \left(\frac{E_c}{E}\right)_z = \left(\frac{\rho_c}{\rho}\right)$$

The last type of core microstructure observed in the spines is that of the tenrec (*Setifer*) (Fig. 5.9d). Its circumferential and radial relative stiffnesses are equal to its relative density while its longitudinal stiffness is negligible.

The cores of the plant stems consist mainly of parenchymatous tissue which can be considered as an isotropic material (Niklas, 1992), (Fig. 5.9e). They are treated similarly to the procupine quills of type 1 microstructure. The relative stiffness of these cores can be conservatively estimated as:

$$\left(\frac{E_c}{E}\right)_x = \left(\frac{E_c}{E}\right)_y = \left(\frac{E_c}{E}\right)_z = \left(\frac{\rho_c}{\rho}\right)^2$$

neglecting the water pressure (turgor pressure) and wall stretching effects.

## 5.3 Mechanical Efficiency of Natural Structures

The analysis of Chapter 3 can be used to describe the mechanical efficiency of natural cylindrical shells in a number of ways. Most obvious, the ratio of the buckling load (under axial compression) or buckling moment (under pure bending) of a natural shell with a compliant core to that of an equivalent hollow shell can be calculated. In addition, the core depth can be compared with that required for the core stresses to decay to 5% of the value at the shell during local buckling, $(c/t)_o$.

From the estimated geometrical and material properties, the theoretical core depth required for the core stress to decay to 5% of the value at the shell during local buckling, $(c/t)_o$, were calculated according to the analysis of Chapter 3 (eqns 3.18) and are listed in Tables 5.2A and 5.2B. The theoretical values are compared with the measured values of c/t in Figure 5.10. The results of Chapter 3 (eqns 3.18) were obtained by treating the core as a two dimensional elastic foundation with isotropic properties in the x-z plane. The

core resists the movements of the shell by extension-compression in the z-direction and by shearing in the x-z plane. This analysis is exact for the case of the natural structures with isotropic cores of type 1 microstructure (quills and all plant stems), and is equally valid for the quills and spines of microstructures of types 2 and 3 . It is however not applicable to type 4 microstructures (*Setifer* spines) where the foundation cannot provide any shearing resistance due to its longitudinal discontinuity in the x-direction. The *Setifer* spine specimen was therefore dropped from the following analysis.

The efficiency of the natural cylindrical microstruc-tures was evaluated by comparing their failure loads to those of equivalent hollow sections of the same radius and total mass. Assuming the Poisson's ratios of both the cores and the shells to be equal to 0.3, the ratios of the buckling stress, $\sigma_{cr}/(\sigma_o)_{eq}$, the axial buckling load, $P_{cr}/(P_o)_{eq}$, the Brazier moment, $M_{Brazier}/(M_{Brazier})_{eq}$, and the local buckling moment, $M_{l.b.}/(M_{l.b.})_{eq}$, were all calculated. The type 1,2, and 3 microstructures were analyzed by modifying the equations of Chapter 3 (eqns 3.44 3.47) to account for the transversely isotropic properties of the cores and their measured depth as follows:

- in the elastic foundation calculations of the critical buckling parameter, $\lambda_{cr}/t$, and the function $f_1$ (eqns 3.18 and 3.19) the radial stiffness modulus ratio, $(E_c/E)_z$, was used.

The spring constant of the foundation was claculated according to eqn 4.2 accounting for the depth of the foundation.

- in the terms correcting for the axial load carried by the core (eqn 3.20) and for the increase in the moment of inertia due to the core (Appendix Ch.3) the longitudinal stiffness modulus ratio, $(E_c/E)_x$, was used.

- in the equations giving the ratios of buckling load or moment of the shell with the core to that without the core (eqns. 3.44 to 3.47), the core depth needed for 95% stress decay, $(c/t)_o = 5\lambda_{cr}/t$, was replaced by the measured core depth c/t.

- the radial stiffness modulus ratio, $(E_c/E)_z$, was used in the calculations of the ovalisation of the core and the Poisson effect (Appendix Ch.3). The effect of the lower circumferential stiffness modulus ratio, $(E_c/E)_y$, in the case of type 2 and 3 core microstructures (Fig. 5.9b and c) was neglected. The error resulting from this simplification affects only the amount of ovalisation due to Brazier's effect which for all good purposes falls below 2% and is negligible for any stiffness modulus ratio in the range considered.

Carrying out all the modifications described above the following equations are obtained:

$$\frac{\sigma_{cr}}{(\sigma_o)_{eq}} = \frac{\sqrt{3(1-v^2)}}{\left[1 + \frac{c}{2t}\frac{\rho_c}{\rho}\left(2 - \frac{c/t}{a/t}\right)\right]} f_1 \qquad (5.1)$$

$$\frac{P_{cr}}{(P_o)_{eq}} = \frac{\sqrt{3(1-v^2)}\left[1 + \frac{c}{2t}\alpha'\left(2 - \frac{c/t}{a/t}\right)\right]}{\left[1 + \frac{c}{2t}\frac{\rho_c}{\rho}\left(2 - \frac{c/t}{a/t}\right)\right]^2} f_1 \qquad (5.2)$$

$$\frac{M_{Brazier}}{(M_{Brazier})_{eq}} = \frac{\left[1 + \frac{2}{3}(1-v^2)\alpha\beta\left(\frac{a}{t}\right)^3\right]^{\frac{1}{2}}\left[1 + \frac{\alpha'}{4}\frac{a}{t}\left(1 - \left(1 - \frac{c/t}{a/t}\right)^4\right) + \frac{\alpha\beta'}{8}\frac{a}{t}\right]^{\frac{3}{2}}}{\left[1 + \frac{\alpha'}{4}\frac{a}{t}\left(1 - \left(1 - \frac{c/t}{a/t}\right)^4\right)\right]\left[1 + \frac{c}{2t}\frac{\rho_c}{\rho}\left(2 - \frac{c/t}{a/t}\right)\right]^2} \qquad (5.3)$$

173

$$\frac{M_{l.b.}}{(M_{l.b.})_{eq}} = \frac{\left[1 + \dfrac{\dfrac{\alpha\beta'}{8}\dfrac{a}{t}}{1 + \dfrac{\alpha'}{4}\dfrac{a}{t}\left(1 - \left(1 - \dfrac{c/t}{a/t}\right)^4\right)} - \dfrac{3}{2}\xi_{lb}\right]\left[1 + \dfrac{\alpha'}{4}\dfrac{a}{t}\left(1 - \left(1 - \dfrac{c/t}{a/t}\right)^4\right)\right]\left(\dfrac{1 - 3\xi_{lb}}{1 - \xi_{lb}}\right)f_1}{0.312\left[1 + \dfrac{c}{2t}\dfrac{\rho_c}{\rho}\left(2 - \dfrac{c/t}{a/t}\right)\right]^2}$$

(5.4)

where the ovalisation at the local buckling moment, $\xi_{lb}$, is obtained similarly to eqn. 3.40 from:

$$\sqrt{\left(\frac{\xi_{lb}}{1 - \nu^2}\right)}\left(\frac{1 - \xi_{lb}}{1 - 3\xi_{lb}}\right) = \frac{\left[1 + \dfrac{\alpha'}{4}\dfrac{a}{t}\left(1 - \left(1 - \dfrac{c/t}{a/t}\right)^4\right)\right]^{\frac{1}{2}}}{\left[1 + \dfrac{2}{3}(1 - \nu^2)\alpha\beta\left(\dfrac{a}{t}\right)^3\right]^{\frac{1}{2}}}f_1$$

(5.5)

$f_1$ was calculated from eqn. 3.19 with $\lambda_{cr}/t$ taken from Tables 5.2A and 5.2B; and the parameters $\alpha$, $\alpha'$, $\beta$, and $\beta'$ defined as follows:

$$\alpha = \left(\frac{E_c}{E}\right)_z$$

$$\alpha' = \left(\frac{E_c}{E}\right)_x$$

$$\beta = 2.88\left(1 - \left(1 - \frac{c/t}{a/t}\right)^2\right)$$

$$\beta' = 0.762\left(1 - \left(1 - \frac{c/t}{a/t}\right)^4\right)$$

(5.6)

These failure load ratios are presented in Tables 5.3A and 5.3B, and Figures 5.11, 5.12 and 5.13.

## 5.4 Discussion

In Figure 5.10, the measured core depth to thickness ratio, $c/t$, is plotted versus the depth required for 95% stress decay, $(c/t)_o$, for the quills and spines on one hand and the plant stems on the other. The data for the plant stems falls consistently along, but slightly below, the $c/t = (c/t)_o$ line. It is fitted with a high correlation, R=0.96, by a line of a slope of 0.95, which is very close to 1.0 and can be practically considered equal to it. The data for the quills and spines does not fall along the $c/t = (c/t)_o$ line. However, it does show a very clear trend of its own, best fitted by a line of slope 2.9, with a high correlation factor of R=0.94. The growth or development of the reinforcing foam cores of the plant stems seems clearly driven and controlled by the stresses generated in the core at impending local buckling of the shell. The decay of stresses away from the shell reduces the amount of material needed to resist them causing a continuous foam density reduction (Fig.5.6b); at $c/t = (c/t)_o$, the foam core is simply stopped and no more material is needed as no more stresses are felt. The spines of *Erinaceus* and *Hemiechinus* are the only ones in the animal group that have a core only partially spanning the inside of the shell. They do however contain thin widely spaced diaphragms. The data points corresponding to their

cores fall at the intersection of the $c/t = (c/t)_0$ line and the quills and spines trend. Though fully filled, the quills of the porcupines ( *Hystrix, Erethizon, Coendou*) all show a marked decrease in the core density towards the center (Fig. 5.1a, 5.2a and 5.3a) supporting the stress controlled growth hypothesis. The purely theoretical measure of the stresses in the core at local buckling, $(c/t)_0$, derived in the analysis of Chapter 3, is shown to be one, but possibly not the only, major variable controlling the growth of foam cores in quills and spines. Physiological and physical conditions, not investigated in this analysis may well explain the need for fully filled cores or cores with diaphragms.

Figures 5.11 shows the failure load and moment ratios for the quills and spines to those of a hollow cylinder of equal mass and radius. Figure 5.11a shows $P_{cr}/(P_0)_{eq}$ for the different species investigated. Only the hedgehog spines, with the square honeycomb-like cores which have a stiffness proportional to their density are above the 1.0 line showing more than 50% improved performance under axial load. Figure 5.11b shows the Brazier moment ratio, $M_{Brazier}/(M_{Brazier})_{eq}$, with all surveyed species showing improvements between 100 and 900%, except of course for the hollow *Tachyglossus Aculeatus* specimen. Although in practice, local buckling precedes Brazier buckling, this does imply that the Brazier ovalization and associated loss of moment of inertia aretotally prevented. Figure 5.11c presents the improvements in local buckling resistance under bending, $M_{l.b.}/(M_{l.b.})_{eq}$. The best improvements, over 300%, are achieved again by *Erinaceus* and *Hemiechinus* because of their square honeycomb cores. The *Hystrix* family reaches modest results ranging from nothing to about 40%. *Tachyglossus Aculeatus, Erethizon,* and *Coendou* fail to realize any improvements in local buckling moment resistance, and actually decrease that resistance by as much as 30% (Table 5.3A). Note that the model used in the analysis to estimate the stiffness of the foam core for the porcupine quills of type 1 microstructure (Fig. 5.9a) neglected the wall stretching effect and may have been overconservative. Figure 5.8c shows the cell

walls of *Erethizon*'s foam core to contain a substantial fraction of the total solid material. A more involved microstructural investigation would have been required in order to correctly account for this stiffening effect.

All animal quills and spines succeed in controlling the mode of failure by eliminating Brazier ovalization. The improvements in local buckling resistance under axial load or bending moment are mixed, with most species achieving some improvement in local buckling moment resistance (Fig. 5.11c). The function of the quill or spine may dictate the level of performance. The short spines of the hedgehog (*Erinaceus* ) and the spiny rat (*Hemiechinus* ) are required to act as shock absorbers as much as armour and protection to discourage predators, hence the high structural efficiency requirement and the need to delay local buckling until the internal stresses have almost reached material failure limits (Vincent and Owers, 1986). The longer quills of the porcupines may only be needed to act as a deterrent to predators with less of a mechanical shock absorbing function (Vincent and Owers, 1986). The efficiency ranking of the species surveyed varies little from one measure to another in Figs 5.11a through 5.11c. This ranking could possibly be used to establish the relative positions of these animals along the evolutionary scale and the effect of geography on their development. Both *Coendou* and *Erethizon* are New World porcupines, *Hystrix* is the family of Old World porcupines, *Tachyglossus Aculeatus* is an echidna native to Australia, Tasmania and New Guinea. The tenrec (*Setifer* ) is found in Madagascar and the hedgehog (*Erinaceus Europaeus* ) is of course a European insectivorous mammal.

Figures 5.12 summarizes the results for the ratios of axial buckling load, Brazier moment, and local buckling moment for the plant stems. Losing axial stiffness because of the three dimensional core, plant stems have their axial buckling resistance reduced between 10 and 40% (Fig. 5.12a). Brazier moment resistance is improved increasingly with increasing a/t, ratios, up to 900% at a/t=60 (Fig. 5.12b). Local buckling moment

177

resistance is nearly without improvements at a/t ratios below 20, but manages a significant 20 to 50% improvement at higher a/t ratios (Fig. 5.12c). The apparently poorer performance of stems with pithy parenchymatous cores is due to the fact that in this analysis the relative density of the foam was used to estimate its relative modulus of stiffness neglecting the effect of turgor pressure. Parenchyma cells are living cells with a protoplast. They fulfill many physiological functions among which water storage, and act as stacked pressurized containers in the core. The pressurized protoplast stiffens the cell walls against bending and acts as an elastic foundation (Niklas, 1992). The impact of this water pressure (or turgor pressure) on the effective stiffness properties of plant stems and other tissues has been investigated by Niklas and O'Rourke (1987) and Niklas (1989) showing its importance. In the case of species occupying wet habitats (hydrophytes) mechanical support is mainly provided by hydrostatic tissues (Niklas, 1992). Experimental investigations have showed the turgor pressure to increase the effective stiffness of chive (*Allium schoenoprasnum* ) leaves by threefold (Niklas and O'Rourke, 1987) and that of parenchyma plugs from potato tubers by fivefold (Niklas, 1992). Nilsson et al. (1958) derived a formula that predicts the apparent elastic modulus of parenchyma for any turgor pressure, and Gibson and Ashby (1988) proposed a similar one for pressurized synthetic foams. Both models show the increase in the relative stiffness ratio, $E_c/E$, to be proportional to $p/E$, where p is the internal cell pressure. If the internal pressure effect was included in the previous analysis it would have introduced an important stiffening of the parenchymatous cores and would have resulted in a marked improvement in mechanical performance. Measurements of this pressure and estimates of the pressurized parenchyma apparent modulus were however beyond the scope of this study.

The plant stems show more consistent results than the animal quills and spines. For a porcupine or a hedgehog the quills and spines represent a fraction of their total

weight and perform a limited and very specific function that depends on the specie and that may or not be critical for survival. This does not impose a very high evolutionary stress on the animal to develop the most efficient and adapted structure. The spines density was estimated from the hide of one of the sacrificed hedgehogs that furnished the spine specimens, to be as high as 114 spines per $cm^2$. The average spine weight was measured to be aroung 5.4 mg. Treating the hedgehog as a spheroid covered with spines, the weight of the spines was estimated to be of the order of 10% of the total weight of the animal. This is a relatively important fraction of the hedgehog weight and it can explain the higher mechanical efficiency of its spines.

On the other hand the stem of a plant is its most important biomass investment, providing structural support and carrying lifelines from the roots to the leafs and reproductive organs. It is critical for survival. In a competition for sun light and exposure, the plant able to minimize its structural weight for the required strength, will maximize its growth rate, attaining greater heights in shorter times, and hence securing its evolutionary niche and insuring its perpetuation.

Finally, Figure 5.13 compiles the calculated ovalisation at local buckling under bending, $\xi$ lb, for the quills, spines and stems. It is plotted versus a/t showing the dramatic decrease in ovalisation from 0.145 for a hollow tube to less than 0.01. This decrease is more important at higher a/t ratios. This ovalisation measure can be used as a single parameter to compare and rank, albeit approximately, both the Brazier moment and local moment resistances of different natural foam core cylindrical structures.

## 5.5 Engineering design and biomimetics

The theoretical and experimental analysis of foam core cylinders in Chapters 3 and 4, inspired from natural structures, have suggested new avenues of research and new

configurations that optimize the use of materials. The survey and analysis of natural tubular structures in this chapter has identified some well designed and complicated structures. The solutions achieved by natural organisms also have to meet many other requirements imposed by growth and physiological function that could not have possibly been included in our analysis.

More so than by blindly copying a final solution from nature, the engineer can learn by mimicking in design the evolutionary process. Take the quills and spines, for example. These are modified hairs whose original dimensions, utility and density, may have been determined by a minimum heat transfer condition (Bejan, 1992). Their main function is a structural beam-column with loading stresses caused typically by an eccentrically applied compressive force on the free end (Vincent and Owers, 1986). The mechanical design problem can be stated as follows: for a given length, the spine or quill has to meet or exceed a set of stiffness and strength requirements keeping the mass to a minimum. At the scale of the quill, the mechanical constraints are: global bending stiffness to resist bending and Euler buckling and bending strength to avoid failure under the expected loads.

Figure 5.14 presents a set of sketches illustrating the development of increasingly mechanically efficient structures. Starting with a solid hair, or a rod, the first step to improve material efficiency is to go to a hollow cylinder of some radius to thickness ratio, a/t, that meets the bending stiffness requirement without increasing the mass (Fig. 5.14a). When that a/t ratio is attained, the section becomes more sensitive to Brazier ovalization. This jeopardizes the bending stiffness at high curvatures and compounds the problem of local buckling which becomes the controlling mechanism of failure. The design problem is now taken one step further to the level of the cross section. Brazier ovalisation can be thought of as a distributed pressure load acting in the plane of the cross section trying to change its shape. To counteract this distributed load an isotropic foam

core is introduced providing for uniform support with a minimum amount of material (Fig. 5.14b).

At this stage local buckling of the shell becomes the next problem to solve in order to meet the strength requirement. The problem of local buckling under bending is in fact that of a thin sheet on an elastic foundation under axial compressive stresses. One way to improve the resistance to local buckling is to provide for immediate support of the shell in the most efficient way, which is to align some core material radially. This radial reinforcement can be provided in the form of longitudinal, circumferential or orthogonal stiffeners (Fig. 5.14c). If these stiffeners are massively built they can also resist Brazier ovalization and the isotropic foam core can be dispensed of (Fig. 5.14d). Finally a stiff efficient core microstructure (such as a square honeycomb) is reached and local buckling is adequately resisted the depth of the material in the central part of the core can be removed without affecting the mechanical performance (Fig. 5.14e).

The different quill and spine microstructures surveyed in this study support this design evolution scenario. Plant stems design can be deduced from a different scenario as proposed by Niklas (1992) that involves in addition physiological factors.

The iterative engineering design process is similar to the hierarchical design process proposed for quills and spines. In treating tubular structures, we have moved from solid to hollow sections, then from hollow to reinforced hollow sections. The manufacturing problems encountered in making orthogonally reinforced metallic shells with thin deep stringers and rings have prevented the improvement of our designs. Metallic honeycombs can today bridge this technological gap and may provide new ways of manufacturing reinforced shells inspired from natural structures. The use of foams as stabilizing foundations has been recently introduced to reinforce the honeycomb cores of sandwich panels against local buckling. Recent advances in materials microstructuring processes such as foaming, are giving the engineer the same operating power as nature to

181

produce better designs by following a hierarchical design optimization process at ever smaller scales, going from structure to microstructrue to nanostructure.

## 5.6 Conclusion

The characterization of several natural tubular structures (quills, spines and plant stems) revealed them to be close to the optimal configurations predicted by the analytical model. The analysis of their mechanical efficiency has improved our understanding of their function and design evolution; it did not however account for physiological and growth requirements.

Engineering design can benefit at two levels: at the level of outright biomimicry, copying a given successful design such as that of the hedgehog spines, or at the level of the design process, following a hierarchical approach, satisfying optimally the most immediate mechanical constraint at the scale under consideration.

# References

Bejan,A. (1992), "Surfaces covered with hair: Optimal strand diameter and optimal porosity for minimum heat transfer",Biomimetics, Vol.1(1), pp 25-40

Cenci, C.A., Grando, S. and Ceccarelli, S. (1989), "Culm anatomy in barley (*Hordeum vulgare* )", Can. J. Bot., Vol. 62, pp 2023-2027

Dunn, G.J. and Briggs, K.G. (1989), "Variation in culm anatomy among barley cultivars differing in lodging resistance", Can. J. Bot., Vol. 67, pp 1838-1843

Esau, K., (1977), Anatomy of Seed Plants, 2nd ed., John Wiley and Sons, New York

Gibson, L.J. and Ashby, M.F. (1982),"The mechanics of three-dimensional cellular materials",Proc. R. Soc. Lond., Vol A382, pp 43-59

Gibson, L.J. and Ashby, M.F. (1988), Cellular Solids, Structure and Properties , Pergamon Press, New York

Gunderson, S.L., Gunnison, K.E. and Sawvel, J.W., (1992) "Hierarchical structure of a natural composite:insect cuticle", Mat. Res. Soc. Symp. Proc., Vol. 255, pp 159-169

Niklas, K.J. and O'Rourke, T.D. (1987), "Flexural rigidity of chive and its response to water potential", Amer. J. Bot., Vol. 74 (7), pp 1034-1044

Niklas, K.J. (1989), "Mechanical behavior of plant tissues as inferred from the theory of pressurized cellular solids", Amer. J. Bot., Vol. 76 (6), pp 929-937

Niklas, K.J. (1992),Plant Biomechanics, an Engineering Approach to Plant Form and Function, The University of Chicago Press, Chicago

Nilsson,S.B., Hertz, S.H. and Falk,S. (1958),"On the relation between turgor pressure and tissue rigidity 2.Theoretical calculations on model systems", Physiol. Plant., Vol 11, pp 818-837

Stevens, P. (1993), personnal communication, Herbarium, Harvard University, Cambridge, MA.

Ueno, O., Samejima, M. and Koyama, T. (1989), "Distribution and evolution of C4 syndrome in *Eleocharis* , a sedge group inhaiting wet and aquatic environments, based on culm anatomy and carbon isotope ratios", Ann. Bot., Vol. 64, pp 425-438

Underwood, F.E. (1970), Quantitative Stereology, Addison-Wesley Publishing Co., Reading, Massachusetts

Vincent, J.F.V. and Owers, P., (1986), "Mechanical design of hedgehog spines and porcupine quills", J. Zool. Lond., Vol. A210, pp 55-75

Wilson, J.R., Anderson, K.L. and Hacker, J.B. (1989), "Dry matter digestibility in vitro of leaf and stem of buffel grass (*Cenchrus ciliaris* ) and related species and its relation to plant morphology and anatomy", Aust. J. Agr. Res., Vol. 40, pp 281-291

Table 5.1A. Section properties of animal quills and spines

| Animal Genus/Specie (common name) | Information Source | Outer radius, (mm) | Shell thick -ness (mm) | Shell relative density, $\rho$ (-) | Core relative density, $\rho_c$ (-) | Core depth, c (mm) |
|---|---|---|---|---|---|---|
| **Type 1: isotropic three dimensional foam core** | | | | | | |
| •*Coendou prehensilis* (Brazilian Porcupine) | Vincent and Owers (1986) | 0.48 | 0.033 | 1.0 | 0.2 | foam filled core |
| •*Erethizon*, (North American porcupine) | SEM investigation | 0.89 | 0.048 | 1.0 | 0.1-0.15 | foam filled core |
| •*Tachyglossus Aculeatus*, specimen 1 (echidna) | SEM investigation | 1.34 | 0.48 | 1.0 | 0.11 | foam filled core |
| •*Tachyglossus Aculeatus*, specimen 2 (echidna) | SEM investigation | 0.90 | 0.33 | 1.0 | 0.0 | empty thick walled tube |
| **Type 2: longitudinal solid ribs with isotropic three dimensional foam core** | | | | | | |
| •*Hystrix Galeata* (porcupine) | SEM investigation | 1.34 | 0.074 | 1.0 | 0.037 ribs, 0.10 foam | foam filled core |
| •*Hystrix Indica-Cristata* (porcupine) | Vincent and Owers (1986) | 1.33 | 0.133 | 1.0 | 0.03 ribs, 0.15 foam | foam filled core |
| •*Hystrix Subcristatus* (porcupine) | SEM investigation | 1.25 | 0.12 | 1.0 | 0.07 ribs, 0.11 foam | foam filled core |

Type 3: orthogonal longitudinal and circumferential stiffeners in a square honeycomb

| | | | | | | |
|---|---|---|---|---|---|---|
| •*Erinaceus Europaeus* (hedgehog) | SEM investigation | 0.36 | 0.025 | 1.0 | 0.1 | 0.17 |
| •*Erinaceus Europaeus* (hedgehog) | Vincent and Owers (1986) | 0.52 | 0.04 | 1.0 | 0.1 | 0.285 |
| •*Hemiechinus spinosus* (spiny rat) | Vincent and Owers (1986) | 0.53 | 0.04 | 1.0 | 0.1 | 0.21 |

Type 4: closely spaced thin septa

| | | | | | | |
|---|---|---|---|---|---|---|
| •*Setifer* (tenrec) | Vincent and Owers (1986) | 2.65 | 0.53 | 1.0 | 0.1 | filled core |

Table 5.1B. Section properties of plant stems

| Plant name (description) | Information Source | Outer radius, (mm) | Thick-ness (mm) | Shell relative density, $\rho$ (-) | Core relative density, $\rho_c$ (-) | Core depth, c (mm) |
|---|---|---|---|---|---|---|
| Group I: vascular bundles in core | | | | | | |
| •*Avena*, (oat) | Esau, (1977) | 3.82 | 0.06-0.08 | 0.95-1.0 | 0.1 without vascular bundles | 0.824 |
| •*Eleocharis* (sedge grass) | Ueno et al. (1989) | 0.35 | 0.016 | 0.9 | 0.2 | 0.1 |
| •*Elytrigia repens*, specimen 1 (grass) | SEM investigation | 0.97 | 0.036 | 0.9-1.0 | 0.13 (0.2 with vascular bundles) | 0.285 |
| •*Elytrigia repens*, specimen 2 (grass) | SEM investigation | 1.17 | 0.05 | 0.9-1.0 | 0.13, (0.2 with v.b.) | 0.4 |
| •*Hordeum vulgare*, (barley) | Dunn and Briggs (1989) | 1.5-2.0 | 0.03-0.09 | 0.8-1.0 | 0.1-0.2 | 0.3-0.68 |
| •*Secale*, (rye) | Esau, (1977) | 2.90 | 0.06 | 0.8 | 0.075 | 0.704 |
| Group II: vascular bundles in shell | | | | | | |
| •*Artemisia*, specimen 1 | SEM investigation | 1.6 | 0.381 | 0.9-1.0 | 0.1-0.3 | foam filled |
| •*Artemisia*, specimen 2 | SEM investigation | 2.55 | 0.762 | 1.0 | 0.2 | foam filled |
| •*Cenchrus Ciliaris* (buffel grass) | Wilson et al. (1989) | 0.83 | 0.14 | 0.8 | 0.2 | foam filled |
| •*Latuca Biennis*, | Optical microscopy | 7.5 | 0.127 | 1.0 | 0.07-0.10 | 1.54 |

| | | | | | |
|---|---|---|---|---|---|
| •*Phytolacca Americana*, (wild-berry type) | Optical microscopy | 7.75 | 0.41 | 0.95 | 0.03 | 5.0 |

Table 5.2A. Dimensionless material and geometrical properties of animal quills and spines

| Animal Genus/Specie (common name) | Radius to thick-ness ratio a/t (-) | Core to shell density ratio $\rho_c/\rho$ (-) | Core depth to thickness ratio c/t (-) | c/t ratio for 95% stress decay $(c/t)_0$ (-) | Buckling wave length para-meter† $\lambda_{cr}/t$ (-) | Radial core to shell stiffness ratio $(E_c/E)_z$ (-) | Longitu-dinal core to shell stiffness ratio $(E_c/E)_x$ (-) |
|---|---|---|---|---|---|---|---|
| •*Coendou prehensilis* (Brazilian Porcupine) | 14.0 | 0.2 | 13.5 | 8.25 | 1.65 | 0.04 | 0.04 |
| •*Erethizon*, (North American porcupine) | 18.0 | 0.125 | 17.5 | 10.50 | 2.10 | 0.0156 | 0.0156 |
| •*Tachyglossus Aculeatus*, specimen 1 (echidna) | 2.3 | 0.11 | 1.8 | 4.15 | 0.83 | 0.012 | 0.012 |
| •*Tachyglossus Aculeatus*, specimen 2 (echidna) | 2.20 | 0.0 | 0.0 | 4.08 | 0.0 | 0.0 | 0.0 |
| •*Hystrix Galeata* (porcupine) | 17.6 | 0.137 | 17.1 | 8.40 | 1.68 | 0.047 | 0.047 |
| •*Hystrix Indica-Cristata* (porcupine) | 9.5 | 0.18 | 9 | 7.24 | 1.45 | 0.052 | 0.052 |
| •*Hystrix Subcristatus* (porcupine) | 10.0 | 0.18 | 9.5 | 6.77 | 1.35 | 0.081 | 0.081 |
| •*Erinaceus Europaeus* (hedgehog) | 13.7 | 0.10 | 6.8 | 6.86 | 1.37 | 0.10 | 0.05 |

| | | | | | | | |
|---|---|---|---|---|---|---|---|
| •*Erinaceus Europaeus* (hedgehog) | 12.5 | 0.10 | 7.1 | 6.75 | 1.36 | 0.10 | 0.05 |
| •*Hemiechinus spinosus* (spiny rat) | 12.75 | 0.10 | 5.25 | 6.75 | 1.36 | 0.10 | 0.05 |
| •*Setifer* (tenrec) | 4.5 | 0.1 | 4 | NA†† | NA | 0.10 | 0.0 |

†the ratio of the critical buckling wavelength parameter to the thickness, $\lambda_{cr}/t$, was calculated form eqn 3.36
††NA: not applicable

Table 5.2B. Dimensionless material and geometrical properties of plant stems

| Plant name (description) | Radius to thickness ratio $a/t$ (-) | Core to shell relative density $\rho_c/\rho$ (-) | Core depth to thickness ratio $c/t$ (-) | c/t ratio for 95% stress decay $(c/t)_0$ (-) | Buckling wave length parameter† $\lambda_{cr}/t$ (-) | Radial core to shell stiffness ratio $(E_c/E)_z$ (-) | Longitudinal core to shell stiffness ratio $(E_c/E)_x$ (-) |
|---|---|---|---|---|---|---|---|
| **Group I** •*Avena*, (oat) | 54 | 0.10 | 12 | 14.01 | 2.85 | 0.01 | 0.10 |
| •*Eleocharis* (sedge grass) | 21.4 | 0.22 | 6.35 | 8.645 | 1.729 | 0.05 | 0.22 |
| •*Elytrigia repens*, specimen 1 (grass) | 26.4 | 0.22 | 7.9 | 8.78 | 1.76 | 0.05 | 0.22 |
| •*Elytrigia repens*, specimen 2 (grass) | 22.9 | 0.22 | 8 | 8.70 | 1.743 | 0.05 | 0.22 |
| •*Hordeum vulgare*, (barley) | 28.7 | 0.17 | 9 | 10.02 | 2.007 | 0.03 | 0.17 |
| •*Secale*, (rye) | 48 | 0.094 | 11.7 | 14 | 2.80 | 0.009 | 0.094 |
| **Group II** •*Artemisia*, specimen 1 | 3.7 | 0.22 | 3.2 | 5.06 | 1.015 | 0.05 | 0.05 |
| •*Artemisia*, specimen 2 | 2.84 | 0.20 | 2.3 | 4.53 | 0.908 | 0.04 | 0.04 |
| •*Cenchrus Ciliaris* (buffel grass) | 5.4 | 0.25 | 4.9 | 5.84 | 1.169 | 0.0625 | 0.0625 |
| •*Latuca Biennis*, | 58.6 | 0.10 | 12.1 | 14.5 | 2.892 | 0.01 | 0.01 |

| *Phytolacca* | 18.4 | 0.032 | 12.2 | 11.7 | 2.347 | 0.001 | 0.001 |
| *Americana,* | | | | | | | |
| (wild-berry | | | | | | | |
| type) | | | | | | | |

†the ratio of the critical buckling wavelength parameter to the thickness, $\lambda_{cr}/t$, was calculated form eqn 3.36

Table 5.3A. Failure load ratios for animal quills and spines

| Animal Genus/Specie (common name) | Buckling stress ratio $\sigma_{cr}/(\sigma_o)_{eq}$ (-) | Axial buckling load ratio $P_{cr}/(P_o)_{eq}$ (-) | Brazier moment ratio $M_{Br.}/(M_{Br.})_{eq}$ (-) | Local buckling moment ratio $M_{lb}/(M_{lb})_{eq}$ (-) | Ovalisation at local buckling $\xi_{lb}$ (-) |
|---|---|---|---|---|---|
| •*Coendou prehensilis* (Brazilian Porcupine) | 0.91 | 0.51 | 2.76 | 0.77 | 0.0074 |
| •*Erethizon*, (North American porcupine) | 0.74 | 0.40 | 3.00 | 0.73 | 0.0054 |
| •*Tachyglossus Aculeatus*, specimen 1 (echidna) | 0.91 | 0.82 | 0.89 | 0.88 | 0.134 |
| •*Tachyglossus Aculeatus*, specimen 2 (echidna) | 1.00 | 1.00 | 1.00 | 1.00 | 0.145 |
| •*Hystrix Galeata* (porcupine) | 1.14 | 0.73 | 5.26 | 1.27 | 0.0055 |
| •*Hystrix Indica-Cristata* (porcupine) | 0.87 | 0.55 | 2.57 | 0.96 | 0.0134 |
| •*Hystrix Subcristatus* (porcupine) | 1.14 | 0.85 | 4.02 | 1.44 | 0.0125 |
| •*Erinaceus Europaeus* (hedgehog) | 2.05 | 1.70 | 10.04 | 3.25 | 0.0107 |
| •*Erinaceus Europaeus* (hedgehog) | 1.90 | 1.58 | 9.07 | 2.98 | 0.0109 |

| •*Hemiechinus spinosus* (spiny rat) | 2.06 | 1.71 | 9.38 | 3.36 | 0.0129 |

## Table 5.3B. Failure load ratios for plant stems

| Plant name (description) | Buckling stress ratio $\sigma_{cr}/(\sigma_o)_{eq}$ (-) | Axial buckling load ratio $P_{cr}/(P_o)_{eq}$ (-) | Brazier moment ratio $M_{Br}/(M_{Br})_{eq}$ (-) | Local buckling moment ratio $M_{lb}/(M_{lb})_{eq}$ (-) | Ovalisation at local buckling $\xi_{lb}$ (-) |
|---|---|---|---|---|---|
| **Group I** •*Avena*, (oat) | 1.31 | 0.70 | 8.41 | 1.36 | 0.0024 |
| •*Eleocharis* (sedge grass) | 1.396 | 0.81 | 5.22 | 1.54 | 0.0084 |
| •*Elytrigia repens*, specimen 1 (grass) | 1.48 | 0.80 | 5.82 | 1.52 | 0.0068 |
| •*Elytrigia repens*, specimen 2 (grass) | 1.32 | 0.72 | 5.05 | 1.35 | 0.007 |
| •*Hordeum vulgare*, (barley) | 1.28 | 0.69 | 5.71 | 1.31 | 0.005 |
| •*Secale*, (rye) | 1.19 | 0.66 | 7.60 | 1.28 | 0.0026 |
| **Group II** •*Artemisia*, specimen 1 | 0.84 | 0.66 | 1.24 | 0.96 | 0.0667 |
| •*Artemisia*, specimen 2 | 0.86 | 0.71 | 1.01 | 0.91 | 0.0989 |
| •*Cenchrus Ciliaris* (buffel grass) | 0.83 | 0.58 | 1.66 | 0.96 | 0.0334 |
| •*Latuca Biennis*, | 1.39 | 0.74 | 9.06 | 1.44 | 0.0024 |
| •*Phytolacca Americana*, (wild-berry type) | 0.83 | 0.66 | 2.06 | 1.15 | 0.0297 |

Figure 5.1: Micrographs showing North American porcupine quill (*Erethizon*) (a) and (b) cross section
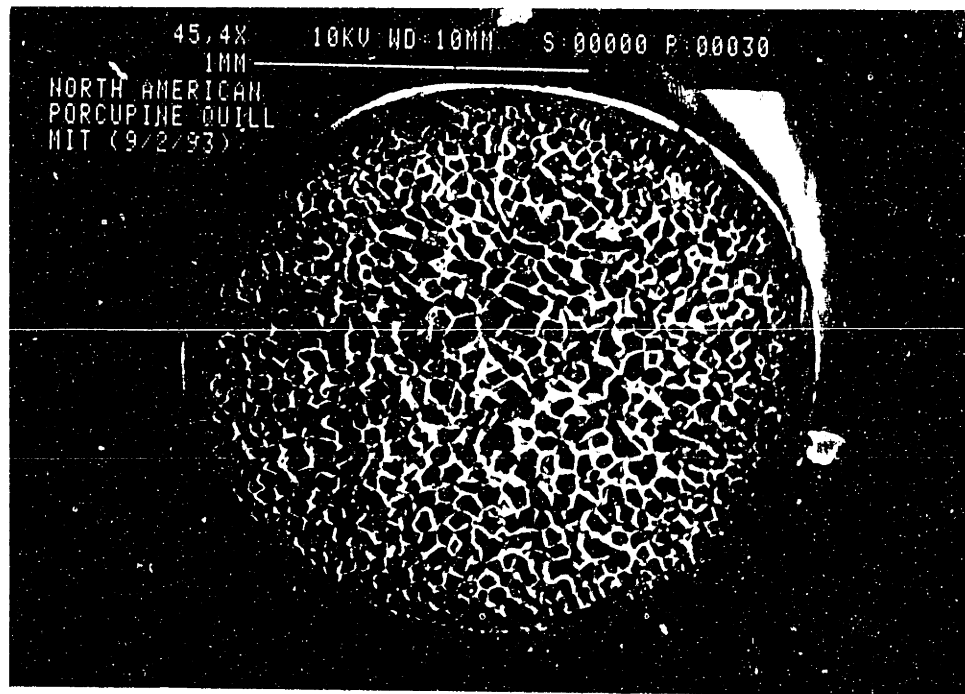


(a)
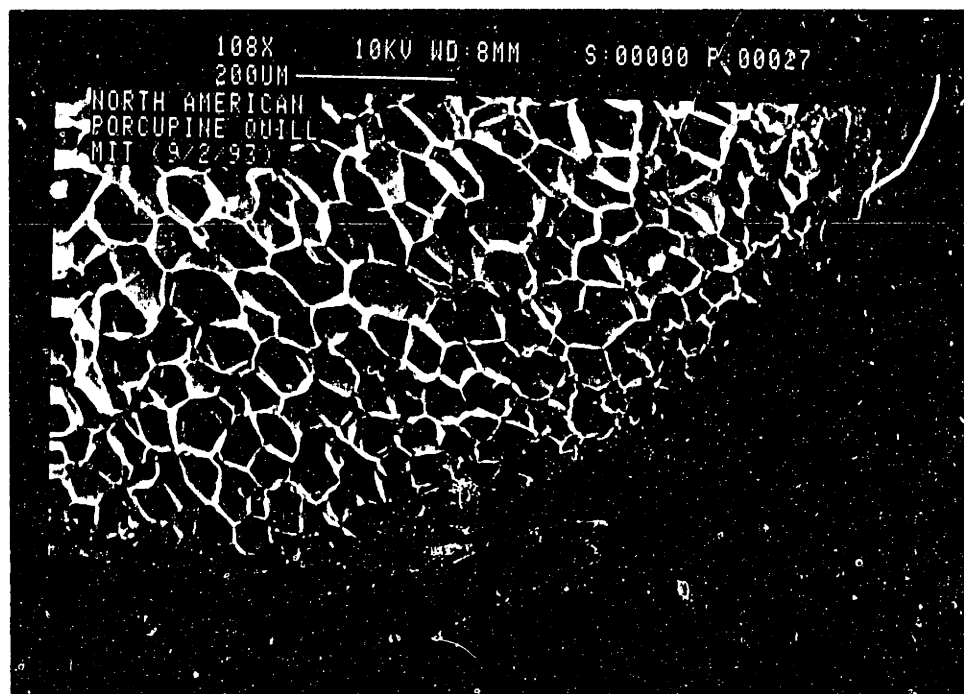


(b)

Figure 5.1: (c) and (d) longitudinal section
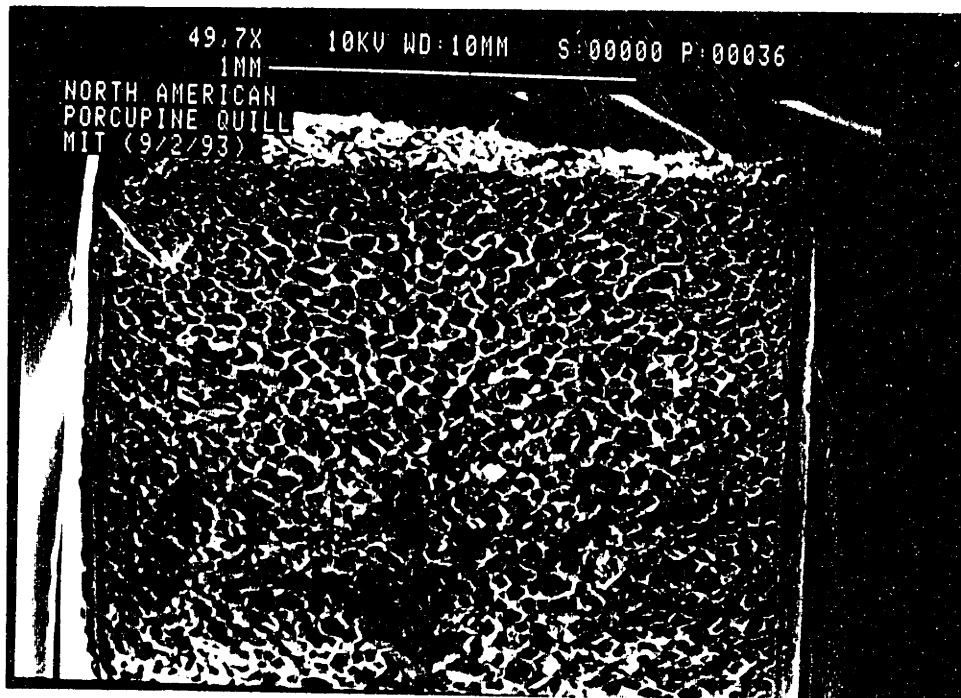


(c)
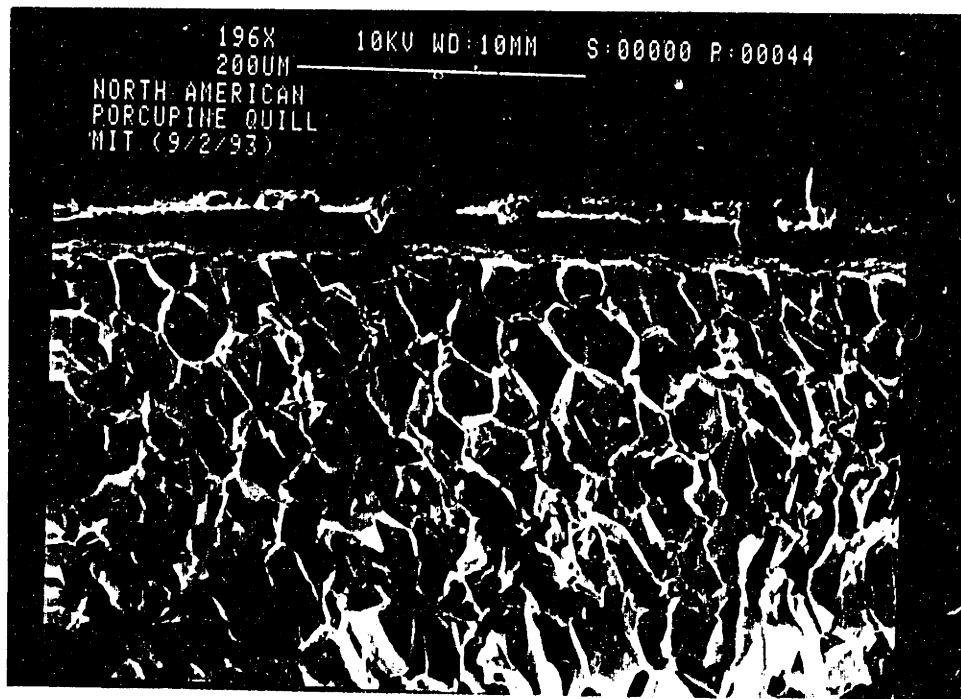


(d)

Figure 5.2: Micrographs showing echidna (*Tachyglossus Aculeatus*) quills: (a), (b)
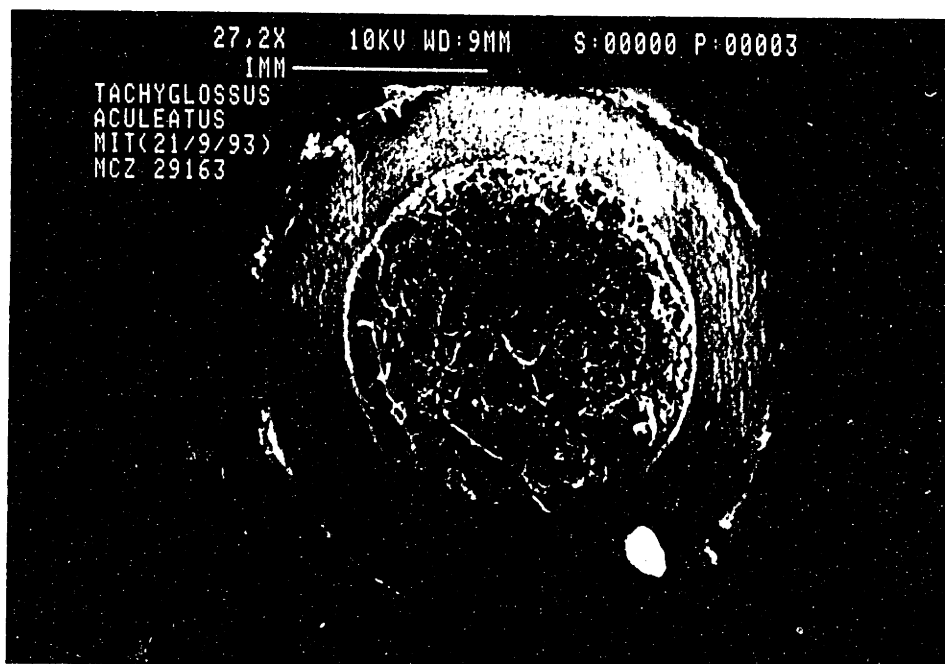


(a)
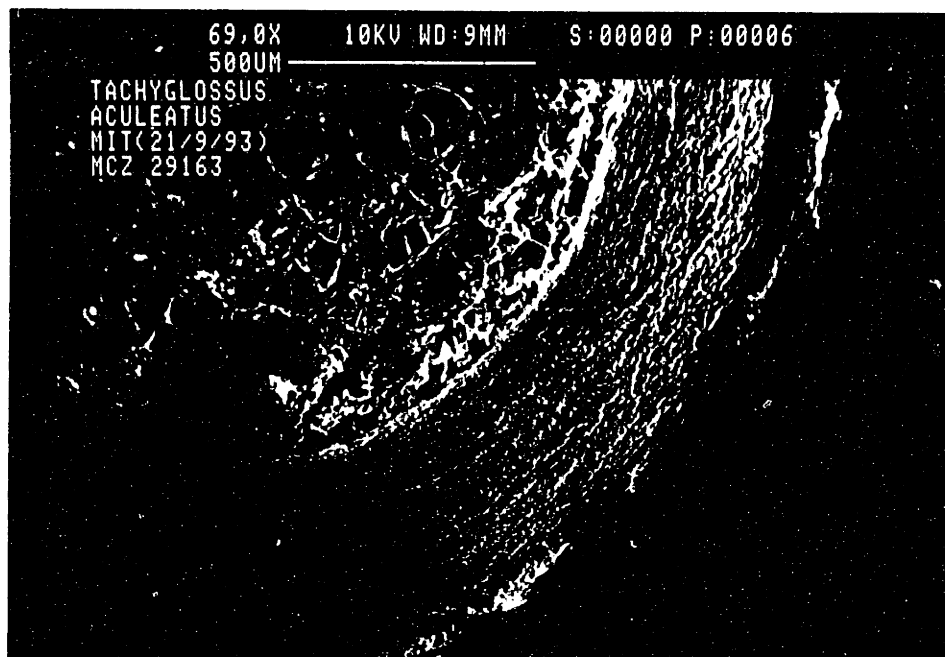


(b)

Figure 5.2: (d) cross sections and (c) longitudinal section
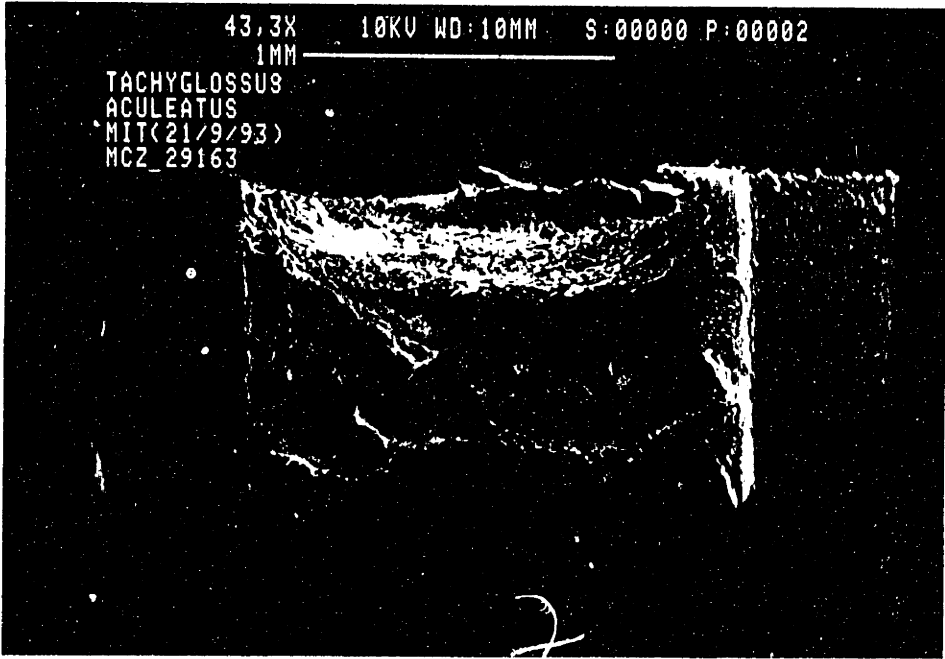


(c)
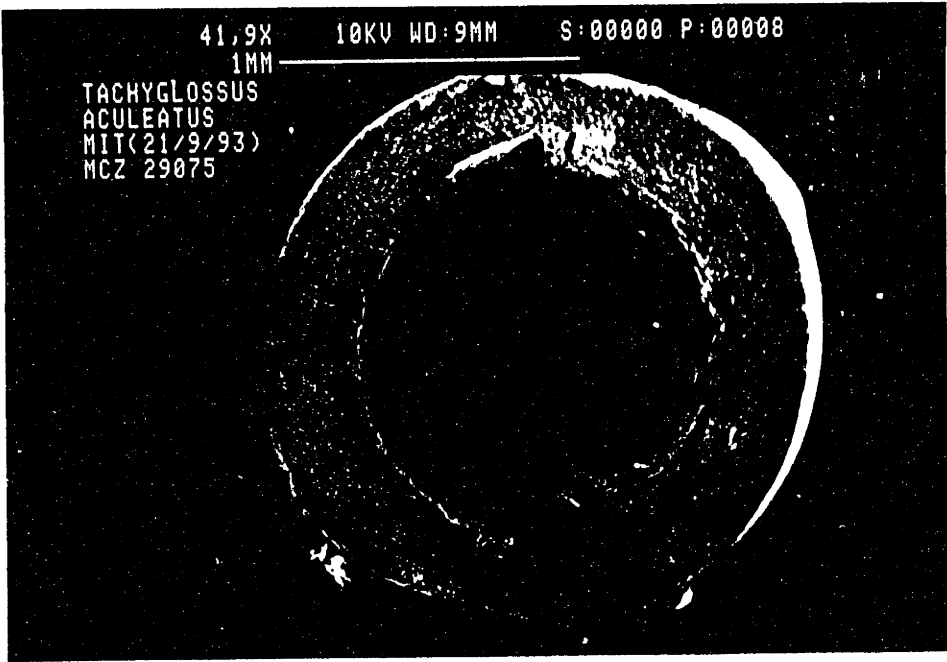


(d)

Figure 5.3: Micrographs showing *Hystrix Subsristata* quill : (a) and (b) cross section
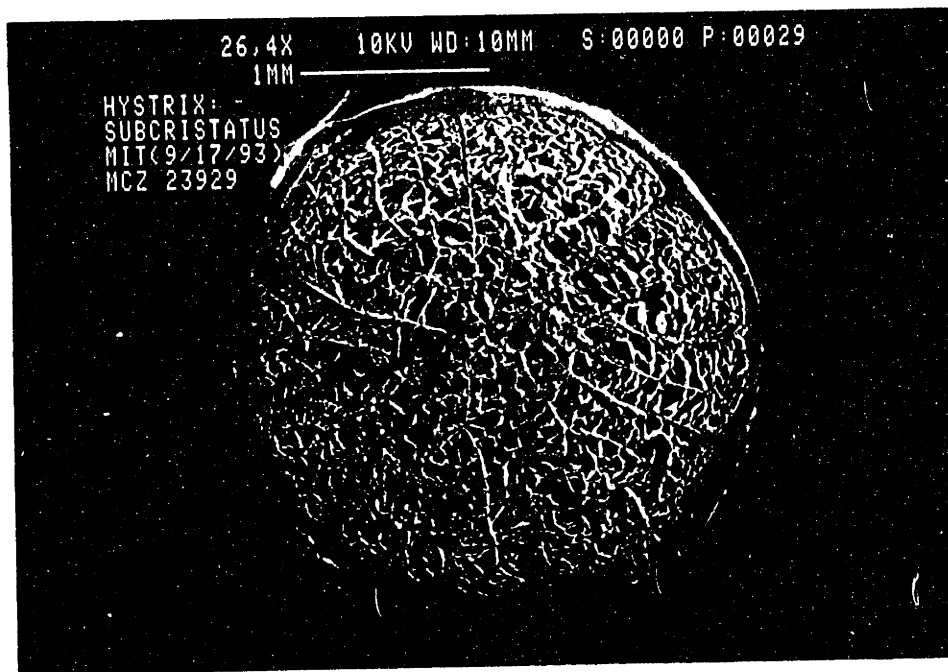


(a)
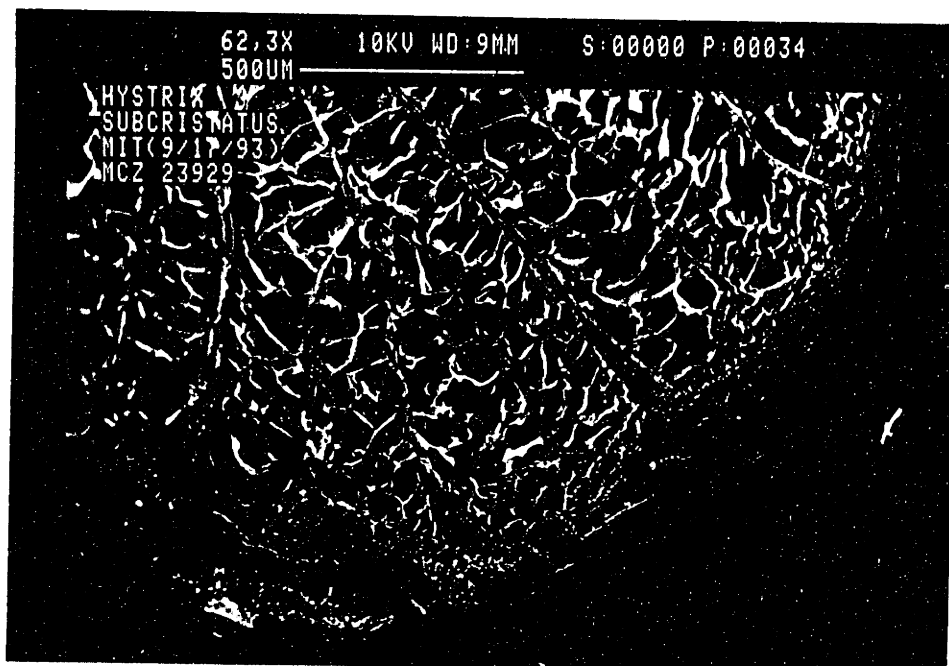


(b)

Figure 5.3: (c) and (d) longitudinal section
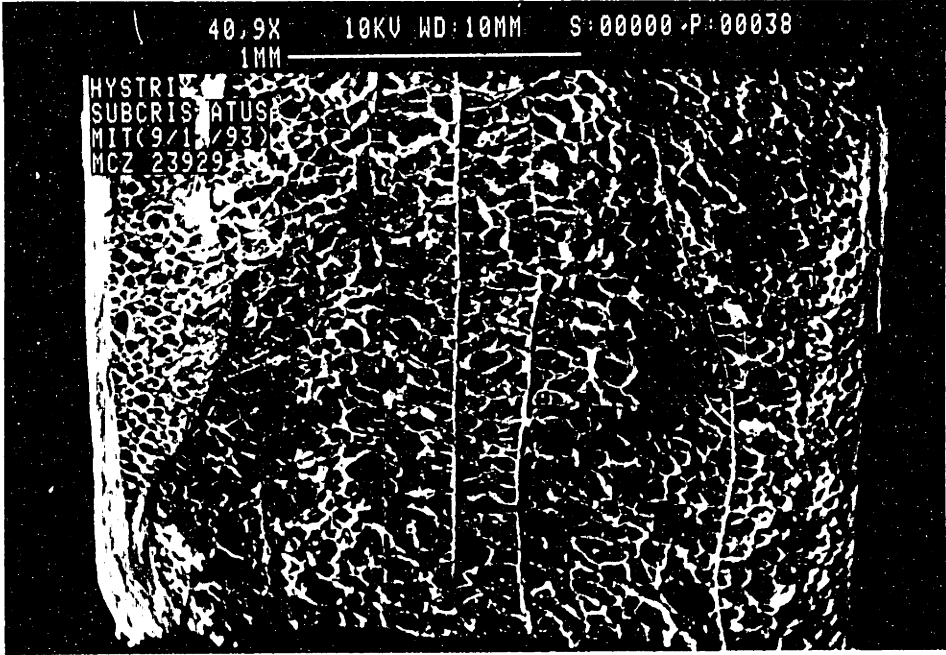


(c)
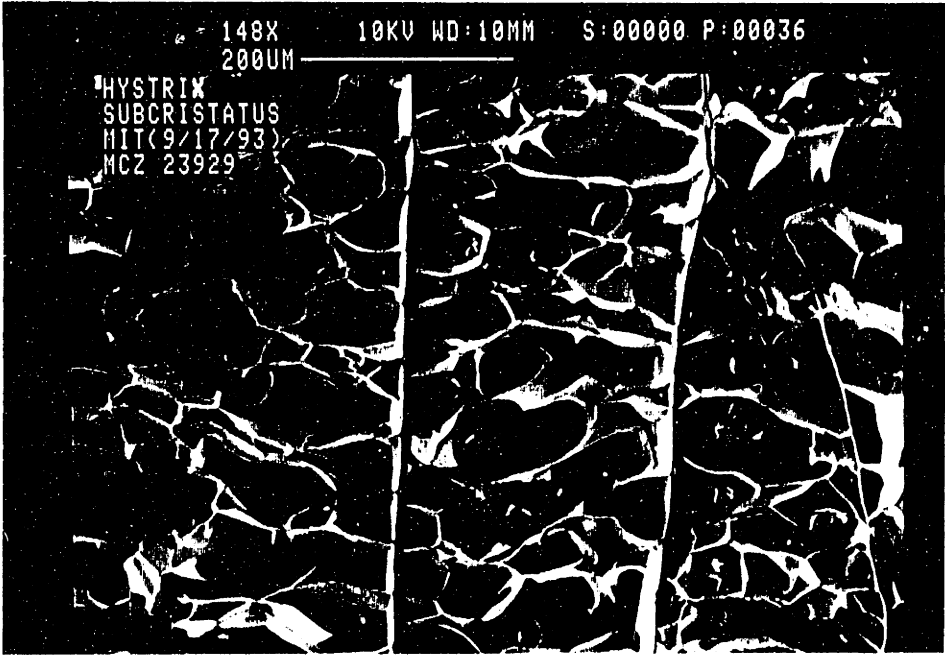


(d)

Figure 5.4: (a) and (b) Micrographs showing *Hystrix Galeata* quill cross section
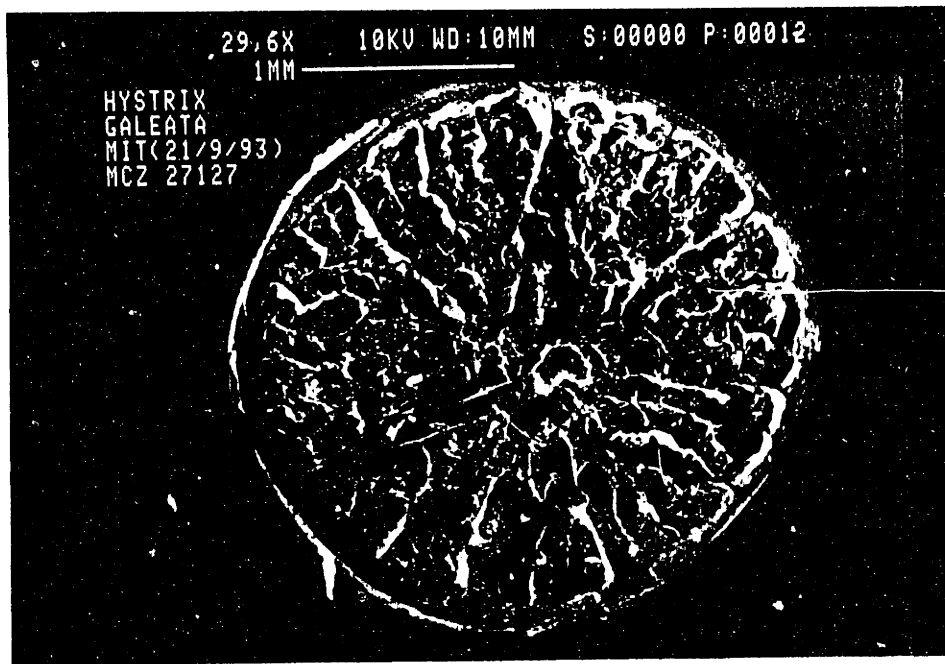


(a)
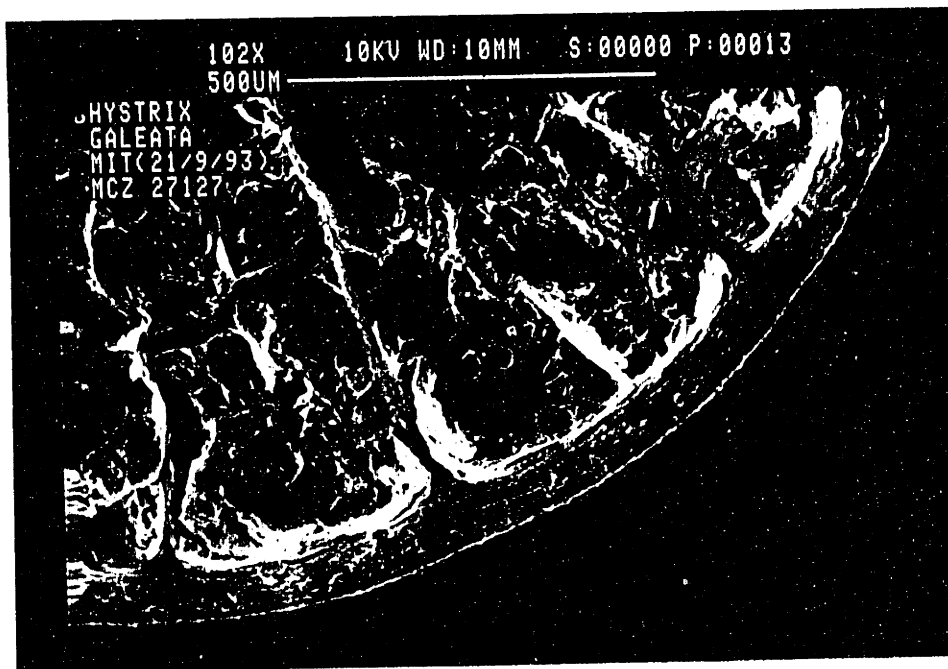


(b)

Figure 5.5: Micrographs showing hedgehog (*Erinaceus Europaeus*) spine: (a) and (b) cross section ,
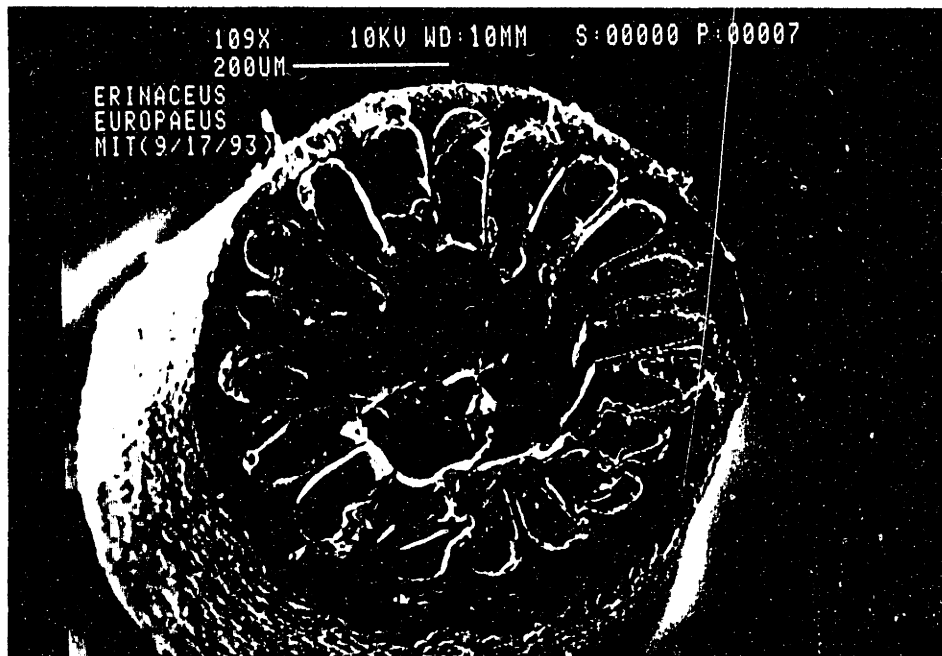


(a)



(b)

Figure 5.5: (c), (d) longitudinal sections
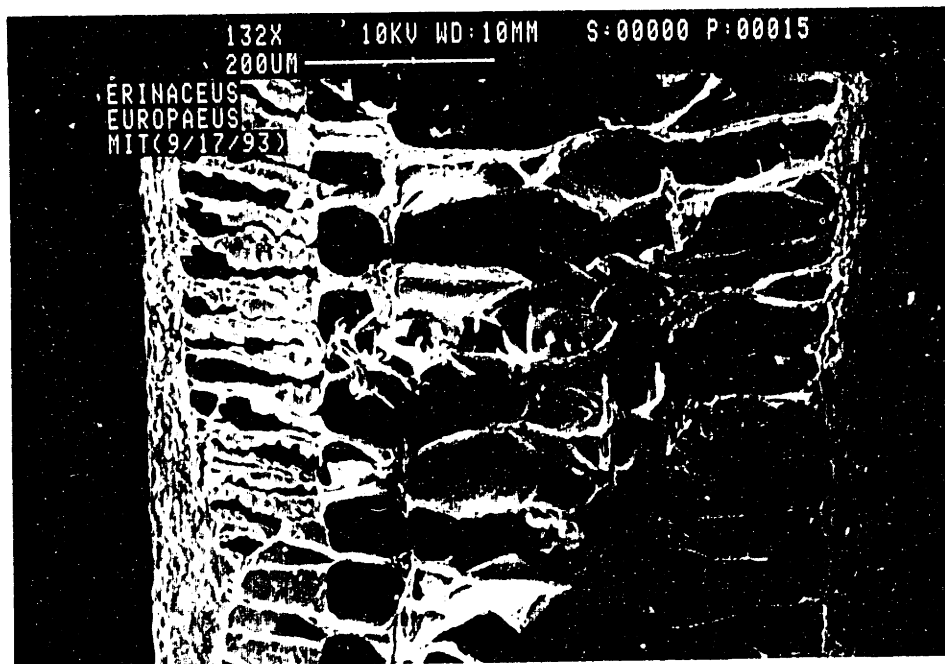


(c)
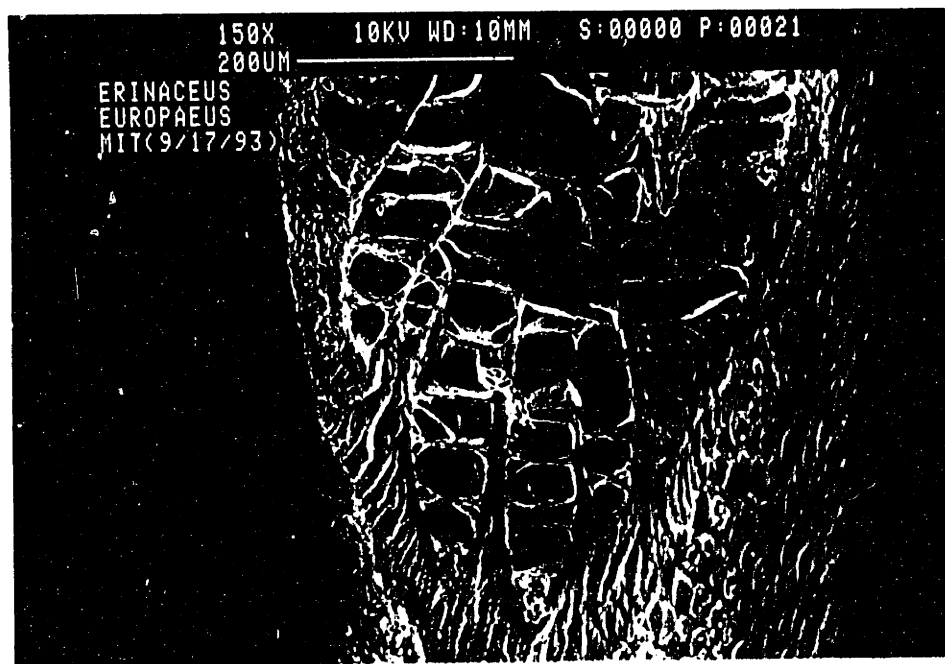


(d)

Figure 5.5: (e) longitudinal section, core as seen from inside of shell
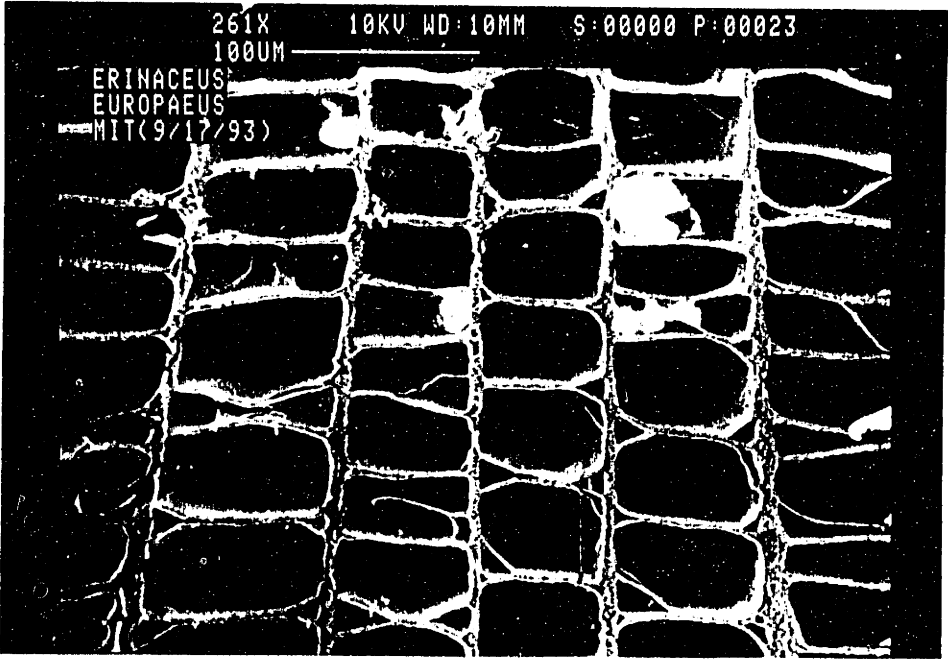
Figure 5.6: Micrographs showing grass (*Elytrigia repens*) stems (a) and (b) cross sections
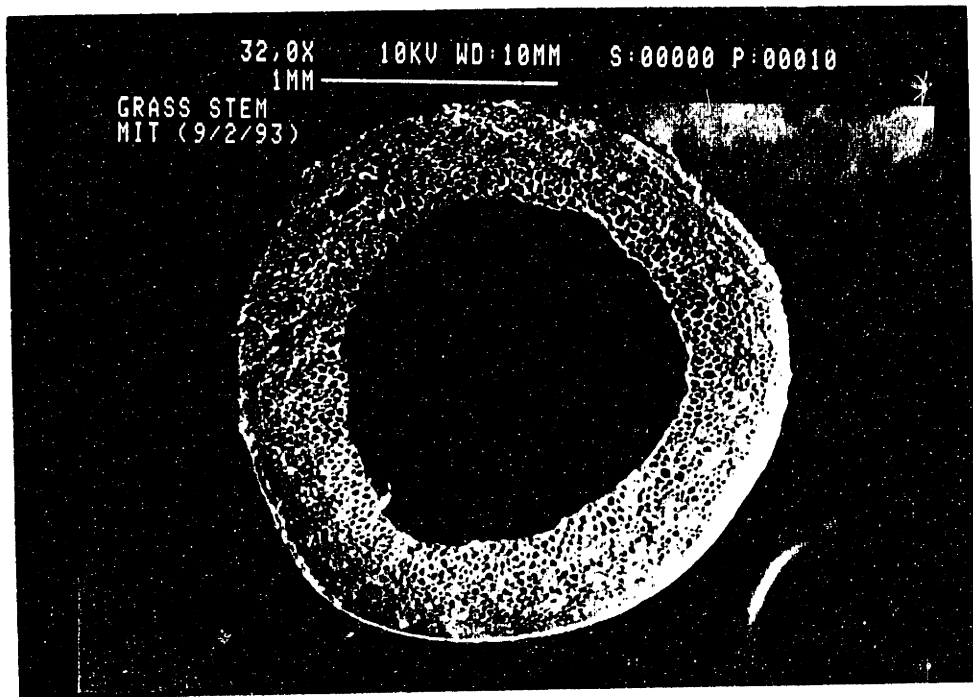


(a)
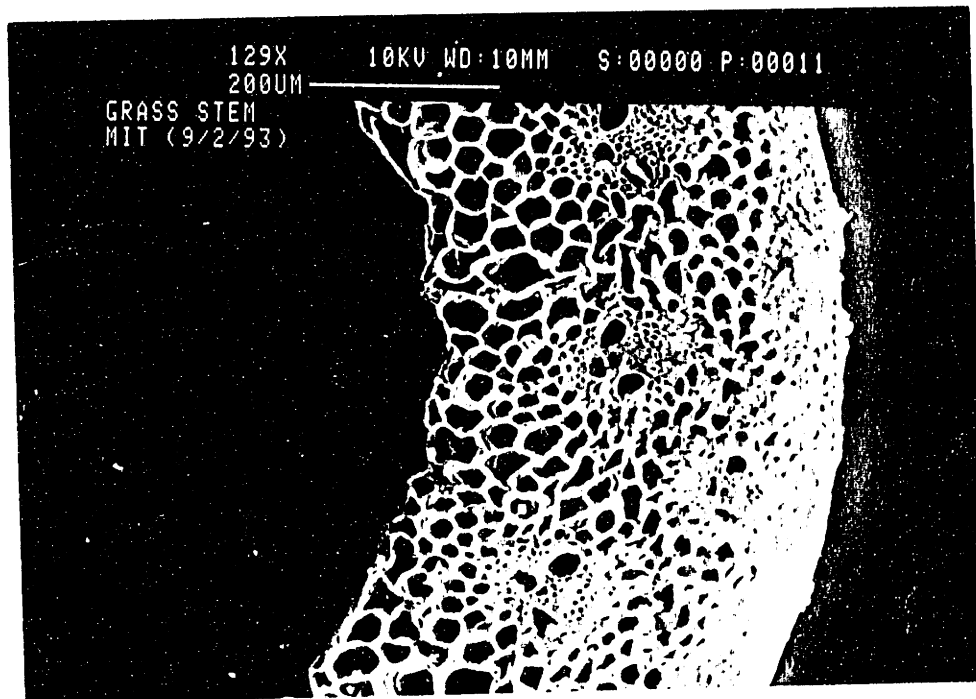


(b)

Figure 5.7: Micrographs showing stem (*Artemisia*) : (a) and (b) cross sections
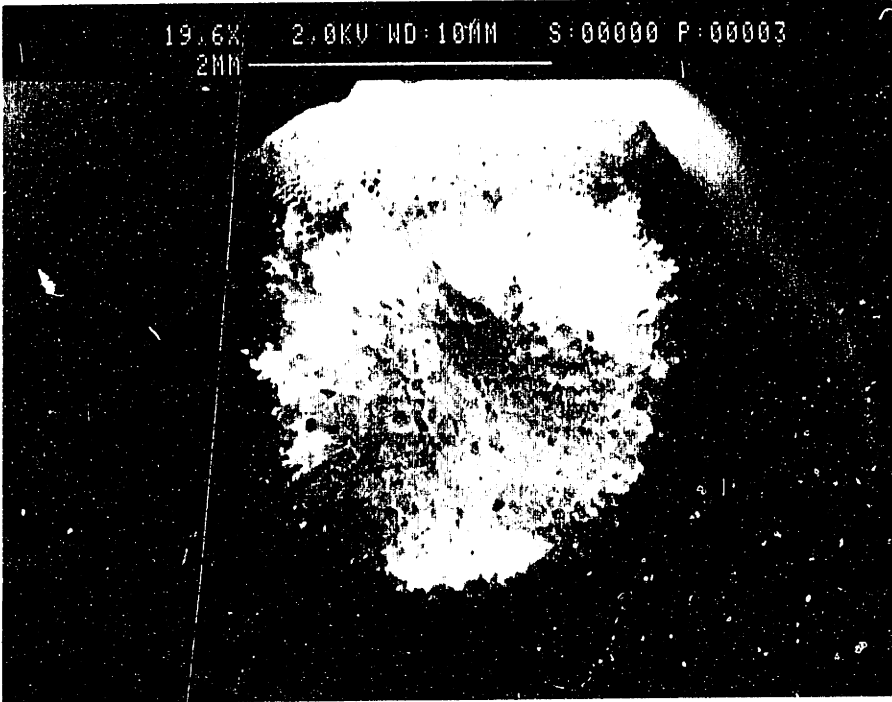


(a)
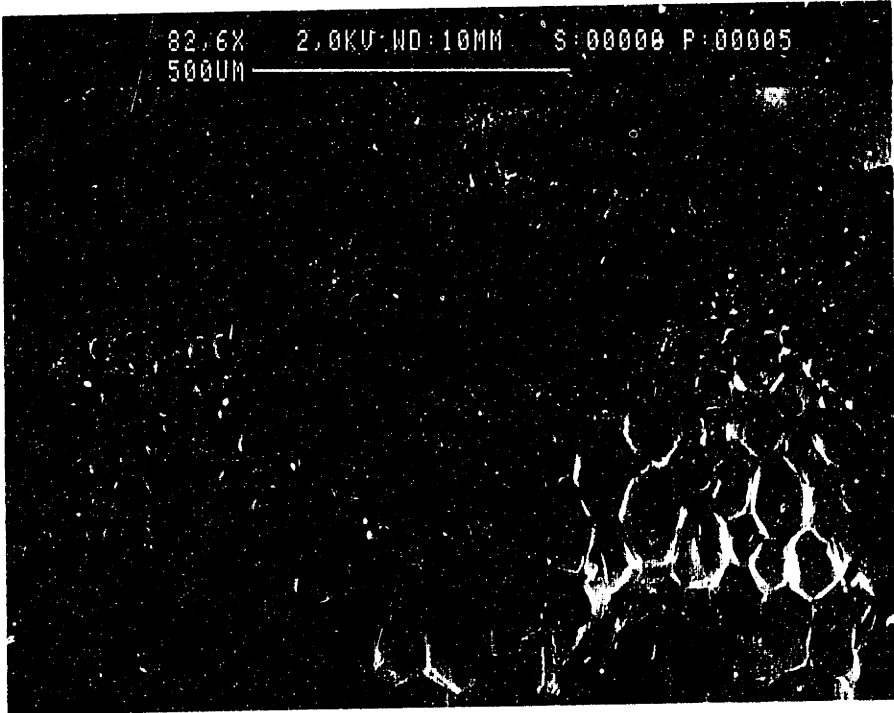


(b)

Figure 5.8: Micrographs showing North American porcupine quill (*Erethizon*) : (a) high magnification of solid shell material showing fibrous structure (b) three dimensional foam core microstructure
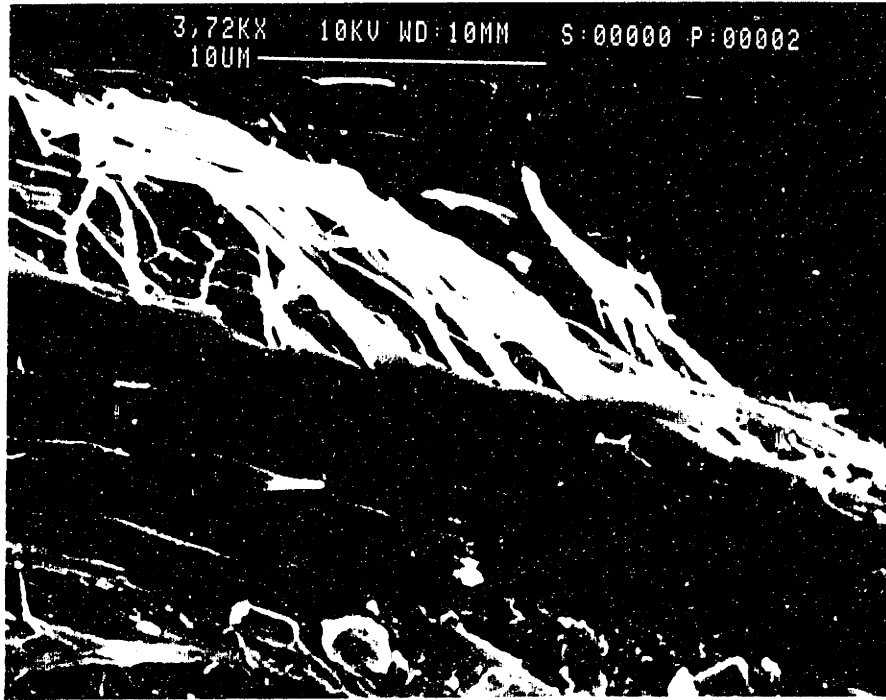


(a)
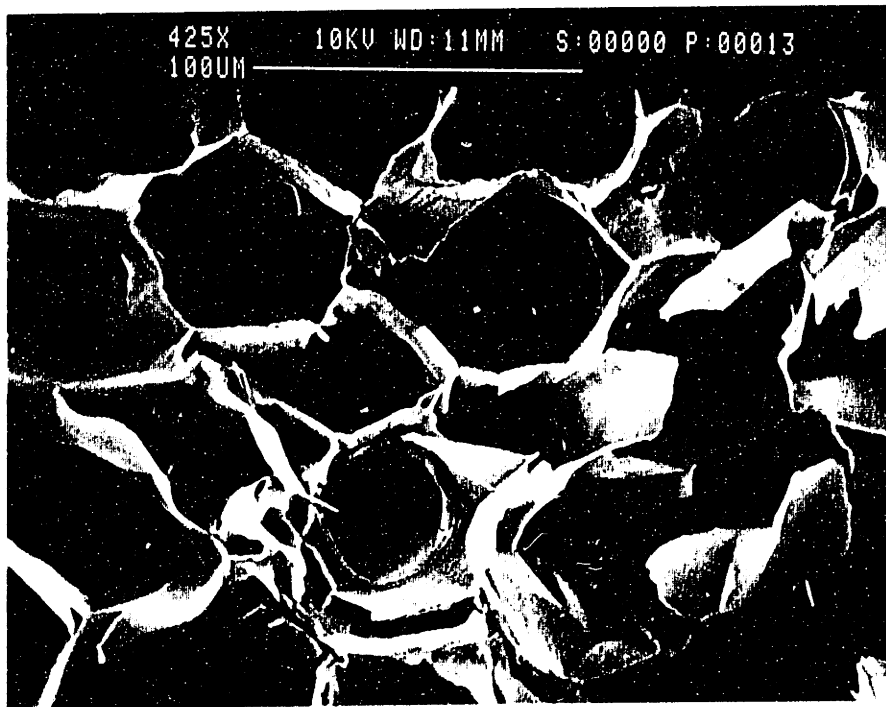


(b)

Figure 5.8: (c) high magnification of foam core cell wall
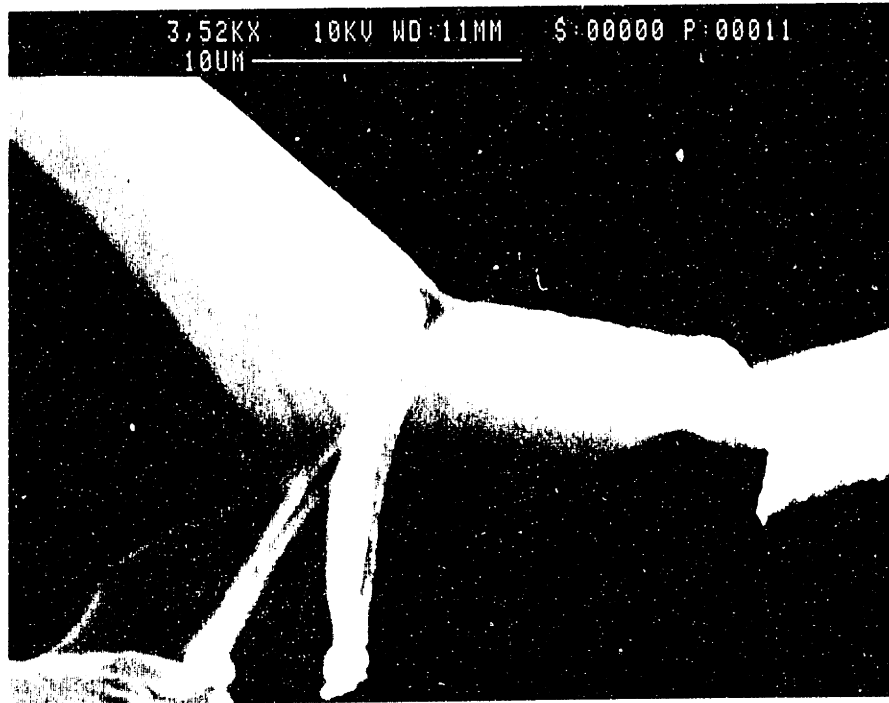
Figure 5.9: Microstructural core types and stiffness models:(a) Type 1 quills and plant stems (b)Type 2,quills
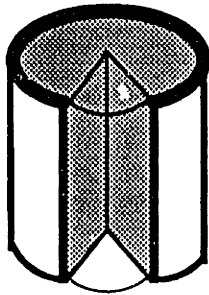


(a) Type 1 porcupine quill and plant stem microstructure:

$$(E_c/E)_x = (E_c/E)_y = (E_c/E)_z \approx (\rho_c/\rho)^2$$
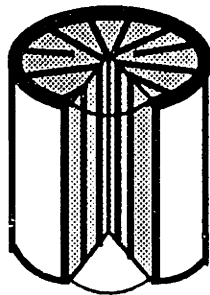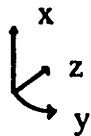


(b) Type 2 porcupine quill microstructure:

$$(E_c/E)_x = (E_c/E)_z \approx$$

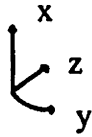$$(\rho_c/\rho)_{ribs} + [1-(\rho_c/\rho)_{ribs}](\rho_c/\rho)^2_{foam\ core}$$

$$(E_c/E)_y \approx \left\{ (\rho_c/\rho)_{foam\ core} / [1-(\rho_c/\rho)_{ribs}] \right\}^2$$

Figure 5.9: (c) Type 3, spines (d)Type 4, spines
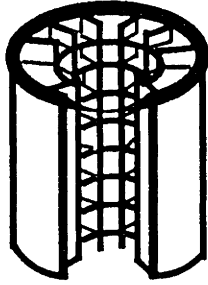


(c) Type 3 hedgehog spine microstructure:

$$2(Ec/E)x = 2(Ec/E)y = (Ec/E)z \approx (\rho c/\rho)$$
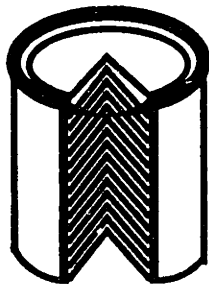


(d) Type 4 tenrec spine microstructure:

$$(Ec/E)y = (Ec/E)z \approx (\rho c/\rho)$$

$$(Ec/E)x \approx 0$$

Figure 5.10: Measured core depth to thickness ratio, c/t, versus core depth to thickness ratio required for 95 % stress decay, $(c/t)_O$
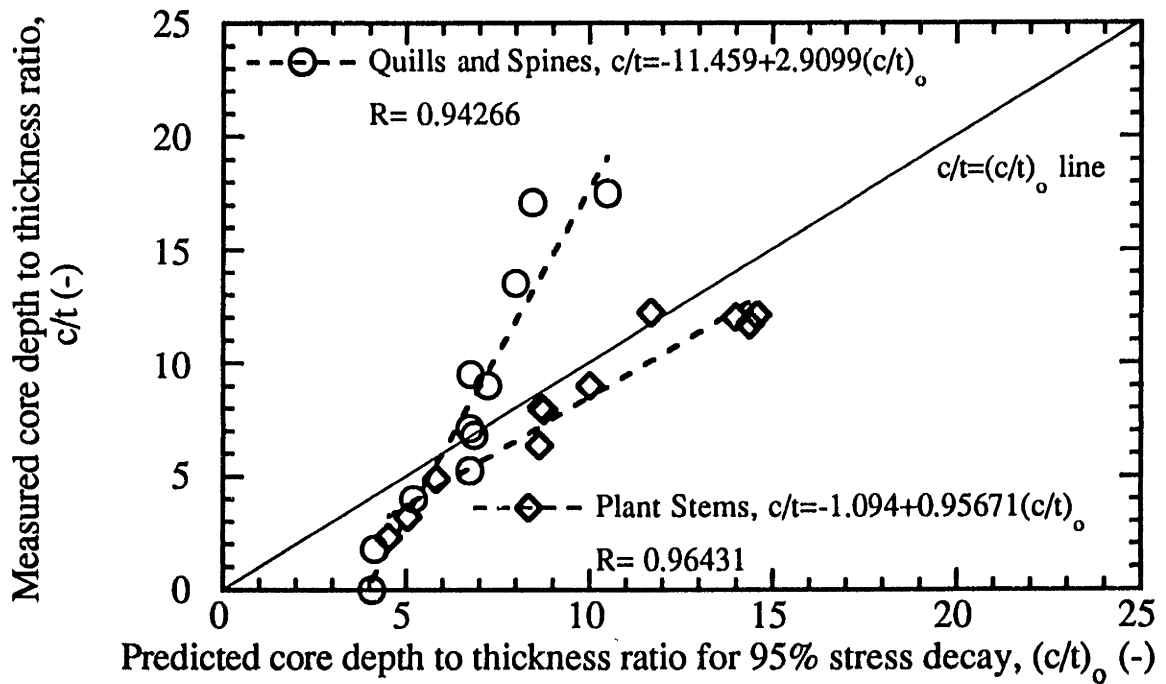
Figure 5.11: Ratio of the failure loads of animal quills and spines to those of the no core cylinder with equal radius and mass: (a) Axial buckling load
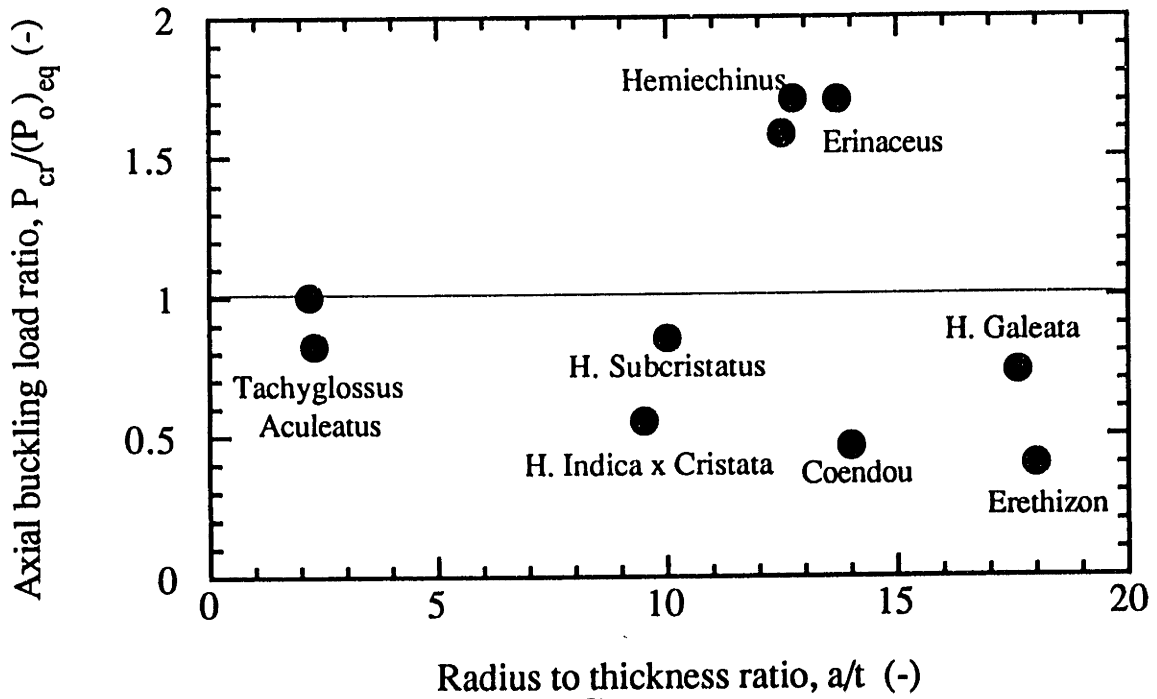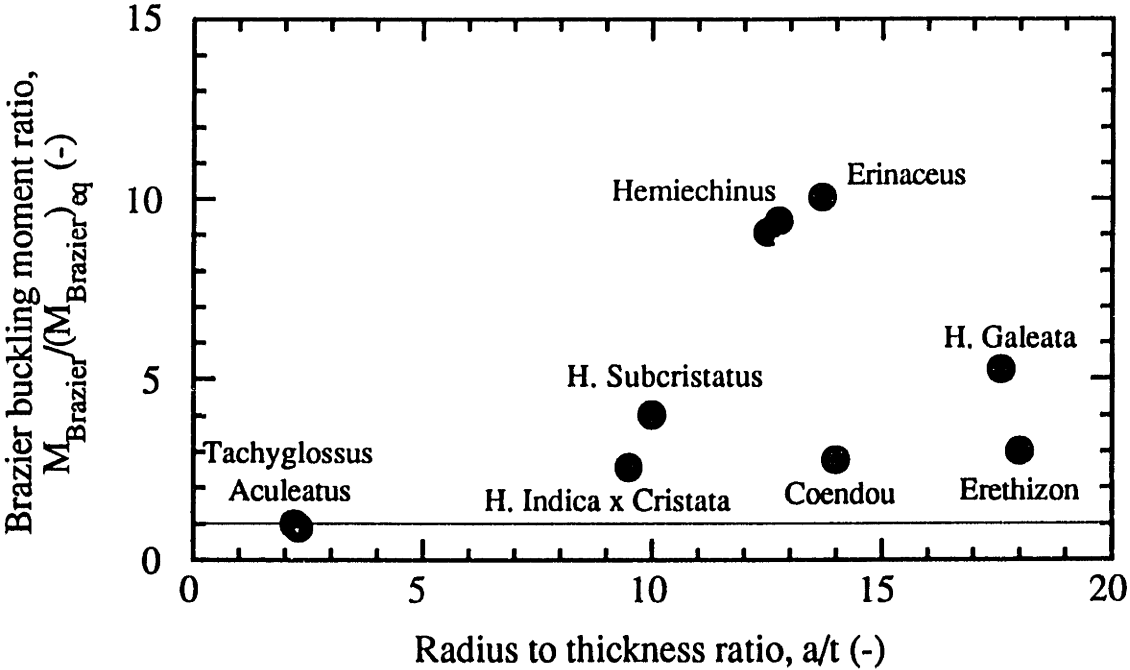
Figure 5.11: (b) Brazier moment



213

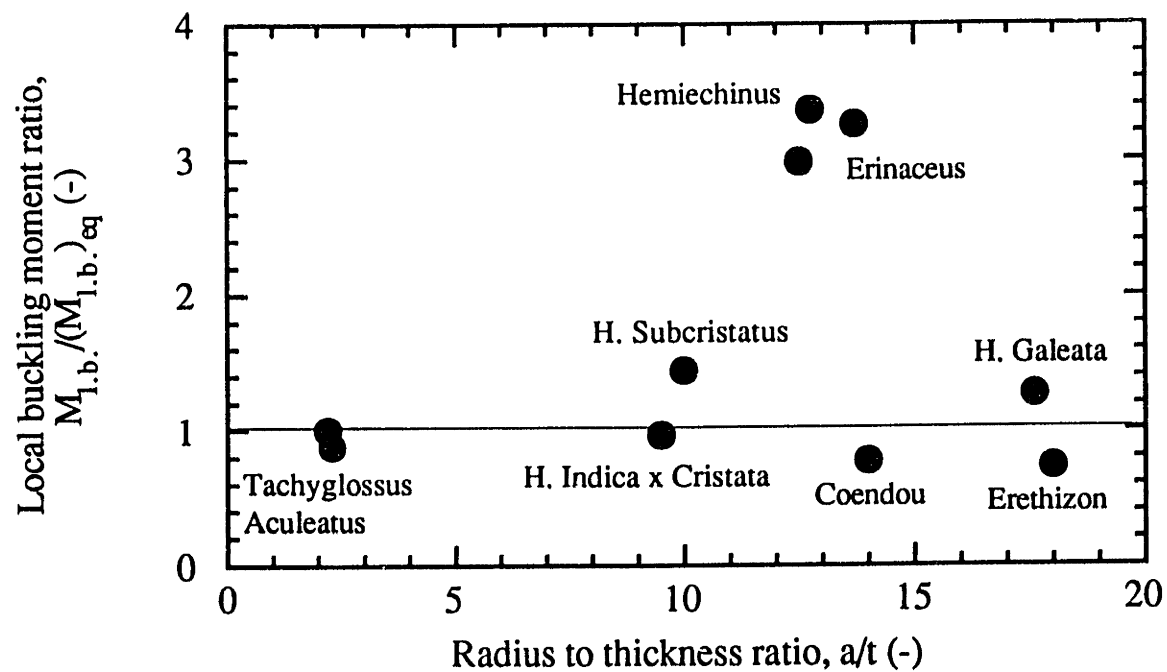Figure 5.11: (c) local buckling moment

Figure 5.12: Ratio of the failure loads of plant stems to those of the no core cylinder with equal radius and mass: (a) Axial buckling load
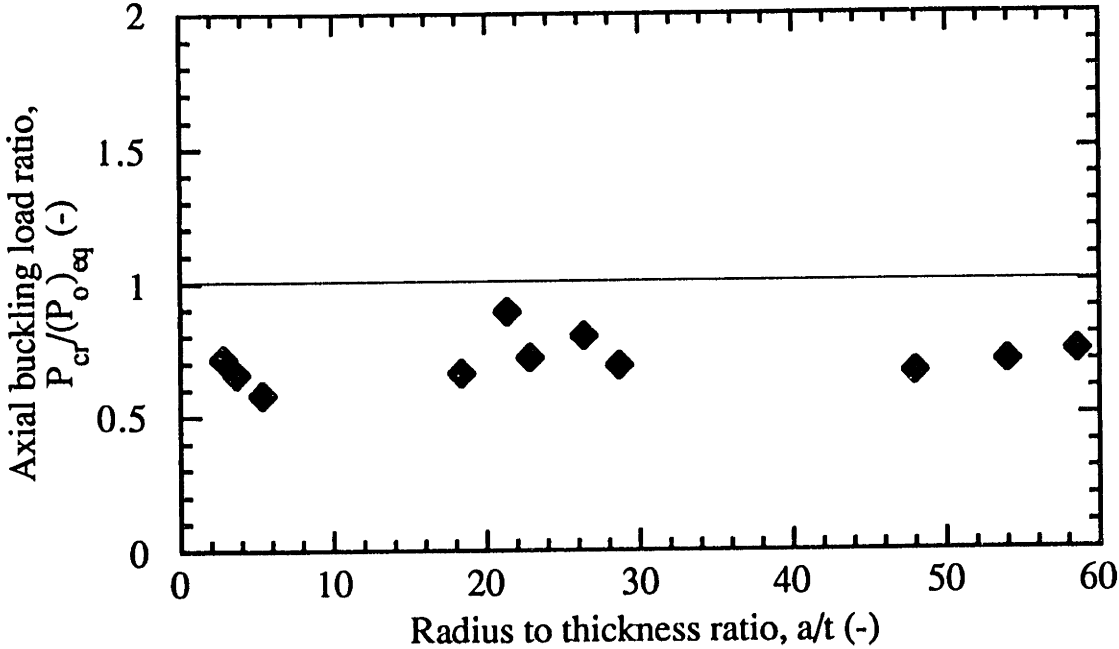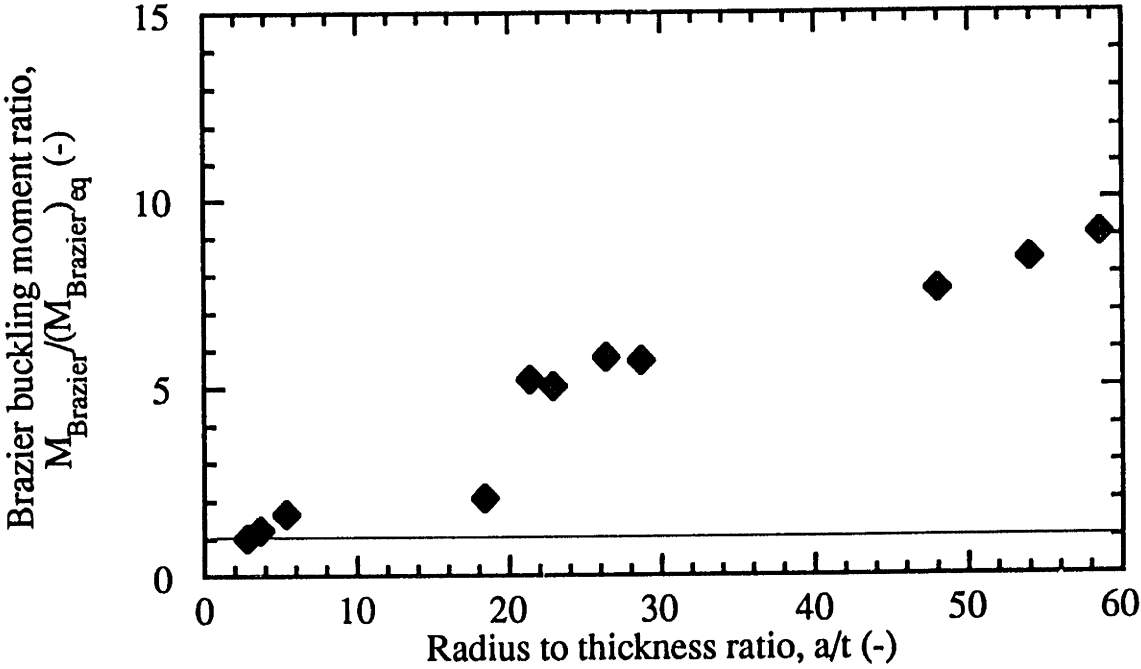
Figure 5.12: (b) Brazier moment

Figure 5.12: (c) local buckling moment

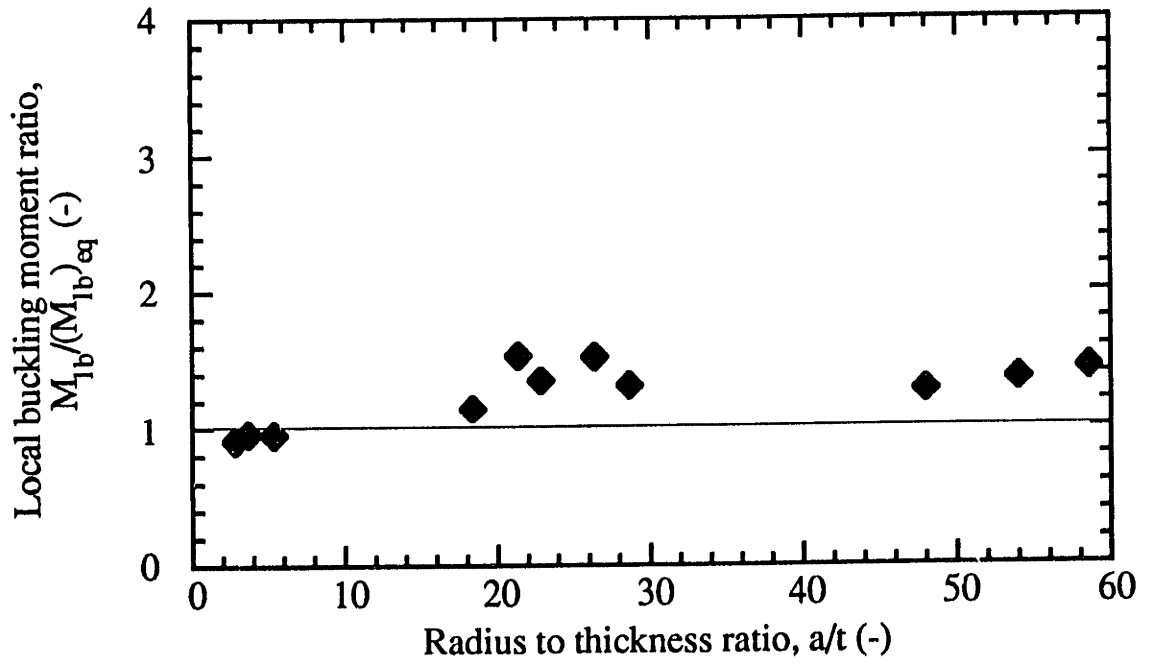Figure 5.13: Ovalisation at local buckling versus radius to thickness ratio, a/t, for quills, spines and stems.
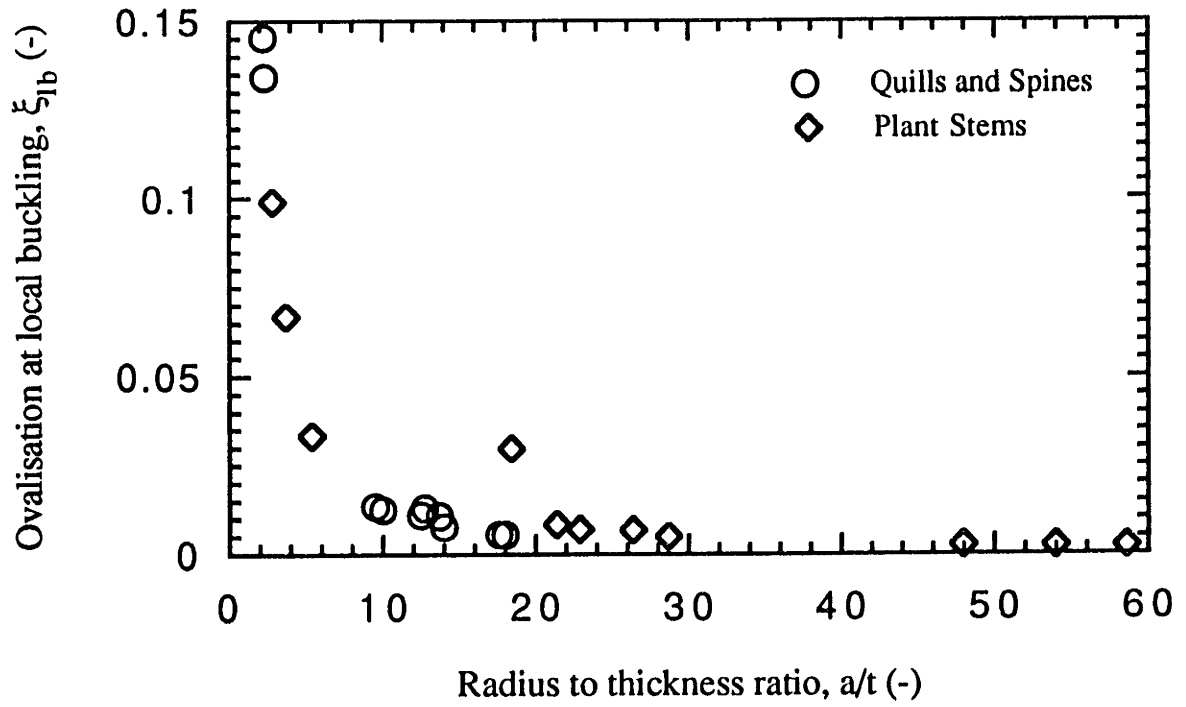
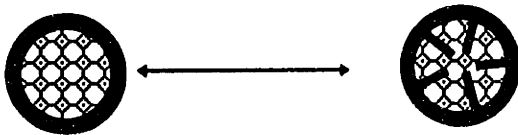Figure 5.14: (a) to (e) Evolutionary design process in animal quills and spines

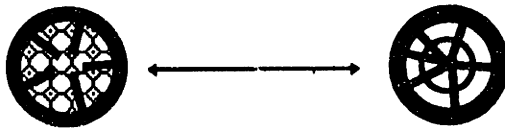(a) Step 1: Global bending stiffness

(b) Step 2: Brazier ovalization resistance

(c) Step 3: Local buckling resistance

(d) Step 4: Local buckling resistance improvement

(e) Step 5: Removing unstressed material in middle core

## CONCLUSIONS AND SUGGESTIONS

## FOR FUTURE WORK

*"You believe in a God who plays dice, and I in complete law and order"*
Albert Einstein (letter to M. Born, ca. 1930)

### 6.1 Conclusions

To investigate the mechanical efficiency of natural tubular structures with a cellular core an analytical model was developped to describe their elastic stability under axial compression, Brazier's ovalisation, and local buckling under bending. Treating the shell as a beam on an elastic half space, a simplified analysis of the buckling under axial compression was developed. It captures the most important elements of more complicated models and provides excellent predictions of the increase in buckling stress in a tractable mathematical form. The axial buckling stress was used as the local buckling criterion to derive a general solution for the stability in pure bending of cylindrical shells with a soft elatic core, including Brazier's ovalisation of the shell and core, and the Poisson's ratio effects in the core due to bending.

The analysis of the stress decay showed that at a depth of 1.6 half buckling wavelengths, the stresses in the core drop to less than 5% of the maximum value they reach at or near the shell. The removal of the material beyond this depth does not affect the buckling stress of the shell. A parametric analysis showed that cylinders with this core depth can reach higher buckling loads than hollow cylinders of equal mass and radius.

An extensive experimental program was carried out on uniaxial compression and four point bending specimens of silicone rubber shells with and without foam cores. The data for uniaxial compression buckling loads, the effect of core depth, the buckling wavelength, local buckling moments and Brazier's ovalisation are well described by the analytical model. Foam core cylinders under axial compression showed a reduced imperfection sensitivity and a stable postbuckling behavior. The axial compression results fell along the trend compiled from literature and extended substantially the experimental verification range of the theoretical models. The presence of a foam core practically eliminated ovalisation at local buckling in bending. The critical bending moments of partially filled cylinders achieved improvement of up to 400% over equivalent hollow cylinders as suggested by the analysis.

The analytical and experimental results suggest that their is a great potential for biomimicking of natural structures in engineering. Recent developments in materials manufacturing and microstructuring technologies have opened the door to new configurations such as cylindrical shells stabilized by a uniform honeycomb or a foam foundation instead of traditional stiffening. In addition to improved buckling resistance this may offer higher reliability due to reduced imperfection sensitivity and stable postbuckling behavior.

The characterization of 11 different animal quill and spine specimens and another 11 plant stem specimens revealed their microstructure to be close to the optimal configurations predicted by the analysis. Their structure seemed to be directed towards resisting applied bending loads in the most efficient way and with the least amount of material. The hierarchical design of these natural tubular structures can be mimicked in the engineering design process and microstructuring adopted to achieve optimal materials use on every scale.

On a broader perspective, the work described in this dissertation has presented a good example of a structural biomimetic study. It validates the applicability of the biomimetic approach to designing better structural and materials systems. An integrated interdisciplinary research effort, combining sound engineering knowledge with biological and evolutionary observations can speed the improvement of engineering designs and suggest a few new ones while providing the biological sciences with a rationale for its observations.

## 6.2 Suggestions for future work

On the particular problem of the cylindrical shells with a foam core, more detailed analytical and experimental work are needed before moving to engineering applications. The model developed has to be extended to treat non linear material behavior in shells and cores, especially elasto-plastic behavior in view of its applications (eg automotive and aerospace) to metallic engineering structures . The model can also be generalized to the case of a fully orthotropic shell and core to model more accurately natural structures and to allow a higher degree of optimization in engineering design by the use of advanced composites (fibre reinforced plastics and metal matrix composites) with properties tailored in each direction towards meeting the applied stresses.

The problem of the debonded shell, or the "zero tension foundation" problem, needs to be investigated in view of assessing the efficiency of an unbonded core and to determine the strength decrease caused by partial or total debonding.

Of all structures prone to elastic buckling (struts, plates, shells), cylindrical shells are among the ones that dangerously and dramatically lose their load carrying capacity after buckling. The presence of a core can prevent that and even provide for a stable increasing load deflection behavior beyond buckling as the experimental results of this

study have suggested. The analytical investigation of the postbuckling behavior is one of the most pressing extensions of this work, and can be of utmost importance in the use of foam stabilized thin sections in automotive frames that are designed to optimize their crashworthiness.

In the course of this investigation the core depth effect was only investigated with respect to resisting local buckling of the shell. And the parametric analysis carried out for configurations with the core depth necessary to achieve 95% stress decay. Only axial load, bending moment and their combination have been treated being the ones that pertain most to the function of the natural structures investigated. A general optimization procedure can be developed to identify the configurations and the material properties that will meet any combination of mechanical constraints (axial load, bending moment, stiffness, external or internal pressure, impact etc...) for a minimal weight. Requirements such as crashworthiness and reliability, and the plastic behavior of the shell or core may suggest totally different optimal configurations than the ones identified from the elastic analysis of natural tubular structures.

Other closed thin sections, such as tubes of square and rectangular cross section, common in engineering structures, can benefit from a stabilizing foam core; the same simple analytical model used for circular cross sections can be adapted to those shapes.

On a more general note, the extension of the derivations developed in this work to model more closely natural materials (pressurized core, orthotropic shell and core properties) can help in the understanding of the biological evolution of these different structures; for example the evolution of plants from water based environments to land based environments of varying dryness. The problem of barley (*Hordeum vulgare*) varieties selection to maximize lodging resistance offers an immediate application for the model presented in this work. Lodging in barleys is caused by local buckling failure

under wind induced bending in the lower two internodes of the stem. So far botanists and agricultural engineers have not been able to formulate a comprehensive scientific method to select the most resistant variety, besides trial plots and actual planting, for lack of accurate mechanical models. This problem may represent the first practical challenge to our work.

Finally, the biomimetic analysis of natural structures other than cylindrical shells with a foam core, such as palm stems, feather shafts and cuttlefish bone (described in Chapter 1), promises to yield interesting results. Further more the extension of the structural biomimetic approach to include not only single structural elements, but the whole structural system such as the "tiered" system of the feather (rachis, vanes, barbs) or the "branched network" of the tree, holds great promise in introducing the engineer not only to efficient solutions but also to elegant methods of design.

# Biographical Note

The author was born (14/4/1966) and raised in Beirut, Lebanon, the eldest of two sons of Nada Taleb and Nizar Karam. He finished highschool at the Grand Lycée Franco-Libanais de Beyrouth, graduating first in his class with a Baccalauréat Français d'Etudes Secondaires Série C (mention bien) and the Baccalauréat Libanais Deuxième Partie Math (mention très bien). He then attended the American University of Beirut (AUB) graduating in 6/1988 with a Bachelor of Engineering degree in Civil Engineering (with distinction). Joining the Civil Engineering depatment at the Massachusetts Institute of Technology in 9/1988 for gradute studies, the author obtained a SMCE degree in 6/1990 with a thesis on the mechanics of wood cement composites. A professional engineer (fully registered in Lebanon and registered as a jr. engineer in Québec) the author is a member or associate member of many professional and scientific societies (ASCE, BSCE, CSCE, ASME, ACI, ASTM, CGS, IABSE, MRS, Rheo. Soc. and Sigma Xi ).

The author in c·rrently engaged to Diane Zreik, a PhD candidate in the Civil and Environmental Engineering Department at MIT, and they plan to get married in summer of 1994.

The author's publications to date are:

• Karam, G.N. (1991) "Effect of fibre volume on tensile properties of real unidirectional fibre reinforced composites", Composites, Vol. 22, No.2, pp 84-88

• Karam, G.N. (1991) "Effect of fibre volume on the strength properties of short fibre reinforced cements with application to the bending strength of WFRC", Proceedings of the Sixth Technical Conference of the American Society for Composites, Albany NY, Oct.6-9, 1991, Technomics Pub., Lancaster PA, pp 548-557

• Karam, G.N. (1992) "Optimal design for prestressing with FRP sheets in structural members", Advanced Composite Materials in Bridges and Structures, K.W.Neale and P.Labossière eds., published by the Canadian Society for Civil Engineers, pp 277-285

• Karam, G.N. (1993) "Theoretical and empirical modeling of the rheology of fresh cement pastes" in Flow and Microstructure of Dense Suspensions, L.J. Struble, C.E. Zukoski and G.C. Maitland eds., Mat. Res. Soc. Symp. Proc., Vol. 289, pp 167-172

• Karam, G.N. and Tonyan, T.D. (1993) "Fractal morphology of cement foams", Materials Letters, Vol. 16, pp 278-280

• Karam, G.N. and Gibson, L.J. "Evaluation of commercial wood-cement composites for sandwich panels facing" to be published J. Matls. Civ. Eng., Vol. 6 (1) (1994)

• Karam, G.N. "On the ovalisation in bending of nylon and plastic tubes" to be published Int. J. Press. Vess. and Piping (1994)

• Karam, G.N. "Effect of fibre-fibre interaction on the strength properties of short fibre reinforced cements" to be published J. Comp. Tech. and Res., April 1994,